CHAPTER 1

Introduction

1.1 General

The stability of mineral particles in aqueous solution plays an important role in the industry practice of minerals engineering, such as coagulation, dispersion and flotation. In general, the suspension stability can be described quite well by the DLVO theory (1, 2), which was derived from the surface forces, i.e. the electrostatic force and van der Waals force, between the solid particles. The theory can be simply expressed as follows,

$$F_t = F_{ele} + F_{vdw} \qquad [1]$$

in which F_t is the total interaction between solid surfaces in close proximity, F_{ele} is the electrostatic force arising from the overlaping of electrostatic double layers, and F_{vdw} is the van der Waals force.

Heretofore, the validity of DLVO theory in describing and predicting the colloid stability has been proved widely by many evidences. However, when hydrophobic materials are involved, the theory met some difficulties in explaining both the experiment results and industry practice. For example, Derjaguin and Dukhin (3) modeled flotation (or bubble-particle interaction) using the surface forces, including only the electrostatic force and the van der Waals dispersion force. However, both of these forces are repulsive in most of the conditions encountered in flotation, which makes it difficult to model flotation, which is fast and spontaneous, using the DLVO theory. The presence of the non-DLVO interaction was first recognized by Laskowski and Kitchener (4). They found that methylated and pure silica particles had practically the same ζ-potentials and yet the former floated while the latter did not, which led to the suggestion that a long-range '*hydrophobic influence*' may be responsible for the rupture of the wetting film and flotation. They thought that the hydrophobic influence was caused by the instability of the water structure in the vicinity of a hydrophobic surface. Later, Blake and Kitchener (5) showed that the thin film of water (wetting film) between a hydrophobic solid and an air bubble ruptures fast and spontaneously at a separation of about 64 nm, which is much larger than predicted by the classical DLVO theory. These investigators suggested, therefore, the presence of a '*hydrophobic force*' in wetting films.

It was not until 1982 that the hydrophobic force was measured directly by Israelachvili and Pashley (6) using the surface force apparatus (SFA). Many follow-up experiments showed the existence of even longer range hydrophobic forces with the decay lengths in the range of 10-30 nm (7-14).

Despite of the fact that various theories have since been proposed and many experiments have been carried out, there is still no consensus on the origin of the hydrophobic force. For example, the strongest opposition to the existence of the hydrophobic force came from those who observed nano-bubbles on hydrophobic surfaces during measurements (15-19). However, it was recently reported (14) that the hydrophobic forces were observed both in degassed and air-saturated solutions. Therefore, it is highly suggested that more systemic investigations of hydrophobic force

should be carried out and the results will shed light on the origin of the complex yet important surface force.

The stability of minerals particles in solutions can also be described using the concept of interfacial surface free energy, γ_{sl}. In general, a high interfacial surface free energy (tension) suggests instability of the suspension; while a low solid/liquid interfacial tension results in a stable suspension.

It is therefore important to know the surface free energy, γ_s, of the solid minerals, from which one can obtain the interfacial tension (surface free energy) between the solid particles and the solution. In practice, it is even applicable to quantify the surface free energies of minerals before and after the addition of chemicals and the obtained information will help choose the suitable type and dosage of the added regents, which may be designed to serve as collector or depressant.

1.2 Literature Review

1.2.1 The hydrophobic force

The non-DLVO "hydrophobic force", without being included in Eq [1] has long been reported to exist between hydrophobic surfaces (7-14). So far, no consensus on the origin of this attractive force has arrived, yet the deviation of force measurement results from the DLVO theory suggests that this non-DLVO hydrophobic force may account for the instability of hydrophobized mineral particles in solution.

When the additional non-DLVO hydrophobic force F_h is taken into account, Eq [1] is extended to as follows,

$$F_t = F_{ele} + F_{vdw} + F_h \qquad [2]$$

In general, the hydrophobic force can be represented by a double-exponential function,

$$F / R = C_1 \exp\left(-\frac{H}{D_1}\right) + C_2 \exp\left(-\frac{H}{D_2}\right) \qquad [3]$$

in which, $H$is the closest separation distance between two curved surfaces with curvature R; C_1 , D_1 , C_2 , and D_2 are constants as fitting parameters.

Sometimes, the force is expressed in a single-exponential function,

$$F / R = C \exp\left(-\frac{H}{D}\right) \qquad [4]$$

where C and D are both constants.

Hydrophobic can also be described by a power law,

$$F / R = -\frac{K}{6H^2} \qquad [5]$$

in which K is a constant.

The fact that no consensus was reached may be due to the discrepancies between the reported experiment results of the hydrophobic force. The magnitude and range of measured forces were found to be strongly dependent on the methods of hydrophobizing the solid substrate. In their review, Christson and Claesson (20) emphasized this point and further classified the reported hydrophobic forces into three classes according to the different hydrophobizing methods for the substrates. 1) Stable hydrophobic surfaces (i.e. neutral hydrophobic polymers). It was usually reported that between these surfaces there was a comparatively short-range interaction in the range of ~30 nm. 2) Silylated silica surfaces, between which a very long-range attractive force was observed and the attraction is believed to be due to the existence of sub-microscopic bubbles on the hydrophobic substrates. 3) Mica surfaces are hydrophobized by coating with LB films or by surfactant in-situ adsorption. The observed attractions follow an exponentially function with rather long range and amounts the maximum in the vicinity of the point of charge neutralization (p.c.n.).

It is redundant to go over the experiment works which have already been nicely reviewed by Christson and Claesson (20). In present review, only the experiment results and theories reported thereafter are specifically discussed in detail. The works carried out before are summarized only when necessary.

1.2.1.1 The nanobubble hypothesis

The strongest opposition to the existence of the hydrophobic force came from those who observed nano-bubbles on hydrophobic surfaces during measurements (16-19). It was proposed that the "so-called hydrophobic force" is actually the capillary force introduced by the coalescence of preexisting nano-bubbles when two hydrophobic surfaces approach each other. From the beginning of the new century, the surface force measurements are carried out mainly to clarify the gas cavity/nanobubble origin of the long range hydrophobic attraction.

Ishida *et al*. (16) studied the effect of silanation on the long-range attraction between hydrophobic surfaces in water using an AFM. They reported that the interaction between the surfaces silanated by usual method was long-ranged with a discontinuous step observed in the approaching and separating force curves. On the other hand, only a short ranged and smooth interaction was observed between the silica surfaces silanated without being exposed to air. They attributed the long range attraction to the incompletely removed air on the hydrophobic surfaces during the hydrophobizing process.

Ishida *et al*. (17) further studied the OTS coated silicon wafer in water by tapping-mode AFM. It was reported the nano-size domain images were found on the hydrophobic surface, while no domain was observed in the case of the surfaces being hydrophobized in-situ in an AFM fluid cell without exposure to air. The same group later (21) claimed the existence of the gas bridge between hydrophobic surfaces from the study using a combined apparatus of an atomic force microscope and an optical inverted microscope.

Sakamoto *et al*. (19) conducted AFM force measurements between silica sphere and fused-silica plate in aqueous octadecyltrimethylammonium chloride (C_{18}TACl) solutions, and concluded that long-range attractive force is not observed in carefully degassed solutions.

Ederth *et al*. (22-24) studied the long-range attraction between self-assembled thiolate monolayers on gold surfaces in water through direct force measurement. It was reported that whenever the water contact angle exceeds 90°, the long-range 'hydrophobic' attraction was observed from a separation of 20 to 40 nm and the force curves were discontinuous and contained steps, which was attributed to the bridging of microscopic bubbles residing on the hydrophobic surfaces. When contact angle is less than 90°, no long-range attraction was observed.

Yang *et al*. (25) claimed the formation of nanobubbles at structured solid-water interfaces using the tapping mode atomic force microscopy (TMAFM) imaging technique. They observed randomly distributed small bubbles on methylated surfaces of controlled roughness. It was also reported that small bubbles did not form on smooth, hydrophilic, or dehydroxylated silicon oxide wafer surfaces in water even under known levels of gas supersaturation.

Tyrrell and Attard (18, 26) reported the observance of domains or nanobubbles on a hydrophobic glass surface in water using a tapping mode AFM. The domains were claimed to be close packed and irregular in cross section, with 'a radius of curvature of the order of 100 nm, and a height above the substrate of 20–30 nm.' The AFM images were further correlated to force measurement results. It was therefore concluded that these nanobubbles evoked the long-range hydrophobic force.

Steitz *et al*. (27) carried out Neutron reflectivity measurement on the thin water film in the vicinity of a perdeuterated polystyrene (d-PS) spin-coated silicon surface. It is proposed that the observed depletion water layer was a precursor layer of submicroscopic gas bubbles on hydrophobic surface.

Holmberg *et al*. (28) observed nanobubbles on unmodified gold surfaces in clean water using a standard silicon AFM probes. It was claimed that these nanobubbles were unstable and they may disappear or reappear from contact mode AFM images depending on the scaning force.

Nguyen *et al*. (29) measured the interaction between an AFM hydrophobic probe and a flat hydrophobic surface in water, in water–ethanol mixtures, and in water saturated by gases with different solubility using an AFM. It was found that the long-range attraction, with steps, decreased with an increase in the ethanol content and disappeared in pure ethanol. Gas solubility was reported to affect the steps size on the force curves rather than the measured forces. The surface roughness and heterogeneity were also considered to be important.

Zhang *et al.* (30) investigated the degassing and temperature effects on the formation of nanobubbles at the mica/water interface. It was claimed that the dissolved gas in the liquids was essential for the formation of nanobubbles. In addition, the density of nanobubbles increased with the temperature of liquid.

1.2.1.2 Capillary force or surface force?

Despite of the claims that the long range hydrophobic attraction is due to gas cavity, some authors proposed, on the other hand, that the nanobubble hypothesis may not be the final answer for the real hydrophobic force.

Mao *et al.* (31) studied the interface between water and hydrophobized silicon wafers using an ellipsometer and concluded that the obtained optical measurements results were inconsistent with the existence of continuous air films that are greater than

about 0.1 nm in thickness. It was then suggested that the putative bubbles would be sparsely distributed on hydrophobic surface. However, the possibility of the existence of air cavity during surface force measurements could not be ruled out.

Evans *et al.* (32) inferred the hydrophobic surface in water using an AFM imaging technique. They proposed that the nanobubbled or domains reported by Tyrrell and Attard were likely to be due to polymeric contamination.

Stevens *et al.* (33) studied the interactions between hydrophobic amorphous fluoropolymer surfaces in water with and without dissolved air. The range of the attraction was found significantly decreased in deaerated water as compared to aerated water. It is interesting to note that, however, the range and strength of the attraction in deaerated water were still greater than the van der Waals attraction. It was then proposed that the attractions obtained in deaerated water were the 'pristine hydrophobic attraction unobscured by nanobubbles'.

The group of Israelachvili (34) conducted a careful examination of degassing effects on the hydrophobic attraction between double-chained surfactant monolayers coated mica surfaces using a surface forces apparatus (SFA). They found that the hydrophobic interaction followed a double-exponential function down to separations of 5 nm and became even stronger at shorter separations (35). The range of the attraction was reduced a little after degassing, while the short-range attraction (<25 nm) remained unchanged.

Zhang *et al.* (14) conducted AFM force measurements between glass sphere and fused-silica plate in aqueous C_{18}TACl solutions. It was reported that an attractive force that was much stronger than the van der Waals force both in air-saturated and degassed solutions. The strongest attraction was observed at the concentration close to the charge compensation point (ccp). The force followed an exponential function and was effectively screened by an added electrolyte (NaCl).

In the big review of Christson and Claesson (20), nanobubles were suggested to be the origin for the extremely strong attraction observed between very hydrophobic surfaces, for example, the OTS coated silica surfaces and the thiolated gold surfaces. However, this can not be generalized to the case of surfactant in-situ adsorption system, which was classified as the third category in the review. Sakamoto *et al*. (19) conducted AFM force measurements between silica sphere and fused-silica plate in aqueous octadecyltrimethylammonium chloride (C_{18}TACl) solutions, and claimed that long-range attractive force was not observed between moderate hydrophobic surfaces with contact angle less than 80º in carefully degassed solutions. They proposed that "alkyl chains of surfactants in the powder state accompany air when the surfactants are dissolved into water" and these refractory air bubbles account for the long-range attractions observed between hydrophobized silica surfaces in C_{18}TACl solutions. However, this mechanism is short of theoretical background, because the cavitations are only thermodynamically stable on hydrophobic surfaces with contact angle larger than 90^o. In addition, the classical theory of micelles formation applies well without considering the attached air on surfactant alkyl chains.

In literatures, the results of surface force measurements are usually plotted in a surface force vs. separation coordinate. Most reported surface force curves in literatures show that the force scale is generally less than 2-10 mN/m (36-40), even when the scale of surfaces separation is as small as 30 nm. To clarify this, we plotted an extremely strong electrostatic attraction assumed to occurr between two reversely charged solid

surfaces with surface potentials as high as 150 mv. The calculated force curve shows that when plotted in a coordinate with a force scale of 100 mN/m, the force is almost zero at the separation of 30 nm. It is clearly seen that, however, the attractions reported in Fig. 3 and Fig. 7 in Ref. 19 are much larger than even such a strong electrostatic attractive force. Therefore, before investigating the force curves, one has to acknowledge the fact that the long-range attractions reported by Sakamoto *et al*. (19) are extremely strong and long-ranged. These super long-range attractions are clearly far beyond real surface force in both range and magnitude.

In Sakamoto *et al*.'s work (19), quite stiff cantilevers were employed. The spring constant was determined to be almost 50 N/m, which was approximately 25 times larger than that of the cantilevers used in common force measurements (36-40). In theory, AFM cantilevers with any a spring constant can be applied for surface force measurement. However, in practice, AFM probes are only chosen from those of which the stiffness is in a suitable range concerning the magnitude of the surface force under investigation. A soft cantilever is sensitive to even weak surface force, and it is beneficial for describing in detail the tail of the force curve. However, a too soft cantilever may result in two drawbacks. First, the force/distance gradient may exceed the spring constant of a soft cantilever easily, introducing the force instability and evoking the sphere to jump onto the plate at a rather large separation. The force information at a close surface separation is therefore no longer available. Second, the AFM piezo has to travel a quite long distance to make the sphere on a soft cantilever to detach the plate in a retract cycle due to the strong adhesion between the hydrophobic surfaces. Therefore, soft cantilever is generally used to measure weak surface force. While using a too stiff cantilever, one can only obtain the force information at a short surface separation in stead of that at a large separation. In particular, a stiff cantilever is generally used in the cases when the solid surfaces are very hydrophobic and a strong adhesion is observed. In practice, some investigators used both soft and stiff in their force measurements. For example, Teschke and Souza (41) studied the force between an AFM tip and a hydrophobic surface using the cantilevers with spring constant of 0.03N/m and 0.1N/m respectively. Meagher and Craig (42) measured the forces between polystyrene surfaces employing the cantilevers with a nominal spring constant of 0.3 N/m and 59.5 N/m. In both these experiments, cantilevers of different spring constant were purposely chosen to obtain the force information in short and large separations separately.

As to the measurements of long-range attraction between silica surfaces immersed in C_nTACl solutions, the force range is of the most important concern. Therefore, it is beneficial to use a soft cantilever, with the precondition of not sacrificing the force curve much at short separations, to get clear information of the tail (long-range part) of the force curve. It was shown (14) that the cantilever with a nominal spring constant of 0.58 N/m has been proved to be beneficial for both high sensitivity and wide force range. For example, the force curve is available from a separation of 24 nm to 100 nm for the strongest long-range attraction. Therefore, one can clearly see the effect of surfactant, salt or degassing on the force curves.

It is unfortunate that Sakamoto *et al*. (19) measured the capillary force rather than the real surface force between silica surfaces in normal $C_{18}TACl$ solutions. In that case, a very stiff cantilever had to be applied in their force measurement due to the extremely large magnitude of the capillary force compared to that of the real surface force. One

direct consequence is the loose of specifics of the real surface force, as shown in Fig. 10 in Ref. 19, when the capillary force is absent after the solution being carefully degassed. Furthermore, their results were plotted in a scale that was ten times larger than used in our work (compare Figure 10 of Ref. (19) to Figure 7 of Ref. (14). Close inspection of their published results reveals an attractive force that is similar in magnitude to the force measured in Figure 7 (14). Unfortunately, only considering the disappearance of capillary force before and after degassing, Sakamoto *et al.* (19) jumped to a conclusion that the long-range attraction between silica surfaces in C_{18}TACl solutions was due to gas cavity, without further investigating the effect of degassing on the real surface force.

One thing worthy of being mentioned is that, with such a stiffer cantilever as the authors used in their experiments, it may be hard to tell the difference between the long-range parts of the 'real surface force' curves obtained before and after degassing due to the great loose in sensitivity. What is more, as discussed before, the data of real surface force will not be discernible on a force scale of 100 mN/m at a separation larger than 30 nm. That is, no long-range attraction will be observed in such a large force scale.

1.2.1.3 Degassing effect on the long-range attraction

The direct way to tell whether the long-rang attraction origins from nanobubble is to compare the surface forces obtained before and after degassing (17-21). Meagher and Craig (42) studied the degassing effect on the surface force between polypropylene surfaces (θ=90º~111º) in aqueous solution using an AFM. It was found that an attraction stronger than the van der Waals force existed before and after degassing. The degassing process only makes the jump distance changes from 21.0$\pm$5.2 nm to 15.2$\pm$4.2 nm. The partial overlap of these results suggests that the change of the attractive force upon degassing is not dramatic and the jump distance after degassing treatment still can be as large as 19.4 nm, which is clearly beyond the range of the van der Waals force.

Considine *et al*. (43) investigated the force between polystyrene spheres in aqueous media using an AFM. It was reported that some attraction, which is clearly much larger than the van der Waals force, pulled the two spheres into contact from a quite long range (20-400 nm) and the range of the strong attraction was found to decrease significantly after degassing. After scrutinizing the reported results, however, one can see that the jump distance on the force curve, obtained after the degassing treatment, can still be as large as 30 nm! (See Fig. 3. of Ref. (43))

Mahnke *et al*. (44) reported the jump distances on the force curves obtained between methylated silica surfaces (θ=73º) before and after degassing. The results showed that degassing process significantly reduced the jump distance, which is above 25 nm; while it has little effect on 'small' jump distance, which is still beyond the range of the van der Waals force. There are two things worthy of being mentioned. First, the degassing processing was carried out using freeze-thaw procedure, which is supposed to better degas the solution. Second, the force curves were obtained in the presence of 0.1mM KNO_3, the existence of which may reduce the range of the long-range attraction.

Most recently, Meyer *et al.* (34) studied the effects of dissolved gas on the hydrophobic attraction between surfactant-coated mica surfaces using a SFA. They claimed that degassing reduced the range of attraction while the short-range attraction (<25nm) remained unchanged.

At first glance, the above force measurements show that the long-range attraction is greatly reduced or even 'disappeared' due to degassing the solution. However, a careful reexamination of the experimental results reveals that an attraction which is long ranged than the van der Waals force always exists between two hydrophobic surfaces. First, the substrates studied in most of these force measurements are of quite hydrophobic surface, such as polypropylene, polystyrene and methylated or silanated silica, with a contact angle generally above 90 degree. Second, the force curves obtained after degassing process show that, even though a 'very' long-range attraction is dramatically reduced, there is still a jump-in occurring at a separation of 15~30 nm, which is clearly beyond the range of the van der Waals force.

Eriksson and Ljunggren (45) concluded that 'no stable bubble can form and adhere to hydrophobic surfaces insofar as (macroscopic) equilibrium surface thermodynamics is applicable'. However, when surface imperfections, for example, roughness, are present, a bridging bubble mechanism of the hydrophobic force can't be excluded. In theory, Yushenko *et al*. (46) predicted cavitations between hydrophobic surfaces (θ>90º) at close separations. In practice, gas cavitation has been directly observed between hydrophobic surfaces (θ>90º) in SFA experiments (47, 48). Therefore, it is possible to detect capillary force between the rather hydrophobic surfaces with a contact angle larger than 90 degree. A character of this macroscopic force is its 'super' long range and large magnitude comparing to those of real surface forces, such as van der Waals force, electrostatic force, hydration force and hydrophobic force *etc*. Therefore, the 'super' long-range attraction is generally expressed in a coordinate of 40-400 mN/m in magnitude and 100-300 nm in range (19). When the solution is degassed, it is not a surprise at all that the 'super' long-range attraction disappeared due to the submicron bubbles are removed from hydrophobic surfaces. It is in essential the disappearance of capillary force rather than that of a true surface force, which is hard to discern in a coordinate with such a large force scale. As mentioned before, Sakamoto *et al*. only observed the change of capillary force after degassing, without further investigating the 'small' attraction shown in figure 10 of Ref. 13.

1.2.1.4 Long-range attraction between hydrophobic surfaces obtained by in situ surfactant adsorption

Hydrophobic attraction was firstly observed between mica surfaces immersed in CTAB solutions (6, 49). Since then, lots of force measurements (36-40, 50) have been carried out between the hydrophobic surfaces obtained by surfactant in situ adsorption. The reported results, in summary, showed that there are two properties in this specific system. First, the contact angle on solid surface after surfactant in situ adsorption is generally less than 90º. This is especially true in the case of silica substrate, due to its relatively low surface charge density in aqueous solutions. Second, the strongest long-range attraction is always observed in the vicinity of the point of charge neutralization (p.c.n.) (20).

The relatively low contact angle, less than 90º, suggests that it is not likely for the submicron bubble to be stable on the hydrophobized surface. Christenson and Claesson (20) stated that 'Cavitation has only rarely been observed, and possibly only with double-chain surfactant.' In fact, most force curves (36-40) obtained in surfactant in situ adsorption system are reported in a coordinate similar in the order as what we used (14). In addition, no long-range attraction as large as what Sakamoto *et al*. has ever been

reported in literatures. It is not clear yet in Sakamoto *et al.*'s work why the bubbles exist on a moderate hydrophobic solid surface with contact angle less than 90 degree.

Considering the results reported by Sakamoto *et al*. (19), two more things are worthy of being mentioned. First, the reported experiment results show fluctuation in a quite large extent. For example, under the same condition, the force curves obtained in 3×10^{-5} M C_{18}TAC solution and listed in Fig. 1, Fig. 2 and Fig. 3 of Ref. 19 are different from each other. This is especially evident when they are redrawn in a same coordinate. It may be due to difference of bubble size and this further indicated that the forces measured by these authors were indeed the capillary force. Second, the separation force curve in Fig. 10 of Ref. 19 shows almost no adhesion at all! It is unlikely to happen at the interface of water and a hydrophobic surface ($\theta\approx80^{o}$ (19)), where a strong adhesion is anticipated due to the rather large interfacial surface free energy. The absence of adhesion at the interface with high interfacial energy simply casts doubts on the hydrophobicity or smoothness of the solid surface applied in these authors' experiments.

The origin of the long-range hydrophobic attraction has been studied for more than twenty years. Various theories could be referred in literatures without being reiterated in present work. However, it is still beneficial to mention some extremely important fundamentals. In thermodynamics, the interfacial energy between hydrocarbon and water is approximately 50 mJ/m^2, which is considerably larger than that due to van der Waals force. It suggests that another attraction, stronger than van der Waals force, should exist between hydrophobic surfaces, even though no prediction as to the range of the interaction has been inferred from the state function yet.

From the above review of surface force measurements, one can clearly see that what Sakamoto *et al*. (19) observed is essentially the capillary force rather than the true surface force. They used cantilevers with unsuitable stiffness for the force measurements in the specific system. In addition, they plotted the force data in a coordinate with a extremely larger scale. Therefore, they failed to resolve the change of real long-range attraction, which is several orders smaller than the capillary force, after the solution was degassed. It is then suggested that submicron bubbles may not be the cause of the true hydrophobic force. In present investigation, careful surface force measurements are carried out between silica surfaces in C_nTACl solutions. The effects of degassing, salt addition and surfactant chain length are systemically studied. The origin of hydrophobic force is also discussed in terms of the obtained surface force results.

1.2.2 Surface free energy

In industrial mineral processing practices, such as adhesion, flotation and dewatering, the interfacial surface free energy between the minerals and the media usually plays an important role in the stability of solid particles in solutions. In general, a high interfacial tension (surface free energy) suggests instability of the suspension; while a low interfacial tension results in a stable suspension. For example, water molecules in fact always attract solid particles. However, sometimes the interactions between water molecules are much stronger than those between water and solid; therefore, it seems that water repels the 'hydrophobic' solids, resulting in the instability of solid in solution.

It is therefore important to know the surface free energy of the solids, from which one can obtain the interfacial tension (surface free energy) between the solid particles and the solutions. In practice, some chemicals, such as collectors and depressants, are usually

applied to change the surface properties, especially the surface free energy, of minerals, which were then made either separate from or disperse in the solutions. The obtained information of solid surface free energy can then be used to quantify the stability of colloidal suspensions in terms of the interfacial tension of solid/liquid interface.

1.2.2.1 Surface tension component or the Acid/Base theory

It is well known that surface tension arises from the unbalanced intermolecular force at the interface. Fowkes (51, 52) firstly proposed that the surface free energy (tension) is consisted of the sum of same kinds of components and intermolecular interactions across the interface. In other words, surface tension can be expressed as a sum of surface tension components, each due to a particular type of intermolecular force. Later the surface tension components concept is developed by van.Oss *et al.* (53). In general, the concept is expressed as follows,

$$\gamma_i = \sum_j \gamma_i^j = \gamma_i^{\,d} + \gamma_i^{\,p} + \gamma_i^{\,i} + \gamma_i^{\,h} + \gamma_i^{\,AB} + \ldots = \gamma_i^{LW} + \gamma_i^{AB} \qquad [6]$$

where the superscripts *d, p, i, h* and *AB* denote the dispersion (London), orientation (Keesom), induction (Debye) van der Waals components, hydrogen bond and acid-base force respectively. Furtherly, the three Lifshitz-van der Waals components namely the dispersion (London), orientation (Keesom) and induction (Debye) parts are concluded as apolar components; the acid-base parts are referred as polar components.

$$\gamma_i = \gamma_i^{LW} + \gamma_i^{AB} = \gamma_i^{a} + \gamma_i^{p} \qquad [7]$$

To calculate the interactions between two completely apolar condensed states across the interface, it was proposed that (53),

$$\gamma_{12}^{LW} = \left(\sqrt{\gamma_1^{LW}} - \sqrt{\gamma_2^{LW}}\right)^2 = \gamma_1^{LW} + \gamma_2^{LW} - 2\sqrt{\gamma_1^{LW}\gamma_2^{LW}} \qquad [8]$$

Later, van Oss *et al*. developed the ideas from Lewis acid-base theory and proposed that the polar components can be concluded as the acid-base interaction to express electron donor-acceptor interaction. It is expressed as:

$$\Delta G_{ij}^{AB} = -2\sqrt{\gamma_i^{+}\gamma_j^{-}} - 2\sqrt{\gamma_i^{-}\gamma_j^{+}} \qquad [9]$$

thus,

$$\gamma_i^{AB} = 2\sqrt{\gamma_i^{+}\gamma_i^{-}} \qquad [10]$$

so,

$$\gamma_i = \sum_j \gamma_i^j = \gamma_i^{LW} + \gamma_i^{AB} = \gamma_i^{LW} + 2\sqrt{\gamma_i^+ \gamma_i^-} \quad [11]$$

From the Dupre equation, which is applicable to any type of interactions,

$$\Delta G_{12} = \gamma_{12} - \gamma_1 - \gamma_2 \quad [12]$$

also,

$$\Delta G_{12}^{LW} = \gamma_{12}^{LW} - \gamma_1^{LW} - \gamma_2^{LW} = -2\sqrt{\gamma_1^{LW}\gamma_2^{LW}} \quad [12a]$$

$$\Delta G_{12}^{AB} = \gamma_{12}^{AB} - \gamma_1^{AB} - \gamma_2^{AB} \quad [12b]$$

thus, combining with Eq. [11], one get:

$$\gamma_{12}^{AB} = 2(\sqrt{\gamma_1^+} - \sqrt{\gamma_2^+})(\sqrt{\gamma_1^-} - \sqrt{\gamma_2^-}) \quad [13]$$

$$\gamma_{12} = \gamma_{12}^{LW} + \gamma_{12}^{AB} = \left(\sqrt{\gamma_1^{LW}} - \sqrt{\gamma_2^{LW}}\right)^2 + 2(\sqrt{\gamma_1^+} - \sqrt{\gamma_2^+})(\sqrt{\gamma_1^-} - \sqrt{\gamma_2^-}) \quad [14]$$

From the Young's equation, assuming that $\gamma_{lv} \approx \gamma_l$ and $\gamma_{sv} \approx \gamma_s$,

$$\gamma_l \cos\theta = \gamma_s - \gamma_{sl} \quad [15]$$

and Dupre equation (Eq.[12]), one gets:

$$-\Delta G_{SL} = \gamma_l(1 + \cos\theta) = -(\Delta G_{sl}^{LW} + \Delta G_{sl}^{AB}) \quad [16]$$

Finally, one obtains the OCG equation:

$$(1 + \cos\theta)\gamma_l = 2(\sqrt{\gamma_s^{LW}\gamma_l^{LW}} + 2\sqrt{\gamma_s^+\gamma_l^-} + 2\sqrt{\gamma_s^-\gamma_l^+}) \quad [17]$$

So, by using three different kinds of liquid whose γ_l^+, γ_l^-, γ_l^{LW}, γ are known and measuring contact angle of each respective liquid on the unknown solid, one can get three equations. Combining and solving the equations, we can get values of the three unknown γ_s^+, γ_s^-, γ_s^{LW} and then the γ_s. The interfacial free energy is therefore calculated using Eq. [14].

1.2.2.2 Contact angles for powder minerals

As shown by Eq. [12], in order to get the interfacial tension values, it is important to know the contact angles of liquids on the target solid surface. Water contact angle has

long been used as a measure of surface hydrophobicity, For example, a high water contact angle suggests that the solid surface is hydrophobic, and a low contact angle means high hydrophilicity.

The contact angles on a smooth and flat surface are easily obtained by means of a contact angle goniometer. It could be done either using the sessile drop technique by dipping a water drop on solid surface or using the captive bubble method by processing a gas bubble directly against the solid plate. Unfortunately, in the practice of minerals engineering, one has to deal with mineral particles rather than smooth and well defined mineral plates. Due to the difference in particle size, the surface free energy values of the particles are usually different from those of the plates. Therefore, because of the difficulties associated with the direct contact angle measurements, one has to apply the indirect methods, such as the capillary rising (54-56) and thin layer wicking (57-62) techniques, to determine the contact angles of powdered solids.

Thin layer wicking technique is specially developed to measure contact angles of the liquids on powdered materials (62) by determining the capillary rise rate of the wicking liquids in packed beds of those particulate materials. It is proposed that the wicking process follows the Washburn's equation (63):

$$\frac{2\eta h^2}{t} = R_{eff} * \gamma_L * \cos\theta \qquad [18]$$

in which η is the viscosity of the liquid, h is the height to which the wicking liquid has risen at elapsed time t, R_{eff} is the effective interstitial pore radius of packed powder bed, γ_L is the surface tension of wicking liquid and θ is the contact angle.

The parameter R_{eff} of Eq. [18] is generally determined by wicking with low-energy spreading alkanes, for which the contact angle, θ is assumed to be zero on the solid. Thus, Eq. [18] is reduced into the following equation:

$$\frac{2\eta h^2}{t} = R_{eff} * \gamma_L \qquad [19]$$

After wicking with several low energy alkanes, one can draw a plot of $2\eta h^2/t$ vs. γ_L. The slope of the straight fitting line passing through origin gives the effective interstitial pore radius R_{eff}, which is to be used for further surface free energies calculation using high energy wicking liquids.

Following the same wicking procedure described above, one can obtain the contact angle of high energy liquid, such as water, on powder surface by wicking with the liquid on thin powder layer. With the R_{eff} value obtained from wicking result with low energy alkanes, it is easy to calculate the water contact angle by solving Eq. [18], in which contact angle is the only unknown parameter.

1.2.2.3 Applications

1) Make better understanding of surface tension (surface free energy)

The Surface Tension Components theory correlates intermolecular force to surface tension components. That is surface tension can be expressed as a sum of surface tension components, each due to a particular type of intermolecular force. Also it gives practical solution by showing that surface tension can be determined from contact angle measurements through Young's equation.

2) Validity in LW (apolar) components of surface tension

From Lifshltz approach, Israelachvili (64) used the following equation to calculate γ_1

$$\gamma_1 = A_{11} /(24\pi l_0^{\,2}) \qquad [20]$$

in which A_{11} is the Hamaker constant, l_0 is the separation distance between the two infinite plate when they are in van der Waals contact. (Usually l_0=0.158±0.008nm) For example, at 25℃, for Heptane, apolar liquid:

$$\begin{aligned}\gamma_{Heptane} &= \gamma_{Heptane}^{LW} = A_{Heptane} /(24\pi l_0^{\,2}) \\ &= 4.03\times10^{-20} /(24\times\pi\times(0.158\times10^{-9})^2) \\ &= 21.4(mJ/m^2) \\ &\approx \gamma_{Heptane}^{Experiment} = 20.3(mJ/m^2)\end{aligned}$$

also, for Water:

$$\begin{aligned}\gamma_{Water}^{LW} &= A_{Water} /(24\pi l_0^{\,2}) \\ &= 4\times10^{-20} /(24\times\pi\times(0.158\times10^{-9})^2) \\ &= 21.3(mJ/m^2) \\ &\approx \gamma_{Water}^{LW_{Proposed}} = 21.8(mJ/m^2)\end{aligned}$$

These results show that the correlation of intermolecular force to surface tension components is applicable for the Lifshitz-van der Waals (apolar) component of surface tension (free energy).

3) OCG equation gives roughness information of apolar solid (low energy surface)

Under some particular situation, γ_s^+ and γ_s^- equal zero because of its apolar property. When the testing liquid is water, the OCG equation is reduced to

$$(1+\cos\theta)\times 72.8 = 2(\sqrt{\gamma_s \times 21.8}) \qquad [21]$$

Thus, by measuring contact angles of water on the unknown apolar solid, we can get the value of solid surface free energy. From Eq. [21], water contact angle can be expressed as function of solid surface tension γ_s. One can see that when γ_s is 20 mJ/m^2, the maximum water contact angle on the solid surface is 115^0. In practice, when the solid surface is methylated, the resulting low energy surface is ended with $-CH_3$ group with a

typical γ_{-CH3} of 21~23 mJ/m^2. That means the maximum water contact angle on methylate solid surface is nearly 115^0. The conclusion has been confirmed by lots of experiments results. In other words, if the water contact angle is larger than 115^0 on a solid surface, the solid surface must be rough and the roughness increases the apparent contact angle θ_a.

4) To calculate interfacial surface tension (γ_{12})

From surface tension of each condensed state, one can calculate interfacial surface tension through Eq. [14]. Further, the interaction of two condensed states across the interface can be mathematically determined from Eq. [12]. In terms of ΔG_{12} value, one can tell the relative solubility of one state in the other; also the adhesion bond strength between two surfaces. In general, a more negative ΔG_{12} value results in greater solubility of one state in the other and a greater adhesion bond strength between two surfaces (65). Further, one can also apply the calculated surface free energies results into DLVO theory and describe the stability of particles in solutions, for example, dispersion and flocculation.

1.3 Research Objectives

The overall objective of present work is to examine the existence of the long range hydrophobic forces between oxides surfaces in cationic surfactant solutions. The factors that may affect the hydrophobic force are to be carefully studied. The force measurement results will help make better understanding of the origin of the non-DLVO hydrophobic forces.

The specific goals of this research include:

1. To conduct direct force measurements between silica surfaces both in air-saturated and degassed C_{18}TACl solutions for the "degassing effect";
2. To conduct direct force measurements between silica surfaces in C_{18}TACl solutions at different salt concentration for the "salt effect";
3. To conduct direct force measurements between silica surfaces in C_nTACl (n=12,14,16,18) solutions at different surfactant concentration for the "chain length effect";
4. To conduct direct force measurements between TiO_2 surfaces in C_nTACl (n=12,14,16,18) solutions at different C_nTACl concentrations for the "substrate effect";
5. To obtain the surface free energies for talc powders of different particle size using the thin layer technique for the "particle size effect";
6. To obtain the surface free energies for talc powders before and after being treated by different reagents such as CMC, EO/PO, SOPA and simple ionic surfactants using the thin layer technique for the "chemicals coating effect";
7. To obtain the interfacial tension between silica and water from the detachment force attained using AFM force measurement and correlate the values to those obtained from thin layer wicking technique. The linkage between surface force and surface free energy is therefore the surface hydrophobicity, i.e. the contact angle.

1.4 Report Organization

The results obtained in the present work have been reported in Chapters 2 to 7. Each chapter comprises of the introduction, experimental, results and discussion, conclusion and references sections.

Chapter 2 reports the repeat of the AFM force measurements conducted by Sakamoto *el al*. (19), who claimed that long-range attractive force was not observed in carefully degassed C_{18}TACl solutions. In present work, AFM force measurements were conducted exactly following the procedures described by Sakamoto *et al.* (19) The results showed the presence of an attractive force that was much stronger than the van der Waals force both in air-saturated and degassed solutions. The force was most attractive at $5x10^{-6}$ M C_{18}TACl, where contact angle was the maximum. At this concentration, which is close to the point of charge neutralization (p.c.n.) of the glass sphere, the long-range decay lengths (*D*) were 34 and 38 nm in air-saturated and degassed solutions, respectively. At 10^{-5} M, the decay length decreased from 30 to 4 nm upon degassing and this decrease in decay length can be explained by a pH increase (from 5.7 to 6.6), which in turn causes additional surfactant molecules to adsorb on the surface with inverse orientation. The attractive force was screened by an added electrolyte (NaCl), indicating that the attractive force may be of electrostatic origin. Therefore, the very long decay lengths observed in the absence of electrolyte may be ascribed to the fact that the p.c.n. occurs at a very low surfactant concentration.

Chapter 3 reports the surface forces measurements using an AFM with silica surfaces immersed in C_nTACl (n = 12-18) solutions in the absence of added salt. The results showed long-range attractive forces that cannot be explained by the DLVO theory. The long-range attractions increased with increasing surfactant concentration, reaching a maximum at the point of charge neutralization (p.c.n.) and then decreased. The long-range forces decayed exponentially, with the decay lengths increasing from 3 to 32 nm as the chain length of the surfactants increased from C-12 to C-18. The measured forces can be fitted to the charged-patch model of Miklavic *et al.* (66) by assuming patch sizes that are much larger than the values reported in the literature.

It was found that the decay length decreases linearly with the effective concentration of the CH_2/CH_3 groups of the C_nTACl homologues raised to the power of -1/2, which is in line with the Eriksson *et al.'s* (67) hydrophobic force model derived using a mean-field approach. It appears, therefore, that the long-range attractions observed in the present work are hydrophobic forces originating from changes in water structure across the thin surfactant solution film between the silica surfaces. It is conceivable that hydrocarbon chains in solution disrupt the surface-induced water structure and cause a decrease in hydrophobic force. This observation may also provide an explanation for the very long-range forces observed with silylated, LB-deposited, and thiol-coated surfaces.

Chapter 4 reports the direct surface force measurements for TiO_2 surfaces in salt (NaCl) and C_nTACl (n = 14, 18) solutions have been carried out using an Atom Force Microscope (AFM). The Hamaker constant for the TiO_2/water/TiO_2 system is found to be of $4\pm1\times10^{-20}$ J from the force curves obtained both in water and in electrolyte solutions. The p.c.n. (point of charge neutralization) for the TiO_2/C_{14}TACl case is 3×10^{-4} M, which is larger than the value of 1×10^{-5} M in the TiO_2/C_{18}TACl system. In surfactant solution, the force curves show a repulsive/attractive/repulsive transition changing with surfactant concentration. This trend is the same as the one obtained in SiO_2/C_nTACl system (14)

and the force measurement results suggest that the cationic surfactant adsorbs at TiO_2/water interface in a similar manner as that at SiO_2/water interface. A long-range attraction beyond the realm of the DLVO theory is observed between TiO_2 surfaces in both C_{14}TACl and C_{18}TACl solutions in the vicinity of respective p.c.n.. The range of the attraction increases, while the p.c.n. decreases, with the surfactant chain length increasing.

The charged-patch model of Miklavic *et al.* (66) explains the long-range forces measured in high electrolyte concentrations. However, as to the long-range attractions measured in the absence of salt, the calculated patch sizes from the model were substantially larger than those measured experimentally and reported in the literature. The relationship between the decay lengths of the strongest attraction measured at p.c.n.'s *vs.* the concentration of salt or surfactant in solution is in support of the hydrophobic force model derived by Eriksson *et al.* (67) It suggests that the long-range attractions observed in the present work are hydrophobic forces originating from the changes of water structure near hydrophobic surfaces. It is very likely that the 'foreign' species in solution may break the structure of the water and decrease the observed long-range attraction.

In Chapter 5, thin layer wicking technique was used to determine the contact angles (θ) of different liquids on powdered talc samples. The measured contact angles were used to calculate the surface free energies (γ_S) of talc and its components such as dispersion (γ_S^d), acidic (γ_S^+), basic (γ_S^-), and acid-base (γ_S^{AB}) surface free energies, using the van Oss-Chaudhury-Good (OCG) equation. It is found that the penetration of wicking liquids follows the Washburn's equation and the effective interstitial pore radius $R_{eff,}$ which is obtained by wicking with low-energy alkenes, is linear proportional to powder size, D_{50}. The surface free energy characterization was conducted on both the basal and edge surfaces. The results showed that talc is a low surface energy solid, and that its basal surfaces are weak basic, while its edge surfaces are acidic.

In Chapter 6, thin layer wicking technique was used to determine the contact angles (θ) of several wicking liquids on powdered talc samples. The obtained contact angle values were used to calculate the surface free energy components of talc using the acid/base interaction theory developed by van Oss-Chaudhury-Good (OCG). The obtained surface free energy data of talc powders, in quantity, describe the surface properties, e.g. hydrophobicity, of talc. The thin layer wicking results of talc coated with CMC (carboxymethyl cellulose sodium salt) shows that the wetting reagents make talc surface hydrophilic by increasing solid surface free energy, especially the γ^{-lw} and γ^-. Also, increasing CMC reagent level from 0.4wt% to 1wt% doesn't change the solid surface free energy further. Adsorption of higher molecular weight CMC, FinnFix30, results in a higher γ_s^-. However the increase of γ_s^- and surface hydrophilicity are limited. Addition of EO/PO only weakly increases the zeta potential of talc sample; however, it increases γ^- and γ^{AB} greatly. Therefore, talc sample was made hydrophilic when being coated with dispersion reagents. Addition of SOPA alone has little effect on γ^- and γ^{AB}; while it changes the zeta potential of talc powder greatly. The reagent is designed to change surface charge rather than surface free energy. This information obtained in present investigation will be helpful for the application of these chemicals as a depressant/wetting reagent on talc in flotation and paper industry

In Chapter 7, finally, the adhesions between glass/silica surfaces in CnTACl solutions, obtained from AFM surface force measurement, are used to calculate the silica/water interfacial surface free energy using the JKR model. The results shows that

the interfacial surface free energy, γ_{sl} increases with surface hydrophobicity (water contact angle) and the values are compared to those obtained from the thin layer wicking technique.

1.5 References

(1) B. V, Derjaguin and L. Landau, USSR Acta Physicochim. 1941, 14**,** 633.
(2) E. J. Verwey and J. Th. G. Overbeek, Theory of the Stability of Lyophobic Colloids, Elsiever, New York, 1947.
(3) B. V. Derjaguin, S. S. Duhkin, Trans. Inst. Min. Metall. 1961, 70, 221.
(4) J. Laskowski, J.A. Kitchener, J. Colloid Interface Sci. 1969, 30, 391.
(5) T. D. Blake, J. A. Kitchener, J. Chem. Soc Faraday Trans. 1972, 68, 1435-1442.
(6) J. N. Israelachvili, R. M. Pashley, Nature, 1982, 300, 341.
(7) H.K. Christenson, P.M. Claesson, Science, 1988, 239, 390.
(8) Ya.I. Rabinovich, B.V. Derjaguin, Colloids Surf., 1988, 30, 243.
(9) Y. H. Tsao, D. F. Evans, H. Wennerström, Science 1993, 262, 547-550.
(10) J. L. Parker, P. M. Claesson, P. Attard, J. Phys. Chem. 1994,98, 8468-8480.
(11) J. Wood, R. Sharma, Langmuir 1995, 11, 4797-4802
(12) M. Hato, J. Phys. Chem. 1996, 100, 18530-18538.
(13) R.-H. Yoon, S. A. Ravishankar, J. Colloid and Interface Sci., 1996, 179, 403-411.
(14) J. Zhang, R.-H. Yoon, M. Mao, W. A. Ducker, Langmuir, 2005; 21, 5831-5841.
(15) P. Attard, Langmuir 1996, 12, 1693-1695.
(16) N. Ishida, M. Sakamoto, M. Miyahara, K. Higashitani, Langmuir, 2000, 16*,* 5681.
(17) N. Ishida, T. Inoue, M. Miyahara, K. Higashitani, Langmuir, 2000, 16, 6377-6380
(18) J. W. G. Tyrrell, P. Attard, Langmuir, 2002, 18, 160-167.
(19) M. Sakamoto, Y. Kanda, M. Miyahara, K. Higashitani, Langmuir 2002, 18, 5713-5719.
(20) H. K. Christenson, P. M. Claesson, Adv. Colloid Interface Sci., 2001, 91, 391- 436.
(21) N. Ishida, M. Sakamoto, M. Miyahara and K. Higashitani, J. Colloid Interface Sci. 2002, 253, 112–116.
(22) T. Ederth, J. Phys. Chem. B 2000, 104, 9704-9712.
(23) T. Ederth and B. Liedberg, Langmuir 2000, 16, 2177-2184.
(24) T. Ederth, K. Tamada, P. M. Claesson, R. Valiokas, R. Colorado, Jr. M. Graupe, O. E. Shmakova, and T. R. Lee, J. Colloid and Interface Sci., 2001, 235, 391–397.
(25) J. Yang, J. Duan, D. Fornasiero, and J. Ralston, J. Phys. Chem. B 2003, 107, 6139-6147.
(26) J. W. G. Tyrrell and P. Attard, Physical Review Letters, 2001, 87, 1761.
(27) R. Steitz, T. Gutberlet, T. Hauss, B. Klosgen, R. Krastev, S. Schemmel, A. C. Simonsen, and G. H. Findenegg, Langmuir 2003, 19, 2409-2418.
(28) M. Holmberg, Anders Kuhle, J. Garnæs, K. A. Mørch, and A. Boisen, Langmuir, 2003, 19, 10510-10513.
(29) A. V. Nguyen, J. Nalaskowski, J. D. Miller, H.-J. Butt, Int. J. Miner. Process. 72 (2003) 215– 225.
(30) X. Zhang, X. Zhang,, S. Lou, Z. Zhang, J. Sun, and J. Hu, Langmuir 2004, 20, 3813-3815.
(31) M. Mao, J. Zhang, R.-H. Yoon, W. A. Ducker, Langmuir. 2004, 1843-1849.

(32) D. R. Evans, V. S. J. Craig, T. J. Senden, Physica A, 339 (2004), 101-105.
(33) H. Stevens, R. F. Considine, C. J. Drummond, R. A. Hayes,. and P. Attard, Langmuir 2005, 21, 6399-6405.
(34) E. E. Meyer, Q. Lin, J. N. Israelachvili, Langmuir, 2005, 21, 256-259.
(35) Q. Lin, E. E. Meyer, M. Tadmor, J. N. Israelachvili and T. L. Kuhl, Langmuir 2005, 21, 251-255.
(36) P.C. Herder, J. Colloid Interface Sci. 1990, 134, 346.
(37) J. L. Parker, V.V.Yaminsky, P.M. Claesson, J. Phys. Chem. 1993, 97, 7706.
(38) M.W. Rutland, J.L. Parker, Langmuir 1994, 10, 1110.
(39) R.-H. Yoon, S. A. Ravishankar, J. Colloid and Interface Sci. 1994, 166, 215.
(40) R.-H. Yoon, S. A. Ravishankar, J. Colloid and Interface Sci. 1996, 179, 391.
(41) O. Teschke and E. F. de Souza, Langmuir 2003, 19, 5357-5365.
(42) L. Meagher, V.S.J. Craig, Langmuir 1994, 10, 2736.
(43) R. F. Considine, R. A.Hayes, R. G. Horn, Langmuir 1999, 15, 1657-1659.
(44) J. Mahnke, J. Stearnes, R. A. Hayes, D. Fornasiero,; J. Ralston, Phys. Chem. Chem. Phys., 1999, 1, 2793-2798.
(45) J. C. Eriksson, S. Ljunggren, Langmuir 1996,11, 2325-2328.
(46) V. S. Yushchenko, V. V. Yaminsky, E. D. Shchukin, J. Colloid and Interface Sci., Vol. 96(2), 307-314.
(47) R. M. Pashley, P. M. McGuiggan, B. W. Ninham, D. F. Evans, Science 1985,229, 1088.
(48) H. K. Christenson, P. Claesson, Science 1988, 239, 390.
(49) J. Israelachvili, R. M. Pashley, J. Colloid and Interface Sci. 1984, 98, 500-514.
(50) P. Kekicheff, O. Spalla, Phys. Rev. Lett. 1995, 75, 1851.
(51) F. M. Fowkes, J.Phys. Chem., 1963, 67, 2538.
(52) F. M. Fowkes, J.Adhension, 1972, 4, 155.
(53) C. J. van.Oss, Chaudhury and R. J. Good, Chem,Rev. 1988,88.927-941.
(54) H. G. Bruil, and J. J. van Aartsen, Colloid & Polymer Sci., 1974, 252, pp. 32-38.
(55) D. T. Hansford, D. J. W.Grant, and J. M. Newton, J. C. S. Faraday I, 1980, 76, 2417-2431.
(56) R. Crawford, L. K.Koopal, and J. Ralston, Colloids and Surfaces, 1987, 27, 57-64.
(57) C. J. van Oss, W. Wu and R. F. Giese, Jr. Particulate Science and Technology, 1993, 11, 193-198.
(58) W. Wu, R. F. Giese, Jr, C. J. van. Oss, Colloids and surface A 89(1994) 241-252.
(59) W. Wu, R. F. Giese, Jr, C. J. van. Oss, Colloids and surface A 89(1994) 253-262.
(60) W. Wu, R. F. Giese, Jr, C. J. van. Oss, Colloids and surface B 14(1999) 47-55.
(61) E. Chibowski, L. Holysz. Langmuir, 1992.8; 710-716.
(62) I. Yildirim, Ph.D. Thesis, Virginia Tech, April 2001.
(63) E. W. Washburn, Physical Review, 1921, 1, 273.
(64) J. Israelachvili, "Intermolecular and surface force", 2nd edition, 1992.
(65) I. Yildirim, J. Zhang, and R.-H. Yoon, "Effect of Surface Treatment on the Acid/base Properties of Fillers and Pigments", SME 2002.
(66) S. J. Miklavic, D. Y. C. Chan, L. R.White, T. W. Healy, J. Phys. Chem. 1994, 98, 9022-9032.
(67) J. C. Eriksson, S. Ljunggren, P. M. Claesson, J. Chem. Soc., Faraday Trans. 2, 1989, 85, 163-176.

CHAPTER 2

Effects of Degassing and Ionic Strength on AFM Force Measurements in Octadecyltrimetylammonium Chloride Solution

Abstract

Sakamoto *et al*. (*Langmuir* 2002, 18, 5713) conducted AFM force measurements between silica sphere and fused-silica plate in aqueous octadecyltrimethylammonium chloride (C_{18}TACl) solutions, and concluded that long-range attractive force is not observed in carefully degassed solutions. In the present work, AFM force measurements were conducted by following the procedures described by Sakamoto *et al.* The results showed the presence of an attractive force that was much stronger than the van der Waals force both in air-saturated and degassed solutions. The force was most attractive at $5x10^{-6}$ M C_{18}TACl, where contact angle was the maximum. At this concentration, which is close to the charge compensation point (ccp) of the glass sphere, the long-range decay lengths (*D*) were 34 and 38 nm in air-saturated and degassed solutions, respectively. At 10^{-5} M, the decay length decreased from 30 to 4 nm upon degassing. This decrease in decay length can be explained by a pH increase (from 5.7 to 6.6), which in turn causes additional surfactant molecules to adsorb on the surface with inverse orientation. The attractive force was screened by an added electrolyte (NaCl), indicating that the attractive force may be of electrostatic origin. Therefore, the very long decay lengths observed in the absence of electrolyte may be ascribed to the fact that the ccp occurs at a very low surfactant concentration.

Published on Web 05/21/2005

2.1 Introduction

Pioneering work by Blake and Kitchener (1) on the thickness of wetting films on methylated silica and by Isrealachvili and Pashley (2) on the forces between surfactant-coated mica sheets in aqueous solutions led to the concept that there is an attractive force between hydrophobic surfaces that is longer ranged than the few layers of water molecules that are usually considered in a solvation shell. The long-range attractive forces are observed with solids that have high water contact angles and, therefore, with solids that have high interfacial tensions in water, so the force is commonly known as the hydrophobic force. The term 'hydrophobic force' was first used by Blake and Kitchener (1) to explain the catastrophic failure of the wetting film on a methylated surface occurring at a separation distance (64 nm) that was much larger than predicted by the DLVO theory. In fact, an earlier work of Laskowski and Kitchener (3) speculated the presence of a 'third force', without calling it a hydrophobic force, to explain the observation that both clean and methylated silica exhibited essentially the same ζ-potentials and yet only the latter was floatable, i.e., wetting films rupture catastrophically. The air-water interface also has a high interfacial energy, so the possibility of long-range attraction existing between air bubbles has also been discussed (4-6).

Isrelachivili and Pashley (2) explained the long-range attraction using the concept of 'hydrophobic effect', which is widely used to explain mutual attraction between hydrophobic solutes (e.g., hydrocarbons) in water. Eriksson *et al.* (7) related the forces measured in the range (~10 nm) of the force in the original work of Israelachvili and Pashley to surface-induced perturbation of water structure using a mean-field theory with a square-gradient assumption. However, follow-up experiments only made the 'range problem' worse. Numerous workers measured forces out to about 80 nm (e.g. (8)); whereas some workers measured forces with a very small range (9). These discrepancies suggest that there may not be a single explanation for all the measurements.

Alternate explanations for the long-range attractive force have focused on two concepts: 1) the idea that it is due to the presence of small bubbles that are attached to the solid surface (10), and 2) an attractive force caused by correlations between surface dipoles (11,12). The existence of the bubbles solves the range problem because the distance between the air-water interfaces of the adsorbed bubbles is much less than the distance between the solid-liquid interfaces, and the apparent range of the force depends on the height of the bubble. Support for the idea that the force is due to adsorbed gas bubbles comes from an observed decrease in the attractive force when the solutions are degassed, and AFM images of the adsorbed gas bubbles (13-15). Recently, we used ellipsometry to show that gas bubbles are very rare on isolated (single) hydrophobic solids (16). We suggested that gas bubbles could be formed during atomic force microscope (AFM) force measurements when a second solid (colloid probe) approaches or separates from a substrate rather than bubbles preexisting at the isolated interface.

Attard (12) suggested that the hydrophobic patches formed as a result of surfactant adsorption can create anomalous electrostatic response to the adjacent aqueous fluid and give rise to long-range attraction. He suggested that hydrophobic patches are formed when a mica surface, coated with a Langmuir-Blodgett-deposited surfactant film, is plunged in water, due to changes in interfacial tensions. According to his theoretical model, the long-range attraction should decay as one-half of Debye length. Comparison of his model and the experimental data reported in the literature suggested that the

hydrophobic patches should have a length scale of approximately 100 nm. Tsao and Evans (11) observed long-range attractive forces with mica surfaces coated with double-chain cationic surfactants. They found that the forces were screened by electrolyte and, therefore, concluded that they are electrostatic in origin. Further, long-chain surfactants self-assembled at solid-water interfaces form domains and the hydrocarbon chains are tilted relative to the interface. The tilted structure generates in-plane dipole moment, which creates electric fields extending large distances. More recently, one of us developed a mathematical model relating attractive forces to the dipole moments of the domains (or patches) that are formed during self-assembly processes (17). Miklavic et al. (18) also suggested that net-neutral surfaces consisting of charged patches can create attractive double-layer forces, provided that the charged species are free to migrate.

Recent work from the group of Higashitani (13, 19-22) offered support for the preexisting adsorbed bubble hypothesis, which may be acceptable for the surfaces whose water angles (θ) were greater than 90^o due to hydrophobization with silanes Thermodynamically, cavitation should occur at $\theta>90^o$. However, Sakamoto, *et al*. (22) reported that air bubbles are also the cause for the hydrophobic forces observed with surfaces coated with a water-soluble surfactant (octadecyltrimethylammonium chloride, $C_{18}TACl$). They observed long-range (60-250 nm) attractive forces between silica surfaces in $1\text{-}3\times10^{-5}$ M $C_{18}TACl$ when the solution was equilibrated with air. The force *vs*. distance curves exhibited discontinuities (or steps), as were also reported by other investigators (23-24). When the measurement was conducted in a degassed solution, both the steps and the long-range attraction disappeared, which lead to the conclusion that the long-range attraction is caused by the gas bridges formed between two hydrophobic surfaces interacting with each other. They stated further that long-range attraction never appears in completely air-free $C_{18}TACl$ solutions.

The aim of this communication is to repeat the AFM force measurements conducted by Sakamoto *el al*. (22) in $C_{18}TACl$ solutions. In contrast to their conclusions, we have observed long-range attractive forces (i.e. forces greater than van der Waals forces) in solutions degassed in the manner described by these authors. In view of the results obtained in the present work, possible origins of the long-range attractive forces are discussed.

2.2 Experimental

Materials

Nanopure water was obtained by Nanopure III (Barnstead, IA) water system. The conductivity of the water was 18.3 MΩ/cm at 25°C and the surface tension was 72.5mN/m at 22°C. Unless otherwise noted, the water and surfactant solutions in the present work were equilibrated with air before use. These air-equilibrated solutions had a pH of 5.6-5.8. The surfactant ($C_{18}TACl$, 97% purity, TCI) was purified by recrystallization in acetone twice. The surface tensions of the aqueous solutions measured as a function of concentration showed no minimum near the cmc, indicating that there are few impurities that are more surface active at the air-water interface than $C_{18}TACl$. Solutions were prepared in containers with a volume of at least 100 mL to prevent significant depletion of surfactant *via* adsorption to the glass walls. NaOH (99%, Mallinckrodt Baker) was used without further purification. NaCl (99%, Sigma) was

roasted in air at 560°C to decompose organic impurities. Liquid reagent, such as Chloroform (99.9%, Burdick & Jackson), H_2SO_4 (98%, VMR International) and H_2O_2 (30%, VMR International) were used as received without further treatment.

Quartz plates (Hareaus Amersil Inc.) were boiled in a H_2SO_4/H_2O_2 solution (7:3 by volume) for 30 minutes. The plates were rinsed thoroughly with nanopure water, equilibrated with the nanopure water in a sealed vial for at least 20 minutes, and then used for experiments.

Degassing Procedure

To conduct AFM force measurements under air-free conditions, surfactant solutions were degassed by following the procedure described by Sakamoto *et al.* (22) Nanopure water was boiled for one hour, frozen in a vessel with liquid nitrogen, evacuated for two hours with a final air pressure at 20mbar, and then melted under reduced pressure. This procedure was repeated three times. During the third degassing step, a known amount of surfactant was placed on the ice and evacuated for two hours. The vessel containing the ice and surfactant powder was then allowed to reach thermal equilibrium with ambient temperature before use. According to Sakamoto *et al.* (22), this procedure "guarantees that the solution is completely free from dissolved gas".

When the target surfactant concentration was very low, i.e., 10^{-6} M, it was difficult to add accurately a desired amount of dry surfactant to frozen water unless a very large amount solution was boiled, frozen, and degassed. Therefore, we prepared a 1 mL of 10^{-4} M C_{18}TACl solution and 125 mL of water, degassed them in the manner described above, mixed the two, and boiled the mixture for 1 hour. During the boiling, only about 25 mg of water evaporated so that the surfactant concentration remained close to 10^{-6} M. The boiled solution was frozen by liquid nitrogen, degassed, melted under vacuum, and allowed to reach a thermal equilibrium with the ambient before use. For comparison purpose, we prepared higher concentrations of C_{18}TACl solutions using this modified procedure and Sakamoto *el al*.'s, and conducted AFM force measurements. We found no significant differences between the two methods of obtaining air-free solutions.

Air-equilibrated solutions

Air-equilibrated C_{18}TACl solutions were prepared in a vessel such that the amount of air above the liquid was greater than the amount of air in the equilibrated solution. This was easily accomplished because the concentration of gas molecules in air (~40 mM) at STP is about 40 times that in water. In each experiment, a solution vessel was thoroughly shaken to speed equilibration, and then was left sealed for 30 minutes. At the end of this period, the seal was broken to allow mixing with ambient air for a few minutes. This procedure was repeated 4 times.

Surface Force Measurement

Surface forces were measured using a Digital Instrument Nanoscope IIIa AFM at room temperature (~22°C) using the colloidal probe technique (25, 26). The separation distance (H) between the probe (glass sphere) and the substrate (silica plate) was measured by monitoring the deflection of the cantilever on which the sphere was attached. Silicon-

nitride NP-20 cantilevers were obtained from Veeco, CA. Triangular cantilevers with nominal spring constant of 0.58 N/m were used. The springs were calibrated in the present work using the resonant frequency technique (27). The calibrated spring constants were in the range of 0.3 to 0.6 N/m, which were approximately a hundred-times smaller than those (~50 N/m) used by Sakamoto *et al*.[22] The error associated with the calibration technique employed in the present work was ±7%. The glass spheres (12-20μm in diameter) were obtained from Polysciences Inc. Warrington, PA. They were soaked in chloroform for 30 minutes and UV-irradiated for 30 minutes to remove possible organic contaminants. In each experiment, a glass sphere was glued onto a cantilever with EPON 1004 resin (Shell Chemical Co.). The diameter of the glass sphere was measured using an Olympus BH-2 light microscope with a video caliper with an error of ±0.5 μm. The combined error between the measurements of the spring constants and the sphere diameters was about ±12% in force/diameter (F/R) calculations.

Surface forces were measured for a series of surfactant concentrations. For a given series of measurements, the surfactant solutions were injected into an AFM liquid cell starting from the lowest concentration and continuing to the highest. For each new concentration, the glass sphere and silica plate were exposed to the surfactant solution for a period of 20 minutes before force measurements were commenced. Forces reported in this paper were recorded about 1 hour after exposure of the solids to a new solution. Although the forces measured during the periods of 20 minutes to 1 hour were reproducible, we found that the forces varied slowly with time after 1 hour, presumably because of slow adsorption kinetics and possible rearrangement of the surfactant molecules on the surface. Thus, we have no evidence that the forces reported here were at adsorption equilibrium.

All reported forces, F, are normalized by the particle radius, R. For measurements at equilibrium, when R is much greater than the range of the force, $F/2\pi R$ is equal to the energy of interaction per unit area for an infinite flat plate interacting with another infinite flat plate of the same material (28).

AFM Imaging

All AFM images reported in this communication are height (constant force) images captured at 22±1°C with integral and proportional gains of about 2. Silicon nitride cantilevers with nominal k=0.12 Nm^{-1} were used. The images are of the same type of silica plate as used in the force measurements.

ζ-Potential Measurement

The silica plates and glass spheres that were used for the AFM force measurements were subjected to ζ-potential measurements. The glass spheres were suspended in water, and the coarser spheres were allowed to settle. The finer spheres (<3 μm) left in suspension were used for the ζ-potential measurements. For silica plates, the measurements were conducted after pulverizing the plates by means of an agate mortar and pestle and isolating the finer particles by sedimentation. The ζ-potential measurements were conducted in both air-equilibrated and degassed $C_{18}TACl$ solutions using a Lazer Zee meter, Model 501 (Pen Kem, Inc, NY). The ζ-potentials were calculated from the

mobilities using the Smoluchowski equation. Reported results represent arithmetic averages of six measurements.

Ellipsometry

The adsorption of C_{18}TACl on the silica surface from solution was determined using a phase-modulationed ellipsometer (Beaglehole Instruments, Wellington, New Zealand) at λ=632.8 nm (HeNe laser) and 23±1°C. The cross section of the laser beam was about 1 mm^2. Ellipsometry was facilitated by the use of a reflective solid, so the measurements were performed with silicon wafers (100 oriented, MOD 2 Polished Wafer, 0.5-35 Ω cm, Sumco, Oregon) which were cut into ~15×15 mm^2 pieces. To calculate the surface excess from the ellipticity, we assumed that the refractive index increment (dn/dc) of C_{18}TACl was 0.15 mL^{-1}. This approximate value was based on the measured values for $C_{12\text{-}16}$TABr surfactants (29).

Contact Angle Measurement

A silica plate was immersed in a surfactant solution for a desired period of time, removed from the solution, and dried by blowing nitrogen gas over the surface. A drop of the surfactant solution was then placed on the surface and the contact angles were measured by means of a contact angle goniometer. The contact angles were also measured using the captive bubble technique, in which silica plates were kept in solution while air bubbles were brought to contact. A total of six contact angles were measured at a given experimental condition and averaged.

2.3 Results and Discussions

2.3.1 Solubility and Purity

We find that C_{18}TACl was water soluble to at least 1 mM at 22°C. Figure 2.1 shows the measured vapor–solution interfacial tension as a function of the surfactant concentration for the aqueous solutions prepared from the purified C_{18}TACl. The absence of a minimum in the surface tension demonstrates the absence of contaminants that are more surface active than C_{18}TACl at the vapor–solution interface. It is possible, however, that there are contaminants that are more surface active at the silica–solution interface. All further experiments utilized the purified surfactant.

From our surface tension measurements, we found that the cmc was approximately 4×10^{-4} M, which is close to $3.4\text{x}10^{-4}$ M reported by Sakamoto *et al*. (22). Solutions prepared at concentrations above the cmc were still clear at 15°C; therefore, all our experiments were well above the Krafft point. Our experiments focused on the concentration range of $0.5\text{–}5.0\times10^{-5}$ M C_{18}TACl because this was where Sakamoto *et al*. conducted their force measurements.

2.3.2 Kinetics of Adsorption

It is important to note that the adsorption from 10^{-5} M solutions of C_{18}TACl is quite slow, which is consistent with earlier work on C_{18}TABr (30). Figure 2.2 shows the surfactant adsorption on the native oxide layer on a silicon wafer as a function of time. The

measurements were conducted at the natural pH. This surface was similar but not identical to the glass and silica surfaces that were used in the force measurements. The adsorption was measured in two different ways: (1) by first exposing the silicon wafer to pure water and then to the C_{18}TACl solution, and (2) by direct exposure to the solution. Both methods gave similar results, suggesting that mixing in the ellipsometry cell is not the limiting step in adsorption. The adsorption process continues up to about 40 h after the silica was exposed to the solution. Most of our AFM force measurements were performed about 1 h after injection of surfactant. Therefore, the forces were measured before the adsorption reached equilibrium.

Ellipsometry measures the surfactant adsorption through detection of the changes in refractive index at the interface. We observed an increase in ellipticity that we can attribute to the adsorption of a substance with a positive refractive index increment (surfactant). If a substance with a negative refractive index increment, for example, air bubbles, were to adsorb, then the ellipticity would decrease. We never observed a decrease in ellipticity, so we have no optical evidence for the adsorption of air-bubbles.

Figure 2.3 shows the images of the fused silica plate immersed in 10^{-5} M C_{18}TACl solution as a function of time. After 30 minutes, patches with high perimeter-to-area ratios were sprinkled across the surface. A typical patch was about 20 nm across. At 60 minutes, these patches cover a larger area of the surface, and by 4 hours, even larger area was covered by the patches. Ellipsometry measurements suggested that these patches were not dense because the coverage was only about 0.9 molecules/nm^2 after 4 hours. After 21 hours, the surface was difficult to image because there was an over-layer of very weakly held objects that changed upon imaging.

An important conclusion to reach from the imaging data was that the surface was inhomogeneous. Inhomogeneity was observed on the original silica surface and also, patches formed on the surface after the C_{18}TACl was introduced. In contrast, both C_{12}TABr and C_{14}TABr produced homogeneous surface coatings of micelles within minutes (31-33). Note that there are lines on the surface that do not show surfactant coatings. The same lines existed on the surface before addition of surfactant, and may be the grain boundaries or scratch marks on the fused silica. Apparently, they have different surface properties from the surrounding areas. There are also circular regions where no patches were observed even after 21 h of exposure to the surfactant solution.

Particularly in the early stages, the patches were very easily disturbed by imaging. Therefore, we had to image at the smallest possible force to avoid disrupting them. Comparing figures B and C, which were consecutive images captured one minute apart, we see that some patches are different. It appears that the adsorbed patches have a degree of mobility in the presence of the AFM tip.

Figure 2.4 shows the equilibrium contact angles of the fused silica plates immersed in 10^{-5} M C_{18}TACl solutions. The contact angles measured with the captive bubble technique reached a maximum after approximately 2 hours, which was shorter than suggested by ellipsometry. The maximum contact angles were less than 60^o despite the long chain length of the surfactant, which may be attributed to the possibility that some of the surfactant molecules adsorb with the head group facing toward the solution. We will describe this as inverse (or flip-flop) orientation.

Figure 2.5 shows the forces measured as a function of immersion time between a flat silica plate and a glass sphere of 12 μm radius in a 10^{-5} M C_{18}TACl solution. The

measured forces were normalized by the radius of the sphere. The solution was prepared several days in advance of the force measurement by the "air-equilibrated" method. As shown, the measured forces changed significantly with time. After the silica plate and glass sphere were in contact with the surfactant solution for 5 minutes, a strong attractive force was observed. The attractive forces decreased with increasing time, which indicated that the adsorption is a slow process and that additional surfactant molecules may adsorb with inverse orientation forming a 'flip-flop' or bilayer, as will be discussed further later in this communication. The attractive force was much stronger than the van der Waals force, which is represented by the solid line. The non-retarded van der Waals forces were calculated from the following approximate relation:

$$\frac{F}{R} = -\frac{A}{6H^2} \qquad [1]$$

where A is the Hamaker constant, which is 8×10^{-21} J for silica (34).

The two surfaces jumped into contact from a separation distance of 34 nm, as indicated by an arrow. Jumps occur when the gradient of the surface force exceeds the spring constant and can be identified from the rapid acceleration of the tip. As the immersion time was increased, the measured forces became less attractive; however, the jump distances were still large, indicating the presence of a strong attractive force not considered in the DLVO theory.

2.3.3 Forces in Air-Equilibrated Solution

Figure 2.6 shows the results of the AFM force measurements conducted as a function of the C_{18}TACl concentration in air-equilibrated solutions. It shows the same general trend as the forces measured previously in cationic surfactant solutions (35-37). Addition of a small amount of the cationic surfactant reduces the repulsive force between the negatively charged surfaces, and a further increase in concentration lead to a repulsive force. In the present work, however, the changes in force were observed at lower concentrations of C_{18}TACl than of C_{12}TABr or C_{16}TABr, as expected of a longer chain surfactant. Also, the range of the forces was much greater. This can be attributed to the fact that the changes in forces was brought about at substantially lower surfactant concentrations than with C_{12}TABr, as will be discussed further later. It is important to note here that a) the most attractive force is much greater than the van der Waals force between either silica solids or hydrocarbon solids, and that b) there is a very large gradient in the force as a function of concentration near the minimum (most attractive) force. The measured force was most attractive at 5×10^{-6} M and became progressively weaker at higher concentrations. The force became net repulsive above 3×10^{-5} M. The concentration at which the measured force became most attractive was close to the charge compensation points (ccp) of the glass sphere and silica plate, as will be shown later. Other investigators also showed that long-range force is most attractive near ccp (38, 39).

One important contributing factor to the decrease in the magnitude of the net attractive force and eventual occurance of repulsive force above the ccp (5×10^{-6} M) is due to the adsorption of the cationic surfactant in excess of the negative charge sites available on silica. The ability of the cationic surfactant to adsorb above ccp is due to the net attraction between hydrocarbon chains, which is known as "hydrophobic effect".

According to Fuerstenau and Somasundaran (40), the standard free energy change (ΔG^o) associated with this process is given by $\Delta G^o = -0.85n$ kcal/mole, where n is the number of CH_2 groups of a hydrocarbon chain that are in contact with the CH_2 groups of the neighboring hydrocarbon chains. This value is comparable to the free energy of transferring hydrocarbon chain to water, 0.88 kcal (1.48 kT) per mole of CH_2 group (41).

The adsorption of surfactant above the ccp will lead to charging of the surfaces and eventually to a repulsive double-layer force. It is possible that the $C_{18}TA^+$ ions adsorbing above ccp may do so with inverse (or flip-flop) orientation, i.e., with the head groups pointing toward the solution. The inverse orientation may occur after the surface has become hydrophobic by virtue of the normal mode of orientation, i.e., the head group in touch of the surface and the tails pointing to the solution. The possible inverse orientation may provide an explanation for the relatively low contact angles observed in C_{18}TACl solutions (Figure 2.4).

The forces measured by Sakamoto *et al*. (22) in air-equilibrated C_{18}TACl solutions are about 30-100 times larger than shown in Figure 2.6. Furthermore, we did not observe the steps that were observed by these investigators and attributed to bridging air bubbles. Other investigators also observed the steps and attributed them to bridging bubbles (23, 24).

2.3.4 Effect of Degassing on AFM Force Measurement

Figure 2.7 shows the forces between glass sphere and fused silica plate in solutions that were degassed. Overall, the forces in degassed and air-equilibrated solutions show the same trends. The measured forces in degassed solutions were attractive at a concentration as low as 10^{-6} M. The strongest attractive force was observed at $5x10^{-6}$ M, as was the case with the measurements conducted in air-equilibrated solutions (Figure 2.6). In fact, the force measured in degassed solution was slightly more attractive than in the air-saturated solution (Figure 2.8a). The reason that Sakamoto *et al.* (22) did not clearly resolve attractive forces in degassed C_{18}TAC solutions was most probably due to the fact that they used approximately one hundred-times stiffer cantilevers than those used in the present work. Furthermore, their results were plotted in a scale that was ten-times larger than used in the present work (compare Figure 2.10 of Ref. 19 with Figure 2.7). Close inspection of their published results reveals an attractive force that is similar in magnitude to the force measured in Figure 2.7. As the concentration was increased to 10^{-5} M, the measured force in degassed solution became repulsive while the force measured in air-saturated solution remained attractive (Figure 2.8b). Below we explain these differences without using the theory of bridging air bubbles.

Note here that the glass sphere and the fused silica plate jumped into contact in the degassed 10^{-5} M C_{18}TACl solution at a separation distance of 12 nm, suggesting the presence of an attractive force not considered in the DLVO theory. The solid line of Figure 2.7 represents the DLVO fit of the data obtained in 10^{-5} M degassed solution. The dashed lines represent an extended DLVO theory, which considers contributions from an additional force term without regard to its origin. Details of the fitting procedures will be discussed later.

The results given in Figures 2.6 and 2.7 show that, although the effect of degassing was quite dramatic at some individual concentrations of surfactant, degassing the solution did not change the overall trends, and caused only a small change in magnitude

particularly at the concentration of maximum attractive force. In the remainder of this communication, we will discuss 1) our hypothesis for the mechanism of the changes in force upon degassing surfactant solutions, and 2) further experiments to reveal the nature of the attractive force.

2.3.5 Mechanism of Force Changes upon Degassing

Our hypothesis is that the primary effect of degassing the solution in our experiments was to raise the pH. As the pH increases, the surface charge becomes more negative, which in turn causes an increase in the adsorption of the $C_{18}TA^+$ ions and, hence, a change in surface force. We found that the pH of the air-equilibrated solutions was 5.7, which increased to 6.6 when the solution was degassed. Degassing removes CO_2 from the solution, causing shift in the following set of equilibria to the left (42):

$$H_2O + CO_2(aq) \rightleftharpoons H_2CO_3(aq) \rightleftharpoons H^+(aq) + HCO_3^-(aq) \qquad [2]$$

The fact that the solution remained at pH 6.6 rather than 7.0 suggests that we had not completely degassed the solution, or that some CO_2 had returned on the timescale of our pH measurement. Using the known equilibrium constant for the composite reaction above ($K = 4.47\times10^{-7}$) (42), we can calculate that our degassing procedure decreased the concentration of dissolved carbon dioxide from 8.9×10^{-6} to 1.2×10^{-7} M, i.e. we removed about 99% of the CO_2.

Figure 2.9 shows the forces measured in 10^{-5} M $C_{18}TACl$ solutions that were equilibrated in air and then the pH was changed by addition of either NaOH or HCl. The effect of increasing the pH was very similar to the effect of degassing (compare Figure 2.9 with Figure 2.8). As the pH increases, the surface becomes more negative, which should cause an increase in the adsorption of the $C_{18}TA^+$ ions and render the surface more hydrophobic. As the surface becomes more hydrophobic, additional $C_{18}TA^+$ ions adsorb on the surface, the adsorption mechanism being hydrophobic effect between the hydrocarbon chains. The additional adsorption of the cationic surfactant should lead to an increased surface charge and, hence, an increased repulsive surface force, as shown in Figures 2.8 and 2.9.

To examine the above mechanism, we have measured the ζ-potentials of the glass particles and the pulverized plate. Figure 2.10 shows the ζ-potentials as a function of the $C_{18}TACl$ concentration. The measurements were conducted both in degassed and air-equilibrated solutions. The pH of the degassed solutions was 6.6, and the pH of the air-equilibrated solutions was adjusted to 6.6 with NaOH. Clearly, the effect of degassing on the ζ-potential was reproduced by increasing the pH of the air-saturated solution.

Figure 2.11 compares the ζ-potentials of the silica plate and glass sphere measured at pH 5.7 and pH 6.6. As the pH was increased from 5.7 to that of the degassed solution, i.e., pH 6.6, the ζ-potentials became considerably more positive, indicating that $C_{18}TA^+$ ions adsorb more readily at the higher pH. The increased adsorption of the cationic surfactant at the higher pH (and hence the higher surface potential) may be responsible for the transition of the measured forces from the long-range attraction to long-range repulsion when a 10^{-5} M $C_{18}TACl$ solution was degassed (see Figure 2.8b). That the measured force became net repulsive does not mean that the surface became hydrophilic. It simply indicates that the repulsive force was greater than the attractive force. In the

degassed solution, the two surfaces jumped into contact at 12 nm, which was much larger than predicted by the DLVO theory. It can be stated, therefore, that the long-range attractive force still existed in the degassed 10^{-5} M C_{18}TACl solution.

The ζ-potential measurements also show that the potentials of the glass sphere were different from those of the ground silica plate. This finding suggests that we should consider the possibility that the long-range attractive forces measured in the present work could be attributed to attractive double-layer interactions.

2.3.6 Effect of Salt Concentration on the Forces in C_{18}TACl Solutions

One possible explanation for the attractive forces measured in air-equilibrated and degassed C_{18}TACl solutions and given in Figures 2.6 and 2.7, respectively, is that the force is of electrical origin. In this case, the magnitude of the force should decrease with an increase in salt concentration. Figure 2.12 shows the effect of added salt (NaCl) on the forces measured in 5×10^{-6} and 8×10^{-6} M C_{18}TACl solutions. Attractive forces decreased with increasing NaCl concentration. In all cases, the forces were approximately exponential. It is not likely that the decrease in force was caused by desorption of surfactant because Goloub*, et al.* (43) showed that the addition of salt at the ccp does not change the amount of adsorbed surfactant.

The measured forces were fitted to an exponential function,

$$\frac{F}{R} = C\exp\left(-\frac{H}{D}\right) \qquad [3]$$

where F is the surface force, R the radius of the glass sphere used for the force measurements, H the closest separation distance between the sphere and plate, and C, and D are fitting parameters. It was assumed that the electrical potentials of the silica plates and glass spheres were zero and that C=-1.4 mN/m. Also, the fitting was carried out after subtracting the forces due to van der Waals interaction from the measured forces.

The decay lengths (D) obtained from the fitting procedure described above are given in Table 2.1. Also shown in the table are the Debye lengths (κ^{-1}) calculated from the NaCl concentrations used. The values of D obtained from the force curves obtained in 5×10^{-6} and 8×10^{-6} M C_{18}TACl solutions show the same trends although the values are not identical. Unfortunately, the slow equilibration of the solution complicated the analysis of these results. Nevertheless, the decrease in the attractive force with NaCl suggests that the long-range attractive force may be of electrical origin and, therefore, is screened by the salt.

2.3.7 Origin of the Long-range Attractive Force

We see little merit in attributing the long-range attractive forces observed in this paper to the effects of adsorbed bubbles because: 1) the effects of degassing are minor, and can be explained by the effect of a small pH change, 2) the observed changes in AFM images on addition of surfactant could be explained simply by the adsorption of surfactant, rather than by the adsorption of bubbles, and 3) we did not observe steps (small discontinuities) in force curves that could be attributed to bridging bubbles. Therefore, for the remainder

of this paper, we will consider three alternate hypotheses for the long-range attractive forces: a) attractive double-layer forces; b) a long-range hydrophobic force of electrostatic origin, and c) attractive forces due to correlations between charged patches.

1) Attractive Double-layer Forces?

The possibility of explaining the long-range attractive forces observed in the present work as due to double-layer interaction was considered in an earlier publication of one of us (35). An appeal for this approach was that it is a known interaction, and the measured forces have the appropriate functional form (exponential). In the present work, however, we are immediately in trouble with the assumptions of DLVO theory. Not only do we have the usual problems with additivity of the double-layer and van der Waals forces, but also the fact that C_{18}TACl ions are not point-sized, that there are significant interactions between them, and that the charge regulation is unknown. Furthermore, we have good evidence that the surfaces were inhomogeneous on the length scale of the forces, and the adsorption was not at equilibrium. Nevertheless, we went ahead and estimated the values of the surface potentials (ψ_0) that are required to fit the measured forces assuming that that Poisson-Boltzmann theory applies. We used the constant potential boundary condition.

Figure 2.13 shows the force curve obtained in an air-equilibrated 5×10^{-6} M C_{18}TACl solution. The measured force can be reproduced by assuming that one surface has ψ_1=+48 mV and the other has ψ_2=-48 mV with κ^{-1}=130 nm. However, these potentials were very different to the zeta potential measurements. As shown in Figures 2.10 and 2.11, the ζ-potentials of the silica plate and glass sphere were +34 and +11 mV, respectively, in air- equilibrated solutions of pH 5.7. The force curve obtained with these values as ψ_1 and ψ_2, and κ^{-1}=130.4 nm in only weakly attractive and is not similar to the measured force. Although the long-range attractive force observed in the air-saturated $5x10^{-6}$ M C_{18}TACl solution decayed exponentially, it is not easy to explain via a conventional double-layer force.

2) Long-Range Hydrophobic Forces of Electrostatic Origin?

Isrelachivili and Pashley (2) were the first to report that macroscopic surfaces hydrophobized with a surfactant exhibited surface forces stronger than the London-van der Waals force. The measurements were conducted using a surface force apparatus (SFA) between two curved mica surfaces immersed in cetyltrimethylammonium bromide (C_{16}TABr). They found that the non-DLVO attractive force decayed exponentially but was insensitive to the type and concentration of electrolyte present. However, many other investigators (11, 38) showed later that hydrophobic force decreases in the presence of electrolyte, suggesting that the hydrophobic force may be of electrostatic origin.

The non-DLVO attractive forces observed in the present work with C_{18}TACl were much stronger and longer ranged than reported by Israelashivili and Pashly (2). Nevertheless, the force data obtained in degassed solutions and given in Figure 2.7 have been fitted to a single-exponential function (Eq. [3]) as represented by dashed lines. The data were fitted after subtracting contributions from the van der Waals and double-layer forces. The former was calculated using Eq. [1] and the latter using the algorisms of Chan *et al*. (44) with the constant potential boundary conditions. In calculating the double-layer potentials, we used the ζ-potentials of the glass sphere and silica plate measured in the

present work as the surface potentials (Ψ_1 and Ψ_2), while the Debye lengths (κ^{-1}) were calculated from the concentrations of the ionic surfactants. In so doing, we recognized that the potentials of the glass sphere and silica plates were different from each other, as shown in our ζ-potential measurements.

The *C* and *D* values obtained by fitting the force curves obtained in degassed solutions are presented in Table 2.2. Also shown for comparison are the results obtained in air-equilibrated C_{18}TACl solutions. In a degassed 10^{-6} M solution, *D* was 11.5 nm. At $5x10^{-6}$, it increased to 34 and 38 nm in air-saturated and degassed solutions, respectively. As the concentration was increased further to 10^{-5} M, *D* was 30 nm when the surfactant solution was air-equilibrated, while it decreased to 4 nm when the solution was degassed. The sharp decrease in decay length was not due to the disappearance of bridging nanobubbles. Rather it was due to the increase in pH from 5.7 to 6.6 due to the shift in equilibrium involving CO_2 (eq. [2]), as has already been discussed. At 10^{-5} M, which is above ccp, the additional $C_{18}TA^+$ ions would adsorb with inverse (or flip-flop) orientation, and cause a decrease hydrophobic force.

The force data given in Figure 2.6 shows that the long-range attraction begins to decrease at C_{18}TACl concentrations above $5x10^{-6}$ M, which can be attributed to the inverse orientation of the cationic surfactant. The contact angle data given in Table 2.3 provide evidence for the inverse orientation. As shown, the equilibrium contact angle increased with increasing C_{18}TACl concentration up to $5x10^{-6}$ M, where the long-range attraction reached a maximum. At higher concentrations, the contact angle decreased most probably due to inverse orientation. That the inverse orientation occurs at concentrations 34-68 times below cmc ($3.4x10^{-4}$ M) (22) may be attributed to the very long hydrocarbon chains of the cationic surfactant used in the present work.

The decay lengths (*D*) of the hydrophobic forces reported in the literature vary widely depending on the chain lengths of surfactants, methods of deposition, and substrates. With the mica and silica surfaces coated with self-assembled monolayer of 12-carbon chain cationic surfactants, the values of *D* are in the range of 1-3 nm. With double-chain cationic surfactants such as dimethyldioctadecylammonium (DDOA) bromide, they are in the range of 15-20 nm. Kurihara *et al*. (45,46) reported *D* values in the range of 42-62 nm with a polymerized double-chain quaternary ammonium surfactant deposited on mica. Thus, the decay lengths observed in the present work was considerably longer than those observed with shorter chain ionic surfactants.

Parker *et al*. (39) and Kekicheff and Spalla (38) showed that long-range attraction was the maximum in the vicinity of ccp. The ζ-potential measurements conducted in the present work (Figures 2.10 and 2.11) showed that the ccp's of the silica plate and glass sphere were 10^{-6} and $5x10^{-6}$ M C_{18}TACl, respectively. At such low concentrations, hydrophobic force would not be screened significantly, if it originates from an electrostatic interaction. As shown in Figure 2.12, the long-range attractive force decreased with increasing electrolyte concentration, which suggested that hydrophobic force may indeed be of electrostatic origin.

In effect, the very large values of *D* observed with C_{18}TACl are due to the very long hydrocarbon chain, which causes the ccp to occur at very low surfactant concentrations and, hence, minimizes the screening effect. To illustrate this point further, a series of AFM force measurements were conducted with a shorter-chain homologue, i.e., C_{12}TABr. As shown in Figure 2.14, the measured forces were most attractive at 10^{-3} M,

which was 16-times lower than its cmc ($1.6x10^{-2}$ M). At $5x10^{-3}$ M, which was 3.2-times lower than the cmc, the measured forces became repulsive at shorter separations. The dashed lines given in Figure 2.13 show the fitted force curves, which included contributions from the van der Waals, double-layer and hydrophobic forces, while Table 2.4 shows the fitting parameters. The fitting was carried out using a single-exponential function (Eq. [3]). As shown, the decay lengths (D) varied in the range of 1.8 to 6.2, which were substantially smaller than those (D) obtained with the longer-chain homologue. The shorter decay lengths obtained with the C_{12}TABr may be attributed to the high surfactant concentrations required to render the surface hydrophobic. It is possible that the hydrophobic force, which may originate from one of electrostatic interaction, is more readily screened at the higher concentrations of the shorter-chain ionic surfactants.

In Figure 2.15, the values of D obtained at different electrolyte (NaCl) concentrations are plotted versus κ^{-1}. The D values were obtained in 5×10^{-6} and 8×10^{-6} M C_{18}TACl solutions and given in Table 2.1. As shown, D varies approximately as $\kappa^{-1}/2$ at electrolyte concentrations, which is consistent with the theoretical electrostatic models developed by Attard (12), Miklavic, *et al*. (18), and Kekicheff and Spalla (38). It seems, therefore, that the long-range attractive forces observed in the present work may be of electrical origin.

3) Forces Arising from the Inhomogeneous Distribution of Surface Charge?

The data presented hitherto clearly suggest that the $C_{18}TA^+$ ions adsorb with normal mode of orientation at low surfactant concentrations. As the concentration reaches ccp, both the contact angle and the long-range attractive force reach maxima. The adsorption may occur in patches (or domains) as observed in the AFM images, because hydrocarbon association is one way of minimizing the free energy of the system. This would be particularly the case with longer-chain surfactants, as the free energy change is proportional to the number of the CH_2 groups in a chain that are associated with those of the neighboring hydrocarbon chains. As concentration is increased, additional surfactant molecules would adsorb with inverse or flip-flop orientation, with their polar heads pointing toward the aqueous phase. With a C-18 surfactant, this may occur at a relatively low concentration.

The patch-wise adsorption mechanism may offer an explanation for the origin of the long-range attractive force observed in the present work. Water dipoles in the vicinity may have a unidirectional orientation so that each domain can have a large dipole moment. The large dipoles on one surface would then correlate with those on the other to give rise to a strong attraction (47). Based on this concept, a mathematical model for the long-range attraction between the surfaces coated with self-assembled monolayer has been developed (17).

The model based on the correlation of the large dipoles assumes that a charged surface is neutralized locally by the adsorption of ionic surfactant. It is possible, however, that a net neutral surface is created by equal number of positively and negatively charge patches. The charged patches on one surface could correlate with those on the other and give rise to long-range attraction. It is possible that the patch-wise adsorption of $C_{18}TA^+$ ions creates patches of positive and negative charges. The positive sites may be represented by the $C_{18}TA^+$ ions adsorbing in patches, in excess of the negative silica

surface charge, while the negative sites may be represented by the unoccupied silica surface.

Several groups have already shown that a net-neutral surface with a heterogeneous distribution of charges can lead to an attractive force (11,18). In particular, Miklavic *et al*. (18) have shown that, if the charged patches are free to migrate across the surface, then the interaction between two net neutral surfaces is always attractive. We have observed some degree of mobility of the C_{18}TACl surface aggregates in AFM images, which would allow positive patches on one surface to align with negative patches on the other surface, thereby producing a net attractive force. This mobility could either occur through the translation of the entire patch, or the decomposition of old patches and nucleation of fresh ones. Of course, this mobility would have to occur at a sufficient speed to allow for correlations between aggregate positions on the two surfaces within the time for each approach between the surfaces. At this point, we have no direct evidence for this degree of mobility.

Support for the mobile patch mechanism may arise from our observation of the functional form, the range, and the magnitude of the force. Attard (12), Kerkicheff and Spalla (38), and Miklavic *et al*. (18) predict that the attractive forces between heterogeneous surfaces will be exponential, as observed in this communication. The magnitude should decrease with salt concentration because additional salt will decrease the net surface charge in each patch when counterions bind to the surfactant headgroup. This effect is also observed in our force measurements. Also, the range of the force should decrease with salt concentration because the electrostatic forces will be screened by the salt. Miklavic *et al*. predicted that the decay length will be dictated by one-half of the solution Debye-length at high salt concentration and by the charge-patch periodicity at low salt concentration. The complex patterning on the surface makes it difficult to establish a patch length-scale. Although there is a trend of a shorter range of force in more concentrated solutions, our data does not quantitatively show a decay length that is equal to half the Debye-length (Tables 2.1 and 2.2).

An alternate explanation for the production of charge heterogeneity is suggested by the observation that in some cases, attractive forces are only observed on the second and subsequent approach of two surfaces. This phenomenon has been previously ascribed to the generation of small adsorbed bubbles. For surfaces bearing surfactant molecules, however, the contact of the adsorbed layers could also generate heterogeneities. Recent self-consistent field theory (SCF) calculations (by one of us) (48) suggest that when two monolayers or partial monolayers are brought into close proximity, a bilayer is formed in the center with a partial layer of water on either side. We speculate that when the solids are separated, a bilayer could adhere to one or other of the surfaces, creating opposed areas of positive and negative charges, which will then give rise to attractive forces on subsequent approaches of the surfaces.

Thus, we see two limiting mechanisms for generating attractive charge patch forces, depending on the mobility of the surfactant. If the surfactant is highly mobile (transport across the surface is faster than the inter-surface approach speed), then dynamic charge patch correlations can lead to attractive forces. If the surfactant is immobile, then charged patches can be created by heterogeneous fracture of a bilayer and remain frozen in place during subsequent force measurements.

2.4 Conclusions

We have observed long-range (~120 nm) attractive forces between moderately hydrophobic surfaces prepared by the adsorption of C_{18}TACl. The force curves do not show discontinuities (or steps) even at large separations, and the effect of degassing is explicable simply in terms of a pH change. Therefore, we do not explain the forces in terms of adsorbed bubbles. The discrepancy between the results obtained in the present work and those of Sakamoto *et al.* (22) is most probably due to their use of excessively stiff cantilevers used by these investigators.

The attractive force is effectively screened by electrolyte (NaCl), indicating that it may be of electrostatic origin. The force reaches a maximum at $5x10^{-6}$ M, which is close to the ccp of the glass sphere in C_{18}TACl solution. At this concentration, the long-range decay lengths (D) are 34 and 38 nm in air-equilibrated and degassed solutions, respectively. Such long decay lengths may be attributed to the fact that the $C_{18}TA^+$ ions neutralize the surface at a very low concentration, where the solution Debye-length is very long (in the absence of added salt). The force measurements conducted with C_{12}TABr show relatively short decay lengths in the range of 1.8-6.2 nm, which may be attributed to the high surfactant concentrations required to neutralize the surface. It appears, therefore, that the decay lengths of the attractive forces in ionic surfactant solutions depend on the hydrocarbon chain lengths because the surfactant concentration required to neutralize a surface varies with the hydrocarbon chain length.

Using AFM imaging, we have shown that the forces acting on a tip as it scans across the surface is inhomogeneous in the presence of the surfactant, and we attribute this to patchy-wise adsorption of the surfactant. There are two possibilities that the patches can give rise to long-range attraction. One is to assume that each patch is neutral, and the neutral patches present large dipoles that can correlate with those of the opposing surface. The other is to assume that a net neutral surface consists of positive and negative patches which can correlate with those of the opposing surface. However, our work in no way precludes the possibility of an attractive force that is due to the structuring of water in the thin film between non-wetting solids.

2.5 References

(1) Blake, T. D.; Kitchener, J. A. J. Chem. Soc Faraday Trans. 1972, 68, 1435-1442.
(2) Israelachvili, J.; Pashley, R. M. J. Colloid Interface Sci. 1984, 98, 500-514.
(3) Laskowski, J.; Kitchener, J.A., J. Colloid Interface Sci. 1969, 30, 391.
(4) Yoon, R.-H. and Aksoy, S., J. Colloid Interface Sci., 211, 1-10.
(5) Angarska, J.K.; Dimitrova, B.S.; Danov, K.D.; Kralchevsky, P.A.; Ananthapadmanabhan, K.P.; Lips, A. Langmuir 2004, 20,1799.
(6) Wang, L. and Yoon, R-H., Langmuir, 2004, 20, 11457-11464.
(7) Eriksson, J.C.; Ljunggren, S. and Claesson, P.M, J. Chem. Soc., Faraday Trans. 2, 85(3), 163-176.
(8) Claesson, P. M.; Christenson, H. K. J. Phys. Chem. 1988, 92, 1650-1655.
(9) Wood, J.; Sharma, R. Langmuir 1995, 11, 4797-4802.
(10) Claesson, P. M.; Attard, P. J. Phys. Chem. 1994, 98, 8468-8480.
(11) Tsao, Y. H.; Evans, D. F.; Wennerstrom, H. Science 1993, 262, 547-550.
(12) Attard, P., J. Phys. Chem. 1989, 93(17), 6441-6444.

(13) Ishida, N.; Inoue, T.; Miyahara, M.; Higashitani, K. Langmuir 2000, 16, 6377-6380.
(14) Yang, J.; Duan, J.; Fornasiero, D.; Ralston, J. J. Phys. Chem. B 2003, 107, 6139-6147.
(15) Tyrrell, J. W. G.; Attard, P. Physical Review Letters 2001, 8717.
(16) Mao, M.; Zhang, J.; Yoon, R.-H.;Ducker, W.A., Langmuir. 2004, 1843-1849
(17) Pazhianur, R. and Yoon, R.-H., Minerals & Metallurgical Processing, 2003, 20, 178-184.
(18) Miklavic, S. J.; Chan, D. Y. C.; White, L. R.; Healy, T. W. J. Phys. Chem. 1994, 98, 9022-9032.
(19) Ishida, N.; Kinoshita, N.; Miyahara, M.; Higashitani, K., J. Colloid and Interface Sci., 1999, 216, 387-393.
(20) Ishida, N.; Sakamoto, M.; Miyahara, M.; Higashitani, K.; Langmuir, 2000, 16, 5681-5687.
(21) Ishida, N.; Sakamoto, M.; Miyahara, M.; Higashitani, K.; J. Colloid Interface Sci., 2002, 252, 112-116.
(22) Sakamoto, M.; Kanda, Y.; Miyahara, M.; Higashitani, K. Langmuir 2002, 18, 5713-5719.
(23) Parker, J.L.; Claesson, P.; Attar, P. J. Phys. Chem. 1994, 98(34), 8468-8480.
(24) Nuyen, A.V.; Nalaskowski, Miller. J.; Butt, H.-J. Int. J. Miner. Process., 2003, 72, 215-225.
(25) Ducker, W. A.; Senden, T. J.; Pashley, R. M. Nature 1991, 353, 239-241.
(26) Ducker, W. A.; Senden, T. J.; Pashley, R. M. Langmuir 1992, 8, 1831-1836.
(27) Cleveland, J. P.; Manne, S.; Bocek, D.; Hansma, P. K. Rev. Sci. Instrum. 1993, 64, 403-406.
(28) Derjaguin, B.V., Kolloid Z. 69, 155 (1934)
(29) Barry, B. W.; Russell, G. F. T. J. Colloid Interface Sci 1972, 174-194.
(30) Mellott J.M, Hayes W.A, Schwartz D.K. Langmuir 2004, 20, 2341-2348
(31) J.F. Liu, W. A. Ducker J. Phys. Chem. 1999 103 8558-8567
(32) Manne, S, Gaub, H.E. Science 1995 270 1480-1482
(33) Clark, S; W.A. Ducker. J. Phys. Chem. B 2003,107, 9011-9022
(34) Israelachvili, J. Intermolecular and Surface Forces: With Applications to Colloidal and Biological Systems. 1992 2nd ed., Academic Press p190
(35) Subramanian, V.; Ducker, W. J. Phys. Chem. B 2001, 105, 1389-1402.
(36) Lokar, W. J.; Ducker, W. A. Langmuir 2002, 18, 3167-3175.
(37) Lokar, W. J.; Ducker, W. A. Langmuir 2004, 20, 378-388
(38) Kerkicheff, P. and Spalla, O., 1995, Phys. Rev. Lett. 75, 1851
(39) Parker, J.L.; Yaminsky, V.V.; Claesson, P.M., J. Phys. Chem. 1993, 97, 7706.
(40) P. Somasundaran, Thomas W. Healy, D. W. Fuerstenau J. Phys. Chem. 1964, 68, 3562-3566
(41) Tanford, C., 1980, "The Hydrophobic Effect," 2nd ed.. Wiley, New York, p.9.
(42) Stumm, W.; Morgan, J. J. Aquatic Chemistry: Chemical Equilibria and Rates in Natural Waters Environmental Science and Technology; John Wiley & Sons: New York, 1996.
(43) Goloub, T. P.; Koopal, L. K. Langmuir 1997, 13, 673-681
(44) Chan, D.Y.C.; Pashley, R.M.; White, L.R., J. Colloid and Interface Sci. 1980, 77, 283.

(45) Kurihara, K.; Kato, S.; Kunitake, T. Chem. Lett., 1990, 1555.
(46) Kurihara, K.; Kunitake, T.J., J. Am. Chem. Soc. 1992, 114, 10927
(47) Yoon, R.-H. ; Ravishankar, S.A., J. Colloid and Interface Sci., 1996, 179, 403-411.
(48) Lokar, W. J.; Koopal, L. K.; Leermakers, F. A. M.; Ducker, W. A. Submitted to J. Phys. Chem. B 2004.

Table 2.1 Effects of NaCl on Debye Lengths (κ^{-1}) and Decay Lengths (D) in C_{18}TACl Solutions.

NaCl (mM)	κ^{-1} (nm)	D (nm)	
		C_{18}TACl Concentration (M)	
		$5x10^{-6}$	$8x10^{-6}$
0	136	34	28
0.1	30	26	18
1	9.6	7.5	4
3	5.6	3	-

Table 2.2 Fitting Parameters Used to Determine the Hydrophobic Force Parameters in Air-equilibrated and Degassed $C_{18}TACl$ solutions.

$C_{18}TACl$ (M)	Degassing	Ψ_1 (mV)	Ψ_2 (mV)	κ^{-1} (nm)	C (mN/m)	D (nm)
$1x10^{-6}$	Degassed	-17.1	-36.9	300	-1.4	11.5
$5x10^{-6}$	Air-equilibrated	11.2	34.2	130.4	-1.4	34
	Degassed	19.5	50.1	130.4	-2.1	38
$1x10^{-5}$	Air-equilibrated	38.0	58.5	94.9	-1.4	30
	Degassed	75.0[1]	80.0[1]	94.9	-1.4	4

[1]Fitted values; the rest were from measured ζ-potentials.

Table 2.3 Equilibrium Contact Angles on the Fused Silica Plate in C_{18}TACl Solutions.

C_{18}TACl (M)	Contact Angle (degrees)
$1x10^{-6}$	46
$3x10^{-6}$	52
$5x10^{-6}$	64
$8x10^{-6}$	61
$1x10^{-5}$	57

Table 2.4 Fitting Parameters Used to Determine the Hydrophobic Force Parameters in Air-equilibrated C_{12}TABr solutions.

C_{12}TABr (M)	Ψ_1 (mV)	C (mN/m)	D (nm)	κ^{-1} (nm)
$1x10^{-4}$	-50	-1.4	3.3	30.4
$1x10^{-3}$	0	-1.2	6.2	9.6
$5x10^{-3}$	+21	-1.2	1.8	4.3

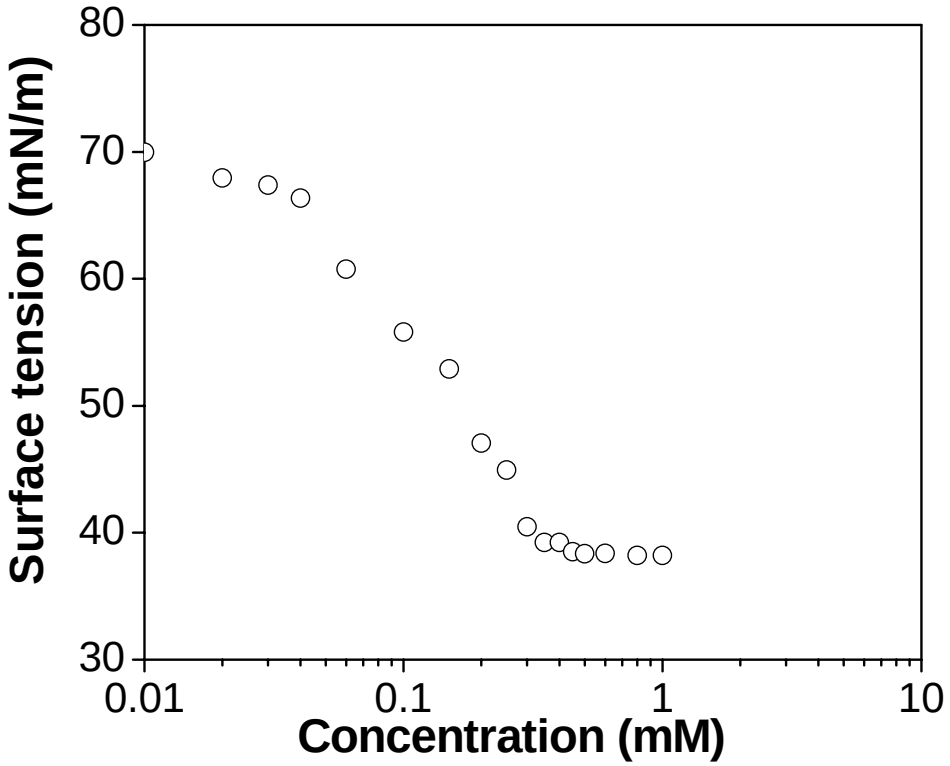

Figure 2.1 Surface tension of aqueous C_{18}TACl solutions.

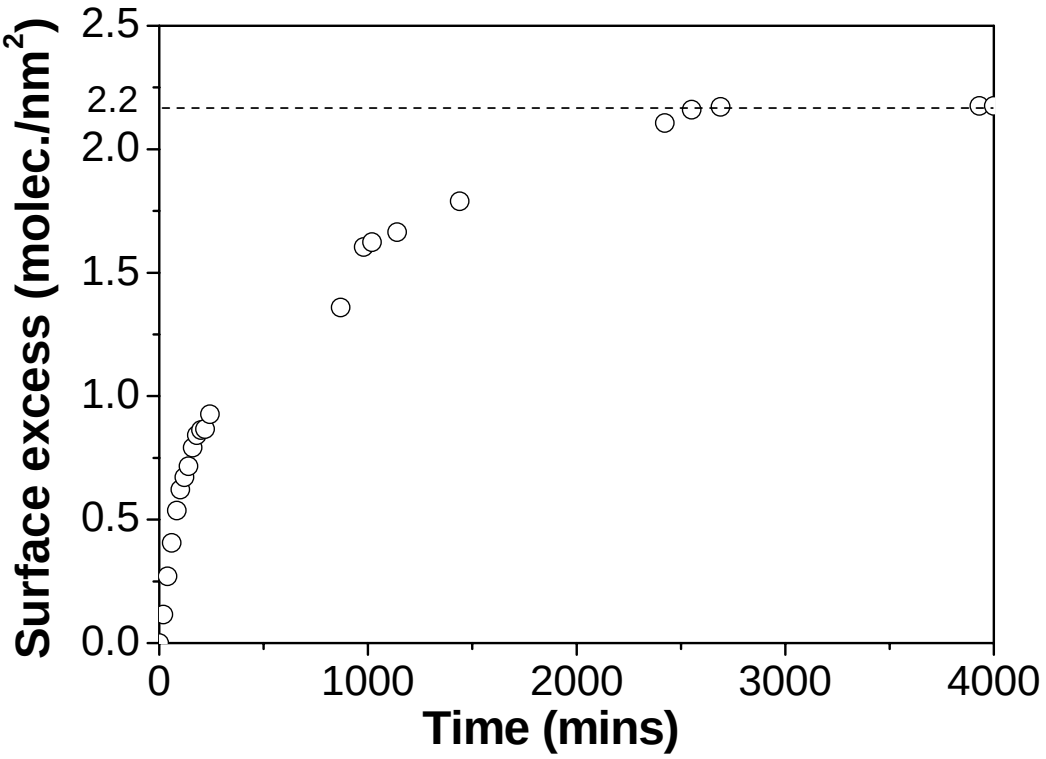

Figure 2.2 Surface excess at the silicon wafer/solution interface at 10^{-5} M C_{18}TACl as a function of elapsed time since exposure to the solution. dn/dc = 0.15 mL/g was used to calculate the data.

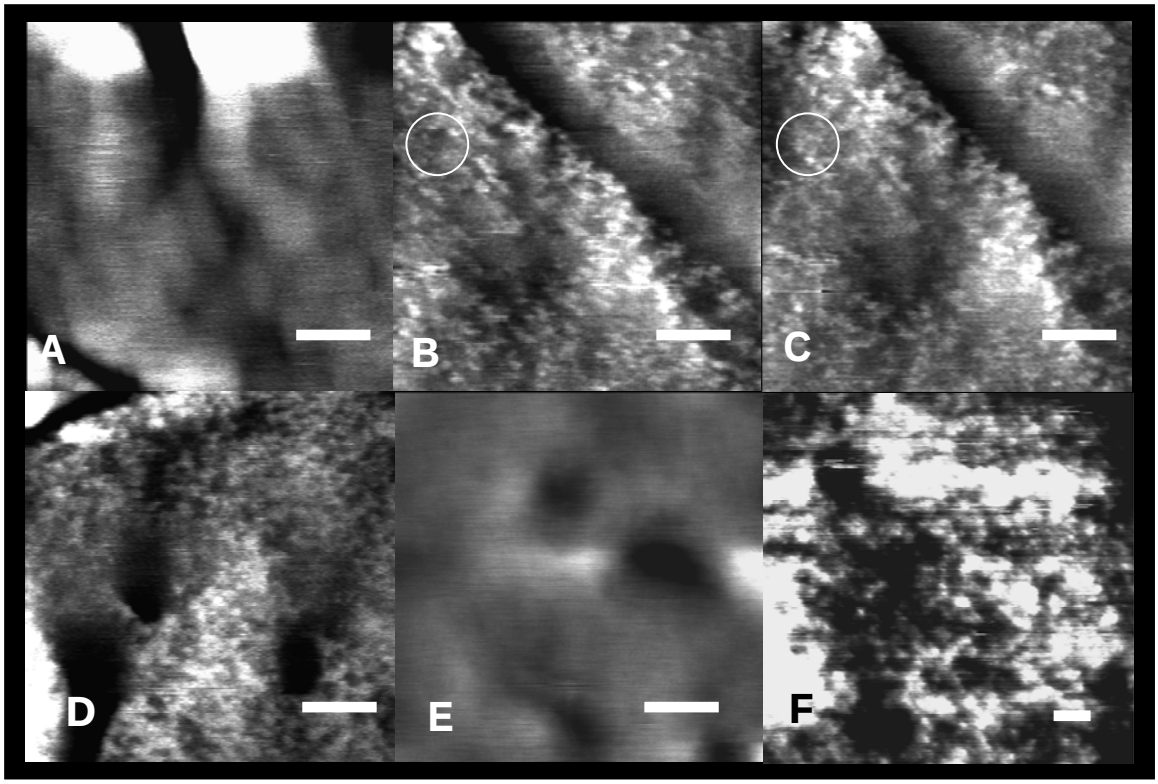

Figure 2.3 AFM contact mode images of the interface between the silica plate and an aqueous 10^{-5} M $C_{18}TACl$ solution over time. The images were captured at constant deflection (force ~0.5 nN) in the liquid cell. In each case, the scale bar is 100 nm. A) in water, before $C_{18}TACl$ was added; B) after 30 min; C) after 31 minutes; D) after 1 hour (the image is similar after 2 hours); E) after 7 h; F) larger scale image after 7 h. The height difference between the patches and the surrounding areas is 0.3–0.6 nm in figures B–D. Note that the some of the patches have moved in the minute between B and C (e.g. within the circle). The lines across the images were present before the introduction of the surfactant and may be grain boundaries in the fused silica.

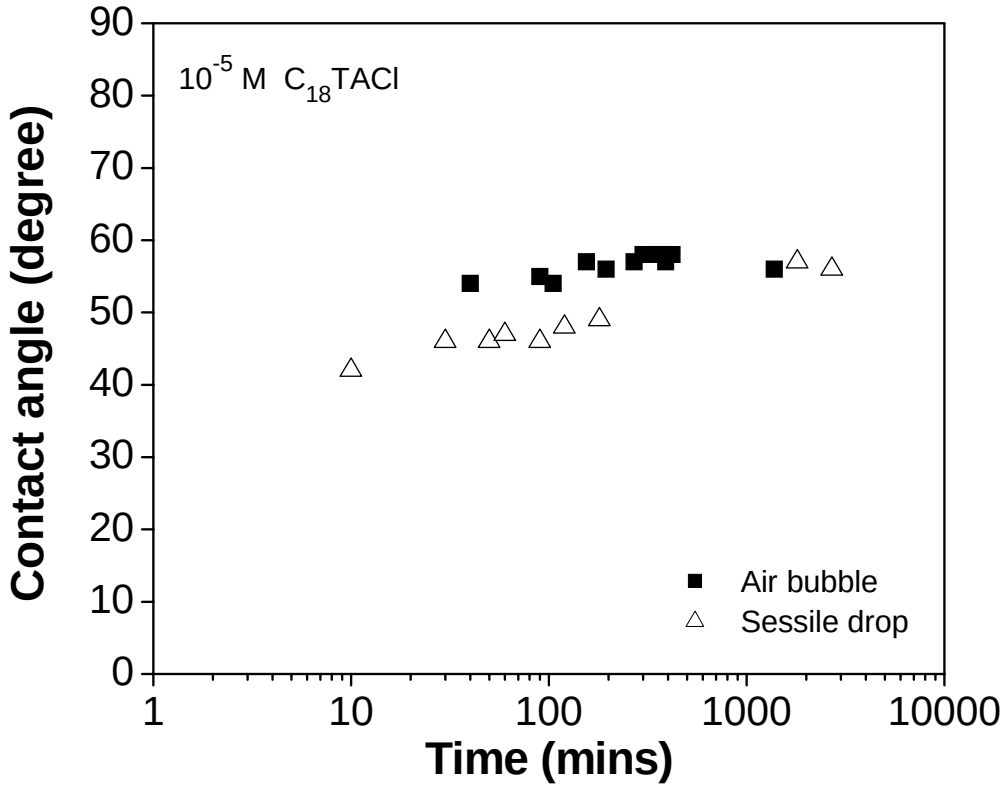

Figure 2.4 Sessile drop and captive bubble contact angles of the fused silica plates as a function of the time that the plate was exposed to 10^{-5} M C_{18}TACl solutions.

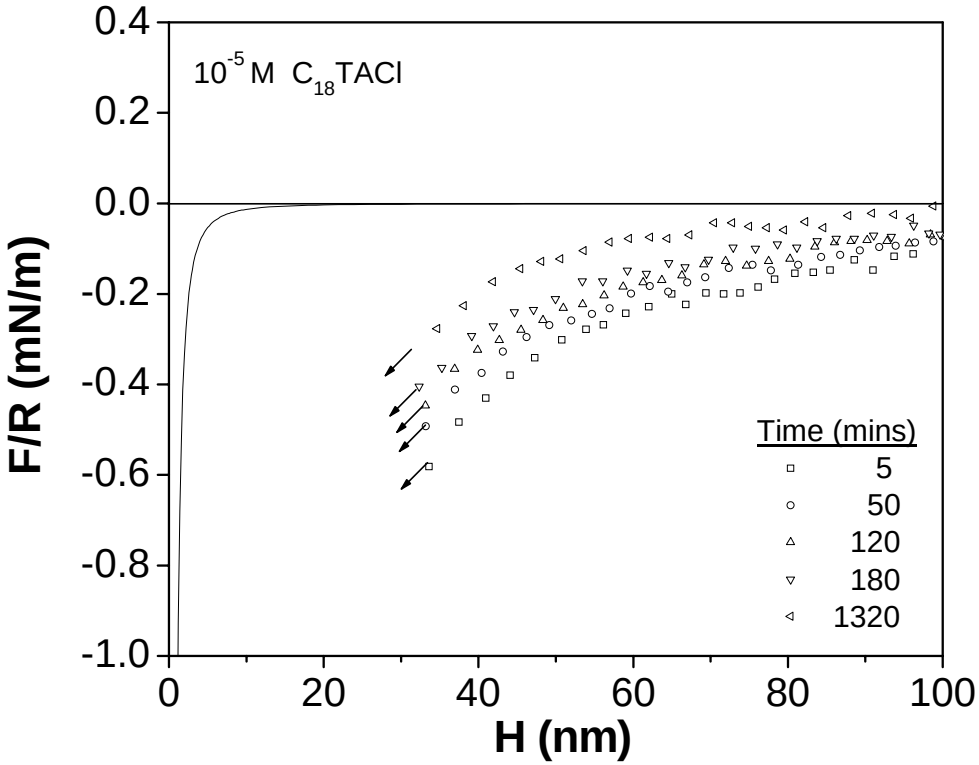

Figure 2.5 The surface forces (F) measured between a glass sphere of radius R and a fused silica plate in an air-equilibrated 10^{-5} M $C_{18}TACl$ solution as a function of immersion time. The measured forces were more attractive than the van der Waals dispersion force represented by the solid line. The arrows represent the distances at which the two surfaces jump into contact. The attractive force decreases with time due to the inverse orientation of the $C_{18}TA^{+}$ ions, which apparently is a slow process for the C-18 surfactant.

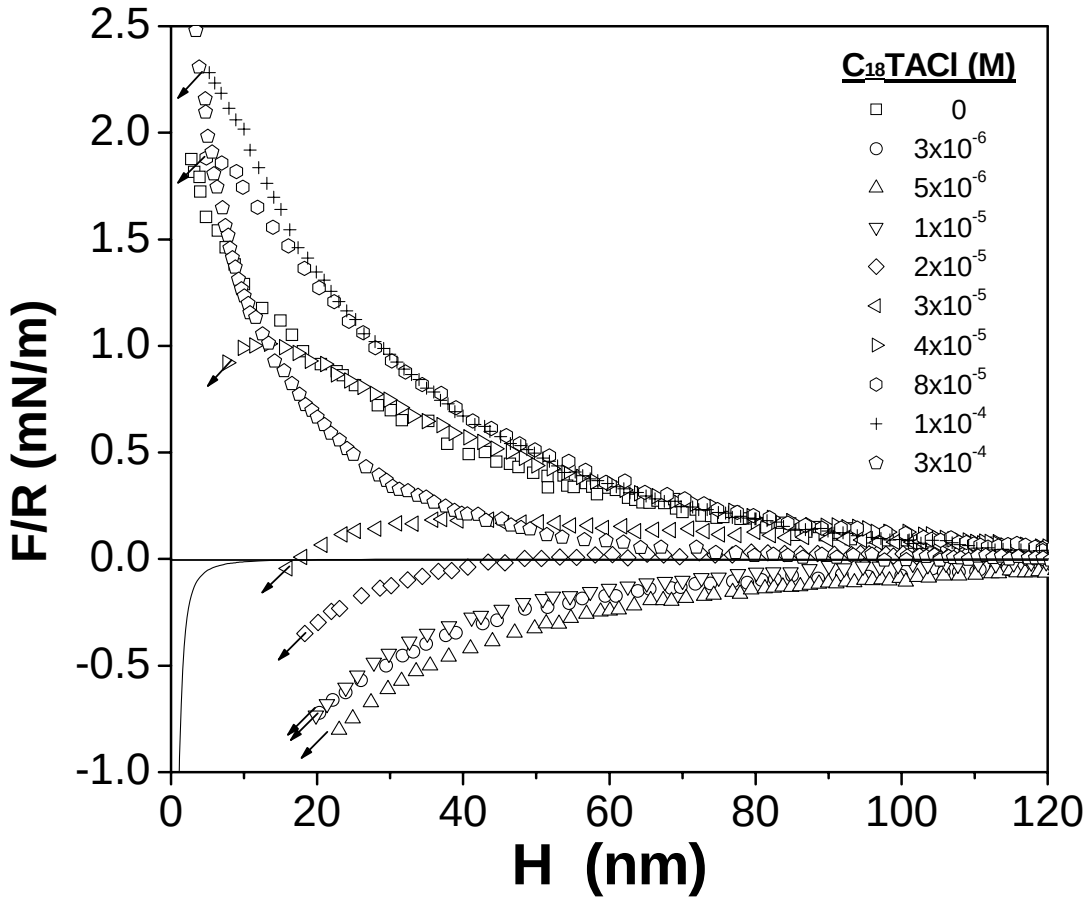

Figure 2.6 Forces (F) normalized by the radius (R) of the sphere in air-equilibrated C_{18}TACl solutions. The solid line represents the theoretical van der Waals force calculated using a Hamaker constant of $8x10^{-21}$ J. The measured forces were repulsive in 0 – $3x10^{-4}$ M C_{18}TACl solutions. The arrows represent the point where the cantilever undergoes a mechanical instability. Forces at smaller separations were measured, but are not reproduced here because the deflection of the spring does not give the surface force when it is not in mechanical equilibrium. Forces were measured in the order of increasing surfactant concentrations with the same sphere-plate combination. The forces were measured ~60 minutes after injection of each new reagent addition.

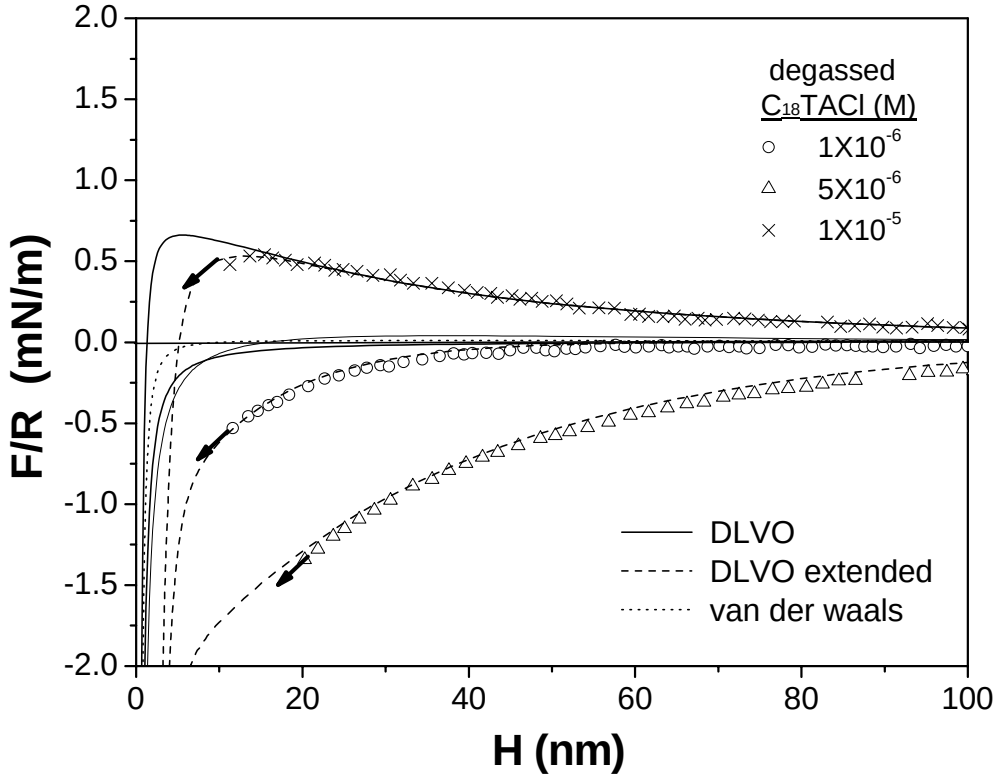

Figure 2.7 Forces (F) normalized by the radius (R) of sphere in degassed $C_{18}TACl$ solutions. The magnitudes of the forces are similar to those measured in air-equilibrated solutions shown in Figure 2.6. The force in $1x10^{-5}$ M solution fits well to DLVO theory that was calculated using an exact numerical solution of the Poisson Boltzmann equation at separations great than ~15 nm, which is shown as a line though the points. The addition of an exponential force term improves the fit as shown by the dashed line. The forces at $1x10^{-6}$ and 5×10^{-6} M are much more attractive than the van der Waals force alone, which is shown as a dotted line. The dashed lines represent the fits by extending the DLVO theory with a single exponential force term (Eq. [3]). The fitting parameters are given in Table 2.2, which shows that D=38 nm at $5x10^{-6}$ M.

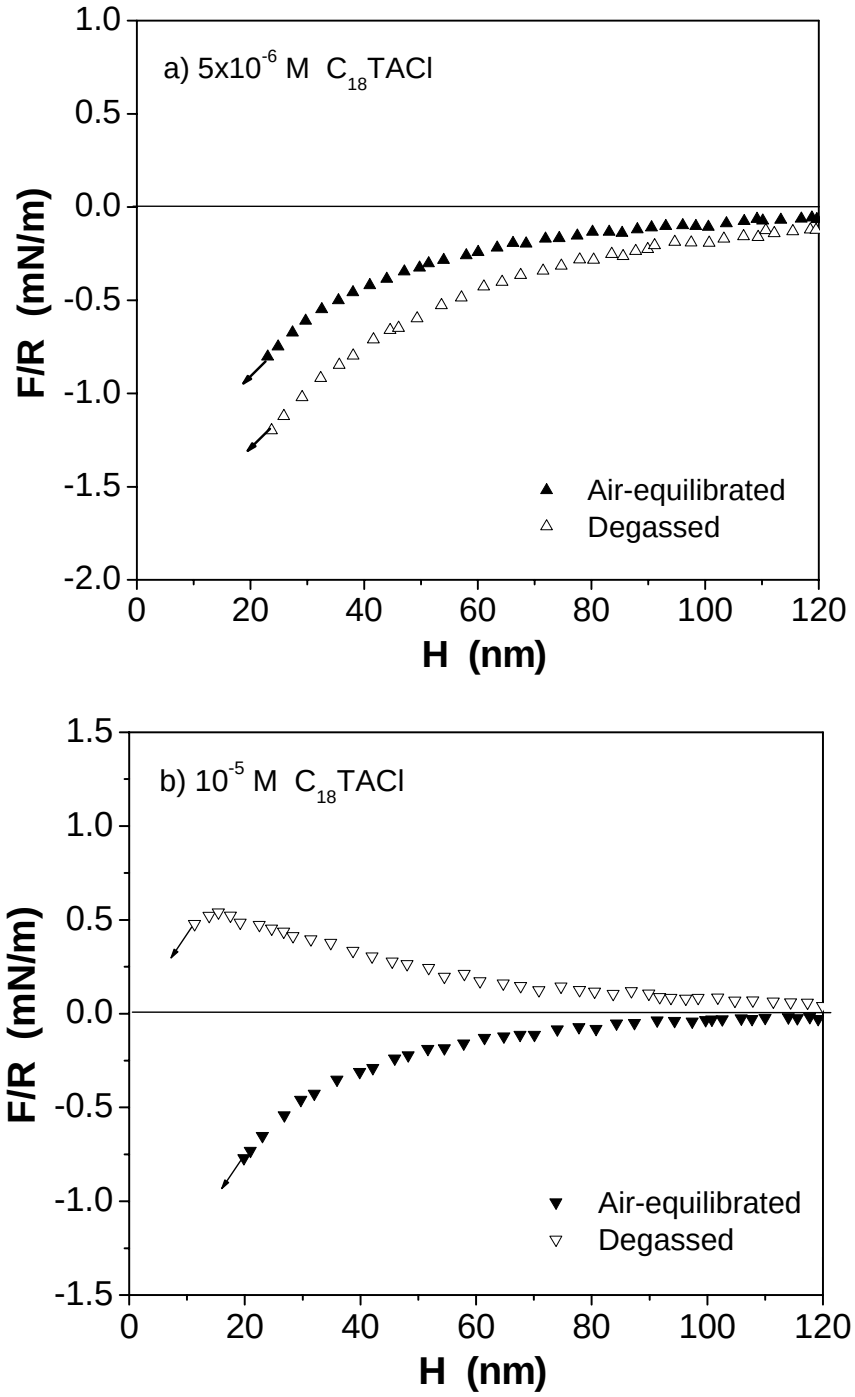

Figure 2.8 Comparison of the forces measured in degassed and air-equilibrated $5x10^{-6}$ and $1x10^{-5}$ M $C_{18}TACl$ solutions. The data were taken from Figures 2.6 and 2.7. At $5x10^{-6}$ M, D is 38 and 34 nm in degassed and air-equilibrated solutions, respectively. At $1x10^{-5}$ M, D is 30 and 4 nm in air-equilibrated and degassed solutions, respectively. The decrease in decay lengths by degassing can be attributed to pH change upon degassing.

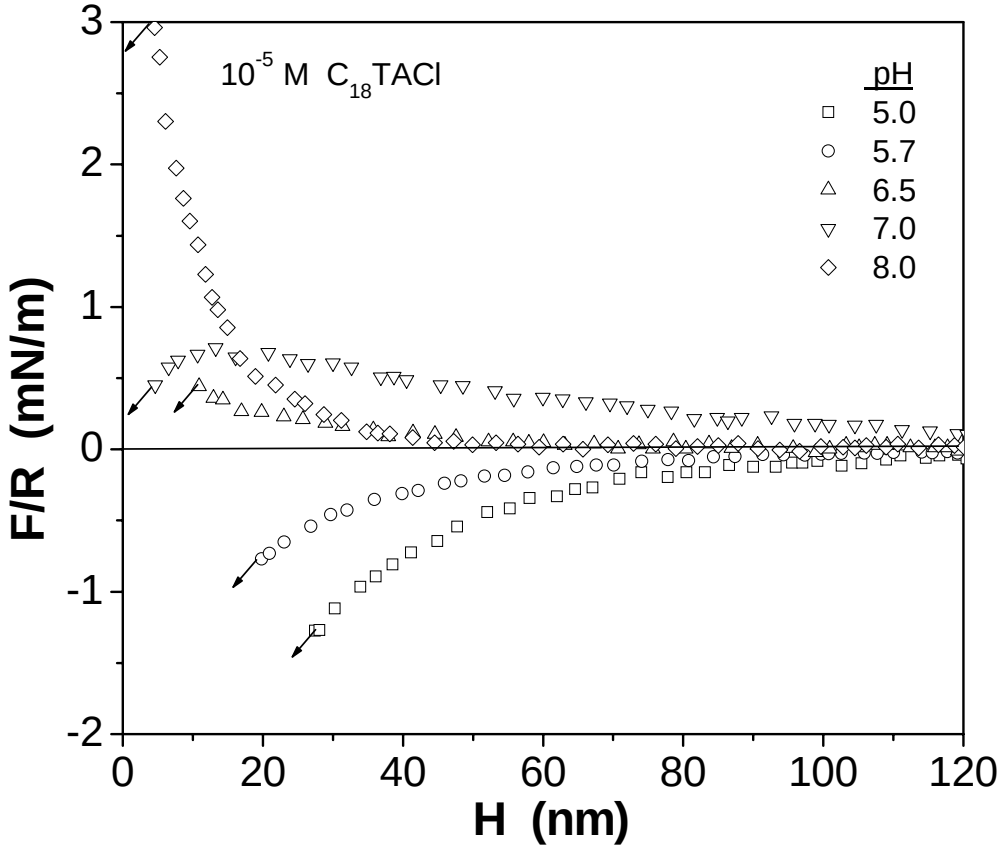

Figure 2.9 Effect of pH on forces in air-equilibrated 10^{-5} M C_{18}TACl solutions. The data for pH=5.7 were taken from Figure 2.6; all other data were for the same particle/plate combination.

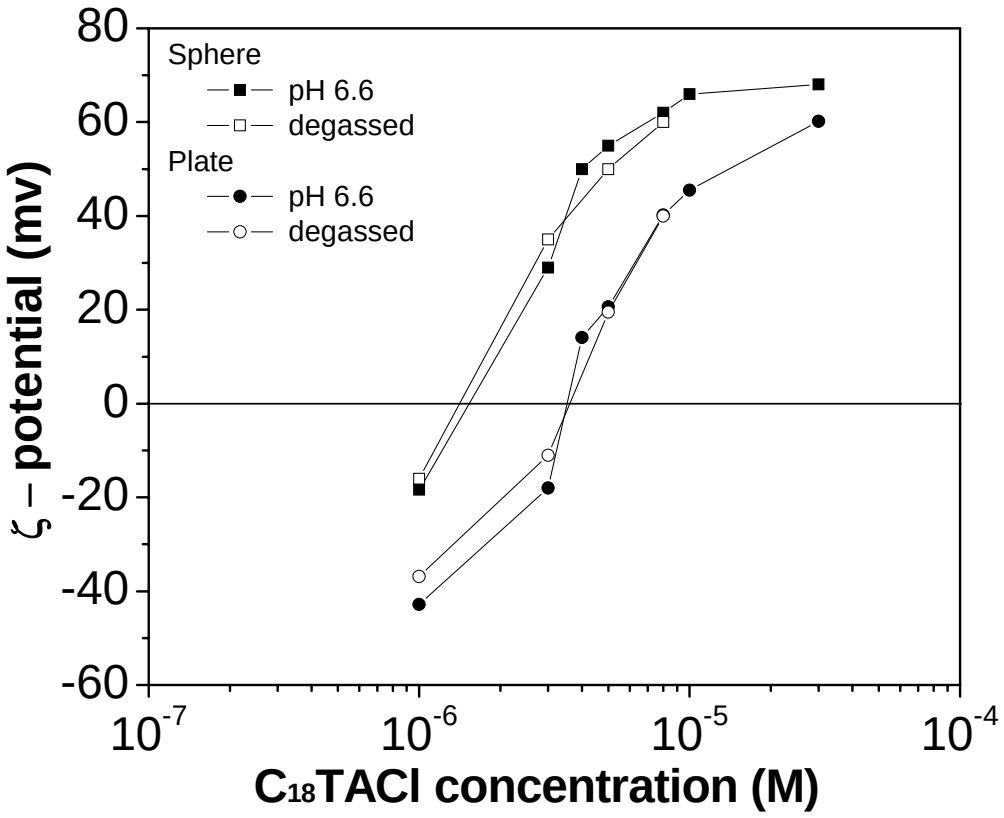

Figure 2.10 Comparison of the ζ-potentials measured in degassed C_{18}TACl solutions with those measured in air-equilibrated solutions whose pH have been adjusted to the same pH (=6.6) as the degassed solutions.

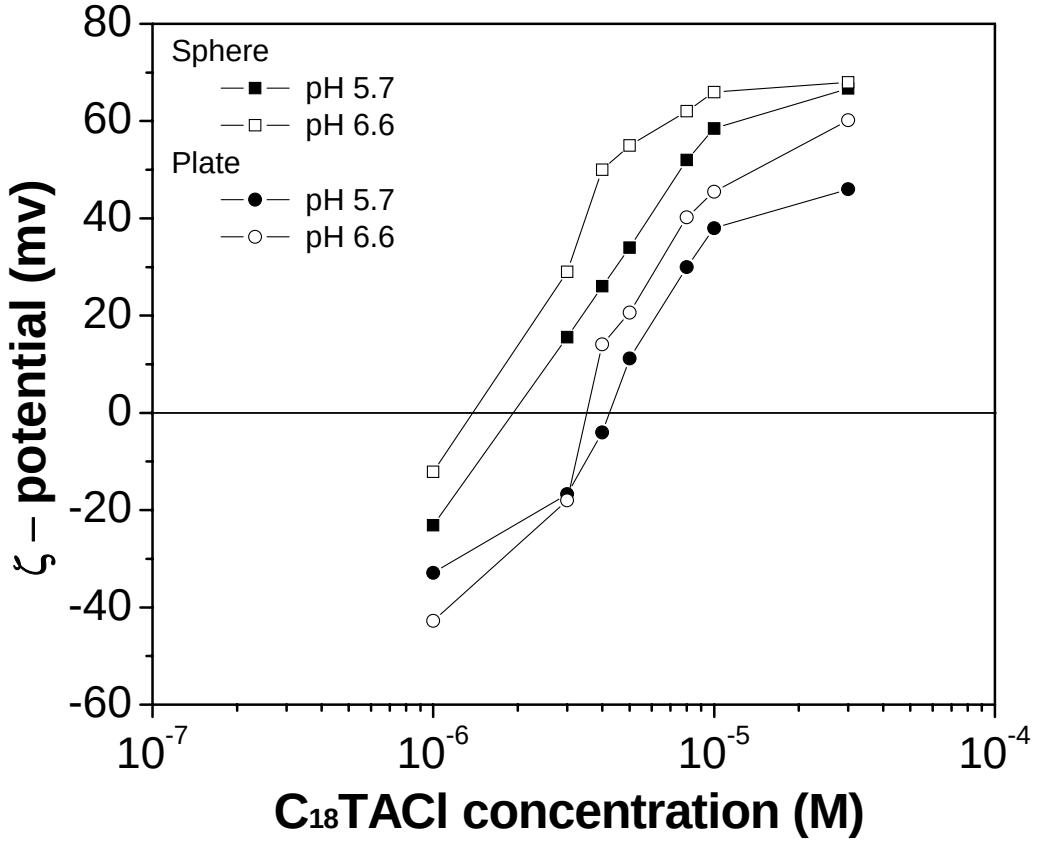

Figure 2.11 Comparison of the ζ-potentials measured in air-equilibrated C_{18}TACl solutions of pH~5.7 with those measured in solutions whose pH was adjusted to pH 6.6.

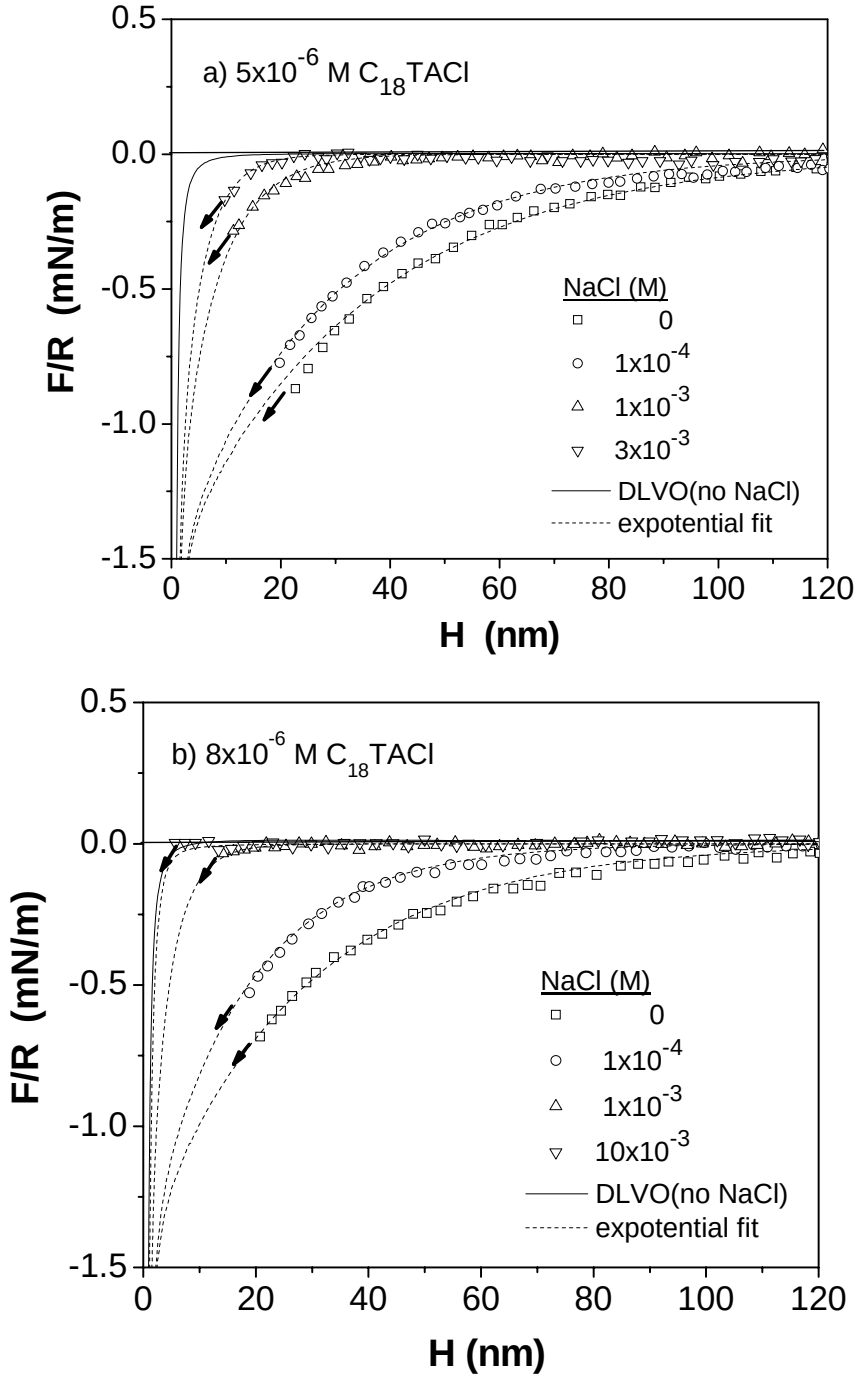

Figure 2.12 Effect of NaCl on the forces measured in air-equilibrated solutions of a) $5x10^{-6}$ M and b) $8x10^{-6}$ M $C_{18}TACl$ solutions. The solid lines represent the DLVO fit, and the dashed lines represent the extended DLVO theory with a single-exponential force term (Eq. [3]). The fitting parameters are given in Table 2.1. The decrease in the long-range attractive force suggests that it may be of electrostatic origin.

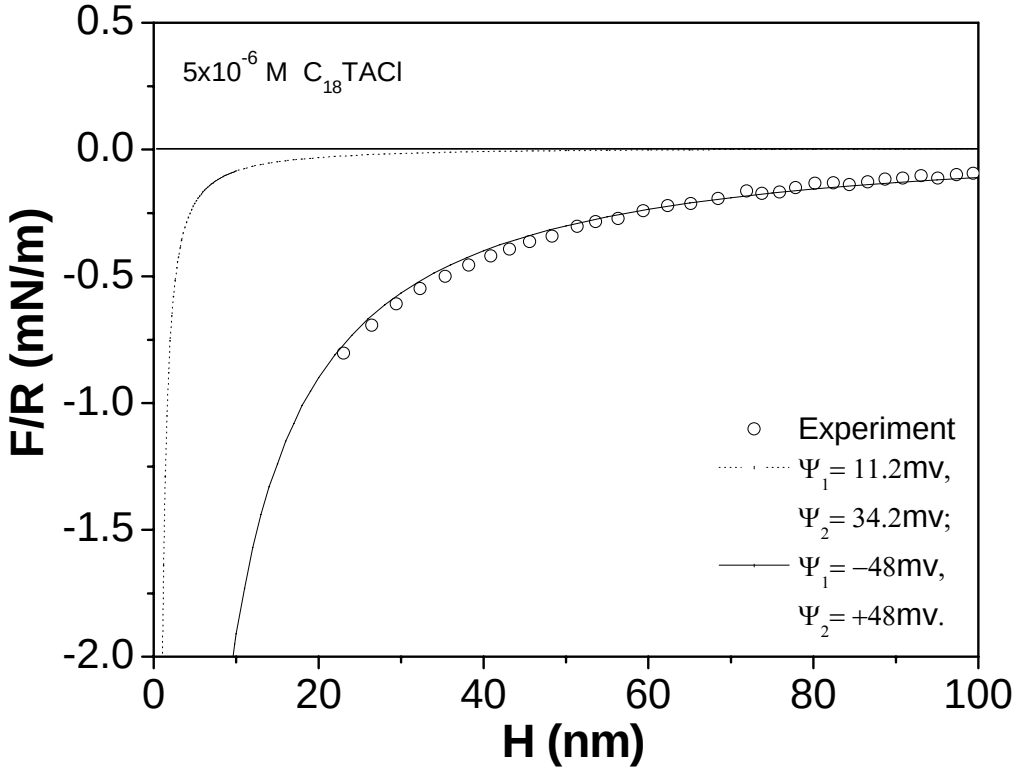

Figure 2.13 Force curves for the silica plate-glass sphere interaction in an air-equilibrated $5x10^{-6}$ M $C_{18}TAC$ solution. The dotted line represents the DLVO fit with Ψ_1=+11.2 mV and Ψ_2=+34.2 mV, which were taken from the ζ-potential measurements. To fit the long-range attractive force, it was necessary to assume that Ψ_1=+48 mv and Ψ_2=-48mv, which is unreasonable.

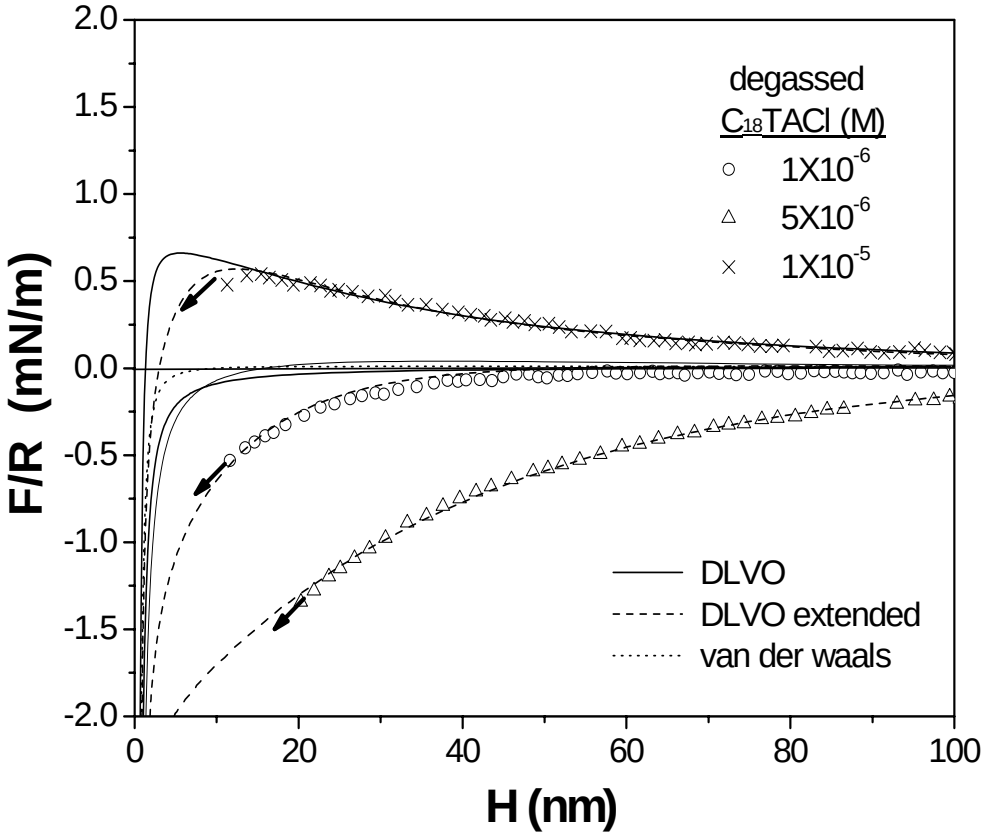

Figure 2.14 Forces between glass sphere and silica plate immersed in degassed C_{12}TABr solutions. Solid lines represent the DLVO theory, while dashed lines represent the DLVO theory extended with a double-exponential force term (Eq. [4]) representing the additional attractive force.

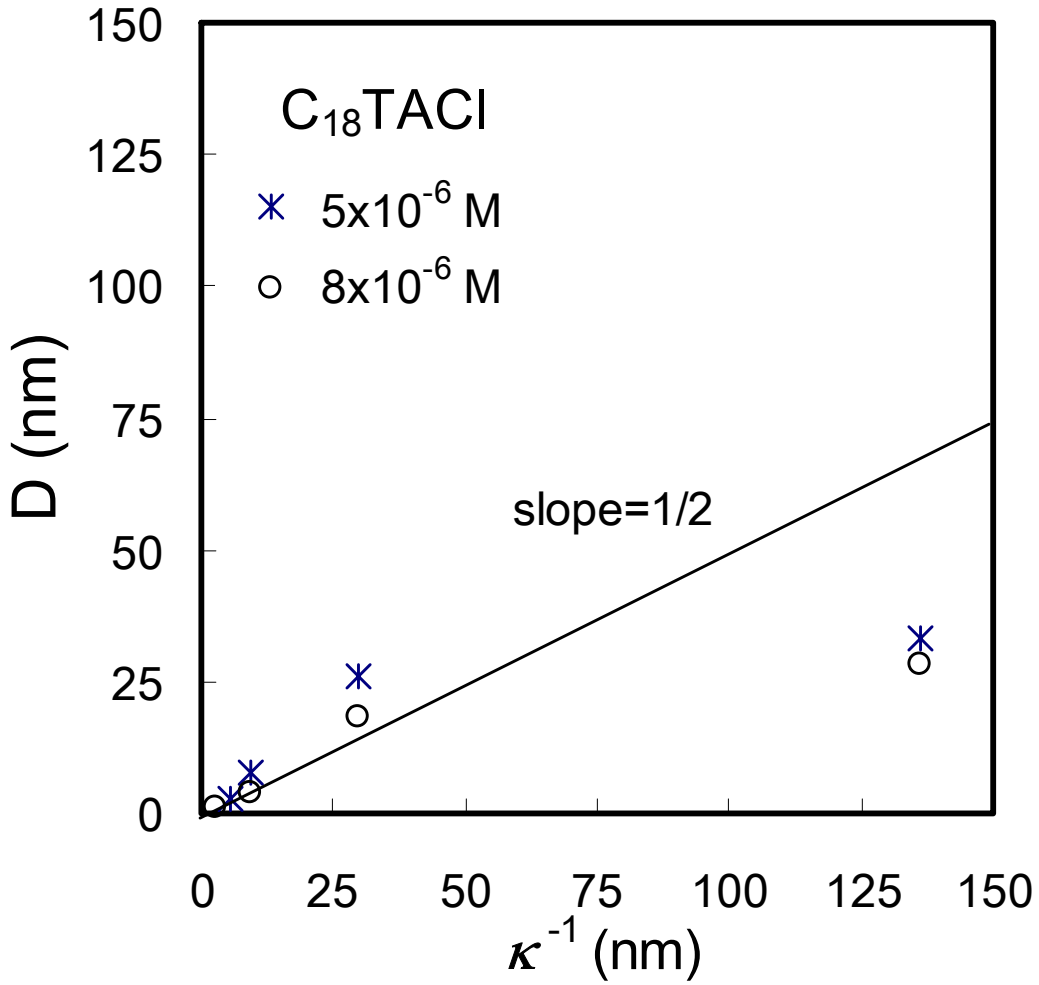

Figure 2.15 Effects of NaCl on Debye Lengths (κ^{-1}) and Decay Lengths (D) in C_{18}TACl Solutions.

CHAPTER 3

AFM Surface Force Measurements Conducted with Silica in C_nTACl Solutions: Effect of Chain Length on Hydrophobic Force

Abstract

Surface forces were measured using an AFM with silica surfaces immersed in C_nTACl (n = 12-18) solutions in the absence of added salt. The results showed long-range attractive forces that cannot be explained by the DLVO theory. The long-range attractions increased with increasing surfactant concentration, reaching a maximum at the point of charge neutralization (p.c.n.) and then decreased. The long-range forces decayed exponentially, with the decay lengths increasing from 3 to 32 nm as the chain length of the surfactants increased from C-12 to C-18. The measured forces can be fitted to the charged-patch model of Miklavic *et al.* (49) by assuming patch sizes that are much larger than the values reported in the literature.

It was found that the decay length decreases linearly with the effective concentration of the CH_2/CH_3 groups of the C_nTACl homologues raised to the power of -1/2, which is in line with the Eriksson *et al.'s* hydrophobic force model derived using a mean-field approach. It appears, therefore, that the long-range attractions observed in the present work are hydrophobic forces originating from changes in water structure across the thin surfactant solution film between the silica surfaces. It is conceivable that hydrocarbon chains in solution disrupt the surface-induced water structure and cause a decrease in hydrophobic force. This observation may also provide an explanation for the very long-range forces observed with silylated, LB-deposited, and thiol-coated surfaces.

3.1 Introduction

Hydrophobicity plays an important role in many different industries such as paper coating, pigment, personal care products, flotation, diamond recovery, and water proofing. It is also important in the processing and handling of the energy minerals such as coal, oil, bitumen, and kerogen, all of which are naturally hydrophobic. In addition, hydrophobicity plays a crucial role in biology, *e.g.*, membrane structure and stability and protein folding. It has also been suggested that the hydrophobicity of bubbles control the stability of foams, which are used in daily lives and many industries. The most widely used measure of hydrophobicity is the water contact angle, which is a thermodynamic property. Hence, it can be used to determine if coalescence, adhesion, wetting or folding can occur, but not how fast. To predict the kinetics of these processes, it is necessary to have information on surface forces.

In colloid chemistry, it is recognized that the kinetics of particle coagulation is controlled by the surface forces. In general, coagulation is *slow* when the surface forces create an energy barrier and conversely coagulation is *fast* when the energy barrier approaches zero. Derjaguin and Dukhin (1) modeled flotation (or bubble-particle interaction) using the surface forces that were known to them at the time, namely, the electrostatic force due to double-layer interaction and the van der Waals dispersion force. However, both of these forces are repulsive in most of the conditions encountered in flotation, which makes it difficult to model flotation, which is fast and spontaneous, using the DLVO theory. Blake and Kitchener (2) showed later that the thin film of water (wetting film) between a hydrophobic solid and an air bubble ruptures fast and spontaneously and that it does so at much larger separation distances than predicted by the classical DLVO theory. These investigators suggested, therefore, the presence of a '*hydrophobic force*' in wetting films. In fact, the presence of the non-DLVO force had been recognized by Laskowski and Kitchener (3) three years prior to the Blake and Kitchener work. They found that methylated and pure silica particles had practically the same ζ-potentials and yet the former floated while the latter did not, which led to the suggestion that a long-range '*hydrophobic influence*' may be responsible for the rupture of the wetting film and flotation. They thought that the hydrophobic influence was caused by the instability of the water structure in the vicinity of a hydrophobic surface.

It was not until 1982 that the hydrophobic force was measured directly using the surface force apparatus (SFA) by Israelachvili and Pashley (4). It decayed exponentially in the 0-10 nm range with a decay length of 1 nm. The authors postulated that the long-range force was related to the hydrophobic effect, which is known to originate from the changes in water structure surrounding hydrocarbon moieties. Many other investigators conducted follow-up experiments and showed the existence of even longer range hydrophobic forces with decay lengths in the range of 10-30 nm (5-11). The strongest opposition to the existence of the hydrophobic force came from those who observed nano-bubbles on hydrophobic surfaces during measurements (12-16). These investigators suggested that the "so-called hydrophobic force" is actually the capillary force caused by the coalescence of preexisting nano-bubbles when two hydrophobic surfaces approach each other. Supporting evidence was shown by Sakamoto *et al*. (16), who observed long-range attraction in air-saturated solutions but not in degassed solutions. However, the repeat experiment conducted by Zhang *et al*. (17) showed that long-range attractions were observed both in degassed and air-saturated solutions. Apparently, Sakamoto *et al.*

had difficulty in detecting the hydrophobic force in degassed solutions because they used stiffer cantilever springs than Zhang *et al.* (17) and the data were plotted in the same scale as the capillary forces they were measuring. Meyer *et al.* (18) showed also that degassing reduced the long-range attractive force but the short-range force remained the same.

It has been shown that hydrophobic forces in general increase with increasing contact angle (19), which in turn increases with increasing chain length of the surfactants used to hydrophobize a surface. However, there has not been a systematic study of the effect of chain length on the hydrophobic forces measured between solid surfaces hydrophobized *in situ* by exposing them in surfactant solutions. It was, therefore, the objective of the present investigation to measure the hydrophobic forces between silica surfaces in water solutions of alkyltrimethylammonium chloride (C_nTACl) homologues. The results are used to discuss the possible origins of the hydrophobic force.

3.2 Experimental

Materials

Nanopure water was obtained by using the Nanopure III (Barnstead IA) water system. The conductivity of the water was 18.2 MΩ/cm at 25°C and the surface tension was 72.5 mN/m at 22°C. The water and surfactant solutions were used without purging with ultra pure nitrogen to exclude atmospheric CO_2. Thus, the pH of the solutions was in the range of 5.6-5.8. NaOH (99%, Mallinckrodt Baker) was used without further purification. Liquid reagents, such as chloroform (99.9%, Burdick & Jackson), H_2SO_4 (98%, VMR International) and H_2O_2 (30%, VMR International) were used as received without further purification. The surfactants used in the present work included dodecyltrimetyl-ammonium chloride (C_{12}TACl), tetradecyltrimetylammonium chloride (C_{14}TACl), hexadecyltrimetylammonium chloride (C_{16}TACl) and octadecyltrimetylammonium chloride (C_{18}TACl) all from TCI and of greater than 97% purity. They were used without further purification. Solutions of low surfactant concentrations were prepared in containers with volumes of at least 100 mL to prevent significant depletion of surfactant *via* adsorption onto the glass walls.

Quartz plates (Hereaus Amersil, Inc.) and silicon wafers (100 oriented, Polished Wafer, Sumco, Oregon) were boiled in a H_2SO_4/H_2O_2 solution (7:3 by volume) at 120^{o}C for 60 minutes. The plates were rinsed thoroughly with a large amount of Nanopure water, equilibrated with the water in a sealed vial for at least 20 minutes, removed and dried by blowing pure nitrogen gas over the surface, and then used for experiments.

Surface Force Measurements

Surface forces were measured using a Digital Instrument Nanoscope IIIa AFM (Digital Instruments, CA) at room temperature (22±1^{o}C) using the colloidal probe technique (20,21). The separation distance (*H*) between the probe (glass sphere) and the substrate (silica plate) was measured by monitoring the deflection of the cantilever on which the probe was attached. Silicon-nitride NP-20 cantilevers were obtained from Veeco, CA. The triangular cantilevers were calibrated using the resonant frequency technique (22). The errors associated with the calibration were within ±7%. The glass spheres (12-20μm in diameter) were obtained from Polysciences, Inc., Warrington, PA. They were soaked

in chloroform for 30 minutes and UV-irradiated for 30 minutes to remove possible organic contaminants. In each experiment, a glass sphere was glued onto a cantilever with EPON 1004 resin (Shell Chemical Co.). The diameter of the glass sphere was measured using an Olympus BH-2 light microscope with a video caliper with an error of ±0.5 μm. Measured forces (F) were normalized with respect to the radii (R) of the glass spheres. Combined errors between the measurements of the spring constants and the sphere diameters were within ±12% in the normalized (F/R) calculations. For a fully equilibrated thin film system, F/R equals 2π times the change in film tension as film thickness decreases from infinity to a finite separation distance of H (23).

For a given surfactant, surface forces were measured at different concentrations. For a given set of measurements, the surfactant solutions were injected into an AFM liquid cell starting from the lowest concentration and continuing to the highest. At a given concentration, the glass sphere and silica plate were equilibrated for 1 hour before starting the measurements. All of the measurements were conducted in air-equilibrated solutions, as it was shown previously that there were no significant differences between the measurements conducted in degassed and air-saturated solutions as long as care was taken to avoid cavitation (17).

AFM Imaging

Images of the surfaces of the silica plates and silicon wafers immersed in water were taken using the Nanoscope IIIa AFM. V-shaped and oxide-sharpened silicon nitride cantilevers with nominal spring constant of $k = 0.12$ Nm^{-1} were used in the present work. All AFM images reported are height (constant force) images captured at 22±1°C with integral and proportional gains of about 1.0. Scan rates of 3-5 Hz were used at contact mode. The images were captured after a substrate was soaked in an aqueous solution for about 1 hour using the soft contact-mode imaging technique. Minimum contact forces were used in order not to disturb the adsorbed surfactant layer.

Contact Angle Measurement

A silica plate was immersed in a surfactant solution for a desired period of time. Contact angles were measured by means of a goniometer using the captive bubble technique, in which silica a plate was kept in solution while an air bubble was brought to contact. At a given experimental condition, a total of five measurements were taken and averaged.

3.3 Results

3.3.1 Force Measurements in Surfactant Solutions

Figure 3.1 shows the surface forces (F/R) measured between a glass sphere of radius R and a flat silica plate in $C_{12}TACl$ solutions as a function of the closest distance (H) separating the two macroscopic surfaces. The inset, which represents the force curve obtained in pure water, shows a strong repulsive force due to the electrostatic repulsion between two negatively charged surfaces. All of the force curves shown in Figures 3.1-3.4 were smooth, without showing steps or kinks, indicating that the adsorption systems were relatively free of contamination or air bubbles.

In the presence of the cationic surfactant, the repulsive force disappeared almost completely due to charge neutralization. The force curve obtained at 8×10^{-4} M $C_{12}TACl$ showed a weakly attractive force at H<10 nm. At 10^{-3} M $C_{12}TACl$, the attractive force became stronger and considerably longer ranged, the net attractive force being detectable at $H\approx25$ nm. As the surfactant concentration was further increased to 3×10^{-3} M, the attractive force was significantly reduced.

Several investigators (24-27) showed that the attractive forces measured between hydrophobic surfaces became the strongest at the surfactant concentrations close to the points of charge neutralization (p.c.n.), which is defined as the concentrations where the surface charge of the substrate is neutralized by the adsorption of an ionic surfactant. The F/R vs. H curves given in Figure 3.1 show the p.c.n. for the silica-$C_{12}TAC$ system is approximately 10^{-3} M, as the attractive force was the strongest at this concentration. At the p.c.n., most of the negative sites are occupied by the $C_{12}TA^+$ ions, forming hemimicelles in which the hydrocarbon tails of the adsorbed surfactant molecules are closely packed (28).

At 3×10^{-3} M $C_{12}TACl$, additional $C_{12}TA^+$ ions adsorb on silica, but most probably with inverse (or flip-flop) orientation. Such an orientation would be favored as it would cost less energy to insert additional surfactant molecules into the adsorption layer with their polar heads farthest apart from each other. The inverse orientation exposes the head groups toward the aqueous phase and, hence, causes the surface to be less hydrophobic. Therefore, the decrease in attractive force at the higher concentration can be attributed to the inverse orientation.

Figure 3.2 shows the surface forces measured between a glass sphere and a silica plate in the presence of a longer-chain ($C_{14}TACl$) homologue. The trend is the same as observed with $C_{12}TACl$. At 8×10^{-5} M $C_{14}TACl$, the repulsive double layer force that was observed in pure water was completely suppressed by charge neutralization, and a net-attractive force was observed. At 10^{-4} M $C_{14}TACl$, the net-attractive force became stronger. As the surfactant concentration was further increased to 5×10^{-4} M $C_{14}TACl$, the measured force became totally repulsive. It appears, therefore, that the p.c.n. is close to 10^{-4} M $C_{14}TACl$. At concentrations above the p.c.n., additional $C_{14}TA^+$ ions adsorbed, causing the observed force totally repulsive. It is likely that additional surfactant ions adsorbed with inverse orientation, rendering the surface hydrophilic. It is interesting to note here that an increase in the number of ethylene groups by two caused a ten-fold decrease in the concentration (p.c.n.) at which the strongest attractive force was observed. This observation is a powerful message that longer-chain surfactants be used to increase the attractive force between hydrophobic surfaces.

Figure 3.3 shows the results obtained with an even longer-chain ($C_{16}TACl$) homologue. At 10^{-5} M $C_{16}TACl$, the repulsive force disappeared completely and a net-attractive force appeared. At 3×10^{-5} M, the measured force became most attractive, indicating that the p.c.n. for the silica-$C_{16}TACl$ was close to this concentration. At 5×10^{-5} M, the attractive force was somewhat reduced, most probably due to the inverse orientation of the $C_{16}TA^+$ ions. It is interesting to note here that the attractive forces observed with the C-16 cationic surfactant were substantially longer ranged than those observed with shorter-chain (*i.e.*, C-12 and C-14) homologues.

The results obtained with $C_{18}TACl$ are presented in Figure 3.4. At 3×10^{-6} M $C_{18}TACl$, a very long-ranged and net-attractive force was observed. When the

concentration was raised to 5×10^{-6} M, the attractive force was strongest. At 10^{-5} M, the attractive force was reduced a little. Thus, the p.c.n. of the silica-C_{18}TACl system was approximately 3×10^{-5} M, which was significantly lower than observed for the shorter chain homologues. The most interesting aspect of the data shown in Figure 3.4 was that the C-18 surfactant gave much stronger and longer-range attractive forces than observed for the shorter-chain homologues. With the C_{18}TACl, net attractive forces were observed at separations as large as 100 nm.

The strongest attractive force curves shown in each of Figures 3.1-3.4 are redrawn in Figure 3.5, and were fitted to a single-exponential force law, *viz*.,

$$F / R = -C \exp(-H / D) \qquad [1]$$

where C and D are fitting parameters. Table 3.1 gives the values of these parameters as well as the Debye length (κ^{-1}). From Figure 3.5, it is clearly seen that the maximum attractive force that can be created by the adsorption of a C_nTACl on silica increases with increasing hydrocarbon chain length. As shown in Table 3.1, the decay length (D) of the attractive force increases with chain length. It was only 3 nm at n=12. As n was increased to 14, 16, and 18, D was increased to 6, 14, and 32 nm, respectively. While D was very sensitive to chain length, the values of C stayed practically the same, 1.3-1.4 mN/m. It is important to note here that the surfactant concentration at which surface charge is neutralized and the maximum hydrophobic force observed decreases substantially with increasing chain length.

Using an AFM, one can estimate the adhesion force between two macroscopic surfaces by measuring the force required to detach them from each other after an initial contact. Table 3.3 shows the detachment forces measured between glass sphere and silica plate immersed in C_nTACl (n = 12, 14, 16, 18) solutions at the concentrations where the strongest attractions were observed. The contact angles of the silica plates immersed in the surfactant solutions are also given in the table. As shown in Table 3.3, both the adhesion (or detachment) force and contact angle increased with hydrocarbon chain length. As n was increased from 12 to 18, the contact angle increased from 47 to 64 degrees, while the detachment force increased from 13.4 to 60 mN/m. In principle, the adhesion force, which should be the same in magnitude as detachment force but opposite in sign, should be a function of interfacial tension, which should increase with increasing contact angle, as will be discussed later.

3.3.2 AFM Images

Figure 3.6 shows the contact mode AFM images of a fused quartz plate immersed in water. It shows that the surface is smooth with a roughness of less than 2 nm on a 100×100 nm scale. The AFM images show boundaries between fused silica particles of approximately 100 nm.

The presence of the grain boundaries on the fused silica surfaces can make it difficult to see the surfactant molecules adsorbing on the surface. Therefore, the images of surfactant molecules adsorbing on SiO_2 surfaces were taken using silicon wafers as substrates. Figure 3.7a shows an AFM image of a silicon wafer surface immersed in Nanopure water. Before taking the images, the substrate had been boiled in a H_2SO_4/H_2O_2 solution (7:3 by volume) at 120^{o}C for 1 hour to remove possible organic

contaminants and to generate a "clean" oxide surface. The 10×10 μm image shows that the substrate surface is smooth with 0.2 nm roughness. No lumps or scratches were seen, indicating that the surface was clean and free of contaminants. Figure 3.7b shows an image of a silicon wafer surface that had been immersed in 10^{-5} M C_{18}TACl solution for 1 hour. It shows that the surfactant molecules cover most of the surface with some areas unoccupied, suggesting the formation of patches or hemi-micelles. The height of the adsorption layer is approximately 2.2 nm, which is a little less than the length (2.3 nm) of a fully extended C_{18} hydrocarbon chain.

Figure 3.7c and d show the AFM images of a silicon wafer immersed in a 3×10^{-5} M C_{18}TACl solution which was above its p.c.n. The images obtained at this concentration show that the adsorption occurs in patches. The heights of some of the patches are higher than 2.3 nm, indicating bilayer formation. Some of the patches are of 20-30 nm in dimension, while others are larger.

3.4 Discussion

3.4.1 Adsorption Mechanism

When a glass or silica substrate is immersed in water, its surface becomes eclectically charged by the following mechanism:

$$-\overset{|}{\underset{|}{Si}}-OH_2^+ \overset{H^+}{\Leftrightarrow} -\overset{|}{\underset{|}{Si}}-OH \overset{OH^-}{\Leftrightarrow} -\overset{|}{\underset{|}{Si}}-O^- + H_2O \qquad [2]$$

in which silanol (Si-OH) groups are protonated to become positive ($Si\text{-}OH_2^+$) sites or are hydroxylated to become negative ($Si\text{-}OH_2^-$) sites depending on pH. The point of zero charge (p.z.c.) of silica is approximately pH 2 (29, 30). Thus, silica surfaces are negatively charged at pHs above 2. It has been shown, however, that the negative charge density is low until the pH increases above 6 (31, 32). In the present work, direct force measurements were conducted at pH≈5.7, where surface charge densities are relatively low. Under this condition, the adsorption of cationic surfactants may occur in patches (25, 33).

In 1955, Gaudin and Fuerstenau (34) studied the adsorption of dodecylammonium hydrochloride (DAH) on quartz, and introduced the concept of "hemi-micelle" formation (35). More detailed studies conducted by Somasundaran and Fuerstenau (36) and Wakamatsu and Fuerstenau (37) showed that the onset of the hemi-micelle formation is indicated by a sharp decrease in ζ-potential. Below this concentration, which is referred to as the critical hemi-micelle concentration (c.h.c.), the surfactant molecules adsorb individually by displacing the counter-ions, causing no changes in the ζ-potentials. Above the c.h.c., however, the hydrocarbon chains of the surfactant molecules associate with each other, causing a sharp increase in adsorption density and, hence, a sharp decrease in ζ-potentials. When the surfactant concentration is increased further, the surface charge can be neutralized. Above this concentration, which is referred to as point of charge neutralization (p.c.n.), the surfactant molecules adsorb with inverse (or flip-flop) orientation, causing a decrease in hydrophobicity. Thermodynamically, the inverse orientation is favored as it is not necessary to remove some of the hydrated water molecules from polar heads.

It was shown by Herder (38) that the details concerning the formation of an adsorption layer of an ionic surfactant (DAH) onto an ion-exchanging solid surface (mica) are surprisingly complex. Upon raising the surfactant concentration, a localized (site-wise) adsorption mechanism is gradually being replaced by an adsorption mechanism that in the end involves migrating (mobile) surfactant ions. Simultaneously, hemi-micelles are formed, first as immobile patches at low surfactant concentrations (typically two to three orders of magnitude below the c.m.c.) and possibly also as mobile surfactant aggregates at higher surfactant concentrations (typically one order of magnitude below the c.m.c.) which are more closely related to ordinary surfactant micelles in bulk solution. A full bilayer is as a rule finally formed in the c.m.c. concentration range. Reaching equilibrium for an adsorption layer of this kind is an amazingly slow process (many hours), especially for surfactants with a long hydrocarbon tail (17).

The AFM images of the silicon wafers immersed in surfactant solutions support the adsorption mechanism discussed above. Figure 3.7b, which was obtained at 10^{-5} M C_{18}TACl, which was close to the p.c.n. (=5×10^{-6} M), shows patches (or hemi-micelles) of the $C_{18}TA^+$ ions adsorbed on the silica substrate. Many of the patches have coalesced to form a self-assembled monolayer with parts of the surface unoccupied. At this concentration, it appears that the surfactants have the normal mode of orientation with their head groups in contact with the surface and the hydrocarbon tail stretching out toward water. An evidence for this is that the thickness of the adsorption layer is close to the length of the fully-extended C-18 hydrocarbon chains. At 3×10^{-5} M, which is well above the p.c.n, the adsorption layer was non-uniform and the heights of the clusters are much larger than the hydrocarbon chain length, indicating that additional surfactant molecules adsorb on top of the monolayer most probably with inverse orientation.

3.4.2 Effect of Hydrocarbon Chain Length on Adsorption

It has been suggested that the attractive hydrophobic force becomes the strongest at the p.c.n. of a surfactant (24-27), which was confirmed in an earlier work reported for the silica-C_{18}TACl system (17). Thus, one can determine the p.c.n. from a set of force curves obtained at different concentrations of a given surfactant. Table 3.1 gives the values of the p.c.n.'s determined from the data obtained for the C_nTACl-silica systems studied in the present work. Also shown in the table for comparison are the points of zeta-potential reversal (p.z.r.) obtained by Somasundaran *et al*. (28) for the quatz-alkylammonium acetate system. In Figure 3.8, the p.c.n. values given in Table 3.1 have been plotted *vs*. the number of hydrocarbons (n) in the alkyl chains of the C_nTACl homologues. This plot represents the Stern-Grahame equation (39):

$$\ln C_0 = -n_c(\phi/kT) - \ln\left(\Gamma_{\delta}^{+}\right)_0 - \ln(2r) \qquad [3]$$

in which C_0 is the., ϕ is the standard adsorption free energy per mole of CH_2 or CH_3 group and $\left(\Gamma_{\delta}^{+}\right)_0$ is the adsorption density of the cationic surfactant at ζ=0, r is the radius of the polar head of the surfactant, and k is the Boltzmann constant. If the product of $\left(\Gamma_{\delta}^{+}\right)_0$ and $2r$ remain relatively constant for the C_nTACl homologues studied in the present work, a plot of log (p.c.n) *vs*. n should give a slope of $-\phi/2.3kT$, from which one can obtain the value of ϕ = -0.85 kT (-0.50 kcal per mole). This value is pretty close

to the value of -0.97 *kT* obtained from a plot of log (p.z.r.) vs. *n* for the quartz-primary amine system (28, 40). For the ordinary micelles forming in solutions of ionic surfactants, the corresponding figure is about -0.75 *kT* per CH_2 group.

The above discussion shows that a major driving force for adsorption of a long-chain surfactant is the hydrocarbon chain association, which is commonly recognized as hydrophobic effect (41). Therefore, the longer the hydrocarbon chain length is, the larger the hydrophobic effect becomes, which in turn causes a decrease in the p.c.n.

3.4.3 Effect of Chain Length on Detachment Force

In the present work, adhesion (or pull-off) forces were measured at the p.c.n.'s of the C_nTACl homologues where the measured hydrophobic forces were maximum. As shown in Table 3.2, the adhesion forces increased with increasing chain length and contact angle. If the macroscopic objects used for the measurements (*i.e.*, silica plate and glass sphere) behave as rigid solids, one can use the Derjaguin-Muller-Toporov (DMT) relation (42):

$$F_{ad} / R = 4\pi \gamma_{12} \qquad [4]$$

where γ_{12} is the interfacial tension between solid 1 and aqueous solution 2. However, most real solids are not completely rigid and have a certain degree of elasticity, in which case the Johnson, Kendal, Roberts (JKR) theory (43)

$$F_{ad} / R = 3\pi \gamma_{12} \qquad [5]$$

might apply. Both Eqs. (4) and (5) presuppose, however, that the contact free energy equals zero which may be a poor approximation for the cases under discussion. Nevertheless, they suggest that the adhesion force should increase with increasing interfacial tension, which should in turn increase with increasing contact angle.

According to van Oss (44), the interfacial tensions can be calculated using the following relation,

$$\gamma_{12} = \left(\sqrt{\gamma_1^{LW}} - \sqrt{\gamma_2^{LW}}\right)^2 + 2\left(\sqrt{\gamma_1^+\gamma_1^-} + \sqrt{\gamma_2^+\gamma_2^-} - \sqrt{\gamma_1^+\gamma_2^-} - \sqrt{\gamma_1^-\gamma_2^+}\right) \qquad [6]$$

where γ_i^{LW}, γ_i^+ and γ_i^- are the non-polar, acidic, and basic components of the surface free energy of material *i*, respectively. In the present work, the surface tension data needed to calculate γ_{12} have been obtained from the plots of the surface tension components *vs*. the water contact angles of silica, as reported by Pazhianur and Yoon (45). In this reference, the surface properties of silica were varied by controlling the adsorption of octadecyltrichlorochlorosilane (OTS) on the surface. Table 3.2 shows the values of γ_1^{LW}, γ_1^+, and γ_1^- from the plots at the maximum contact angles obtained with the C_nTACl homologues and the values of γ_{12} obtained by substituting those into Eq. [6]. As shown, the interfacial tensions obtained using Eq. [6] are much larger than those obtained using Eq. [5]. The discrepancy may be attributed to the differences in the surface roughness created by the surfactant coatings. According to Israelachvili (46), asperities of

1-2 nm can significantly lower adhesion forces. In order to fit the two sets of γ_{12} values, the JKR model has been modified as follows:

$$F_{ad} / R = 3\pi \gamma_{12} f \qquad [7]$$

in which f represents a roughness factor. In the present work, Eq. [7] was used to back-calculate the values of f from the experimental values of F_{ad} and the values of γ_{12} calculated using Eq. [6]. As shown in Table 3.3, the roughness factors are in the range of 0.4 to 0.5 for the C-14 to C-18 homologues, while it is only 0.26 for C-12 homologue. Accordingly, it would appear, therefore, that the longer-chain surfactants produce rougher surfaces. Although this result doesn't seem unreasonable in view of our AFM imaging data, one has to keep in mind that Eqs. [5] and [6] rest on the tacit assumption of zero contact interaction free energy.

3.4.4 Possible Origin(s) of Hydrophobic Force

Figure 3.5 and Table 3.1 show that the long-range attraction becomes stronger and longer ranged with increasing hydrocarbon chain length. Further, the concentration at which the strongest attractive force was observed increased with increasing carbon number (n) in a chain.

It has been more than twenty years since Israelachvilli and Pashley (4, 47) observed long-range attractive forces between two mica surfaces hydrophobized with hexadecyltrimethylammonium bromide (C_{16}TABr). Numerous other investigators observed similar results (5-11), and proposed possible causes for the long-range attraction. (12, 16, 23, 48, 49) However, its origin is not yet fully understood. In the following, we discuss the possible origin(s) of the long-range attraction between hydrophobic surfaces. Discussing the effect of the chain length may shed light from a different angle on this complex and continually perplexing issue.

It was shown previously (17) that the long-range attractive force deceases in the presence of inorganic electrolyte, which may be taken as evidence that the non-DLVO force is of electrostatic origin. In this regard, it is of interest to analyze the force data obtained in the present work in terms of the charged-patch model developed by Miklavic *et al*. (49). Their model suggests that the long-range attraction may originate from the electrostatic correlation attraction between the patches of surfactant molecules formed on surfaces. It was necessary to assume, of course, that the patches are electrically charged. The charged-patch model was based on the recognition that long-chain surfactants adsorb in patches (or hemi-micelles) at a relatively low concentration. According to Fuerstenau and Pradip (50), hemi-micelles begin to form at concentrations 2-3 orders of magnitude below the c.m.c. The AFM (17) and SEM (51) images of the surfactant-coated surfaces indeed showed patches, as is also shown in Figure 3.7. Further, the aggregation numbers of the hemi-micelles (or 'soloids') determined using the electron spin resonance (ESR) and fluorescence spectroscopic techniques showed the patch-wise adsorption mechanism (52, 53). Table 3.3 shows that the roughness of the surfactant-coated surfaces increases with increasing chain length, which may serve as an indication that patch size and, hence, hydrophobic force increases with chain length.

Miklavic *et al*. (49) considered that the patches are charged but the surface as a whole is neutral. The model implies that the interaction between the two surfaces covered with patches of positive and negative charges is always attractive when the patches are sufficiently mobile and free to correlate with each other. At an infinite separation, the patches may be distributed randomly. As the separation decreases, the patches migrate laterally on the surface in order for the system to minimize the free energy. Assuming that the patches are distributed in a square lattice with a dimension of *a*, the free energy of interaction per unit area ($G(H)$) is given as follows:

$$G(H) = -\frac{A}{kT}\Omega^2 \exp\left(-2q_{\min}H\right) \qquad [8]$$

where A is the area of the unit cell, Ω is a constant which varies with surface property (surface potential or charge), reciprocal lattice vector, and lateral displacement. As shown, the interaction energy decays exponentially, with a decay length of $\left(2q_{\min}\right)^{-1}$, in which $q_{\min}$ is given as follows:

$$q_{\min} = \left[\left(\pi/a\right)^2 + \kappa^2\right]^{1/2} \qquad [9]$$

where κ is the reciprocal Debye length. At a high electrolyte concentration, $q_{\min} \approx \kappa$; therefore, the interaction energy should decay as $\left(2\kappa\right)^{-1}$. At a low electrolyte concentration, κ is small; therefore, $q_{\min}$ should vary inversely with *a*.

From the decay lengths, D ($=\left(2q_{\min}\right)^{-1}$), measured in the present work, one can obtain the values of $q_{\min}$, which can then be used to obtain the values of *a* using Eq. [9]. In this exercise, the κ values have been calculated from the concentrations of the ionic surfactants used in force measurements. As shown in Table 3.4, the lattice patch size *b*, which may be roughly estimated from the value of *a* by multiplying it with a factor 0.75 used by Miklavic *et al.* (49), increases with chain length. This finding is in agreement with the results obtained by Fan *et al*. (52) and Strom *et al*. (53), who showed that the aggregation numbers of the hem-micelles increased with increasing chain length. These investigators studied the adsorption of C_{12}TABr, C_{14}TABr, and C_{16}TABr on silica and alumina.

Eq. [9] suggests that decay length (or $q_{\min}$) is mainly controlled by two parameters, *i.e.*, *a* and κ. The data presented in Table 3.4 show that the contribution from *a* is more significant than from κ in determining the range of attraction, but κ still plays an important role, particularly with the shorter chain surfactant, *e.g.*, C_{12}TACl. These findings may be anticipated from the fact that all of the force data presented in Table 3.4 were obtained in the absence of supporting electrolyte. Under this condition, the residual concentrations of the ionic surfactants act as electrolytes that can dampen the hydrophobic force.

It has been shown in the present work that the long-range attraction was strongest at p.c.n., and that the adsorption of the C_nTACl on silica is likely to occur as patches. Both of these observations provide a basis for discussing the origin of the long-range attraction

in view of the model developed by Miklavic *et al*. (49). A question remains, however, as to whether it is physically possible for the patches to be positively charged, while unoccupied silica surface remains negatively charged. This would undoubtedly be the case if the adsorption occurs as micelles (54), or as bilayers (55). In both of these cases, the number of the surfactant molecules adsorbing in each patch (aggregation number) can exceed the negative charge sites underneath, causing it net positively charged. However, the micellar or bilayer adsorption should render the surface hydrophilic due to the orientation of the polar heads toward the aqueous phase. Therefore, such adsorption mechanisms cannot explain the experimental observations that both the long-range attraction and contact angle reached the maxima at a p.c.n..

Somasundaran and Fuerstenau (36) showed, on the other hand, that long-chain surfactants adsorb as hemi-micelles, in which the head groups of the surfactant molecules are in touch with substrates and the hydrocarbon tails point toward the aqueous phase. Such orientation renders the surface hydrophobic. Once the surface has been neutralized, the surfactant molecules begin to adsorb with inverse orientation, rendering the surface hydrophilic. Thus, the surface should become most hydrophobic at a p.c.n, as has been demonstrated by Fan *et al*. (52) with a series of vacuum flotation experiments. This finding is in agreement with the force data obtained in the present work and the contact angle data reported previously (17).

For the case of C_nTA^+ ions adsorbing on silica, the hemi-micelles formed at a p.c.n. must be positively charged in order for the surface, which includes the patches of unoccupied negative charge sites, to be neutral as a whole. The positive charges associated with the hemi-micelles should come from the surfactant molecules co-adsorbing into the hemi-micelles along with those that adsorb on negatively charged sites. Fuerstenau and Pradip (50) showed that at p.c.r. the co-adsorption occurs with the head groups in contact with the surface which gives rise to optimal flotation. Beyond the p.c.r., the co-adsorption occurs with the head groups oriented toward the water phase.

Table 3.4 shows the patch sizes vary from 18 to 172 nm with increasing chain length. However, these values are substantially larger than those estimated from the aggregation numbers reported by Fan *et al*. (52): 5.4, 7.1, and 10 nm for the C_{12}-, C_{14}-, and C_{16}-TABr hemi-micelles formed on alumina. These values were obtained by assuming that the cross-sectional area of the surfactant molecules in the hemi-micelles is 1 nm^2, *i. e.* a value somewhat larger than reported for spherical micelles formed in solution (about 0.6 nm^2). Assuming instead that the hydrocarbon chains are closely packed on the surface, one can use the value of 0.21 nm^2 as the cross-sectional area, in which case the patch size becomes even smaller, *i.e.*, 2.5, 3.2, and 4.8 nm^2 for the C_{12}-, C_{14}-, and C_{16}-TABr hemi-micelles. These numbers are close to the value of 6.5±1 nm^2 obtained from the scanning tunneling microscopic (STM) images of the (111) gold surface coated with dodecanethiol. On the other hand, much larger domains (20-30 nm) were observed on silica surfaces coated with OTS (56), most likely due to cross-linking polymerization. It appears, therefore, that the charged patch model of Miklavic *et al*. (49) requires substantially larger patches than observed experimentally with self-assembled monolayers to predict the long-range attractive forces measured in the present work. Moreover, it seems unlikely that the hemi-micelles (patches) formed at or slightly below the p.c.n. can migrate on the surfaces rapidly enough to actually generate an attractive correlation force.

Figure 3.9 shows a plot of D *vs.* κ^{-1} for the data obtained with C_nTACl homologues. Also shown is a plot of the D values obtained with $C_{18}TACl$ in the presence of varying concentrations of NaCl (17). The latter has a slope of ½ as predicted by Eq. [9]. The former, on the other hand, has a slope of ¼, for which there is so far no adequate theoretical explanation.

Figure 3.10 shows a plot of D *vs.* $(C_0 n)^{-1/2}$, where C_0 is the concentration of C_nTACl in bulk solution and n is the number of carbons in a hydrocarbon chain. The linear relationship suggests that the range of hydrophobic force is simply a function $C_0 n$, which is the molar concentration of the CH_2 and CH_3 groups in solution. In effect, the results presented in Figure 3.10 shows that the long-range attraction decreases with increasing concentration of the species that can disrupt the structure of water, *i.e.*, hydrocarbons. That the long-range attraction decreases in the presence of NaCl, as shown in Figure 3.9, may be given the same explanation, that is, the long-range attraction decreases with increasing concentration of the species, *i.e.*, Na^+ and Cl^- ions in this case, that can disrupt the water structure. Thus, the results presented in Figures 3.9 and 3.10 show that the long-range attraction is strongest when water is in its pristine state. Any foreign species added to water causes a decrease in D. Likewise, Wang and Yoon (57) showed that the long-range hydrophobic forces observed in the thin films of water between two air bubbles are at a maximum in pure water and decrease with increasing surfactant and/or electrolyte concentrations.

According to the Derjaguin approximation (58), the surface force (F) normalized by the diameter of the sphere (R) can be given as follows:

$$F / R = 2\pi\left(\gamma^{f} - \gamma_{\infty}^{f}\right) \qquad [10]$$

in which γ^f is the film tension at a separation distance H and γ_∞^f is the same at an infinite separation distance, *i.e.*, in the bulk solution. Figure 3.10 shows a schematic representation of the possible changes in γ^f and γ_∞^f as a function of surfactant concentration. In general, both should decrease with increasing concentration. It has been shown that at very low concentrations, ionic surfactants adsorb as individual ions by substituting the counter ions in the electrical double layer without causing changes in ζ-potentials (37). Therefore, γ^f is higher than γ_∞^f due to a positive (repulsive) surface force. When the surfactant concentration becomes higher than the critical hemimicelle concentration (c.h.m.c.), surfactant adsorption entails a reduction in surface charge and causes γ^f to become lower than γ_∞^f, which in turn creating a negative (attractive) surface force. In this region, γ^f decreases more rapidly than γ_∞^f due to the higher surfactant concentration near the surface and the attractive surface force. At a p.c.n., the adsorption density reaches a plateau. Therefore, an increase in surfactant concentration should cause a sharper decrease in γ^f as shown, which gives rise to a maximum in the attractive force. At still higher concentrations, both γ^f and γ_∞^f decrease rapidly with concentration, but γ^f stays larger than γ_∞^f due to the charged bilayers (or micelles) formed on the surface, creating the second range of repulsive forces. In short, surface force is repulsive at low

concentrations, becomes attractive, and then becomes repulsive again at higher concentrations, as shown in the force curves presented in Figures 3.1-3.4.

Eriksson *et al*. (23) derived theoretical expressions for γ^{f} and γ_{∞}^{f} using a mean field approach based on the 'square-gradient approximation'. By substituting those into Eq. [10], they obtained the following expression for the hydrophobic force:

$$F / R = -B\left[\coth(bH/2) - 1\right] \qquad [11]$$

which can be simplified to:

$$F / R = -2B\exp(-bH) \qquad [12]$$

for large enough separations. Eq. [12] shows that b^{-1} can be identified with D and that $2B$ is equivalent to C of Eq. [1]. Furthermore, according to Eriksson *et al*.,

$$b^{-1} = \sqrt{c_3 / 2c_2} \qquad [13]$$

where c_2 and c_3 are constants which account for the free energy costs of structuring the water and forming order parameter gradients, respectively. From Figure 3.10, it is seen that the decay length D (or b^{-1}) varies as $(C_0 n)^{-1/2}$. According to Eq. [13], such a relationship can be generated if we assume that c_2 is proportional to $(C_0 n)^{1/2}$ and c_3 is inversely proportional to $(C_0 n)^{1/2}$. In other words, the presence of surfactant ions would make it more costly free-energy-wise to obtain a certain ordered water state, whereas it would be less costly with the gradients in the order parameter function in the vicinity of a hydrophobic surface. Although these assumptions seem reasonable, they are nevertheless in need of further justification.

Based on the data obtained in the present work, two possible origins for the long-range attractions have been discussed. The charged-patch model of Miklavi**c** *et al.* (49) seems to provide an explanation at high electrolyte concentration. At low electrolyte concentrations, however, it is necessary to assume that the patch sizes are much larger than known from experimental work. A basic premise of the model is that the patches have lateral mobility. Otherwise, the model predictions are too small to predict the long-range forces measured between hydrophobic surfaces. A question arises then as to whether the charged patches are indeed mobile enough to give rise to long-range attractions. It is conceivable that *physically* adsorbing surfactant molecules might possess the necessary molecular and micellar mobility that is a prerequisite for the applicability of the theory of Miklavic *et al*. (49). However, ionic surfactants adsorb primarily on oppositely charged surface sites rather than being evenly distributed across the surface. For a surfactant molecule to be mobile, it may have to jump from one site to another, which is likely to be a slow process when the surfactant-site bond is fairly strong. Needless to say, the corresponding aggregate mobility should be exceedingly slow. Thus, correlation attraction might possibly arise in the concentration range well above the p.c.n., where, however, electrostatic repulsion as a rule predominates. Further, the charged-

patch model does not explain the long-range forces observed with silylated surfaces and Langmuir-Blodgett-deposited surfaces. The surfactants in neither of these two surfaces are likely to be mobile. It should also be noted here that long-range attractions have been observed with thiolated gold surfaces, which is a well-known chemisorbing system.

The second possibility discussed above is related to water structure. It suggests that surfactant monomers and inorganic electrolytes break the hydrogen bond network present in thin watery films between hydrophobic surfaces, thereby reducing the long-range attraction. A short-chain surfactant requires a higher monomer concentration in solution to obtain a given surface coverage, which would be the reason that it gives a relatively short-range attraction. Chemisorbing surfactants such as thiols would leave very few monomers in solution, which may be conducive to creating long-range attractions. The very long-range attractions observed with silylated and LB-deposited surfaces may be explained in the same vein. The circumstance that the experimental data support Eriksson *et al.*'s theoretical model (23), which is based on the changes in water structure across a hydrophobic surface-solution interface, is yet another reason to further explore the possibility of the hydrophobic force actually being a structural force.

3.5 Conclusions

A series of surface force measurements were measured with silica surfaces coated *in situ* with C_nTACl homologues with n = 12-18 using an AFM. The measured forces decayed exponentially with separation, with the decay lengths varying in the range of 3-32 nm. With a given surfactant, the strongest attractions were observed at the p.c.n. Both the maximum decay lengths measured at the p.c.n.'s and the adhesion forces increased with increasing chain length. The adhesion forces can be predicted from the solid-liquid interfacial tensions, with appropriate corrections for surface roughness. It was found that the roughness increased with increasing chain length.

The long-range forces measured in the present work were analyzed in terms of the migrating charged-patch model, which might explain the forces measured in high electrolyte concentrations. For the long-range attractions measured in the absence of added salt, however, it was necessary to assume that the patch sizes were substantially larger than those measured experimentally and reported in the literature. Furthermore, there is no evidence that hemimicelles are mobile in the p.c.n. concentration range.

A plot of the maximum decay lengths measured at p.c.n.'s *vs.* the concentration of the CH_2 and CH_3 groups in solution shows a linear relationship, which supports the formalism derived by Eriksson *et al.* from the mean-field theory by considering the structural changes across the thin water solution film between the silica surfaces. It is possible that the residual surfactant monomers in solution break the structure of the water and cause the long-range force to decrease.

3.6 References

(1) B. V. Derjaguin, S. S. Duhkin, Trans. Inst. Min. Metall. 1961, 70, 221.
(2) T. D. Blake, J. A. Kitchener, J. Chem. Soc Faraday Trans. 1972, 68, 1435-1442.
(3) J. Laskowski, J.A. Kitchener, J. Colloid Interface Sci. 1969, 30, 391.
(4) J. N. Israelachvili, R. M. Pashley, Nature, 1982, 300, 341.
(5) H. K. Christenson, P.M. Claesson, Science, 1988, 239, 390.

(6) Ya. I. Rabinovich, B.V. Derjaguin, Colloids Surf., 1988, 30, 243.
(7) Y. H. Tsao, D. F. Evans, H. Wennerström, Science 1993, 262, 547-550.
(8) J. L. Parker, P. M. Claesson, P. Attard, J. Phys. Chem. 1994,98, 8468-8480.
(9) J. Wood, R. Sharma, Langmuir 1995, 11, 4797-4802
(10) M. Hato, J. Phys. Chem. 1996, 100, 18530-18538.
(11) R.-H. Yoon, S. A. Ravishankar, J. Colloid and Interface Sci., 1996, 179, 403-411.
(12) P. Attard, Langmuir 1996, 12, 1693-1695.
(13) N. Ishida, M. Sakamoto, M. Miyahara, K. Higashitani, Langmuir, 2000, 16, 5681-5687.
(14) N. Ishida, T. Inoue, M. Miyahara, K. Higashitani, Langmuir, 2000, 16, 6377-6380
(15) J. W. G. Tyrrell, P. Attard, Langmuir, 2002, 18, 160-167.
(16) M. Sakamoto, Y. Kanda, M. Miyahara, K. Higashitani, Langmuir 2002, 18, 5713-5719.
(17) J. Zhang, R.-H. Yoon, M. Mao, W. A. Ducker, Langmuir, 2005; 21, 5831-5841.
(18) E. E. Meyer, Q. Lin, J. N. Israelachvili, Langmuir, 2005, 21, 256-259.
(19) R.-H. Yoon, S.A. Ravishankar, J. Colloid Interface Sci., 1996, 179, 391-402.
(20) W. A. Ducker; T. J. Senden; R. M. Pashley, Nature 1991, 353, 239-241.
(21) W. A. Ducker; T. J. Senden; R. M. Pashley, Langmuir 1992, 8, 1831-1836.
(22) J. P. Cleveland; S. Manne, D. Bocek, P. K. Hansma, Rev. Sci. Instrum. 1993, 64, 403-406.
(23) J. C. Eriksson, S. Ljunggren, P. M. Claesson, J. Chem. Soc., Faraday Trans. 2, 1989, 85, 163-176.
(24) J.L. Parker, V.V. Yaminsky, P.M. Claesson, J. Phys. Chem. 97, 1993, 7706.
(25) M.W. Rutland, J.L. Parker, Langmuir 10, 1994, 1110-1121.
(26) P. Kékicheff, O. Spalla, Phys. Rev. Lett. 75, 1995, 1851.
(27) H. K. Christenson, P. M. Claesson, Adv. Colloid Interface Sci., 2001, 91, 391- 436.
(28) P. Somasundaran, T. W. Healy, D. W. Fuerstenau J. Phys. Chem. 1964, 68, 3562-3566.
(29) Adsorption on Silica Surface, E. Papirer (ed), Surfactant Science Series, Vol. 90, New York, Marcel Dekker, Inc. 2000
(30) G. A. Parks, Chem. Rev., 1965, 65(2), 177-198.
(31) J. Zajac, J. L. Trompette, and S. Partyka, Langmuir, 1996, 12, 1357-1367.
(32) T. P. Goloub, L. K. Koopal, B. H. Bijsterbosch. Langmuir, 1996, 12, 3188-3194.
(33) K. Wong, B. Cabane, R. Duplessix, and P. Somasundaran, Langmuir, 1989, 5, 1346-1350.
(34) M. Gaudin, D. W. Fuerstenau, Trans. AIME, 1955, 202,958.
(35) D. W. Fuerstenau, Pure Appl Chem 1970, 24, 135.
(36) P. Somasundaran, D. W. Fuerstenau, J Phys Chem 1966;70:90.
(37) T. Wakamatsu, D. W. Fuerstenau, Adv Chem Ser 1968;79:161.
(38) P. C. Herder, J. Colloid and Interface Sci., 1990, 134, 2, 346-356.
(39) D. C. Grahame, Chem. Rev., 1947, 40, 441.
(40) P. Somasundaran, L. Huang. Adv. Colloid Interface Sci., 2000, 88, 179-208
(41) C. Tanford,, "The Hydrophobic Effect," 1980, 2nd ed. Wiley, New York.
(42) B. V. Derjaguin, V. M. Muller and Yu. P. Toporov, J. Colloid Interface Sci., 1975, 53, 2, 314-326.
(43) K.L. Johnson, K. Kendall, A.D. Roberts, Proc. R. Soc. London, A324, 1971, 301.

(44) C. J. Van Oss, “Interfacial forces in aqueous media,” Marcel Dekker, 1994.
(45) R. Pazhianur, R. H. Yoon, Miner. Metall. Process. 20, 4, 2003, 178–184.
(46) J. N. Israelachvili, “Intermolecular and Surface Forces: With Applications to Colloidal and Biological Systems,” 1992 2nd ed., Academic Press, p329.
(47) J. N. Israelachvili, R. M. Pashley, J. Colloid Interface Sci., 1984, 98, 500.
(48) P. M. Claesson, H. K. Christenson, J. Phys. Chem. 1988, 92, 1650-1655.
(49) S. J. Miklavic, D. Y. C. Chan, L. R. White, T. W. Healy, J. Phys. Chem. 1994, 98, 9022-9032.
(50) D.W. Fuerstenau,T, Pradip, Adv. Colloid Interface Sci., 2005, 114–115, 9-26.
(51) E. Delamarche, B. Michel, Ch. Gerber, D. Anselmetti, H.-J. Guntherodt, H. Wolf, H. Ringsdorf, Langmuir 1994,10, 2869-2871.
(52) A. Fan, P. Somasundaran, N.J. Turro, Langmuir, 1997, 13, 506.
(53) C. Ström, P. Hansson, B. Jönsson, O. Söderman, Langmuir, 2000, 16, 2469.
(54) T. Gu, Z. Huang, Colloids Surf., 40, 1989, 71.
(55) M. A. Yeskie, J. H. Harwell, J. Phys. Chem., 1988, 92, 8, 2346-2352.
(56) Ya. I. Rabinovich, R.-H. Yoon, Langmuir 1994, 10, 1903-1909.
(57) L.Wang, R-H. Yoon, Langmuir, 2004, 20, 11457-11464.
(58) B.V. Derjaguin, Kolloid Z. 1934, 69, 155.

Table 3.1. The parameters of Eq. [1] obtained for the force curves measured at the p.c.n's of the silica-C_nTACl system

Surfactant	p.c.n. (M)	p.z.r.[1] (M)	C (mN/m)	D (nm)	κ^{-1} (nm)
C_{12}TACl	$1x10^{-3}$	$2x10^{-3}$	1.3	3	9.5
C_{14}TACl	$1x10^{-4}$	$4x10^{-4}$	1.4	6	30
C_{16}TACl	$3x10^{-5}$	$7x10^{-5}$	1.3	14	54.8
C_{18}TACl	$5x10^{-6}$	$8x10^{-6}$	1.4	32	134

*point of zeta-potential reversal, from Somasundaran *et al*. (28).

Table 3.2 The interfacial tensions at the silica/water interface in C_nTACl solutions as calculated using Eq. [6] from the surface tension data given in Ref. (44)

Material	Contact angle (degree)	γ^{LW} (mJ/m^2)	γ^+ (mJ/m^2)	γ^- (mJ/m^2)	γ_{12} (mJ/m^2)
water	-	21.8	25.5	25.5	-
$C_{12}TACl$	47	42	2	22.5	5.51
$C_{14}TACl$	51	41	1.8	21.5	6.07
$C_{16}TACl$	58	40	1.5	16.5	10.3
$C_{18}TACl$	64	38	1	13	13.93

Table 3.3 Comparison of the interfacial tensions at the silica/C_nTACl solution interfaces as obtained from the adhesion forces using the JKR equation and the acid-base theory[1]

Surfactant	p.c.n. (M)	Contact angle (degree)	Adhesion force (mN/m)	γ_{12} (mJ/m^2)		^2f
				Acid/Base	JKR*	
C_{12}TACl	$1x10^{-3}$	47	13.4	5.51	1.42	0.26
C_{14}TACl	$1x10^{-4}$	51	23.0	6.07	2.44	0.40
C_{16}TACl	$3x10^{-5}$	58	49.0	10.3	5.20	0.50
C18TACl	$5x10^{-6}$	64	60.0	13.9	6.37	0.46

[1]Eq. (6); ^2f represents the roughness factor calculated using Eq. (7).

Table 3.4 The parameters of Miklavic *et al.*'s charged-patch model as obtained by fitting the decay lengths obtained at the p.c.n.'s of the silica/C_nTACl system

Surfactant	p.c.n. (mM)	D (nm)	q_{min}	κ^2	$(\pi/a)^2$	a (nm)	b (nm)
C_{12}TACl	1	3	0.167	0.011	0.0168	24	18
C_{14}TACl	0.1	6	0.083	0.0011	0.0058	41	31
C_{16}TACl	0.03	14	0.036	0.00033	0.00097	101	76
C_{18}TACl	0.005	32	0.0156	0.000056	0.000188	229	172

b=0.75a

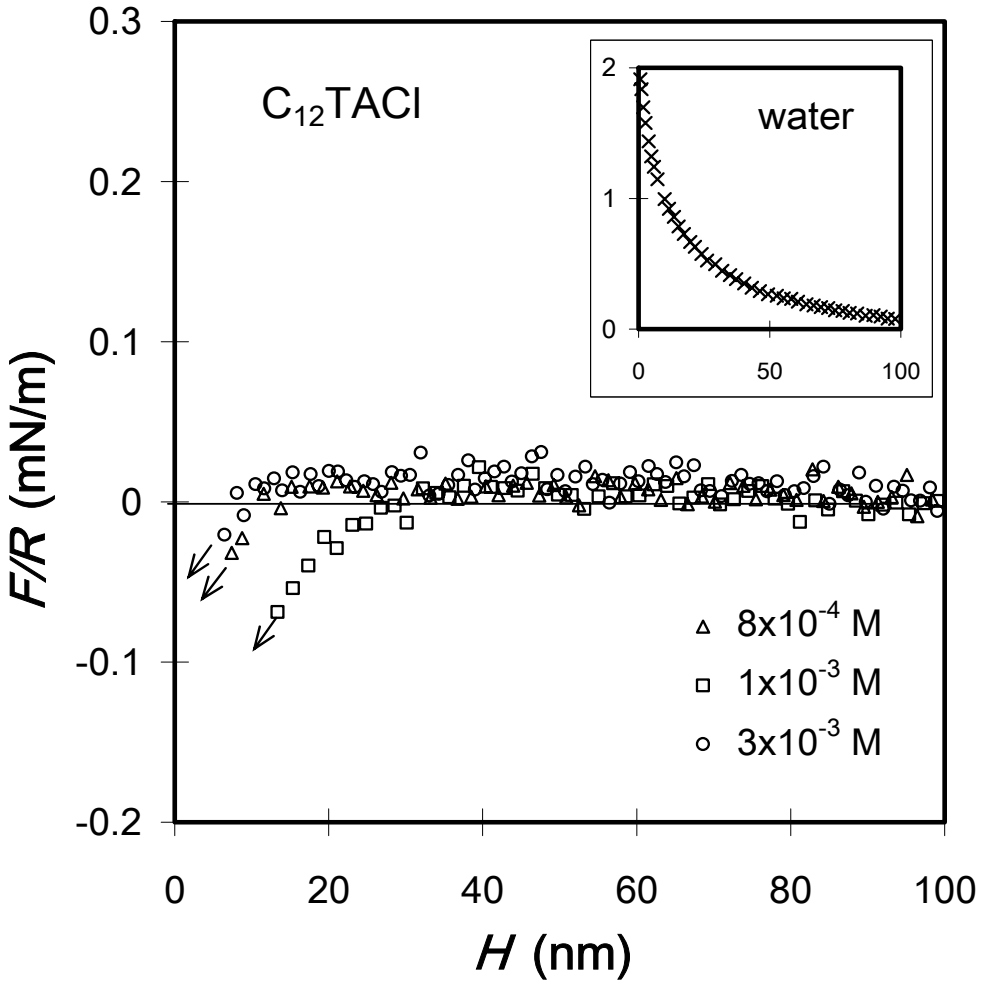

Figure 3.1 The AFM force curves obtained with the glass sphere and silica plate immersed in $C_{12}TACl$ solutions at pH≈6. The repulsive forces measured in the presence of the surfactant are much lower than that obtained in pure water (inset). The arrows represent the distance where the two surfaces jumped into contact due to attractive forces. The attraction was strongest at 10^{-3} M $C_{12}TACl$.

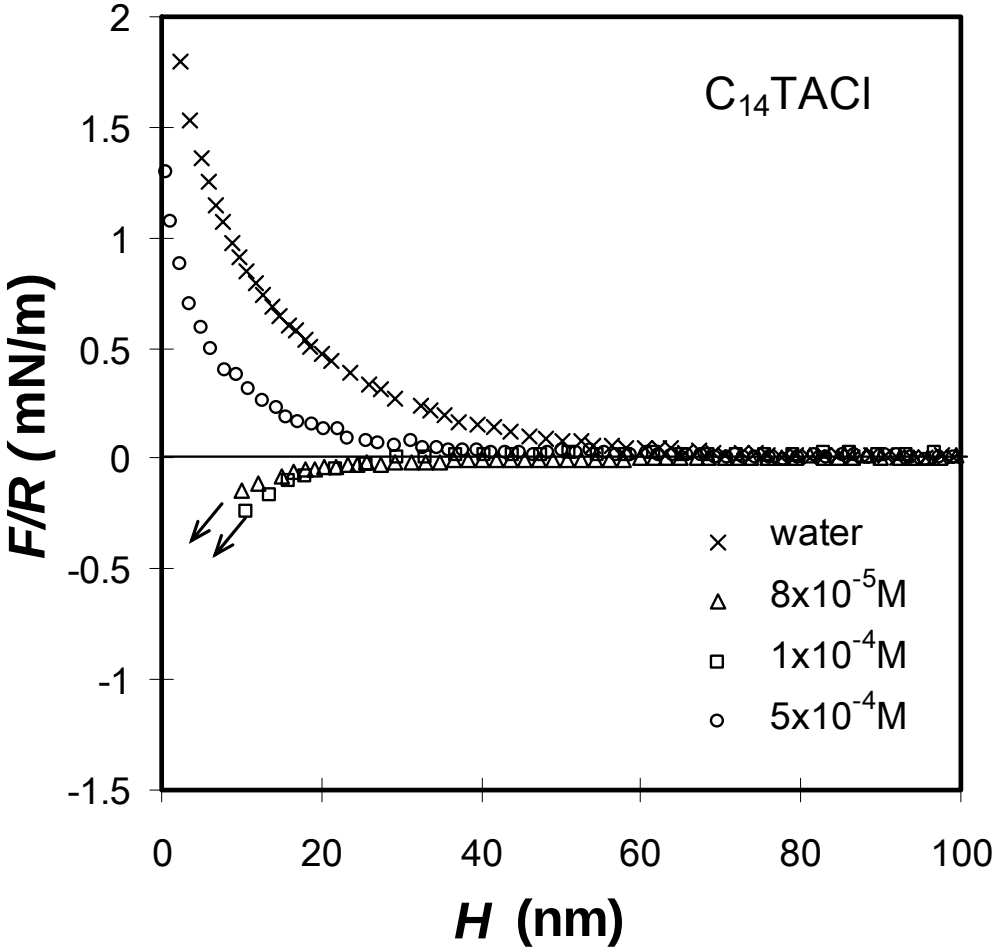

Figure 3.2 The AFM force curves obtained with the glass sphere and silica plate immersed in $C_{14}TACl$ solutions. The measured forces are most attractive at 10^{-4} M $C_{14}TACl$, which is close to the p.c.n. The forces measured above this concentration are repulsive possibly due to the inverse orientation of the surfactant.

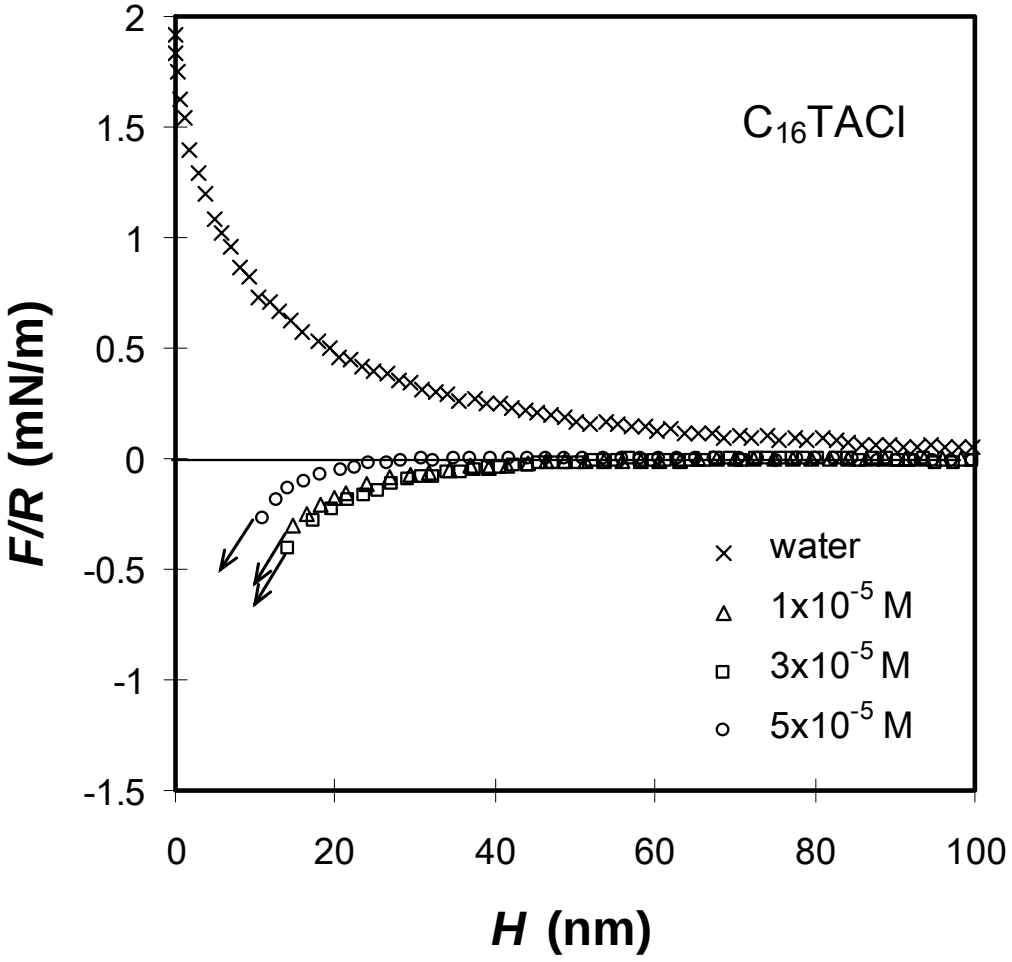

Figure 3.3 The AFM force curves obtained with the glass sphere and silica plate immersed in $C_{16}TACl$ solutions. The measured forces are most attractive at $3x10^{-5}$ M $C_{16}TACl$. The long-range forces become less negative at the higher concentration possibly due to inverse orientation.

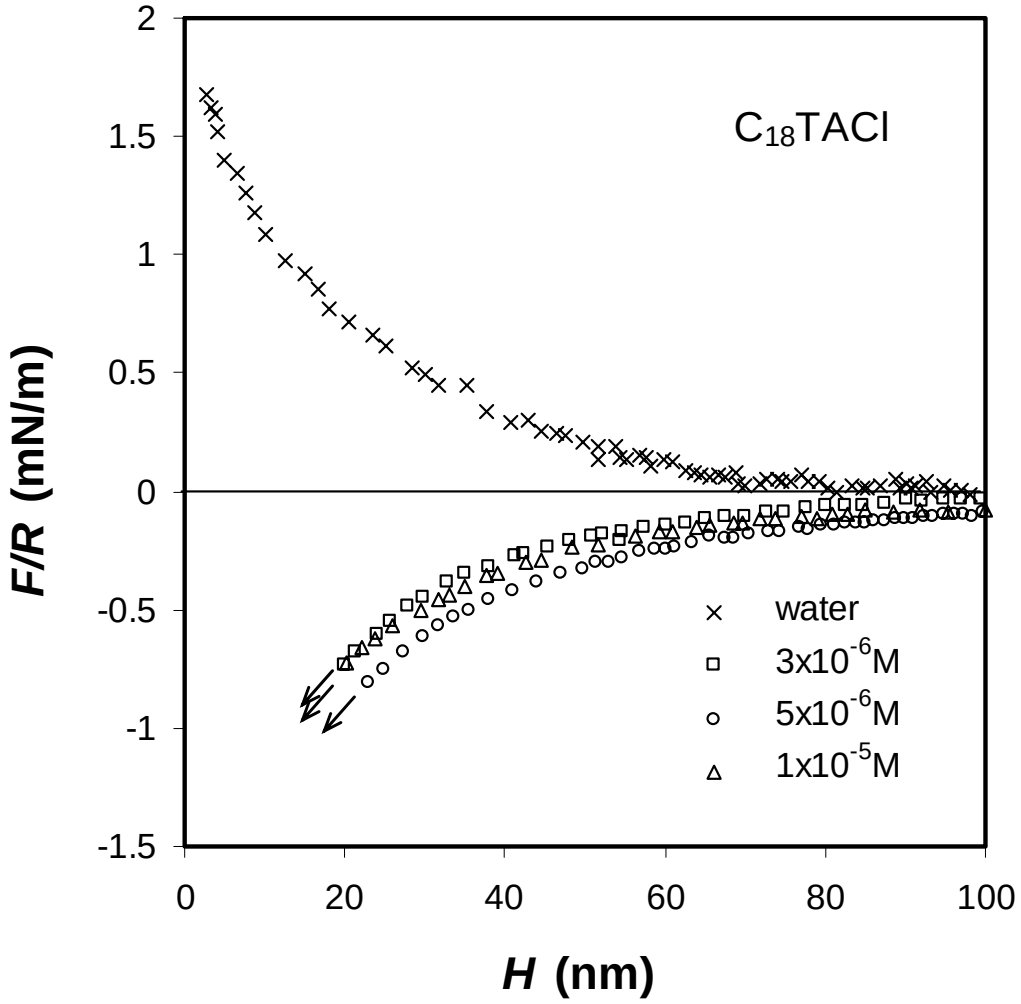

Figure 3.4 The AFM force curves measured with the glass sphere/silica plate immersed in $C_{18}TACl$ solutions. The long-range forces measured are most attractive at $5x10^{-6}$ M $C_{18}TACl$, which is close to the p.c.n.

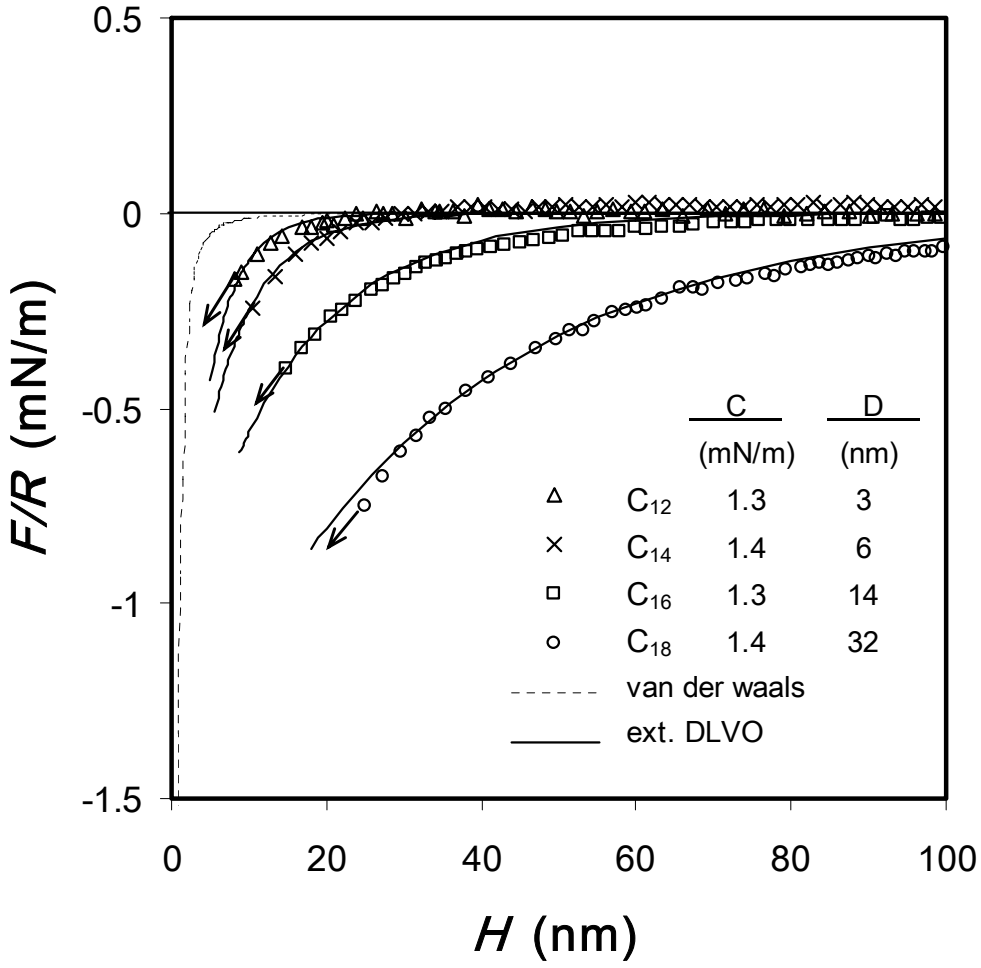

Figure 3.5 The AFM force curves obtained with glass sphere and silica plate at the p.c.n.'s of the C_nTACl homologues (n = 12, 14, 16, 18). The dashed line represents the van der Waals force with the Hamaker constant A = 0.8×10^{-20} J. The solid lines represent the extended DLVO theory which includes contributions from the van der Waals force and the hydrophobic force. (The double layer force is considered to be zero.) The hydrophobic force is represented by the single-exponential force law (Eq. [1]) with a pre-exponential parameter C and the decay length D as fitting parameters. It is shown that the hydrophobic force increases with increasing chain length.

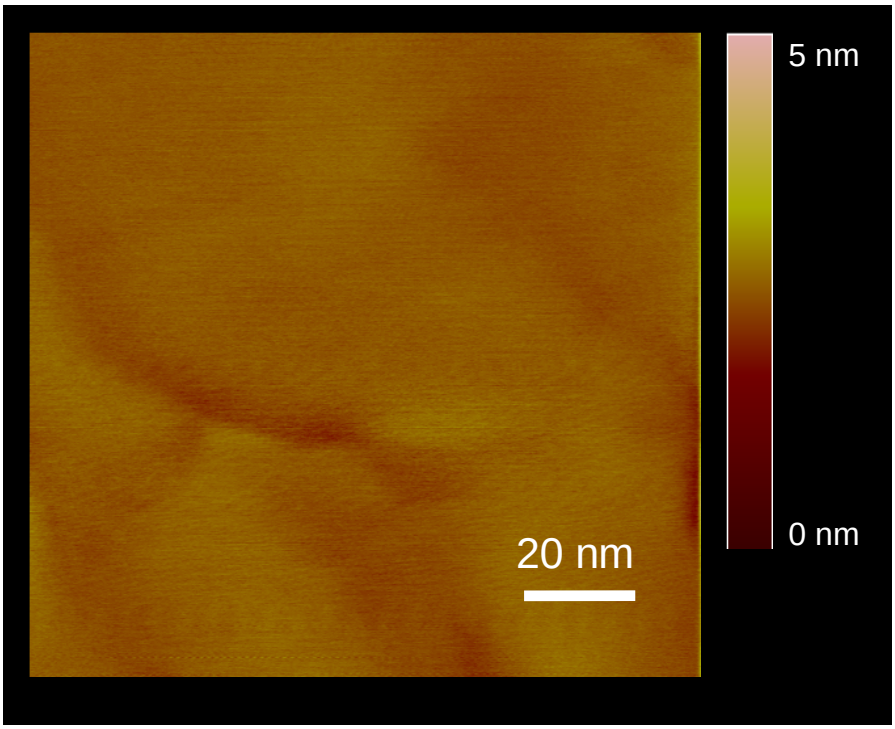

Figure 3.6 A soft contact mode AFM image of the fused silica plate immersed in water. The dimension of the scanning area is given by a scale bar. Height data for the surface were obtained using the scale bar to the right.

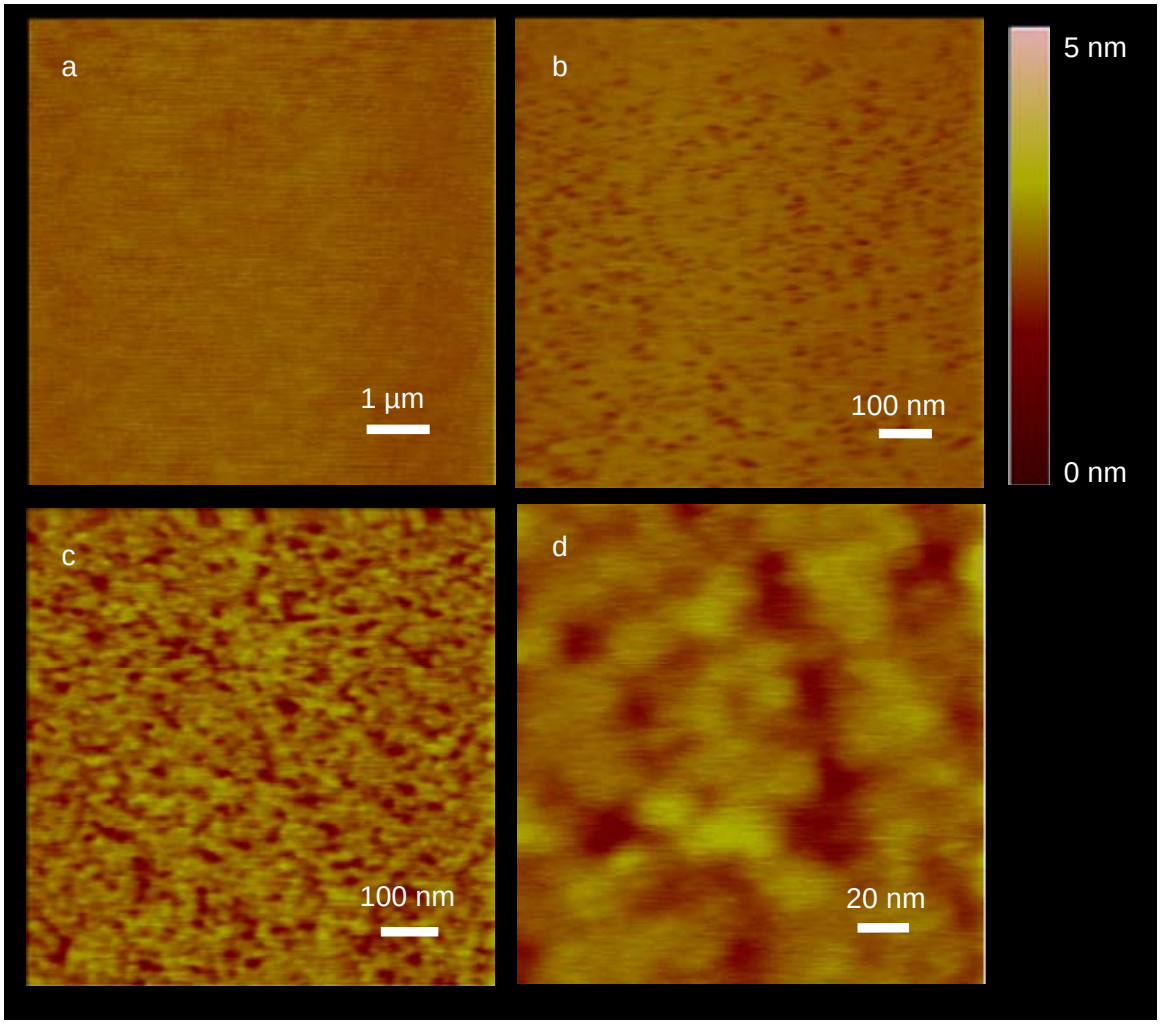

Figure 3.7 The soft contact mode AFM images of the silicon wafer surfaces immersed in $C_{18}TACl$ solutions at different concentrations and scale. The scale of the image is given in each image. The scale bar on the side gives height information. All of the images were taken 1 hour after the solution had been injected into the AFM cell. a) 10×10 µm image in water; b) 1×1 µm image in a 10^{-5} M $C_{18}TACl$ solution; c) 1 × 1 µm image in a 3×10^{-5} M $C_{18}TACl$ solution; d) 200×200 nm image in a $3x10^{-5}$ M $C_{18}TACl$ solution.

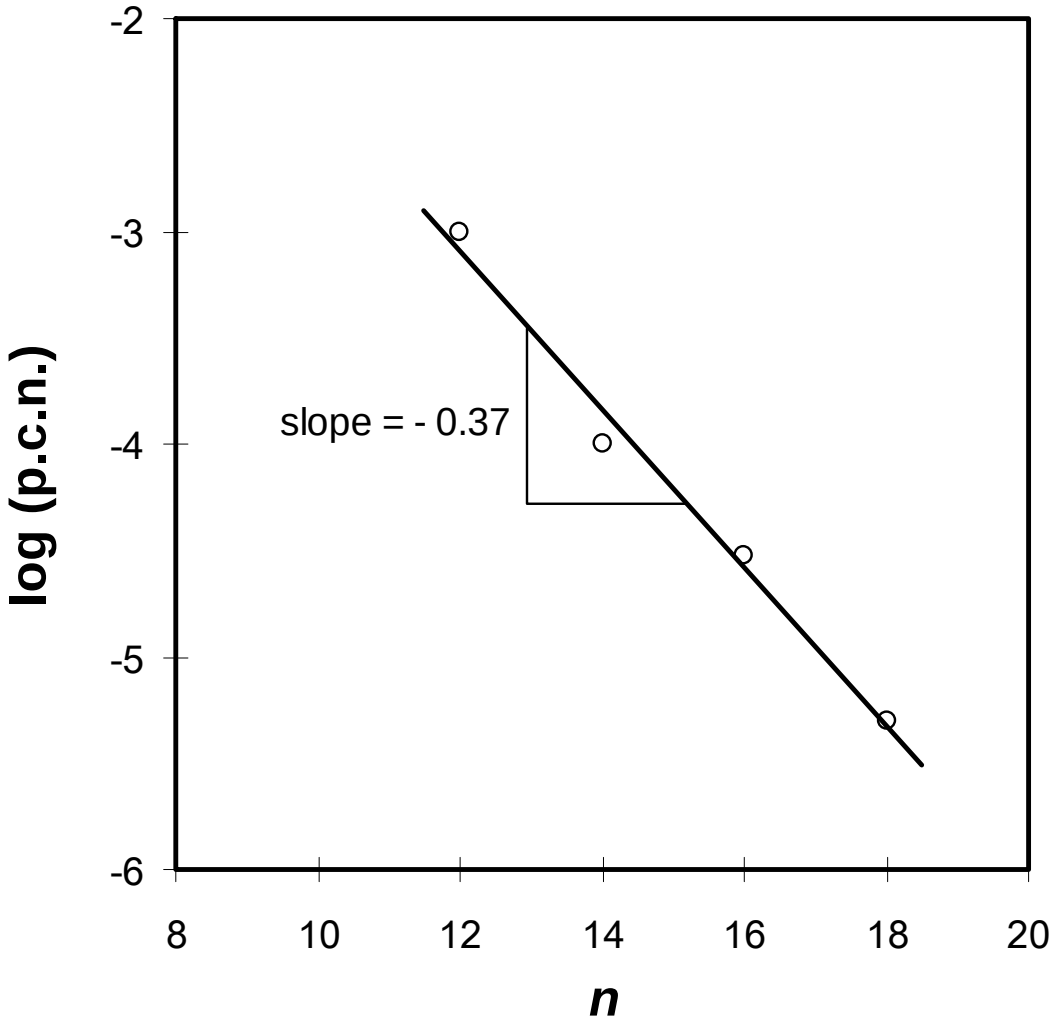

Figure 3.8 A relationship between the p.c.n.'s for the silica-C_nTACl system and the number of carbons in the hydrocarbon chains. According to the Stern-Graham equation (Eq. [3]), the slope of -0.37 gives ϕ = -0.85 kT per CH_2 group.

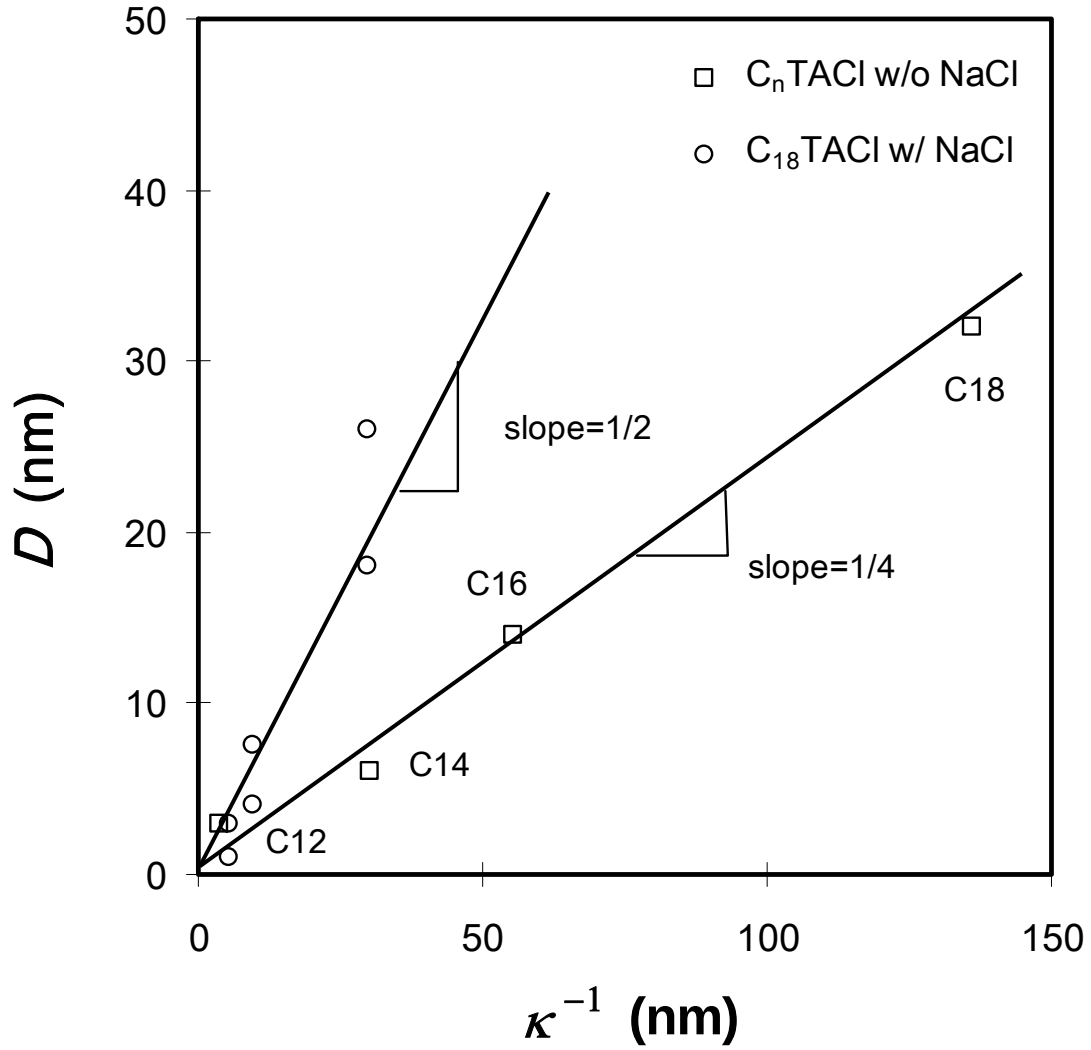

Figure 3.9 Decay length *vs.* the Debye length plots for the data obtained with C_{18}TACl with NaCl (17), and for the data obtained in C_nTACl solutions at the p.c.n.'s in the absence of electrolyte. The former fits the charged patch model of Miklavic *et al.* (49), while the latter cannot be explained with any available theory.

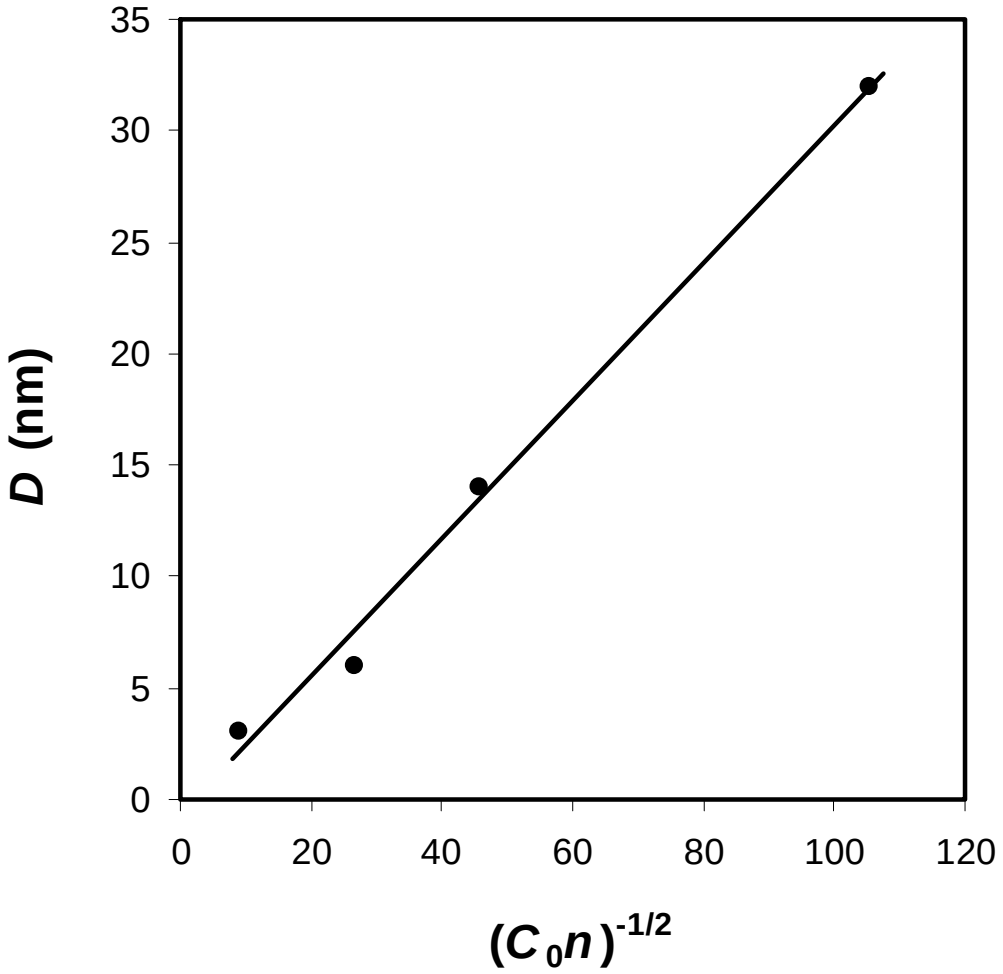

Figure 3.10 A decay length (D) *vs*. $(C_0n)^{-1/2}$ plot for the data obtained in C_nTACl solutions in the absence of electrolyte. C_0 represents the surfactant concentration, and D is equivalent to b^{-1} of Eriksson *et al*.'s hydrophobic force model (Eq. [11]) derived from the mean-field theory. C_0n represents the effective concentration of CH_2/CH_3 species in solution.

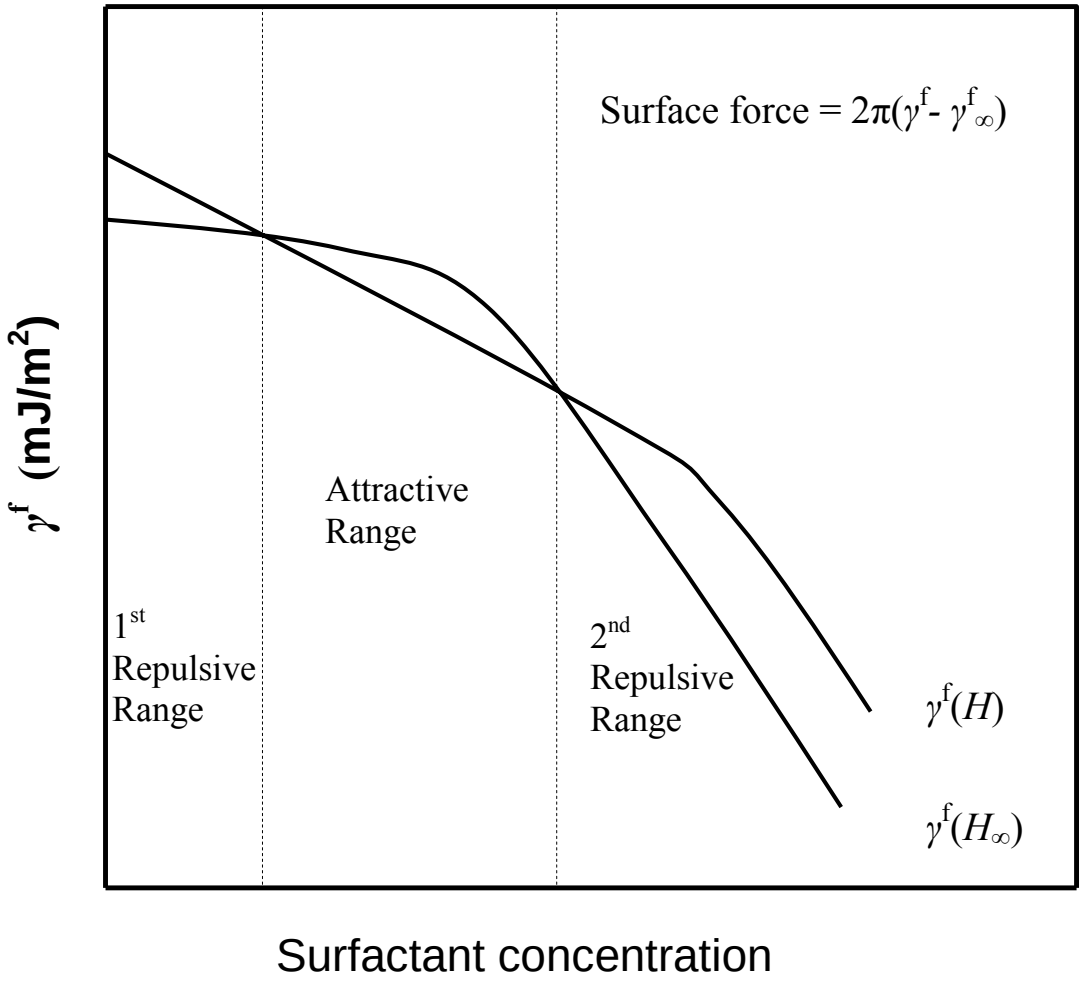

Figure 3.11 A schematic representation of the changes in film tensions with surfactant concentration. At a very low concentration, the tension ($\gamma^f(H)$) of the planar thin film at a distance H from a silica surface is higher than the same ($\gamma^f(H_\infty)$) at the infinite distance (H_∞) from the surface. Under this condition, $\gamma^f(H) > \gamma^f(H_\infty)$, resulting in a positive surface force. The rate of decrease in film tension upon adding surfactant is larger at H than at H_∞; hence, a range with negative (attractive) surface force may arise, reaching a maximum at the p.c.n. At still higher surfactant concentrations, the charged hemi-micelles formed on the silica surface cause $\gamma^f(H)$ to decrease more slowly than $\gamma^f(H_\infty)$, again resulting in a positive surface force.

CHAPTER 4

Surface Forces between TiO_2 Surfaces in C_nTACl Solutions Studied by an AFM

Abstract

Direct surface force measurements for TiO_2 surfaces in salt (NaCl) and C_nTACl (n = 14, 18) solutions have been carried out using an Atom Force Microscope (AFM). The Hamaker constant for the TiO_2/water/TiO_2 system is found to be of $4\pm1\times10^{-20}$ J from the force curves obtained both in water and in electrolyte solutions. The p.c.n. (point of charge neutralization) for the $TiO_2/C_{14}TACl$ case is 3×10^{-4} M, which is larger than the value of 1×10^{-5} M in the $TiO_2/C_{18}TACl$ system. In surfactant solution, the force curves show a repulsive/attractive/repulsive transition changing with surfactant concentration. This trend is the same as the one obtained in the SiO_2/C_nTACl system (19, 21), and the force measurement results suggest that the cationic surfactant adsorbs at TiO_2/water interface in a similar manner as that at SiO_2/water interface.

A long-range attraction beyond the realm of the DLVO theory is observed between TiO_2 surfaces in both $C_{14}TACl$ and $C_{18}TACl$ solutions in the vicinity of respective p.c.n. The range of the attraction increases, while the p.c.n. decreases, with the surfactant chain length increasing.

The charged-patch model of Miklavic *et al.* (56) explains the long-range forces measured in high electrolyte concentrations. However, as to the long-range attractions measured in the absence of salt, the calculated patch sizes from the model were substantially larger than those measured experimentally and reported in the literature.

The relationship between the decay lengths of the strongest attraction measured at p.c.n.'s *vs.* the concentration of salt or surfactant in solution is in support of the hydrophobic force model derived by Eriksson *et al.* (53) It suggests that the long-range attractions observed in the present work are hydrophobic forces originating from the changes of water structure near hydrophobic surfaces. It is very likely that the "foreign" species in solutions may break the structure of the water and decrease the observed long-range attraction.

4.1 Introduction

In oxide (silica, rutile, alumina) flotation, the surface properties of the minerals, such as surface potential and hydrophobicity, are usually modified by addition of the ionic surfactant (collector). In general, the adsorption of the surfactants at the solid/water interface minimizes the solid surface potential and maximizes the surface hydrophobicity; thus correlates to an optimum flotation response (1). Usually hydrophobicity is quantified using a thermodynamic property, water contact angle, which is successfully applied to determine the possibility of wetting, coagulation or adhesion process. As to the kinetics of these processes, one has to refer to the information of surface forces between colloidal particles.

Derjaguin and Dukhin (2) first applied the DLVO theory, which involves the electrostatic force and the van der Waals force, to model flotation (or bubble-particle interaction). However, the DLVO theory only predicts, due to the repulsive DLVO forces, an impossible flotation instead of a fast and spontaneous flotation practice, which occurs in most of the conditions. The presence of the non-DLVO interaction was first recognized by Laskowski and Kitchener (3). They found that methylated and pure silica particles had practically the same ζ-potentials and yet the former floated while the latter did not, which led to the suggestion that a long-range "*hydrophobic influence*" may be responsible for the rupture of the wetting film and flotation. They thought that the hydrophobic influence was caused by the instability of the water structure in the vicinity of a hydrophobic surface. Later, Blake and Kitchener (4) showed that the thin film of water (wetting film) between a hydrophobic solid and an air bubble ruptures fast and spontaneously at a separation of about 64 nm, which is much larger than predicted by the classical DLVO theory. These investigators suggested, therefore, the presence of a "*hydrophobic force*" in wetting films.

Hydrophobic force was first experimentally measured by Israelachvili and Pashley (5) using the surface force apparatus (SFA) in 1982. The measured force was reported to decay exponentially in the 0-10 nm range with a decay length of 1 nm. It was also postulated that the long-range attraction was related to the hydrophobic effect, which is widely used to explain mutual attraction between hydrophobic solutes (e.g., hydrocarbons) in water. Follow-up experiments showed the existence of even longer range hydrophobic forces with decay lengths in the range of 10-30 nm (6-13). One popular explanation for the attraction is the nano-bubble hypothesis, which attributes the force to the nano-bubbles on hydrophobic surfaces during force measurements (14-18). It is suggested that the "so-called hydrophobic force" is actually the capillary force caused by the coalescence of preexisting nano-bubbles when two hydrophobic surfaces approach each other. However, Zhang *et al.* (19) showed that long-range attractions were observed between in-situ hydrophobized silica surfaces both in degassed and air-saturated surfactant solutions. The force curves were smooth all along the separations without showing any kinks or steps. In addition, the range and magnitude of the measured force were much smaller than those reported by Sakamoto *et al*. (18). Meyer *et al.* (20) showed also that degassing reduced the long-range attractive force but the short-range force remained the same.

The purpose of present work is to carry out direct force measurements between TiO_2 surfaces in solutions using an AFM and clarify whether there is a long range attraction, just as the one found in the SiO_2/C_nTACl system, between hydrophobized

surfaces (19, 21). The effects of surfactant chain length on the p.c.n. and the hydrophobic force are also to be studied based on the force measurement results obtained in the solutions of C_nTACl homologues. The results are used to generalize the adsorption of cationic surfactant on negatively charged oxide surfaces and, of course, shed light on the possible origins of the hydrophobic force.

4.2 Experimental

Materials

Nanopure water was obtained by using the Nanopure III (Barnstead, IA) water system. The conductivity of the water was 18.2 MΩ-cm at 25°C and the surface tension was 72.5 mN/m at 22°C. Liquid reagents, such as chloroform (99.9%, Burdick & Jackson, NJ), H_2SO_4 (98%, VMR International, PA) were used as received without further purification. The tetradecyltrimetylammonium chloride ($C_{14}TACl$, 97% purity, TCI, OR) and octadecyltrimetylammonium chloride ($C_{18}TACl$, 97% purity, TCI, OR) are all from TCI and of greater than 97% purity. They were used without further purification. Solutions of low surfactant concentrations were prepared in containers with volumes of at least 100 mL to prevent significant depletion of surfactant *via* adsorption onto the glass walls.

TiO_2 plate (MTI, CA), which is in rutile form, was soaked in 0.01 M HNO_3 over night. The plate was then rinsed thoroughly with copious Nanopure water, equilibrated with the water in a sealed vial for at least 30 minutes, removed and dried by blowing pure nitrogen gas over the surface, and then used for experiments.

TiO_2 microspheres (Phasis, Switzerland) were soaked in ethanol and sonificated for 2 hours, and then they were filtered out with a large amount ethanol rinsing. The above clean procedure was carried out at least three times. TiO_2 spheres of 5-20μm in diameter were finally chosen for the force measurement.

Surface Force Measurements

Surface forces were measured using a Digital Instrument Nanoscope IIIa AFM (Digital Instruments, CA) at room temperature (22±1℃) using the "colloidal probe technique" (22, 23). The separation distance (H) between the probe (TiO_2 sphere) and the substrate (TiO_2 plate) was measured by monitoring the deflection of the cantilever on which the probe was attached. Silicon-nitride DNP-020 probes (Veeco, CA) were UV-irradiated for 30 minutes and soaked in chloroform for 1 hour to remove possible organic contaminants. The triangular cantilevers with nominal spring constant k of 0.12 N/m were used. The exact spring constants were determined using the resonant frequency technique (24). Errors associated with this technique were within ±7%. The precleaned TiO_2 microsphere (5-20μm in diameter) was glued onto the end of a cantilever with EPON 1004 resin (Shell Chemical Co.) using a manipulator. Measured forces (F) were normalized by dividing with the radii (R) of the spheres. Combined errors between the measurements of the spring constants and the sphere diameters were within ±12% in force/diameter (F/R) calculations.

For a given surfactant, surface forces were measured at different concentrations. The surfactant solutions were injected into an AFM liquid cell starting from the lowest concentration and continuing to the highest. At each concentration, the TiO_2 sphere and plate were equilibrated for 1 hour before starting the measurements.

AFM Imaging

Images of the surfaces of the TiO_2 plates immersed in water were taken using the Nanoscope IIIa AFM. The AFM images reported are height images captured at 22±1°C. V-shaped silicon nitride cantilevers with nominal spring constant k = 0.12 Nm^{-1} were used in the present work. The scan rates were set as 3 Hz. The image was captured using the contact-mode imaging technique after the substrate was soaked in water for 1 hour.

4.3 Results

4.3.1 AFM images of the TiO2 plate surface submerged in water

Figure 4.1 shows contact mode AFM images of the interface between a TiO_2 plate and water. The height data for the solid surface were obtained using the scale bar to the right. The image shows that the TiO_2 plate surface is quite smooth in a 500 nm×500 nm scale with a maximum peak-valley distance less than 0.8 nm. No scratches were observed at the TiO_2/water interface from the AFM image. The smoothness of the surface ensures the TiO_2 plate a suitable substrate for surface force measurement in the present work. TiO_2 spheres are shown to be in quite good spherical shape from the SEM picture. However, the AFM image of TiO_2 sphere surface is not available in the present work.

4.3.2 Force measurements in water

Figure 4.2 shows the surface forces (F/R) measured between a TiO_2 sphere of radius R and a flat TiO_2 plate in water at neutral pH as a function of the closest distance (H) separating the two macroscopic surfaces. A repulsive force was detected all along the separation until the sphere jumped onto the plate at a separation of about 6 nm. The obtained force curve is then fitted with the classical DLVO theory, which considers only the contribution of the electrostatic force and the van der Waals force. The former, F_{ele}, is calculated using the constant potential model (25). The later was calculated from the following approximate relation:

$$\frac{F_{vdw}}{R} = -\frac{A_{131}}{6H^2} \qquad [1]$$

where A_{131} is the nonretarded Hamaker constant. The fitting result is shown in Fig. 2 as the solid line, with the fitting parameter of surface potentials for the sphere and plate as -50±3 mv and a Hamaker constant of 4±1×10^{-20} J for the TiO_2/water/TiO_2 system.

It has been reported that the Point of Zero Charge (P.Z.C.) for TiO_2 is about at pH 5~6 (26-30). Therefore, at pH 6 the TiO_2 surface is negatively charged in solutions and this evokes the repulsion between the sphere and plate when two double layers overlap. In the present work, the fitted surface potentials for the sphere and plate are -50±3 mv, which are a little higher than those given in reference (30). The discrepancy may be due to either the difference between TiO_2 substrates or the facts that in the present work, the experiment data were fitted using a constant potential model which was a low limit boundary.

It is worthwhile to note that, as shown in Fig. 2, the sphere jumps and contacts the plate at a separation of about 6 nm due to an overwhelming attraction between sphere and plate over the electrostatic repulsion. The observation is different from the one obtained with silica substrates (18), in which case only a purely repulsive force was observed all along the sphere/plate separation untill the two surfaces contact. This may be due to a smaller Hamaker constant, 8×10^{-21} J, for the SiO_2/water/ SiO_2 system; therefore, the weaker van der Waals attraction can possibly be surmounted by the repulsive hydration force at short separations (31). On the other hand, in the present work, the fitted Hamaker constant for TiO_2 surfaces in water is found to be as large as $4\pm1\times10^{-20}$ J. The strong van der Waals attraction may introduce the force instability/jump-in before the repulsive hydration force predominates.

4.3.3 Force measurements in NaCl solutions

Figure 4.3 shows the surface force curves obtained between the TiO_2 sphere/plate surfaces immersed in electrolyte solutions. When the salt concentration increases from 0.001 M to 0.1 M, the force changes gradually from repulsion to attraction. In 0.001 M NaCl solution, long range repulsion was observed starting from 50 nm to 6 nm; then the sphere jumped onto the plate due to the stronger van der Waals attraction at short separation. In 0.005 M NaCl solution, a strong electrostatic repulsion was also detected before the jump-in occurred. However, the decay length of the repulsive force curve becomes much smaller due to the electrostatic double layer being compressed at a higher electrolyte concentration. When the salt concentration increases further to 0.01 M, the total interaction between the sphere and the plate becomes almost purely attractive, because the repulsive electrostatic force was almost screened out in the presence of high ionic strength. At last, when the salt concentration increases to as high as 0.1 M, the electrostatic repulsion is totally screened out and the total surface force is a result alone from the van der Waals attraction. Therefore, by fitting the force curve obtained in 0.1 M salt solution to the van der Waals force using Eq. [1], one can get an approximate Hamaker constant between TiO_2 sphere/plate surfaces immersed in water, assuming that the addition of electrolytes has little impact on the Hamaker constant. As shown in Fig. 3, the force measurement results obtained in 0.1 M NaCl solution were fitted with the DLVO theory considering only the van der Waals force. The fitting result was shown as the solid line. The fitted Hamaker constant, $A_{\mathrm{TiO2/water/TiO2}}$, gave a value of 3.5×10^{-20} J, which was comparable to the one obtained in pure water.

4.3.4 Force measurements in Cationic surfactant solutions

Figure 4.4 shows the surface forces (F/R) measured between a TiO_2 sphere of radius R and a flat TiO_2 plate in C_{14}TACl solutions as a function of the closest distance (H) separating the two macroscopic surfaces. The force curves were smooth all along the separations, without steps or kinks, indicating that the systems studied in the present investigation were relatively free of air bubbles.

In 1×10^{-4} M C_{14}TACl solution, the repulsion observed between TiO_2 surfaces in water was replaced by a net attraction. The attractive force was a little larger than the van der Waals attraction, which is calculated from Eq. [1] using a Hamaker constant $A_{\mathrm{TiO2/water/TiO2}}$ of 4×10^{-20} J and shown as the dotted line. When the surfactant concentration increased to 3×10^{-4} M, the net-attractive force became stronger and longer ranged. The

jump-in distance also increased from 10 nm to 12 nm. Further, at the surfactant concentration as high as 5×10^{-4} M, the measured force changed from net-attractive to net-repulsive.

This repulsion/attraction/repulsion force transition changing with surfactant concentration was the same as the one obtained in the force measurements with silica substrates in C_nTACl solutions (19, 21). That is, at low surfactant concentrations, the total sphere/plate interaction is dominated by the repulsive electrostatic force. Gradually, with surfactant concentration increasing, the force curves change from repulsive to attractive because of the charge neutralization of solid surfaces. It has been reported (19, 21, 32-35) that the attractive forces measured between hydrophobic surfaces became the strongest at the surfactant concentrations close to the points of charge neutralization (p.c.n.), defined as the concentrations where the surface charge of the substrate is neutralized by the adsorption of an ionic surfactant. The force curves in Figure 4.4 then showed that p.c.n. for the TiO_2-$C_{14}TAC$ system is approximately 3×10^{-4} M, because the strongest attractive force was obtained at this concentration. When the surfactant concentration is above the p.c.n., additional $C_{14}TA^+$ counter ions inversely adsorb on TiO_2 surface with their polar headgroups pointing towards aqueous phase, causing the solid surface to be recharged and become hydrophilic again. Therefore, the decrease in attractive force at the higher concentration is mainly attributed to the inverse orientation.

Figure 4.5 shows the forces measured between TiO_2 sphere/plate surfaces in $C_{18}TACl$ solutions at four different concentrations. The force curves changed in the same trend as what was obtained with the $TiO_2/C_{14}TACl$ system. At 5×10^{-6} M $C_{18}TACl$, the repulsive electrostatic force observed in pure water was completely suppressed by charge neutralization and only a net-attractive force was observed. When the surfactant concentration increases to 1×10^{-5} M, the long range attractive force became stronger. The net attraction became totally repulsive all along the separation between the sphere and the plate with the concentration further increasing to 5×10^{-5} M. The repulsion became even stronger when the surfactant concentration increased to as high as 1×10^{-4} M.

From the above discussion, one can see that the overall trend of the force curve changing with surfactant concentration obtained in the $TiO_2/C_{18}TACl$ system is the same as that in the TiO_2-$C_{14}TACl$ system. The force curves show a repulsion-attraction-repulsion transition, and the strongest attraction was observed at the p.c.n. In addition, there are two things worthy of being mentioned. First, the concentration at which the strongest long range attraction was observed is different for each system. For example, the critical concentration for $C_{14}TACl$ is 3×10^{-4} M, whereas, that for $C_{18}TACl$ is 1×10^{-5} M. That is, the latter is nearly thirty times less than the former. Second, the strongest attraction observed in $C_{18}TACl$ solutions is much larger than that in $C_{14}TACl$ solutions both in magnitude and range. These findings coincide with those obtained in the silica/C_nTACl system in previous work (21).

The strongest attractive force curves shown in Figure 4.4 and 4.5 are redrawn in Figure 4.6, and were fitted to a single-exponential force law, *viz*.,

$$F / R = -C \exp(-H / D) \qquad [2]$$

where C and D are the fitting parameters, the values of which as well as the Debye length (κ^{-1}) are also listed in Table 4.1. The fitting includes the contribution from the van der

Waals force. The electrostatic force is assumed to be zero because the solid surface is net neutral at the p.c.n.. It is clearly shown in Figure 4.6 and Table 4.1 that the maximum attractive force increases with increasing hydrocarbon chain length. For example, the decay length (D) of the attractive force increases from 5.5 nm to 19 nm when the hydrocarbon number in the surfactant straight chain increases from 14 to 18. It is important to note here that the surfactant concentration at which surface charge is neutralized and the maximum hydrophobic force observed decreases substantially with increasing surfactant chain length.

4.4 Discussion

4.4.1 Van der Waals force between TiO_2 surfaces in aqueous solutions

As discussed in the previous section, the van der Waals forces between TiO_2 surfaces in aqueous solutions were calculated using Eq. [1], in which A_{131} is the Hamaker constant for the TiO_2/water/TiO_2 system. In literature (36-38), the Hamaker constant for TiO_2 materials in water media is mainly reported to be in the range of $4\text{-}8\times10^{-20}$J. As far as we know, Larson *et al*. (30) first obtained the $A_{131}$for TiO_2 in water, of which the value is $6\pm2\times10^{-20}$J, from direct force measurement between TiO_2 surfaces using an AFM. Recently, McNamee *et al*. (39) reported an experimental A_{131} value of 2.6×10^{-20}J also from AFM surface force measurements. Unfortunately, the authors mistakenly cited the value of 26×10^{-20}J in reference 40 as 2.6×10^{-20}J.

In this present work, the Hamaker constant for the TiO_2/water/TiO_2 case was obtained by fitting the force curves both in water and in electrolyte solutions. The fitting results are shown in Fig. 2 and Fig. 3 as solid lines. It is found that the value of A_{131} is $4\pm1\times10^{-20}$J, which is close to the one reported by Larson *et al*. (30). In addition, the jump-in shown on the force curves also confirms that a much higher Hamaker constant for the TiO_2/water/TiO_2 system than that for the SiO_2/water/SiO_2 system.

4.4.2 Adsorption of cationic surfactants at the TiO_2/water interface

In general, the surface of TiO_2 is electically charged in an aqueous solution by the following mechanism:

$$Ti-OH_2^+ \overset{H^+}{\Leftrightarrow} Ti-OH \overset{OH^-}{\Leftrightarrow} Ti-O^- + H_2O \qquad [3]$$

in which silanol (Ti-OH) groups are protonated to become positive (Ti-OH_2^+) sites or are hydroxylated to become negative (Ti-O^-) sites according to the pH of the solution. The point of zero charge (p.z.c.) for TiO_2 in water is generally reported to be in the range of pH 5-6 (26-30), which is higher than the value of SiO_2 (PZC=2-3) (26, 41). The difference is due to the fact that the electronegativity difference between Si and O is smaller than that between Ti and O. This results in a higher acidicity for SiOH group, therefore a lower PZC for SiO_2 (41).

For oxide, it was proposed that (1, 42), as a first approximation, the relationship between surface potential and pH can be simply expressed as follows:

$$\Psi_0 = \frac{2.3RT}{F}\left[pH_{PZC} - pH\right] = 59 \times \left[pH_{PZC} - pH\right]\ mv \qquad [4]$$

Therefore, as studied in the present work, the TiO_2 surface is less negatively charged than that of SiO_2 at around pH 6, because the latter has a much smaller PZC. This reasoning was confirmed by the force measurement results shown in Fig. 2, in which the fitted surface potentials for TiO_2 in water is about -50±3 mv. This value is smaller than that for silica substrate (43).

Gaudin and Fuerstenau (44, 45) first introduced the "hemi-micelle" concept after studying the adsorption of dodecylammonium hydrochloride (DAH) on quartz. Later, Somasundaran and Fuerstenau (46) and Wakamatsu and Fuerstenau (47) developed further this concept and correlated the surfactant adsorption mechanism to the results of zeta potential measurement and flotation practice. Their work shows that at a very dilute surfactant concentration, surfactant molecules adsorb at the solid/liquid interface mainly through the electrostatic interaction with the polar head group pointing towards the adsorbent. It was proposed that at a specific surfactant concentration, known as the critical hemi-micelle concentration (c.h.c.), surfactant molecules began to form aggregates on adsorbent with the hydrocarbon chains of the surfactant molecules being associated with each other due to the increased lateral attractions between hydrocarbon chains. Therefore, because of the sharp increase in adsorption density, the surface charge of the adsorbent is greatly reduced. The surface may be totally neutralized when the surfactant concentration further increases to a certain concentration, which is referred to as point of charge neutralization (p.c.n.). When the concentration is above the p.c.n., surfactant molecules adsorb with inverse orientation, resulting in the recharging of solid surface and a decrease in surface hydrophobicity.

4.4.3 Effect of hydrocarbon chain length on adsorption

It has been reported that the long range attraction is the strongest at the p.c.n. of a surfactant (32-35). This finding was also confirmed in our previous work for the silica-C_nTACl system (19, 21). Thus, the p.c.n. was assumed to be approximately the concentration at which the strongest hydrophobic force was observed. The p.c.n. values for the TiO_2 in $C_{14}TACl$ and $C_{18}TACl$ solutions obtained in the present investigation are listed in Table 4.1. This shows that even though the hydrocarbon chain lengths differ only by 4 carbons, the p.c.n. for the $TiO_2/C_{14}TACl$ case, which is 3×10^{-4} M, is much higher than the value of 1×10^{-5} M for the $TiO_2/C_{18}TACl$ case. This discrepancy is directly a result of the "hydrophobic effect" (48), which is related to the hydrocarbon chain length of surfactant monomer. Further, the p.c.n. values given in Table 4.1 were plotted *vs*. the number of hydrocarbons (n) in the alkyl chains of the C_nTACl homologues. This is shown in Figure 4.7, which represents the Stern-Grahame equation (49):

$$\ln C_0 = -n_c\left(\phi / kT\right) - \ln\left(\Gamma_\delta^+\right)_0 - \ln\left(2r\right) \qquad [5]$$

in which C_0 is the surfactant concentration at ζ=0, ϕ is the standard adsorption free energy per CH_2 or CH_3 group, $\left(\Gamma_\delta^+\right)_0$ is the adsorption density of the cationic surfactant at ζ=0, r is the radius of the polar head of the surfactant, and k is the Boltzmann constant.

When ζ equals zero, C_0 is approximately the same as the p.c.n. Therefore, as shown by Eq. [5], a plot of log (p.c.n) *vs*. *n* should give a slope of $-\phi/2.3kT$, if the product of $\left(\Gamma_{\delta}^{+}\right)_0$ and 2*r* remain relatively constant for the C_nTACl homologues studied in the present work.

Figure 4.7 shows that the plot of log (p.c.n) *vs*. *n* for TiO_2 gives a slope of -0.37, from which one can obtain the value of ϕ = -0.85 *kT*. This value is quite close to the value of -0.97 *kT* obtained from a plot of log (p.z.r.) vs. *n* for the quartz-primary amine system (50, 51). In addition, the corresponding figure is about -0.75 *kT* per CH_2 group for the ordinary micelles forming in solutions of ionic surfactants. The value of the slope suggests that the major driving force for adsorption of a surfactant on oxide surface at the p.c.n. is the hydrocarbon chain association recognized as hydrophobic effect (48). Therefore, the longer the hydrocarbon chain length is, the larger the hydrophobic effect becomes. It in turn causes a shift of the p.c.n. to a much lower concentration.

It is interesting to note that the obtained ϕ value is the same as the one reported from the previous work with the SiO_2/C_nTACl system. To clarify this point, the plot of log (p.c.n) *vs*. *n* for the SiO_2/CTACl system is also included in Figure 4.7 for comparison. It is clearly shown in the figure that the two straight lines are parallel to each other with the same slope of -0.37. The finding suggests that the adsorption of surfactants on oxides, which is driven by the charge neutralization and hydrophobic attraction between hydrocarbon chains, is similar for both the SiO_2/CTACl and the TiO_2/CTACl systems. The shift between the two straight lines, however, comes from the difference between surface properties of the two oxide materials, as shown by the term of $\left(\Gamma_{\delta}^{+}\right)_0$ in Eq. [5].

4.4.4 Possible Origin(s) of Hydrophobic Force

The non-DLVO long-range attractive force was first observed experimentally by Israelachvilli and Pashley (5, 52) about two decades ago. In their investigation, the hydrophobic surfaces were prepared by hydrophobizing mica surfaces with hexadecyltrimethylammonium bromide (C_{16}TABr). The process is similar to the case of oxide submerged in C_nTACl solutions, which was also classified as the in-situ adsorption system for the hydrophobic force measurement (35). Since then, numerous other investigators reported long range attractions even in different systems (6-13), and proposed possible causes for the long-range attraction (8, 12, 18, 53-56). However, its origin is not yet fully understood. In our previous works with the SiO_2/C_nTACl system (19, 21), we discussed the possible origin(s) of the long-range attraction between hydrophobic surfaces. In the following section, the discussion is to be continued by combining the findings from our previous work and the results obtained in the present investigation. It will help clarify the intriguing yet complex hydrophobic force observed in this specific surfactant in-situ adsorption system.

Due to the fact that the long range attractions are observed in degassed surfactant solutions and the force curves are smooth without any kinks or steps, the nanobubble hypothesis will not be discussed as the possible origin of hydrophobic force in the specific surfactant in-situ adsorption system.

The charged-patch model developed by Miklavic *et al*. (56), however, has been applied to explain the fact that long-range attractive force deceases in the presence of inorganic electrolyte, which suggests that the non-DLVO force is of electrostatic origin.

It is proposed in the model that the surfactants form patches/aggregates on the solid surfaces and the patches can be charged even though the whole solid surface is neutral. Therefore, the long-range attraction may originate from the electrostatic correlation attraction between the patches of surfactant molecules formed on the solid surfaces. In the following section, the charged-patch model will also be discussed in detail in terms of the existence of charged patches and applicability of the model to experiment results.

It is not at all a new concept that surfactants form patches/aggregates at solid/solution interface even at a quite low surfactant concentration. As mentioned before, the "hemi-micelle" first proposed by Gaudin and Fuerstenau (44) is essentially patches or aggregates of surfactants. Later, the aggregation numbers of the hemi-micelles (or 'soloids') determined using the electron spin resonance (ESR) and fluorescence spectroscopic techniques showed the patch-wise adsorption mechanism (57, 58). AFM (19, 21) images of the surfactant-coated surfaces indeed directly showed patches even at low surfactant concentration. According to Fuerstenau and Pradip (42), hemi-micelles begin to form at concentrations 2-3 orders of magnitude below the c.m.c.

The model predicts that the interaction between the two surfaces covered with patches of positive and negative charges is always attractive when the patches are sufficiently mobile and free to correlate with each other. A question remains, however, as to whether it is physically possible for the patches to be positively charged, while unoccupied silica surface remains negatively charged. For the case of C_nTA^+ ions adsorbing on TiO_2, there should always exist some unoccupied negative charge sites at low surfactant concentrations; therefore, the hemi-micelles formed at a p.c.n. must be somehow positively charged in order to make the whole surface to be neutral.

In the charged-patch model (56), it is assumed that the patches are distributed in a square lattice with a dimension of a. The free energy of interaction per unit area ($G(H)$) is given as follows:

$$G(H) = -\frac{A}{kT}\Omega^2 \exp(-2q_{\min}H) \qquad [6]$$

in which A is the area of the unit cell, Ω is a constant which varies with surface property (surface potential or charge), reciprocal lattice vector, and lateral displacement. As shown, the interaction energy decays exponentially, with a decay length of $(2q_{\min})^{-1}$, in which $q_{\min}$ is given as follows:

$$q_{\min} = \left[(\pi/a)^2 + \kappa^2\right]^{1/2} \qquad [7]$$

where κ is the reciprocal Debye length. At a high electrolyte concentration, $q_{\min} \approx \kappa$; therefore, the interaction energy should decay as $(2\kappa)^{-1}$. At a low electrolyte concentration, κ is small; therefore, $q_{\min}$ should vary inversely with a.

Eq. [7] suggests that decay length (or $q_{\min}$) is mainly controlled by two parameters, a and κ, depending on the ionic strength in the solution. It was experimentally found that in the SiO_2/C_nTACl system, in the presence of varying concentrations of NaCl, the plot of D *vs*. κ^{-1} gives a slope of ½ as predicted by Eq. [7]. When the ionic strength in the

solution is low, especially in the case of long chain C_nTACl homologues without salt addition, the slope of the plot of *D vs.* κ^{-1} is approximately ¼, for which there is so far no adequate theoretical explanation. Figure 4.8 shows a plot of *D vs.* κ^{-1} drawn from the data obtained with rutile in $C_{14}TACl$ and $C_{18}TACl$ solutions. The plot obtained with silica in C_nTACl homologues solutions in the absence of salt addition are also shown in the same figure for comparison. It is interesting to note that the *D vs.* κ^{-1} plot for TiO_2 and SiO_2 substrates follow almost the same straight line with a slope of ¼.

$$D=1/4\kappa^{-1} \qquad [8]$$

In previous work, from Eq. [7], the values of unit cell size, *a*, was obtained through the values of $q_{\min}$, which was calculated from the measured decay length, $D(=(2q_{\min})^{-1})$. The κ values were calculated from the concentrations of the ionic surfactants used in force measurements. The lattice patch size, *b* was roughly estimated from the value of *a* by multiplying it with a factor 0.75 used by Miklavic *et al.* (56). In present investigation, the *b* values were calculated and listed in Table 4.2. It shows that *b* increases from 33 nm to 98 nm when the carbon number of the surfactant increases from 14 to 18. The trend is the same as the one obtained with the SiO_2/CTACl system. Fan *et al*. (57) and Strom *et al*.(58) also reported that the aggregation numbers of the hem-micelles increased with increasing chain length. However, reexamination of Table 4.2 reveals that the values of patch sizes are substantially larger than those estimated from the aggregation numbers reported by Fan *et al*. (57). That is, in the charged patch model of Miklavic *et al*. (56), the patches size required has to be substantially larger than experimentally observed with self-assembled monolayers to evoke the long-range attractive forces measured in the present work. In addition, it is assumed in the model that the charged patches should be mobile in order to evoke a long range attraction. When the two surfaces approach each other, the patches may migrate laterally on the surface in order for the system to minimize the free energy. Yet, the ultimate prerequisite that the charged patches are indeed mobile enough at p.c.n. to give rise to long-range attractions has to be proved by experiments.

According to the Derjaguin approximation (59), the surface force (*F*) normalized by the diameter of the sphere (*R*) can be given as follows:

$$F / R = 2\pi\left(\gamma^{f} - \gamma_{\infty}^{f}\right) \qquad [9]$$

in which γ^{f} is the film tension at a separation distance *H* and γ_{∞}^{f} is the same at an infinite separation distance, (*i.e.*, in the bulk solution). Eriksson *et al*. (53) derived theoretical expressions for γ^{f} and γ_{∞}^{f} using a mean field approach based on the 'square-gradient approximation'. By substituting those into Eq. [9], they obtained the following expression for the hydrophobic force:

$$F / R = -B\left[\coth(bH / 2) - 1\right] \qquad [10]$$

which can be simplified to:

$$F / R = -2B\exp(-bH) \quad [11]$$

for large enough separations. Eq. [11] shows that b^{-1} can be identified with D and $2B$ is equivalent to C of Eq. [2]. Furthermore, according to Eriksson *et al*. (53),

$$b^{-1} = \sqrt{c_3 / 2c_2} \quad [12]$$

where c_2 and c_3 are constants which account for the free energy costs of structuring the water and forming order parameter gradients, respectively. According to Eq. [12], such a relationship as the decay length D (or b^{-1}) is a linear function of $(C_0 n)^{-1/2}$ can be generated if we assume that c_2 is proportional to $(C_0 n)^{1/2}$ and c_3 is inversely proportional to $(C_0 n)^{1/2}$. In other words, the presence of surfactant ions would make it more costly free-energy-wise to obtain a certain ordered water state, whereas it would be less costly with the gradients in the order parameter function in the vicinity of a hydrophobic surface. Although these assumptions seem reasonable, they are nevertheless in need of further justification.

Figure 4.9 shows a plot of D *vs.* $(C_0 n)^{-1/2}$, where C_0 is the concentration of C_nTACl in bulk solution and n is the number of carbons in a hydrocarbon chain. The results obtained with the SiO_2/C_nTACl system in previous work are also shown in the figure. It is clearly seen that in the absence of salt addition, the decay length of hydrophobic force, D, is linear to $(C_0 n)^{-1/2}$, giving a slope approximately of 0.3:

$$D = 0.3(C_0 n)^{-1/2} \quad [13]$$

$C_0 n$ is known as the molar concentration of the CH_2 and CH_3 groups in solution. Therefore, the straight line in Figure 4.9 suggests that the long-range attraction decreases with increasing concentration of the species that can disrupt the structure of water, (*i.e.*, hydrocarbons). In addition, it is interesting to note that the obtained relationship of $D = 0.3(C_0 n)^{-1/2}$ is somehow similar to the one of $D=1/4\kappa^{-1}$obtained in Figure 4.8. In the vicinity of p.c.n., because the solid surface is almost neutral with minor surface potential, κ^{-1} may be simply calculated using $\kappa^{-1} = 0.3C_0^{-1/2}$. Therefore, it can be readily derived from Eq. [8] that:

$$D = 0.3(16C_0)^{-1/2} \quad [14]$$

Comparing Eq. [13] and [14], one can see that they are of nearly the same in essential, as the carbon number, n, is close to 16 when the C_nTACl homologue is chosen from C_{12} to C_{18}.

Hereto, we have a quite good explanation for the linear relationship of D vs.κ^{-1} in the absence of salt addition. The long-range attraction decreases with increasing the concentration of surfactant. The slope of ¼ is simply due to the correction considering the

hydrocarbon number of surfactant chain. In the case of NaCl addition, Na^+ and Cl^- ions, instead of the hydrocarbons, are the main species that can disrupt the structure of water. Therefore, the long-range attraction should be the strongest in pristine water and decrease with the increase of electrolyte concentration. This claim has been experimentally proved in our previous work.

Until now, two possible origins for the long-range attractions have been discussed in terms of the force measurement results obtained with TiO_2 and SiO_2. The charged-patch model explains the force results obtained in high electrolyte concentration rather well. At low electrolyte concentrations, however, the model predicts much larger patch sizes than known from experimental work. Moreover, it still needs to be further proved whether the charged patches are indeed mobile enough to give rise to long-range attractions. Finally, the charged-patch model does not explain the long-range forces observed with silylated and Langmuir-Blodgett-deposited hydrophobic surfaces, which are supposed to be rather stable in aqueous solutions.

The origin of hydrophobic force is also discussed above concerning the water structure from Eriksson *et al.*'s theoretical model (53). It is suggested that 'foreign' species, such as surfactant monomers and inorganic electrolytes, break the hydrogen bond network present in thin watery films between hydrophobic surfaces, thereby reducing the long-range attraction. The smaller p.c.n. for a longer chain surfactant results in a stronger hydrophobic force. While in short chain length surfactant solution, the fact that only a short range attraction can be observed is due to the much larger p.c.n.. Addition of electrolyte in solution helps disrupt the water structure near the hydrophobic surface, resulting in a reduced hydrophobic force. The above reasoning may also explain the fact that very long-range attractions were observed with hydrophobic surfaces obtained with silylation (12, 60).

4.5 Conclusions

Direct surface force measurements have been carried out between TiO_2 surfaces in salt (NaCl) and cationic surfactant C_nTACl (n = 14 and 18) solutions using an Atom Force Microscope (AFM). From the force curves obtained both in water and in electrolyte solutions, the Hamaker constant for the TiO_2/water/TiO_2 system is found to be $4\pm1\times10^{-20}$ J, which is much higher than the value of 8×10^{-21} J for the case of silica/water/silica. The high Hamaker constant results in a stronger van der Waals attraction; thus a jump-in occurs in the surface force curve.

A repulsion-attraction-repulsion transition behavior of the force curves between TiO_2 surfaces in different concentrations of C_nTACl solutions follows the same trend as obtained with the silica/water system. The p.c.n., inferred from the force measurements, for the TiO_2-$C_{14}TACl$ system is 3×10^{-4} M, and this value is much higher than that for the TiO_2-$C_{18}TACl$ case, which is only 1×10^{-5} M. The discrepancy is due to the "hydrophobic effect". That is, for the homologue of C_nTACl, a longer hydrocarbon chain length results in a larger hydrophobic driving force and a shift of p.c.n. to a lower concentration.

In the vicinity of respective p.c.n, there is a long-range attraction observed between TiO_2 surfaces in both $C_{14}TACl$ and $C_{18}TACl$ cationic surfactant solutions. At lower or higher surfactant concentrations, the attraction is weaker. The force curves show that the strongest attraction between TiO_2 surfaces in $C_{18}TACl$ solution is much larger than that in $C_{14}TACl$ solution. The results coincide with the finding achieved in the silica/water

system. All these suggest that the C_nTACl surfactant adsorbs at the oxide (silica, TiO_2) surface in aqueous solutions in a similar manner, in which the electrostatic and hydrophobic interactions are the only two main driving forces for surfactant adsorption.

The long-range forces measured in the present work were analyzed in terms of the charged-patch model, which might explain the forces measured in high electrolyte concentrations. For the long-range attractions measured in the absence of added salt, however, it was necessary to assume that the patch sizes were substantially larger than those measured experimentally and reported in the literature. Furthermore, experimental evidence is still called for to confirm the mobility of hemimicelles in the vicinity of p.c.n.

The linear relationship between the maximum decay lengths measured at p.c.n.'s *vs.* the concentration of the CH_2 and CH_3 groups in solution is in support of the formalism derived by Eriksson *et al.* from the mean-field theory by considering the changes of water structure near hydrophobic surfaces. It is very likely that the 'foreign' species in solution break the structure of the water and decrease the observed long-range attraction. Even though there is no unanimity in the origin of this long-range attraction until now, its existence and its impact on the stability of oxides in aqueous solutions in flotation practice should be greatly acknowledged.

4.6 References

(1) D.W. Fuerstenau; R. Jia, Colloids Surf. A, 250 (2004) 223-231.
(2) B. V. Derjaguin, S. S. Duhkin, Trans. Inst. Min. Metall. 1961, 70, 221.
(3) T. D. Blake, J. A. Kitchener, J. Chem. Soc Faraday Trans. 1972, 68, 1435-1442.
(4) J. Laskowski, J.A. Kitchener, J. Colloid Interface Sci. 1969, 30, 391.
(5) J. N. Israelachvili, R. M. Pashley, Nature, 1982, 300, 341.
(6) H. K. Christenson, P.M. Claesson, Science, 1988, 239, 390.
(7) Ya.I. Rabinovich, B.V. Derjaguin, Colloids Surf., 1988, 30, 243.
(8) Y. H. Tsao, D. F. Evans, H. Wennerström, Science 1993, 262, 547-550.
(9) J. L. Parker, P. M. Claesson, P. Attard, J. Phys. Chem. 1994,98, 8468-8480.
(10) J. Wood, R. Sharma, Langmuir 1995, 11, 4797-4802
(11) M. Hato, J. Phys. Chem. 1996, 100, 18530-18538.
(12) R.-H. Yoon, S.A. Ravishankar, J. Colloid and Interface Sci., 1996, 179, 391-402.
(13) R.-H. Yoon, S. A. Ravishankar, J. Colloid and Interface Sci., 1996, 179, 403-411.
(14) P. Attard, Langmuir 1996, 12, 1693-1695.
(15) N. Ishida, M. Sakamoto, M. Miyahara, K. Higashitani, Langmuir, 2000, 16, 5681-5687.
(16) N. Ishida, T. Inoue, M. Miyahara, K. Higashitani, Langmuir, 2000, 16, 6377-6380
(17) J. W. G. Tyrrell, P. Attard, Langmuir, 2002, 18, 160-167.
(18) M. Sakamoto, Y. Kanda, M. Miyahara, K. Higashitani, Langmuir 2002, 18, 5713-5719.
(19) J. Zhang, R.-H. Yoon, M. Mao, W. A. Ducker, Langmuir, 2005; 21, 5831-5841.
(20) E. E. Meyer, Q. Lin, J. N. Israelachvili, Langmuir, 2005, 21, 256-259.
(21) J. Zhang, J.C. Eriksson and R.-H. Yoon, submitted to J. Colloid Interface Sci., 2006.
(22) W. A. Ducker; T. J. Senden; R. M. Pashley, Nature 1991, 353, 239-241.
(23) W. A. Ducker; T. J. Senden; R. M. Pashley, Langmuir 1992, 8, 1831-1836.

(24) J. P. Cleveland; S. Manne, D. Bocek, P. K. Hansma, Rev. Sci. Instrum. 1993, 64, 403-406.
(25) H. Ohshima, T. W. Healy, L. R. White, J. Colloid Interface Sci. 1982, 89, 484.
(26) Y. G. Bérubé, P. L. de Bruyn, J. of Colloid and Interface Sci., 1968, 27, 2, 305-318
(27) S. M. Ahmed, D. Maksimov, J. Colloid and Interface Sci., 1969, 29, 1, 97-104.
(28) S. Ardizzone, S. Trasatti, Adv. Colloid and Interface Sci., 1996, 64, 173-251.
(29) J. C. Schulz, G. G. Warr, Langmuir, 2002, 18, 3191-3197.
(30) I. Larson, C. J. Drummond, D. Y. C. Chan, F., J. Crieser, Am. Chem. Soc. 1993, 115, 11885-11890.
(31) R. M. Pashley, J. A. Kitchener, J. of Colloid and Interface Sci., 1979, 71, 491.
(32) J.L. Parker, V.V. Yaminsky, P.M. Claesson, J. Phys. Chem. 97, 1993, 7706.
(33) M.W. Rutland, J.L. Parker, Langmuir 10, 1994, 1110-1121.
(34) P. Kékicheff, O. Spalla, Phys. Rev. Lett. 75, 1995, 1851.
(35) H. K. Christenson, P. M. Claesson, Adv. Colloid Interface Sci., 2001, 91, 391- 436.
(36) H. D. Ackler, R. H. French, Y.-M. Chiang, J. Colloid Interface Sci., 1996, 179, 460.
(37) L. Bergström, Adv. in Colloid and Interface Sci., 1997, 70, 125
(38) J. Fernández-Varea, R. Garcia-Molina, J. of Colloid and Interface Sci., 2000, 231, 394–397.
(39) C. E. McNamee, Y. Tsujii, M. Matsumoto, Langmuir, 2005, 21, 11283-11288.
(40) J. N. Israelachvili, "Intermolecular and Surface Forces: With Applications to Colloidal and Biological Systems," 1992 2nd ed., Academic Press, p 294.
(41) G. A. Parks, Chem. Rev., 1965, 65(2), 177-198.
(42) D.W. Fuerstenau, P. Pradip, Adv. Colloid and Interface Sci., 2005, 114-115, 9-26.
(43) H. Yotsumoto; R.-H. Yoon, J. of Colloid and Interface Sci., 1993, 157, 426-433.
(44) M. Gaudin, D. W. Fuerstenau, Trans. AIME, 1955, 202,958.
(45) D. W. Fuerstenau, Pure Appl Chem 1970, 24, 135.
(46) P. Somasundaran, D. W. Fuerstenau, J Phys Chem 1966;70:90.
(47) T. Wakamatsu, D. W. Fuerstenau, Adv Chem Ser 1968;79:161.
(48) C. Tanford,, "The Hydrophobic Effect," 1980, 2nd ed. Wiley, New York.
(49) D. C. Grahame, Chem. Rev., 1947, 40, 441.
(50) P. Somasundaran, T. W. Healy, D. W. Fuerstenau J. Phys. Chem. 1964, 68, 3562-3566.
(51) P. Somasundaran, L. Huang. Adv. Colloid Interface Sci., 2000, 88, 179-208.
(52) J. N. Israelachvili, R. M. Pashley, J. Colloid Interface Sci., 1984, 98, 500.
(53) J. C. Eriksson, S. Ljunggren, P. M. Claesson, J. Chem. Soc., Faraday Trans. 2, 1989, 85, 163-176.
(54) R. Pazhianur, R. H. Yoon, Miner. Metall. Process. 20, 4, 2003, 178–184.
(55) P. M. Claesson, H. K. Christenson, J. Phys. Chem. 1988, 92, 1650-1655.
(56) S. J. Miklavic, D. Y. C. Chan, L. R. White, T. W. Healy, J. Phys. Chem. 1994, 98, 9022-9032.
(57) A. Fan, P. Somasundaran, N.J. Turro, Langmuir, 1997, 13, 506.
(58) C. Ström, P. Hansson, B. Jönsson, O. Söderman, Langmuir, 2000, 16, 2469.
(59) B. V. Derjaguin, Kolloid Z. 1934, 69, 155.
(60) Ya. I. Rabinovich, R.-H. Yoon, Langmuir 1994, 10, 1903-1909.

Table 4.1 Fitting parameters of the strongest attraction force curves obtained between glass sphere and silica plate in respectively C_{18}TACl solution.

Surfactant	**Conc. / M**	**C / mNm^{-1}**	**D / nm**
	1×10^{-4}	1.1	4
C_{14}TACl	3×10^{-4}	1.2	5.5
	5×10^{-4}	-	-
	5×10^{-6}	1.1	14.6
C_{18}TACl	1×10^{-5}	1.2	19
	5×10^{-5}	1.1	7.6
	1×10^{-4}	1.1	4.5

Note. The measured forces were fitted to a exponential function, $F/R=-C\times\exp(-H/D)$, where F is the surface force, R the radius of the glass sphere used for the force measurements, H the closest separation distance between the sphere and plate, and C, D are fitting parameters.

Table 4.2 The parameters of Miklavic *et al.*'s charged-patch model as obtained by fitting the decay lengths obtained at the p.c.n.'s of the TiO_2/C_nTACl system

	p.c.n. (mM)	D (nm)	q_{min}	κ^2	$(\pi/a)^2$	a (nm)	b (nm)
$C_{14}TACl$	0.3	5.5	0.091	0.00336	0.00492	45	33
$C_{18}TACl$	0.01	19	0.0263	0.00011	0.00058	130	98

$b=0.75a$

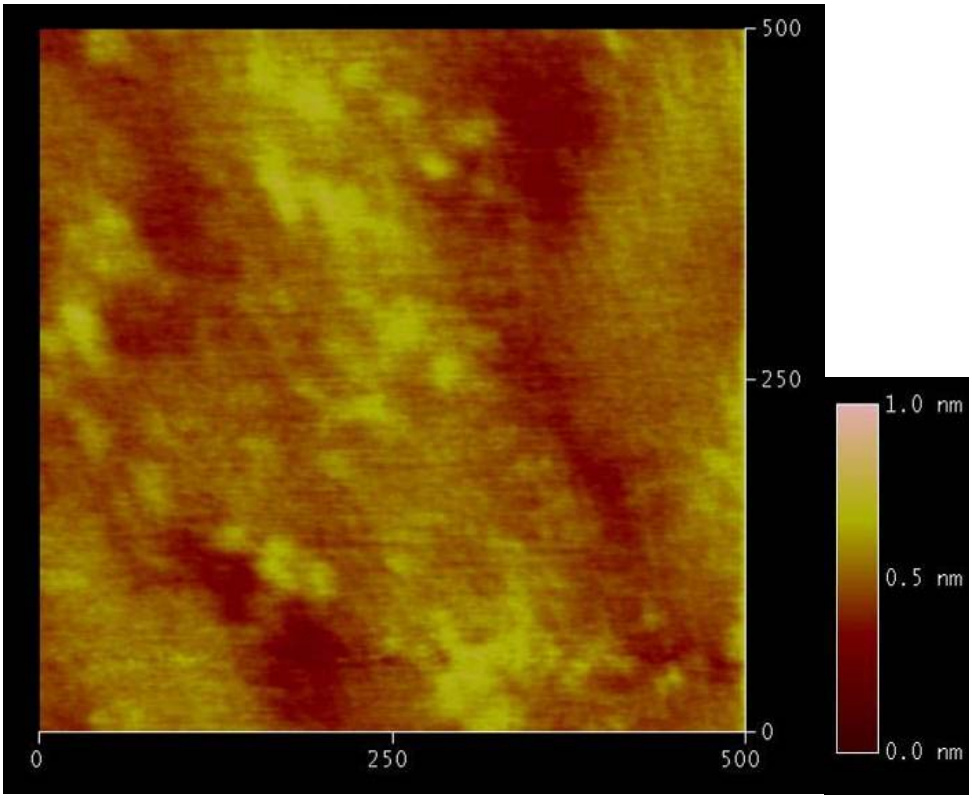

Figure 4.1 Soft contact mode AFM images of the TiO_2 (Rutile plate) surface obtained in water. The dimension of the scanning area is 500 nm×500 nm. Height data for the surface were obtained using the scale bar to the right.

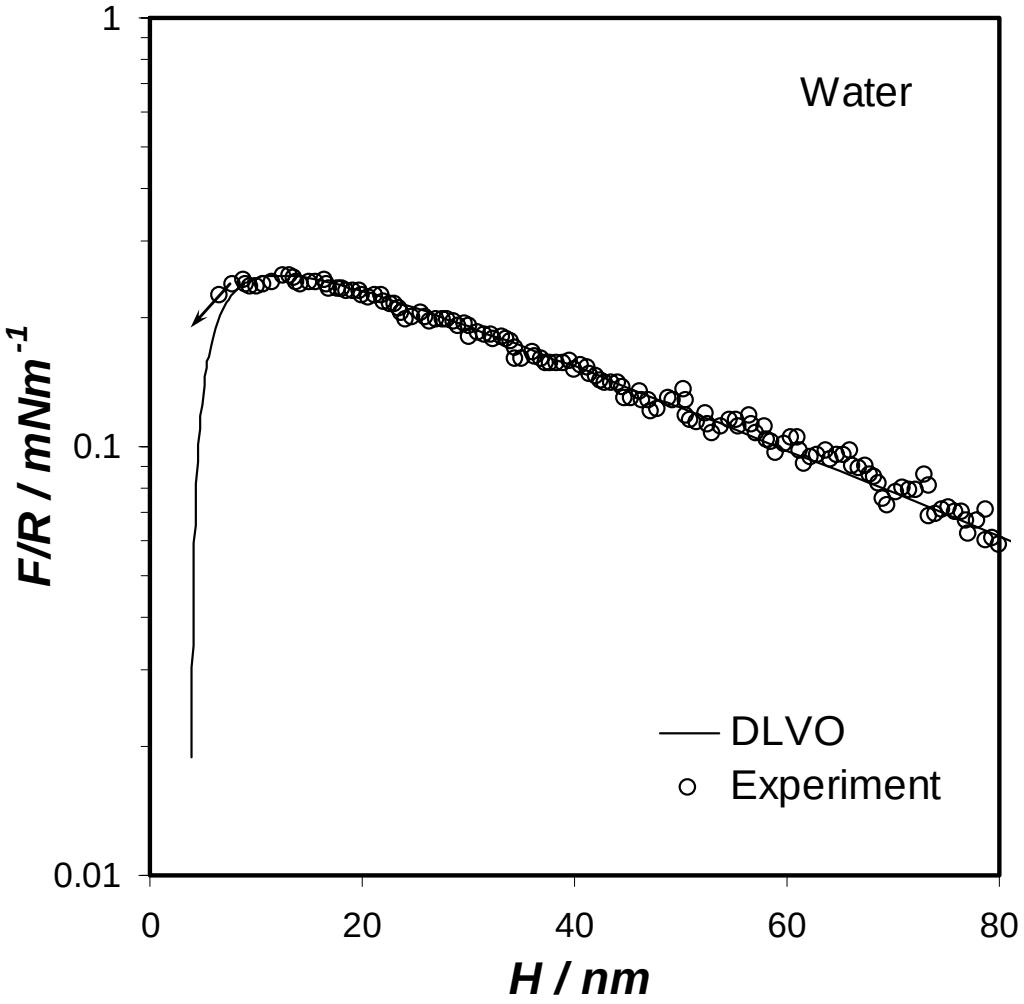

Figure 4.2. Surface force curves for the TiO_2 sphere/plate surfaces immersed in water at pH 6. The solid line is the DLVO fitting curve using a constant potential. The fitting surface potentials for TiO_2 sphere and plate are -50±3mV. The Hamaker constant $A_{TiO2/water/TiO2}$ is $4\pm1\times10^{-20}$ J. The arrows represent the point where the cantilever undergoes a mechanical instability.

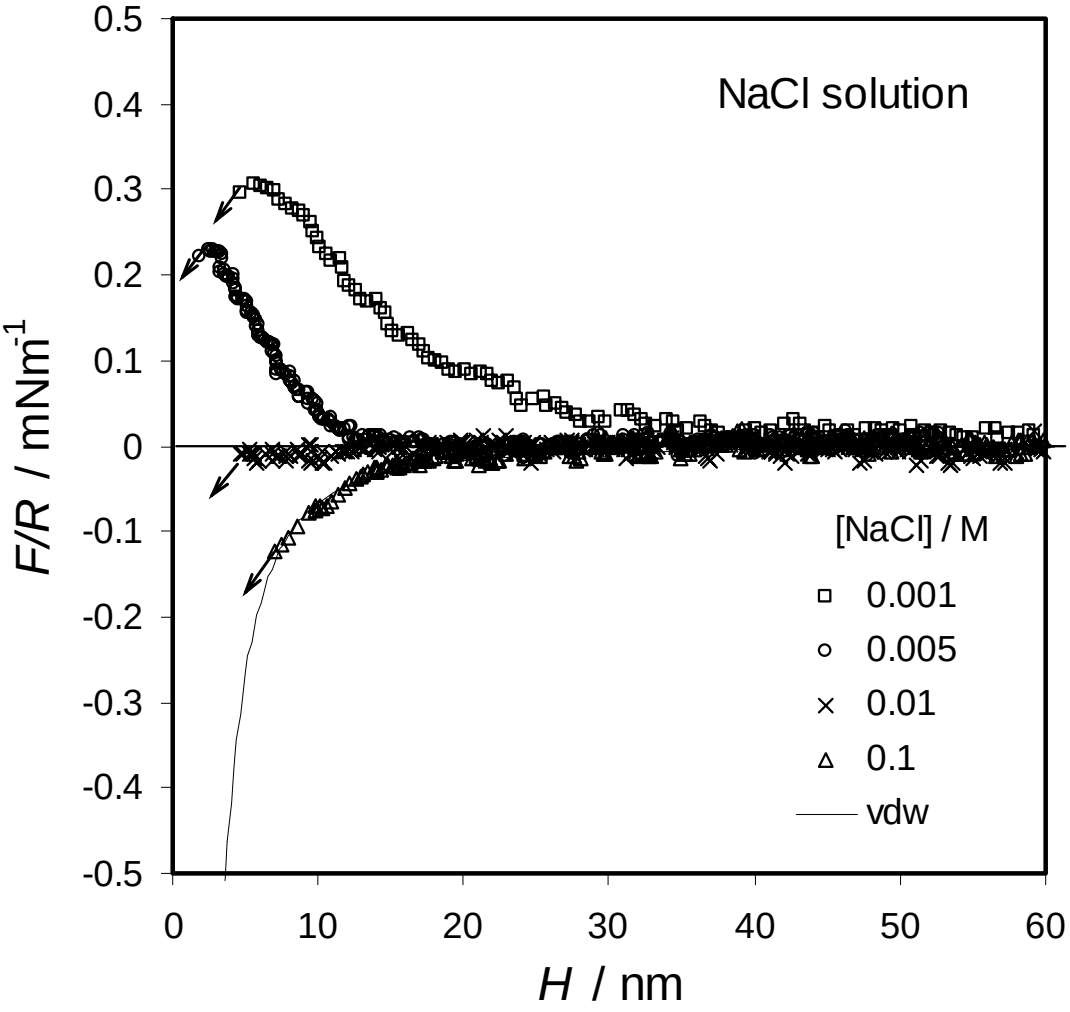

Figure 4.3 Surface force curves for the TiO_2 sphere/plate surfaces immersed in water at different electrolyte concentrations. The solid line is the van der waals force curve with a Hamaker constant $A_{TiO2/water/TiO2}$ of 3.5×10^{-20} J. From top to the bottom, the experimental force curves are respectively obtained in 0.001, 0.005, 0.01 and 0.1 M NaCl solutions. The repulsive electrostatic force is further depressed with electrolyte concentration increasing and only the van der waals force exists, when the salt concentration is as high as 0.1M.

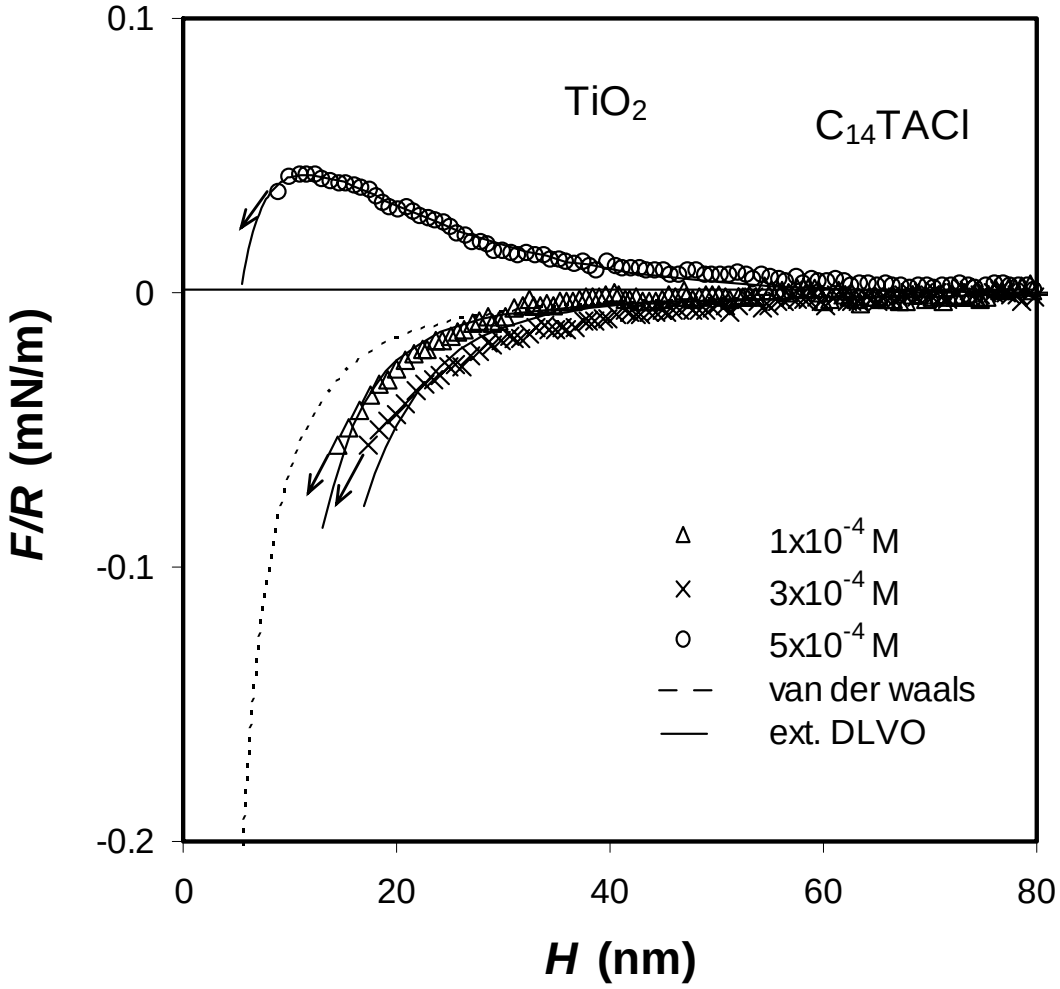

Figure 4.4 Surface force curves for the TiO_2 sphere/plate surfaces immersed in $C_{14}TACl$ solutions at different surfactant concentrations. The solid line is the van der waals force curve with a Hamaker constant $A_{TiO2/water/TiO2}$ of 4×10^{-20} J. Dash lines are the extended DLVO fitting result with an additional single-exponential attraction. The long-range forces measured are most attractive at $3x10^{-4}$ M $C_{14}TACl$, which is close to the p.c.n.

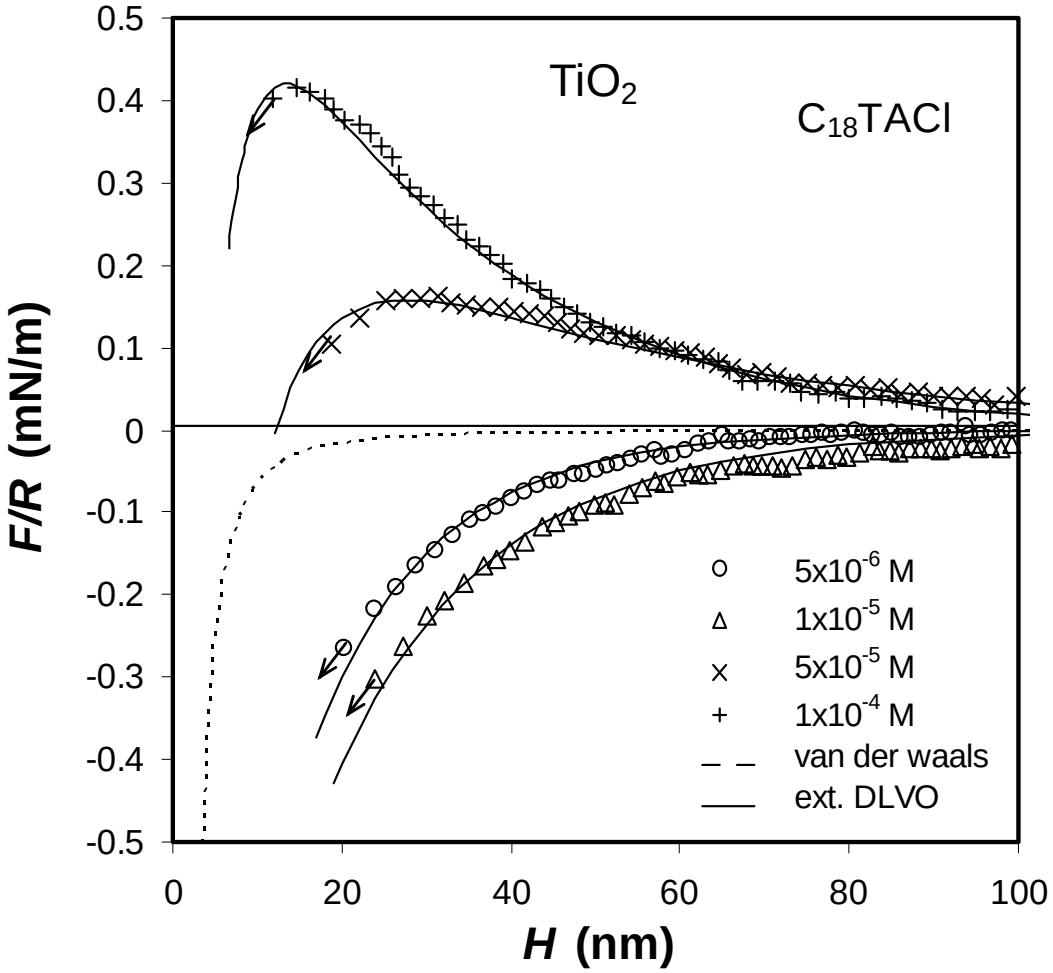

Figure 4.5 Surface force curves for the TiO_2 sphere/plate surfaces immersed in $C_{18}TACl$ solutions at different surfactant concentrations. The long-range forces measured are most attractive at $1x10^{-5}$ M $C_{14}TACl$, which is close to the p.c.n.

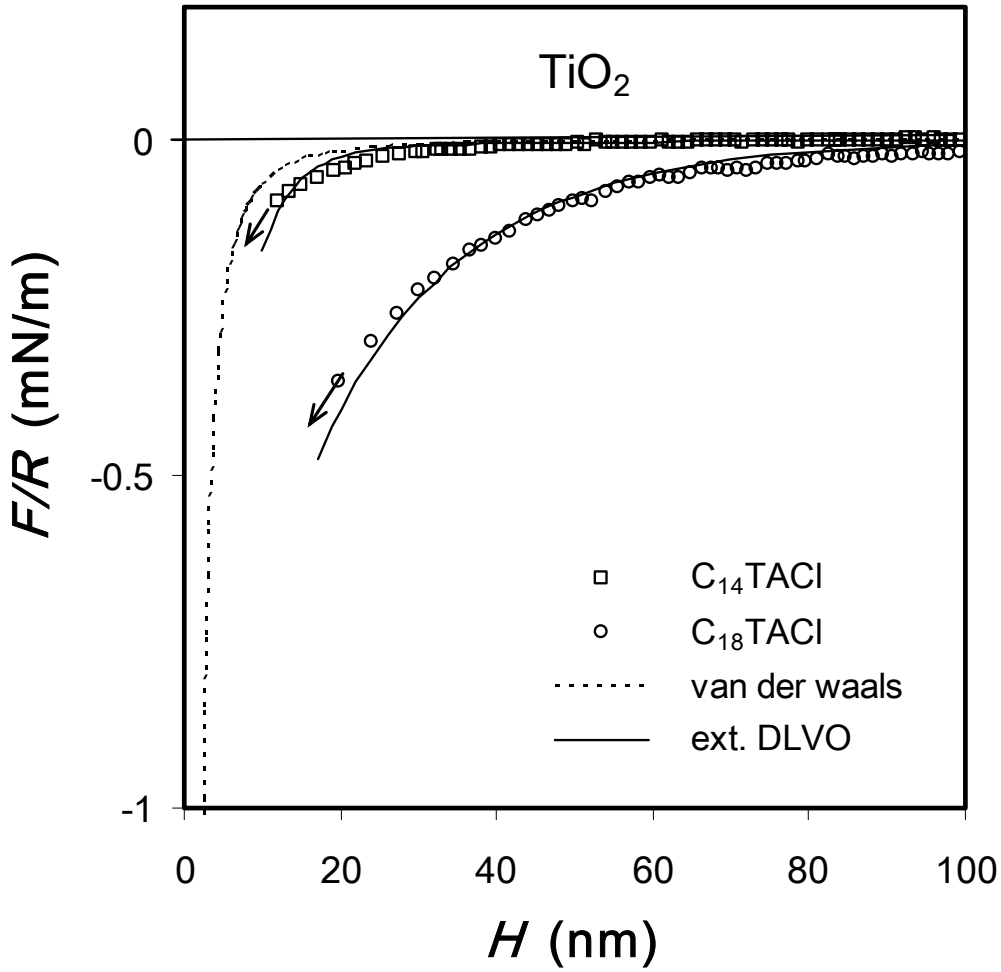

Figure 4.6 The strongest attractive surface force for the TiO_2 sphere/plate combination immersed in each of the C_nTACl (n = 14, 18) solutions. The long range attraction increases both in magnitude and range upon increasing the hydrocarbon chain length of the surfactant.

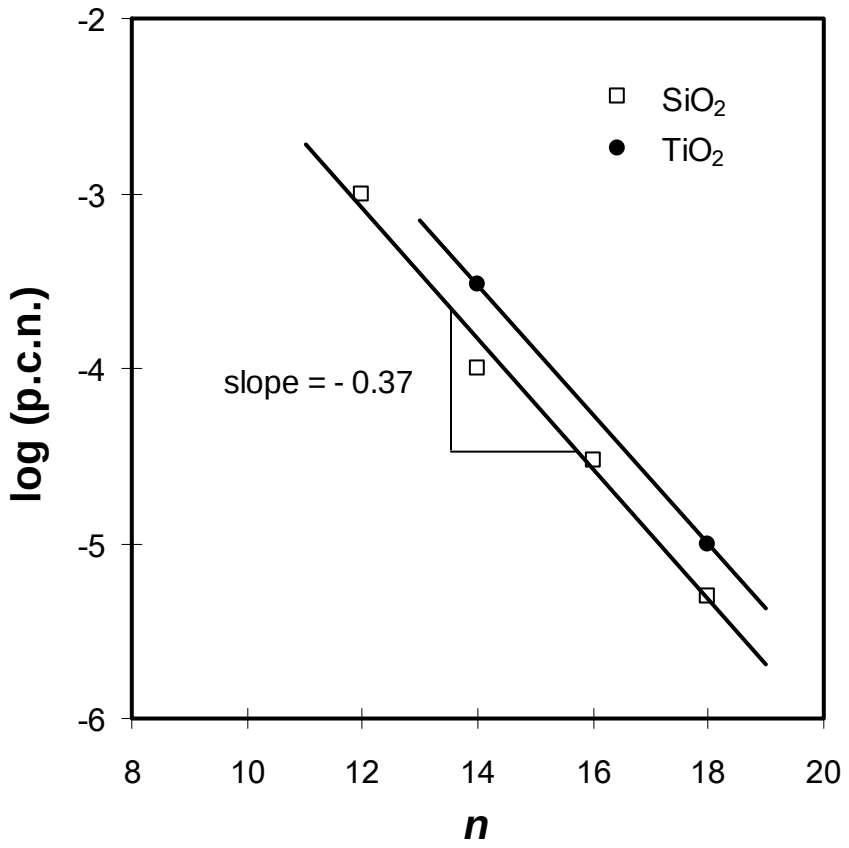

Figure 4.7 A relationship between the p.c.n.'s for the silica-C_nTACl system and the number of carbons in the hydrocarbon chains. According to the Stern-Graham equation (Eq. [5]), the slope of -0.37 gives ϕ = -0.85 kT per CH_2 group.

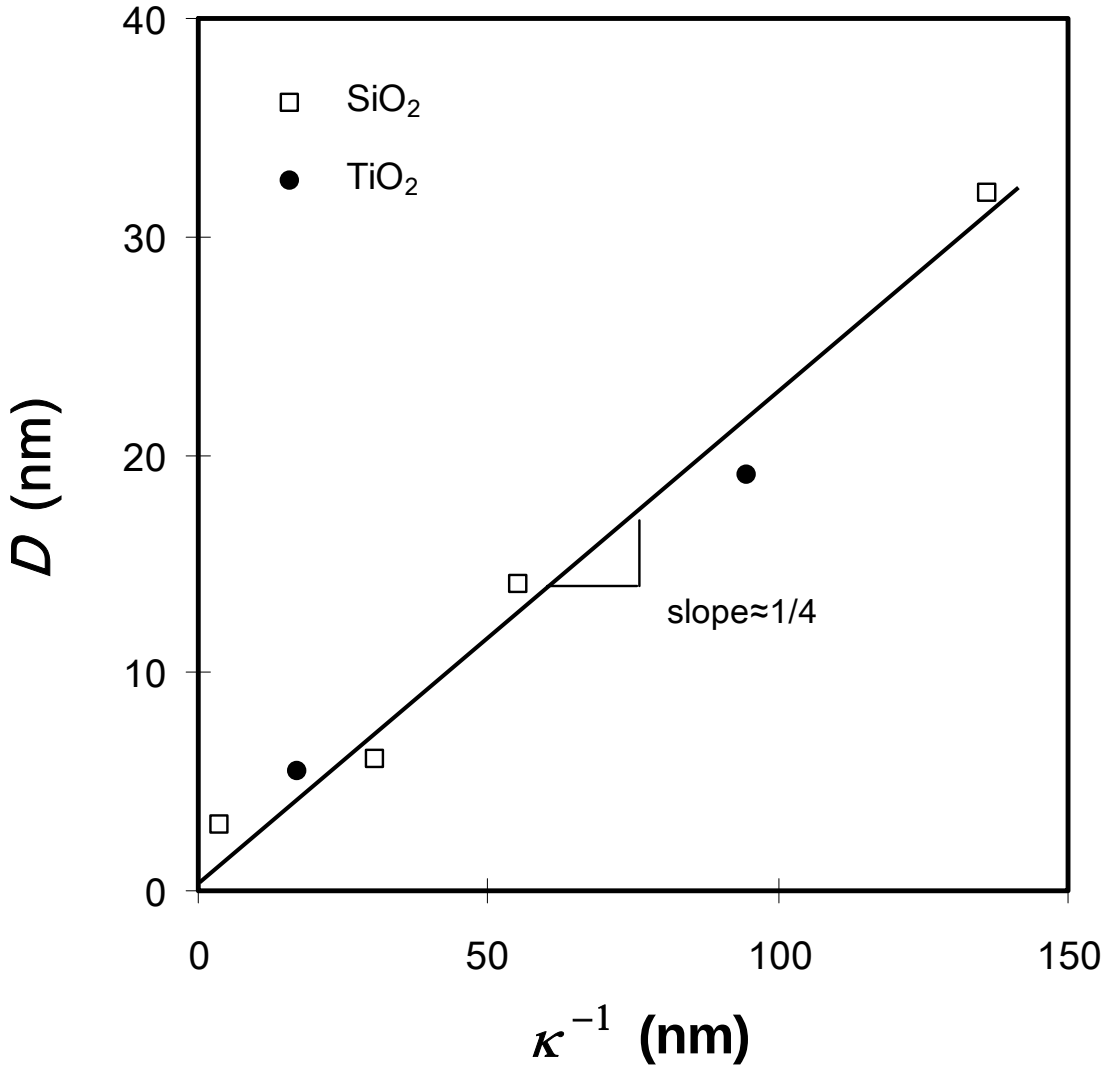

Figure 4.8 Decay length *vs.* Debye length plots for the data obtained between TiO_2 surfaces and SiO_2 surfaces in C_nTACl solutions at the p.c.n.'s in the absence of electrolyte. The experiment results show a linear relationship of D vs. κ^{-1}, giving a slope of ¼.

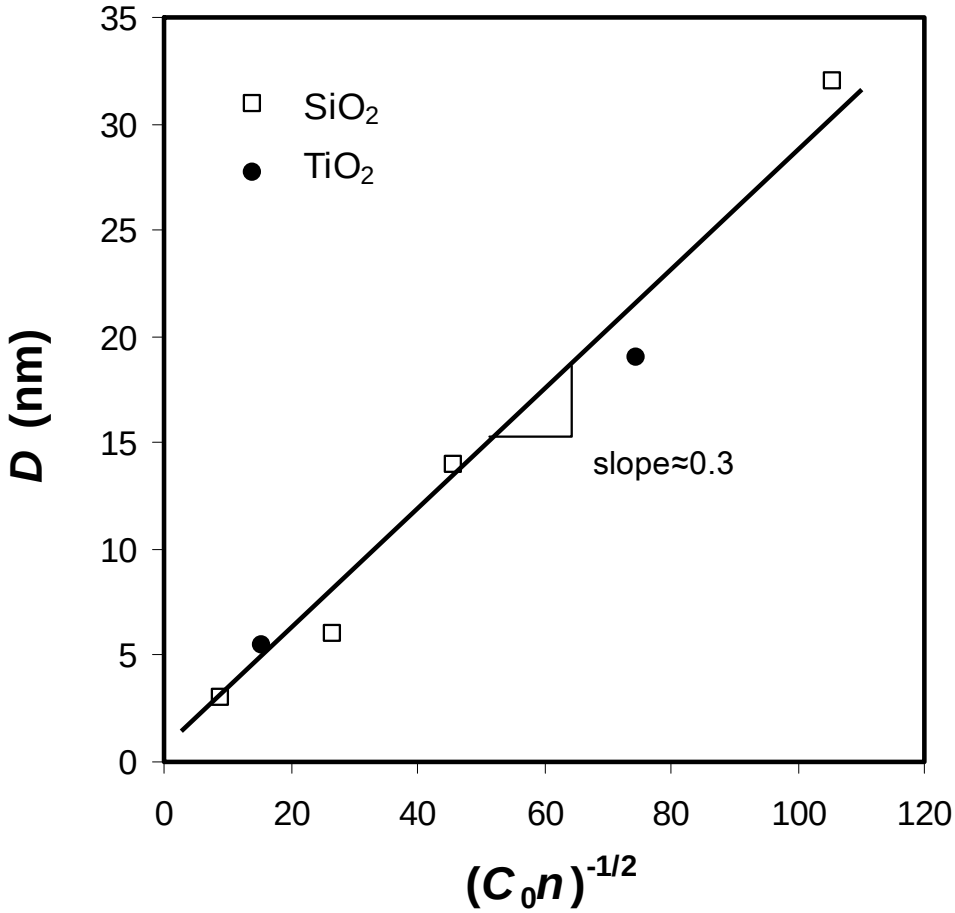

Figure 4.9 A decay length (D) *vs*. $(C_0n)^{-1/2}$ plot for the data obtained between TiO_2 surfaces and SiO_2 surfaces in C_nTACl solutions in the absence of electrolyte. C_0 represents the surfactant concentration, and D is equivalent to b^{-1} of Eriksson *et al*.'s hydrophobic force model (Eq. [12]). (53) derived from the mean-field theory. C_0n represents the effective concentration of CH_2 or CH_3 species in solution.

CHAPTER 5

Characterization of Surface Free Energies of Talc Powders Using the Thin Layer Wicking Technique

Abstract

Thin layer wicking technique was used to determine the contact angles (θ) of different liquids on powdered talc samples. The measured contact angles were used to calculate the surface free energies (γ_S) of talc and its components, which included dispersion (γ_S^d), acidic (γ_S^+), basic (γ_S^-), and acid-base (γ_S^{AB}) surface free energies, using the van Oss-Chaudhury-Good (OCG) equation derived from the Surface Tension Component theory or the Acid/Base Theory.

Experimental results showed that the wicking experiments should be carried out in a gas-tight chamber to eliminate the effects of vaporization, which was especially a serious problem for volatile/low energy wicking liquids. The effective capillary radius in the Washburn equation was found to be in a good linear relationship with the particle size, D_{50}. It suggested that a rather long wicking time was needed for the powder samples with small particle size. It was recommended that, from the analysis of the experiment results, it is better to choose the water as one of the two polar wicking liquids to obviate abnormal results.

The surface free energy characterization was conducted on both the basal and edge surfaces of talc using the novel technique developed in CAST of Virginia Tech. The results showed that talc is a low surface energy solid, and that its basal surfaces are weak basic, while its edge surfaces are acidic. It has also been found in present investigation that in some specific size range, the hydrophobicity of talc increases with decreasing particle size, indicating that fracture occurs preferentially along the basal surface of talc. When the particle size is further reduced to a certain limit, however, the surface free energies of talc increase, indicating that talc begins to fracture along the edge surfaces, thereby exposing more hydrophilic surfaces.

5.1 Introduction

Talc ($Mg_3Si_4O_{10}(OH)_2$) (1) is a natural mineral of which the elementary sheet is composed of a layer of magnesium-oxygen/hydroxyl octahedral sandwiched between two tetrahedral silica layers(2, 3). Its main surface, the face surface, of an elementary sheet shows a high hydrophobicity with no hydroxyl groups or active ions; whereas the edge surface shows some hydrophilicity because of the existence of pH dependent SiOH and MgOH sites(4, 5) This dual surface property of talc plays an important role in many of the industrial applications, including paper coatings, pitch control, ceramics manufacture, and as filler in the plastics, polymer, paint and cosmetics industries.

In the paper industry, for the pitch and sticky control applications, the hydrophilic property of the edges allows the particles to be dispersed in aqueous media, while the hydrophobic property of the basal surfaces attract the sticky hydrophobic substances present in wood pulp. For filler applications, proper control of the adhesion between talc filler and the matrix is essential in controlling the property of the composite material. The strength of adhesion depends on the surface properties of the filler and of the matrix (6). In general, strong filler-matrix interactions result in improved processability, impact strength, and surface quality, while interactions that are too weak lead to decreased strength and increased deformability of the composite (7).

Therefore, determination of surface properties both at the basal and edge surfaces of talc is essential for understanding the origin of molecular interaction and strength of adhesion between two interacting surfaces, i.e., talc and polymers, stickies, etc. It will also be helpful for the proper selection of surfactants used in the surface treatment of talc. Thus, it is crucial to determine the surface free energy and its components at the basal and edge surfaces of talc individually.

In this communication, the thin-layer wicking technique is applied to determine the surface free energy of talc powders. The relationship between solid surface free energy and particle size is thus drawn based on the wicking results. Further, the flow microcalorimetry is utilized to determine the basal/edge surface area ratio of talc powders. Thus, solid surface free energy components on basal and edge of talc surfaces are accordingly inferred based on the unique technique developed in present work.

5.1.1 Acid/Base theory

Surface free energy is a fundamental parameter to quantify the wetting and adhesion phenomena which have been widely studied due to their importance in many industry applications. For example, a low solid surface free energy value suggests a poor wetting of water on this solid and a strong adhesion between the solid particles in aqueous solution. For non-polar materials, the surface free energies values can be directly measured or simply calculated from the van der Waals force interaction. However, how to quantify the surface free energies of polar materials is still under hot debate. The Surface-Tension-Component theory or the Acid/Base Theory developed by van Oss et al. (8-12) is by far the mostly used and applicable theory for the characterization of surface free energies of materials in both fundamental research and industry practice, even though some problems still have to be addressed. The theory can be briefly described as follows.

Fowkes (13-14) first proposed that the surface free energy of a material *i* can be subdivided into separate components:

$$\gamma_i = \sum_j \gamma_i^j \qquad [1]$$

where j refers to types of surface free energy component, e.g., dispersion, H-bonding, and metallic interactions. Later, Van Oss *et al*. (8-12) considered the surface tension as a sum of apolar Lifshitz-van der Waals, γ^{LW}, and polar acid/base interactions, γ^{AB}. Therefore, Eq. [1] can be expressed as:

$$\gamma_i = \gamma_i^{LW} + \gamma_i^{AB} \qquad [2]$$

in which γ_i^{LW} and γ_i^{AB} refer to the non-polar and polar (acid-base) surface free energy components, respectively. The former can be represented by the Lifshitz-van der Waals (or LW) interactions that include the dispersion (London), induction (Debye) and orientation (Keesom) components. The latter represents interactions between Lewis acids (electron acceptor) and bases (electron donor) on the surface.

van Oss *et al.* (8-12) used the geometric mean combining rule to define γ_i^{AB} as follows:

$$\gamma_i^{AB} \equiv 2\sqrt{\gamma_i^+ \gamma_i^-} \qquad [3]$$

where γ_i^+ is the acidic component of the surface tension and γ_i^- is the basic component. Therefore, Eq. [2] can be transformed into

$$\gamma_i = \gamma_i^{LW} + 2\sqrt{\gamma_i^+ \gamma_i^-} \qquad [4]$$

It can be readily shown also that the free energy change (ΔG) associated with the adhesion of a liquid on a solid in the air is given by:

$$\Delta G = -2\left(\sqrt{\gamma_S^{LW}\gamma_L^{LW}} + \sqrt{\gamma_S^+\gamma_L^-} + \sqrt{\gamma_S^-\gamma_L^+}\right) \qquad [5]$$

where γ^{LW} is the Lifshitz-van der Waals component of the surface energy, γ^+ the acidic component, and γ^- is the basic component of the interacting solid (subscript S) and liquid (subscript L) surfaces.

Combining Eq. [5] with the well known Dupre equation:

$$\Delta G_{SL} = \gamma_{SL} - \gamma_S - \gamma_L \qquad [6]$$

one obtains:

$$\gamma_{SL} = \gamma_S + \gamma_L - 2\left(\sqrt{\gamma_S^{LW}\gamma_L^{LW}} + \sqrt{\gamma_S^+\gamma_L^-} + \sqrt{\gamma_S^-\gamma_L^+}\right) \qquad [7]$$

Combining Eq. [7] with the Young's equation,

$$\gamma_L \cos\theta = \gamma_S - \gamma_{SL} \quad [8]$$

where θ is contact angle, one obtains the van Oss-Chaudhury-Good (OCG) equation:

$$(1+\cos\theta)\gamma_L = 2\left(\sqrt{\gamma_S^{LW}\gamma_L^{LW}} + \sqrt{\gamma_S^{+}\gamma_L^{-}} + \sqrt{\gamma_S^{-}\gamma_L^{+}}\right) \quad [9]$$

which can be used to characterize a solid surface in terms of its surface free energy components, i.e., γ_S^{LW}, γ_S^{+}, and γ_S^{-}. In order to determine these values, it is therefore necessary to determine contact angles of three different liquids of known properties (i.e. γ_L^{+}, γ_L^{-}, γ_L^{LW}) on the surface of the solid of interest. One can then set up three equations with three unknowns, which can be solved simultaneously to obtain the values of γ_S^{LW}, γ_S^{+}, and γ_S^{-}.

5.1.2 Thin layer wicking technique

The contact angle of liquid on a flat and smooth solid plate can be easily obtained using the sessile drop method. In practice, however, it is impossible to directly measure the contact angle of liquid on powdered solids, especially for clay particles. Thin layer wicking technique is specially developed to measure contact angles of the liquids on powdered materials (15, 16) by determining the capillary rise rate of the wicking liquids in packed beds of those particulate materials. It is proposed that the wicking process follows the Washburn's equation (17):

$$\frac{2\eta h^2}{t} = R_{eff} * \gamma_L * \cos\theta \quad [10]$$

in which η is the viscosity of the liquid, h is the height to which the wicking liquid has risen at elapsed time t, R_{eff} is the effective interstitial pore radius of packed powder bed, γ_L is the surface tension of wicking liquid and θ is the contact angle.

The parameter R_{eff} of Eq. [10] is generally determined by wicking with low-energy spreading alkanes, for which the contact angle, θ is assumed to be zero on the solid. Thus, Eq. [10] is reduced into the following equation:

$$\frac{2\eta h^2}{t} = R_{eff} * \gamma_L \quad [11]$$

After wicking with several low energy alkanes, one can draw a plot of $2\eta h^2/t$ vs. γ_L. The slope of the straight fitting line passing through origin gives the effective interstitial pore radius R_{eff}, which is to be used for further surface free energies calculation using high energy wicking liquids.

Following the same wicking procedure described above, one can obtain the contact angle of high energy liquid, such as water, on powder surface by wicking with the liquid on thin powder layer. With the R_{eff} value obtained from wicking result with low energy alkanes, it is easy to calculate the water contact angle by solving Eq. [10], in which

contact angle is the only unknown parameter. Table 1 gives a list of liquids that can be used for the contact angle measurements, along with the values of γ_L, γ_L^{LW}, γ_L^+, and γ_L^-.

5.1.3 Surface free energy characterization of basal/edge surfaces

It has been shown that flow microcalorimetry can be utilized for characterizing solid surfaces and their interactions with liquids (18-20). It was also used to estimate the percentage of hydrophilic (polar) and hydrophobic (nonpolar) surface sites on powdered solid surfaces (21-22). In this method, a talc sample is equilibrated initially with heptane and then contacted with a 2 g/l butanol solution while measuring the calorimetric heat effect. The heat effect is due to the butanol displacing heptane from the hydrophilic edge surface of the talc sample. Since heptane is non-polar in nature, it will be adsorbed strongly on the hydrophobic basal surface rather than on the hydrophilic edge surface. By dividing the heat effect with the total surface area of talc sample used in the measurement, one can obtain the molar heat of adsorption ($-\Delta H_{ad}$) of butanol in unit of mJ/m^2. Further, by dividing this value with the heat of adsorption of butanol on silica (197 mJ/m^2), one obtains the fraction of the talc surface area that is hydrophilic, i.e., fraction of edge surface area, (f_e). Also, one can get the basal surface area fraction, f_b, which equals one minus f_e.

The technique has been developed in CAST in Virginia Tech that surface free energy characterization studies should be conducted at two different sizes (D_1 and D_2) (15), in order to determine the surface free energy components at the basal and the edge surfaces of talc. The solid surface free energy (γ_s) and its components (i.e., γ_s^{LW}, γ_s^+, and γ_s^-) for each of the two different samples are obtained using the above described thin layer wicking technique. From the known f_e and f_b values obtained from flow microcalorimetry, one therefore can set up the following equation (15):

$$\gamma_s^{D_1} = f_b^{D_1}\gamma_s^b + f_e^{D_1}\gamma_s^e \qquad [12]$$

in which γ_s^b is γ_s at the basal surface and γ_s^e is γ_s at the edge surface. Eq. [12] suggests that the value of γ_s is a composite of γ_s^b and γ_s^e in proportion to f_b^{D1} and f_e^{D1}. Similarly, one can set up the following equation at size D_2:

$$\gamma_s^{D_2} = f_b^{D_2}\gamma_s^b + f_e^{D_2}\gamma_s^e \qquad [13]$$

In writing Eqs. [12] and [13], it is explicitly assumed that γ_s^b and γ_s^e are intensive properties of talc and do not change with particle size, which is somehow reasonable due to the two materials are nearly of the same. By solving Eqs. [12] and [13] simultaneously, one can obtain the values of γ_s^b and γ_s^e. Likewise, simultaneous equations for γ_s^{LW}, γ_s^{AB}, γ_s^+, and γ_s^- can be set up and the respective values at the basal and edge surfaces of talc are therefore obtained.

5.2 Experimental

Materials

Nanopure water was obtained by Nanopure III (Barnstead, IA) water system. The conductivity of the water was 18.2 MΩ/cm at 23°C and the surface tension was 72.5mN/m at 22°C. Pre-cleaned glass microslides (75x25 mm, Corning, NY) were used without further cleaning.

Wicking liquids used in the present work, Alkanes, such as Heptane, Octane, Decane and Dodecane (Aldrich Chemical Company) were HPLC grade (>99.5% purity). The surface tension and viscosity data of these wicking liquids are listed as Table 1. HPLC-grade acetone and butanol were purchased from Fluka and both had purities greater than 99.5%.

Powdered talc samples of different particle sizes, labeled Luz A to Luz F, were kindly provided by Luzenac America (Englewood, CO.). They are readily used without further treatment.

Thin layer wicking technique

A known amount of a given talc powder was dispersed in deionized water to make a 5% (w/v) suspension. Aliquots of 5 ml suspensions were withdrawn with a pipette and evenly distributed onto a microscopic glass slide, which was kept strictly horizontal. The water was allowed to evaporate overnight at room temperature and then the slides coated with thin talc powder layer are further dried in an oven at 150ºC overnight to remove residual pore water. It was then cooled down in a vacuum desiccator before being used for wicking experiments.

The wicking experiments were carried out in a closed chamber, in which the glass slide was vertically placed with the side with coated talc layer facing the observer. The probe liquid was filled in the chamber beforehand and the slide above the liquid was lowered to contact the wicking liquid as the wicking process starts. A scale was carefully marked along the slide with the edge of the slides to set the zero position. The time for the probe liquid to travel through every 5 mm interval was recorded using a stopwatch. The wicking was stopped after enough wicking time, which is generally 20-30 minutes, has elapsed. With each sample, the tests were repeated at least three times for each probe liquid and the values reported here were the arithmetic averages over three sets of experiment data.

The value of the parameter R_{eff} of Eq. [11] was determined using liquids of low surface free energy (heptane, octane, decane and dodecane), all of which were found to completely spread over the solid surface (i.e., $\theta=0$). Experimental results showed that the $2\eta l^2/t$ vs. γ_L yielded a straight line passing through the origin. This finding confirms the applicability of the Washburn equation, Eq. [11] under the wicking conditions in present work.

Flow microcalorimetry

Heats of adsorption measurements were conducted using a Model 3V flow microcalorimeter (FMC) from Microscal, United Kingdom. Figure 1 shows a schematic diagram of the calorimeter. In each measurement, a talc sample was dried overnight in an oven at 110 ºC. A known amount (usually 0.05-0.15 gram) of the dried sample was placed in the calorimeter cell, and degassed for at least 30 minutes under vacuum (<5 mbar) at ambient temperature. The vacuum system consisted of a vacuum pump and a liquid nitrogen vapor trap. The solvent was then introduced to the calorimeter cell at a

steady flow rate of 3.3 ml/h by means of a syringe pump, and two Valco Instrument changeover valves for switching between solvent and solution. The heat effect was recorded by means of a strip chart recorder and a PC. After the thermal equilibrium was reached, which usually took 8 to 30 minutes, the solvent was switched over to the solvent containing adsorbate and the solution was introduced to the cell at a flow rate of 3.3 ml/h. The heat of interaction of an adsorbate on the solid was also recorded using a strip chart recorder and a PC. The recorded experimental data was analyzed using the Microscal Calorimeter Digital Output-Processing System (CALDOS), which enables the analysis of calibration and experimental data and converts the raw downloaded data into the heat of immersion (Δh_i) and heat of adsorption (Δh_{ads}) values.

5.3 Results and Discussion

5.3.1 Effects of volatility of wicking liquids on the wicking speed

It has been suggested that the wicking experiments should be done in an airtight chamber (23, 24). However till now no specific work has been done to quantify the effect of volatility of probe liquids on the wicking process in an open or a closed chamber. The experiment results, wicking with Heptane, Octane, Decane and Dodecane on talc sample of Luz E, were respectively plotted and shown as Figures 2a to Figures 2d, which clearly show the evaporation effect of different liquid on its wicking behavior. The wicking conditions for each process were also listed in Table 2.

It is shown in Figure 5.2a that when wicking with Heptane, it is suggested to carry out the experiment in a sealed chamber even without exposing the slide in the chamber beforehand. Because of the high volatility of Heptane, the wicking speed is greatly decreased in an open condition. It was even observed in the experiment that in an open chamber the liquid front line on the slide coated with talc powder didn't advance at all after wicking for a specific distance.

Figure 5.2b shows the results of liquid Decane in four different conditions. It is clearly seen that, similar to the one found in the wicking tests with Heptane, the capillary rising speeds of Decane is also somehow decreased in an open condition, when compared to the results obtained in an airtight chamber. Keeping the slides equilibrated in the closed chamber with the liquid vapor has no significant effect on the wicking speed only if the experiment was carried out in an airtight condition.

The wicking tests with Decane are shown in Figure 5.2c. It is interesting to note that the wicking speeds of the probe liquid on talc powder slides are almost the same under four different conditions. That is, the chamber is open or not during the wicking process has no little effects on the results. The reason is believed to be due to the fact that Decane is not a quite volatile liquid; therefore, the wicking speed of Decane will not be reduced evidently because of its volatility even the experiment is carried out in an open chamber.

Figure 5.2d shows that all the thin-layer wicking results obtained with Dodecane, one can see that there was not much difference between wicking results under all these experiment conditions. This finding is the same as the one obtained with Decane. That is, the volatility of liquid has little effect on the capillary rising of the liquid in the thin-layer bed of talc powder. Either pre-equilibrated with liquid vapor or wicking in an airtight chamber has no pronounced effect on thin-layer wicking process when wicking with non-

volatile liquids, such as Decane and Dodecane, which have a relatively high surface tension.

The experiment data obtained in Figure 5.2a to Figure 5.2d are further plotted in the relationship of $2\eta h^2/t$ vs. γ_L and the results are shown in Figure 5.3. It is clearly shown that the data attained under the condition of wicking in an air-tight chamber are almost on the same straight line passing through the origin, which suggests the applicability of the Washburn equation in the wicking test. On the other hand, the data obtained with low surface tension liquids are a little below the straight line, especially in the case of wicking in an open situation. It is clearly shown that the volatility of the liquid greatly decreases the wicking speed of liquids and makes the wicking process away from the Washburn equation. It is worthwhile to mention that, when wicking with low energy liquids, the capillary rising technique, either the column wicking and thin layer wicking, should be carried out in a sealed chamber saturated with vapor of wicking liquid, because the low surface tension wicking alkanes has a high volatility, which greatly decreases the wicking speed when wicking in a open situation (8, 25). Negligence to this prerequisite results in the fitting line of $2\eta h^2/t$ vs. γ_L relationship not passing through the origin with a large intercept on the x-coordinate (25). Another finding is that there is no evaporation effect on wicking results when Decane and Dodecane are used as probe liquids and the pre-equilibrated with vapor is not necessary for wicking with these two liquids. It suggests that when wicking with Decane and Dodecane, it is not necessary to carry out thin-layer wicking experiments with Decane and Dodecane in an airtight chamber.

5.3.2 Determination of the effective pore radius (R_{eff}).

Figure 5.4a shows the results of the thin layer wicking experiments conducted with four different non-polar alkane liquids, namely Heptane, Octane, Decane and Dodecane, on the glass slides coated with Luz C talc powders, of which the average particle size, D_{50} is 3.2 μm. It is clearly shown in the figure that there is a very good linear relationship between the wicking distance square h^2 and wicking time t.

Figure 5.4b shows the thin layer wicking experiment results of four different low surface energy alkanes wicking on glass slides coated with Luz E, of which the average particle size, D_{50} is 7 μm. Same as the one shown in Figure 1, the wicking distance square h^2 and the wicking time t follow a good linear relationship. It suggests that when low surface free energy alkanes are used as wicking liquids, they spread automatically on solid surface and form zero degree contact angles; thus the viscosity of the wicking liquid was the only parameter that determined the wicking velocity.

The wicking experiment results shown in Figure 5.4a and Figure 5.4b were fitted linearly and the slope, which equals h^2/t, was inputted to the left of Eq. [11] to obtain the value of $2\eta h^2/t$ for each wicking liquid. Further, the relationship of $2\eta h^2/t$ vs. γ_L for each wicking liquid was plotted for the Luz C and Luz E samples and shown as Figure 5.5. It is clearly seen form the figure that for each talc sample, $2\eta h^2/t$ vs. γ_L follows a good linear relationship and the straight line passing through the origin, which indicates that the contact angles of these wicking liquids are zero and Eq. [11] is applicable under the present experiment conditions. It is also shown in Figure 5.5 that the slope of $2\eta h^2/t$ vs. γ_L, or the effective pore size (R_{eff}), is larger for Luz E, a coarser talc sample, than that for the finer Luz C talc sample.

5.3.3 Effective pore radius (R_{eff}) vs. particle size (D_{50}).

van Oss *et al*. (26) studied wicking of porous monosized polymer particles using column wicking technique. Their results show that the effective pore radius *(R_e)* increases with particle size *(D_{50})*. However, the scatting of the data suggests that a uniform packing bed is not easily obtained using column wicking technique, resulting in the low repeatability of experiment.

van Oss *et al*. (26) further derived the relationship between R_{eff} and D_{50} for spherical shape particles based on the experiment data. It was written as follows,

$$R_p = \frac{3\Phi}{2(1-\Phi)} \cdot R_{eff} \qquad [14]$$

then, it can be transformed as,

$$R_{eff} = \frac{2(1-\Phi)}{3\Phi} \cdot R_p = \frac{1}{3} \cdot \left(\frac{1}{\Phi} - 1 \right) \cdot D_{50} \qquad [14a]$$

in which Φ is the volume fraction of solid in a packed volume of particles. Eq. [14a] shows that the effective pore size (R_{eff}) of powder bed is determined by the volume fraction of solid (Φ) and particle size (D_{50}) of the powder bed. When other parameters, such as powder shapes are of nearly the same, according to the equation, finer powders not only has a smaller D_{50}, but also makes a dense packing powder bed, which in turn introduces a higher volume fraction of solid (Φ). Both these factors give rise to a smaller effective pore size (R_{eff}). That is, the packing property of a powder bed is mainly determined by powder size (D_{50}).

In present work, the effective pore size (R_{eff}) values of several talc samples of different particle sizes were carefully measured and the obtained values and corresponding powder size (D_{50}) for each talc sample were listed as Table 5.3 and plotted in Figure 5.6. It was clearly shown that R_{eff} increases with D_{50}. In addition, that fact that all the data points are almost on a same straight line suggests a perfect linear relationship between the effective pore size and the powder size. That is, even though Eq. [14a] is specially derived for spherical shape particles, the linear relationship is surprisingly applicable for strongly asymmetrical particles, e.g. talc. Threfore, Eq. [14a] can be simplified as follows:

$$R_{eff} = f\left(\frac{1}{\Phi}\right) \cdot D_{50} \qquad [14b]$$

in which $f(1/\Phi)$ is a constant, which is the slope of the straight line obtained in Figure 5.6. It is interesting to note that the slope of R_{eff}/D_{50} obtained in present study is different from that reported in literature (40). Because talc powder is strongly asymmetrical rather than spherical, it suggests that particle shape must have an impact on the slope of. R_{eff} vs. D_{50}. However, it is clearly shown in Figure 5.6 that the R_{eff}/D_{50} values for several different

talc samples, which are of different sizes, are almost the same. Re-examining Eq. [14b], one may conclude that for the talc samples studied in present work, the volume fraction of solid (Φ) does not much change with particle size. Further, because volume fraction of solid (Φ) of the powder bed is determined by the aspect ratio (l_l/l_w) of particles, a constant Φ reflects little change in the aspect ratio (l_l/l_w) when particle size changes from 2 μm to 8 μm. By the way, l_l and l_b are respectively the dimension of particle in length and in width.

5.3.4 Solid surface free energy components vs. particle size (D_{50})

Table 5.4 shows the contact angles of various probe liquids on powdered talc samples measured with thin layer wicking technique described in the experimental section using the Eqs. [10] and [11]. The table shows that the obtained water contact angles on talc samples are in the range from 76 to 89 degree, which suggests the rather natural floatability and high hydrophobicity of talc samples.

These obtained contact angle data are further used to obtain the value of the various surface free energy components, i.e., γ_s^{LW}, γ_s^{AB}, γ_s^+, γ_s^- and γ_s, by solving three set up of Eq. [9]. The calculation results obtained with different combinations of probe liquids are specifically listed as Table 5.5 a-f and also plotted as a function of average particle size (D_{50}) in Figure 5.7 a-d. The data listed in Table 5.5 e and f is too large to be reasonable; therefore, the figures corresponding to the results of these two tables were not provided.

Figure 5.7a shows the experimental results of surface free energies obtained with water, formamide and methylene iodide as the high energy probe liquids. When talc powder size decreases from 20 to 3.2 μm, the surface free energies decreases a little, especially for the parameters of γ_s and γ_s^{LW}. The fact that the polar components γ_s^+,γ_s^- and γ_s^{AB} are rather small for all these talc samples confirms that talc is a natural hydrophobic mineral with little polar site on the surface. When the particle size further goes down to 2.2 μm, the surface free energies, mainly the parameters of γ_s and γ_s^{LW}, of talc samples increase quite a lot. For example, γ_s^{LW} increases from 29.28 mJ/m^2 to 39.31 mJ/m^2 and γ_s increases from 34.42 mJ/m^2 to 41.15 mJ/m^2. Therefore, the talc samples become not so hydrophobic.

The values of surface free energies obtained with such high energy probe liquids as water, formamide and methylene iodide were plotted as Figure 5.7b. The change of surface free energies as a function of particle size followed almost the same trend as shown in Figure 5.7a. The same finding that the surface free energies decrease with particle size to about 3μm first and then increase with particle size was also observed in Figure 5.7c and Figure 5.7d, which were obtained by wicking with different polar liquids combination. The results suggest that when grinding, talc sample is likely to break along the basal planes with surface free energies change a little; however, when the particle size is less than 2~3μm, the sample tends to break across the basal plane, generating more hydrophilic edge surfaces, resulting in an increased solid surface free energies and especially a higher value of γ_s^+. This finding coincides with the work reported by Lobado.

The results shown in Table 5.5a to Table 5.5d confirms the rather good repeatability and applicability of the thin-layer wicking technique in measureming the surface free energies. However, one thing worthy of being mentioned is that, as shown in Table 5.5e and Table 5.5f, some values of the surface free energies are too large to be reasonable. For example, the γ_s for Luz F in Table 5.5e is as large as 1154.26 mJ/m^2. The abnormal

results suggest that using such polar liquids combination is not applicable in practice, even though theoretically there is no flaw at all. On the other hand, as discussed before, Table 5.5a to Table 5.5d show quite good and repeatable results with water as one of wicking liquid. In fact, it has been suggested by van Oss that it is better to always include water as a wicking reagent, which is clearly short of support in theory.

5.3.5 Surface free energy components at basal/edge surfaces of powdered talc samples

The fraction of hydrophobic surface on some Luzenac talc samples were obtained with a flow microcalorimetry described in the experimental section and the results were also listed in Table 5.3. One can see from the table that for the largest sample Luz F, the fraction of hydrophobic surface is 54%. When the particle size decreases to 3.2 μm, the fraction of hydrophobic surface also increases to 77%. That is, when particle size is larger than 3.2 μm, the fraction of hydrophobic surface increases with D_{50}, which is due to the delamination along the basal plane. The fractions of hydrophobic surface on smaller samples are not available in present work. However, it has been reported (16) that when particle size is smaller than a specific limit, the fraction of hydrophilic surface increases with decreasing D_{50}, which is due to the fracture across the basal plane. This finding correlates to the one obtained with surface free energy analysis shown in Figure 5.7. It is therefore reasonably assumed that in present work the fraction of hydrophobic surface will decrease when the sample size is smaller than 3.2 μm.

In order to obtain the surface free energies of the basal and edge surfaces individually, it is necessary to know the area fractions of the basal surface (f_b) and that of the edge surface (f_e) at two different size fractions, as well as the total (or composite) surface free energies (γ) of the two talc samples of different size fractions. The values of f_b and f_e for the two samples are obtained from the % hydrophobic surface area values listed in Table 5.3. In the present work, some combinations of talc samples were chosen for surface free energies calculation and the calculated results are shown in Table 5.6. The combination of talc samples Luz C/Luz E, Luz E/Luz F and Luz C/Luz F gives negative surface free energy values, which is clearly not realistic. However, no negative values were observed using the combination of Luz A/Luz E. The results show that γ_s^-, which is 0.1 mJ/m^2, on the base surface is a little larger than the value, which is 0.07 mJ/m^2, on the edge surface; while γ_s^+, which is 1.38 mJ/m^2, on the base surface is much smaller than the value of 10.6 mJ/m^2 on the edge surface. Despite the obtained negative surface free energies, which are not realistic, the results show one important finding, that is, the basal surface is almost apolar with little polar components of surface free energies, while the edge surface is mainly acidic due to the relatively high γ_s^+ value. This finding is reasonable because the basal surface of talc can be considered as Lewis base because its basal surface consists only of oxygen atoms without cations. Especially these oxygen atoms are nearly fully-compensated, linked together by siloxane (Si-O-Si) bonds, resulting in small polar surface free energy components. The oxygen atoms can donate electron pairs to a base, thereby meeting the definition of Lewis base. On the other hand, the edge surfaces of talc are composed of MgOH, SiOH and the other substituted cations, e.g. Al^{3+}, Fe^{2+}. Therefore, the edge surfaces, can readily dissociate to give up protons, thereby acting as Bronstead acid.

The negative surface free energies on base/edge talc surface obtained from Eqs. [12] and [13] has already been reported. It was suggested that this may due to the inaccuracies associated in determining the values of f_b and f_e. In the present work, these values were determined using the heats of adsorption of technique, which is used in the talc industry. In this technique, heat of adsorption is measured by immersing a dry talc sample in a butanol-in-heptane solution, and the measured value is divided by the heat of adsorption of silica in the same solution. This method assumes that butanol adsorbs only on the edge surface and that the heat of adsorption on talc is the same as on quartz. In addition, one can see that it is the combination of samples Luz C, Luz E and Luz F that gives negative values. It has already been shown in Figure 7 that the surface free energy components for these samples are rather close to each other. A small inaccuracy associated in determining the values of f_b or f_e may easily result in 'abnormal' calculated values because of the little difference of surface properties between these samples, which can make the combination of Eqs. [12] and [13] 'ill-conditioned'. On the other hand, the calculation using Luz A and Luz E, of which the surface free energy parameters are not of the same, give much more reasonable results. Therefore, in order to obviate the negative surface free energy values, it is recommended better to choose two samples of the relatively large difference between the each other in surface area fractions and surface free energies.

5.4 Conclusions

In present work, thin layer wicking technique was used to determine the surface free energy components on powdered talc samples. The results showed that under the experiment conditions employed in the present work, the penetration of liquids in powder layer follows the Washburn's equation. It was suggested that when wicking with low surface tension liquids, such as Heptane and Octane, it is highly required to carry out thin-layer wicking experiments in an airtight chamber due to their high volatility which may greatly reduce the wicking speed. However, the restriction is not necessary for the liquids with high surface tension, such as Decane and Dodecane. The results also showed that the effective interstitial pore radius (R_{eff}), which is obtained by wicking with low-energy alkenes, varies linearly with particle size size (D_{50}). It was also recommended that it is better to choose the water as one of the two polar wicking liquids to obviate abnormal results.

It was also found that there is a relationship between particle size and the hydrophobic/hydrophilic surface area ratios. As the particle size decreases, the surface free energies parameters decrease and the hydrophobic surface area ratio increases, indicating that the mineral fractures preferentially along the basal surface. When the particle size becomes smaller than approximately 3 μm, however, the surface free energies begins to increase, indicating that the fracture occurs preferentially across the basal surface, resulting in more exposed edge surfaces.

The basal-to-edge surface area ratios of talc samples have been used to calculate the surface free energies using the acid-base theory, the surface free energies of the basal and edge surfaces of the mineral have been determined. The results show that the basal surface is weak basic and the edge surface is mainly acidic.

5.5 References

1. E. Z. Orowan, Phys. 1933, 82, 235.
2. B. W. Evans, S. Guggenheim, Rev. Min. 1988, 19, 225.
3. A.U. Gehring, et al., Clay Minerals, 1988. 33. 661-664.
4. P. Jenkins, J. Ralston, Colloids and Surfaces A, 1998, 139, 27–40.
5. L. J. Michot, F. Villiéras, M. Franqois, J. Yvon, R. Le Dred, and J. M. Cases Langmuir 1994, 10, 3765-3773.
6. G. Fourchet, Polymer Eng. Sci., 1995, 35, 957.
7. B. Pukansky, "Polypropylene: Structure, Blends and Composites", ed. by J. Karger-Kocsis, Vol. 3, pp. 1, Chapman and Hall, London, 1995
8. C. J. Van Oss, R. J. Good, and M. K. Chaudhury, Colloid and Interface Science, 1986, 111, 378.
9. C. J. van Oss, M. K, Chaudhury, and R. J. Good, Adv. in Colloid Interface Sci., 1987, 28, 35.
10. C. J. Van Oss, R. J. Good, and M. K. Chaudhury, Langmuir, 1988, 4, 884.
11. C. J. Van Oss, M. K. haudhury, and R. J. Good, Colloid and Interface Science, 1988, 128, 313.
12. C. J.Van Oss, "Interfacial forces in aqueous media", Marcel Dekker, 1994
13. F. M. Fowkes, J. Phys. Chem., 1962, 66, 382
14. F. M. Fowkes, J. Phys. Chem., 1963, 67, 2538-2541
15. I. Yildirim, Ph.D. Thesis, Virginia Tech, April 2001
16. E. Lobato, , Master Thesis, Virginia Tech, November 2004
17. E. W. Washburn, Physical Review, 1921, 1, 273.
18. A. J. Groszek, Nature, 1962, 196, 531.
19. A. J. Groszek, Proc. Roy. Soc., A, 1970, 314, 473-498.
20. A. J. Groszek,, Chemistry and Industry, 1966 Oct. 1754-1756.
21. A. J. Groszek, Carbon, 1987 Vol. 25, 6, 717-722.
22. A. J. Groszek, S. Partyka, Langmuir, 1993, 9, 2721-2725.
23. E. Chibowski, L. Holysz, Langmuir, 1992, 8(2), 710-716
24. L. Holysz, E. Chibowski, Langmuir, 1992, 8(2), 717-721.
25. J. Y. Lee, S. H. Lee, S. W. Kim, Materials Chemistry and Physics, 2000, 63, 251-255.
26. C. J. Van Oss, W. Wu, and R. F. Giese, Jr., Particulate Science and Technology, 1993, 11, 193-198.

Table 5.1 Surface tension components (mJ/m) and viscosities (mPa • s) values of wicking liquids used in thin layer wicking measurements. (@ 20ºC)

Liquid	γ_l^{LW} (mJ/m)	γ_l^{AB} (mJ/m)	γ_l^{+} (mJ/m)	γ_l^{-} (mJ/m)	η (mPa • s)
Apolar					
Heptane	20.3	0	0	0	0.409
Octane	21.6	0	0	0	0.542
Decane	23.8	0	0	0	0.907
Dodecane	25.35	0	0	0	1.493
1-Bromonaphthalene	44.4	0	0	0	4.89
Methylene iodide	50.8	0	0	0	2.82
Polar					
Water	21.8	51.0	25.5	25.5	1.08
Ethylene glycol	29	19	1.92	47	19.9
Formamide	39.0	19	2.28	39.6	3.76

Table 5.2 Experiment conditions for thin layer wicking test.

Conditions		Before wicking	Wicking
Vapor Equilibrium	1	–	–
	2	–	+
	3	+	+
	4	+	–

Note: To testify the evaporation effects on low-energy alkanes wicking, four wicking conditions are arranged in experiments. They were respectively:

Condition 1: samples were not vapor equilibrated before wicking and wicking was carried out in open condition. It is simply expressed as (–, –); Condition 2: samples were not vapor equilibrated before wicking and wicking was carried out in airtight vapor equilibrium condition. It is simply expressed as (–, +); Condition 3: samples were vapor equilibrated before wicking and wicking was carried out in airtight vapor equilibrium condition. It is simply expressed as (+, +); Condition 4: samples were vapor equilibrated before wicking and wicking was carried out in open condition. It is simply expressed as (+, –).

Table 5.3 Effective pore size, R_{eff} of talc sample obtained with the thin layer wicking technique using low surface free energy liquids.

Talc Sample	Particle Size D_{50} (µm)	% hydrophobic surface area	Effective Pore Size R_{eff} (µm)
Luz A	2.2	30*	0.0806
Luz B	3.2	-	0.2732
Luz C	3.2	77	0.2480
Luz D	3.4	-	0.3065
Luz E	7	62	0.5227
Luz F	20	54	1.3032

* The % hydrophobic surface area ratio for talc sample Luz A is approximately assumed due to the fact that surface free energy parameters increase for this sample.

Table 5.4 Contact angles of various liquids on powdered talc samples measured with the thin layer wicking technique.

Talc Sample	Particle Size (μm)	Contact angle (θ)				
		W	FO	MI	1-Br	EG
Luz A	2.2	76.48	12.32	40.00	19.50	0.00
Luz B	3.2	82.89	50.55	57.57	40.70	45.23
Luz C	3.2	87.06	43.91	55.15	40.47	36.41
Luz D	3.4	88.64	54.34	58.14	44.49	43.44
Luz E	7	87.59	48.49	58.51	44.39	47.67
Luz F	20	80.89	60.11	51.55	44.31	20.42

W= water; FO=Formamide; 1-Br=1-Bromonapthalene; MI= Methylene iodide., EG=Ethylene glycol.

Table 5.5 a) Surface free energy and its components of powdered talc samples obtained with the thin layer wicking technique using water, formamide and methylene iodide combination.

Talc Sample	Particle Size (µm)	Surface free energy (mJ/m^2)				
		γ_s^{LW}	γ_s^-	γ_s^+	γ_s^{AB}	γ_s
Luz A	2.2	39.61	0.08	7.83	1.54	41.15
Luz B	3.2	29.98	1.51	3.27	4.45	34.42
Luz C	3.2	31.36	0.00	5.58	0.18	31.54
Luz D	3.4	29.64	0.36	3.06	2.09	31.73
Luz E	7	29.43	0.08	4.89	1.26	30.69
Luz F	20	33.41	5.84	0.35	2.85	36.25

Table 5.5 b) Surface free energy and its components of powdered talc samples obtained with the thin layer wicking technique using water, formamide and 1-bromonaphthalene combination.

Talc Sample	Particle Size (µm)	Surface free energy (mJ/m^2)				
		γ_s^{LW}	γ_s^-	γ_s^+	γ_s^{AB}	γ_s
Luz A	2.2	41.89	0.08	6.85	1.53	43.42
Luz B	3.2	34.31	1.60	2.02	3.59	37.90
Luz C	3.2	34.41	0.00	4.38	0.26	34.67
Luz D	3.4	32.59	0.39	2.19	1.84	34.43
Luz E	7	32.63	0.10	3.68	1.19	33.82
Luz F	20	32.67	5.81	0.43	3.15	35.82

Table 5.5 c) Surface free energy and its components of powdered talc samples obtained with the thin layer wicking technique using water, ethylene glycol and methylene iodide combination.

Talc Sample	Particle Size (µm)	Surface free energy (mJ/m^2)				
		γ_s^{LW}	γ_s^-	γ_s^+	γ_s^{AB}	γ_s
Luz A	2.2	39.61	1.61	3.25	4.58	44.19
Luz B	3.2	29.98	2.94	1.75	4.54	34.51
Luz C	3.2	31.36	0.36	3.24	2.17	33.52
Luz D	3.4	29.64	0.53	2.63	2.35	31.99
Luz E	7	29.43	1.26	1.88	3.08	32.51
Luz F	20	33.41	0.91	4.20	3.92	37.32

Table 5.5 d) Surface free energy and its components of powdered talc samples obtained with the thin layer wicking technique using water, ethylene glycol and 1-bromonaphthalene combination.

Talc Sample	Particle Size (µm)	Surface free energy (mJ/m^2)				
		γ_s^{LW}	γ_s^-	γ_s^+	γ_s^{AB}	γ_s
Luz A	2.2	41.89	1.54	2.79	4.14	46.03
Luz B	3.2	34.31	2.72	1.07	3.41	37.72
Luz C	3.2	34.41	0.31	2.56	1.78	36.19
Luz D	3.4	32.59	0.46	2.02	1.93	34.52
Luz E	7	32.63	1.15	1.34	2.48	35.11
Luz F	20	32.67	0.93	4.40	4.05	36.72

Table 5.5 e) Surface free energy and its components of powdered talc samples obtained with the thin layer wicking technique using formamide, ethylene glycol and methylene iodide combination.

Talc Sample	Particle Size (μm)	Surface free energy (mJ/m^2)				
		γ_s^{LW}	γ_s^-	γ_s^+	γ_s^{AB}	γ_s
Luz A	2.2	39.61	455.95	162.71	544.75	584.36
Luz B	3.2	29.98	134.14	19.01	100.99	100.99
Luz C	3.2	31.36	142.92	17.00	98.59	129.95
Luz D	3.4	29.64	11.06	16.66	27.15	56.80
Luz E	7	29.43	325.38	120.82	396.55	425.99
Luz F	20	33.41	804.98	390.17	1120.85	1154.26

Table 5.5 f) Surface free energy and its components of powdered talc samples obtained with the thin layer wicking technique using formamide, ethylene glycol and 1-bromonaphthalene combination.

Talc Sample	Particle Size (μm)	Surface free energy (mJ/m^2)				
		γ_s^{LW}	γ_s^-	γ_s^+	γ_s^{AB}	γ_s
Luz A	2.2	41.89	415.16	142.64	486.70	528.59
Luz B	3.2	34.31	90.03	6.86	49.72	84.03
Luz C	3.2	34.41	110.20	8.48	61.15	95.56
Luz D	3.4	32.59	3.54	27.90	19.88	52.47
Luz E	7	32.63	271.13	93.80	318.95	351.59
Luz F	20	32.67	785.20	374.14	1084.02	1116.69

Table 5.6 Surface free energy and its components on the edge and base surfaces of powdered talc samples obtained from the thin layer wicking technique.

γ	Luz C/E		Luz E/F		Luz C/F		Luz A/E	
	γ^b	γ^e	γ^b	γ^e	γ^b	γ^e	γ^b	γ^e
γ_s^{LW}	34.3	21.5	10. 6	60.2	29.3	38.2	17.35	49.15
γ_s^-	−0.12	0.4	−27.3	44.7	−5.8	19.5	0.1	0.07
γ_s^+	6.6	2.0	26.4	−30.3	10.8	−11.9	1.38	10.60
γ_s^{AB}	−1.5	5.7	−6.3	13.6	−2.5	9.10	0.92	1.81
γ_s	32.9	27.2	4.3	73.8	26.8	47.3	18.27	50.96

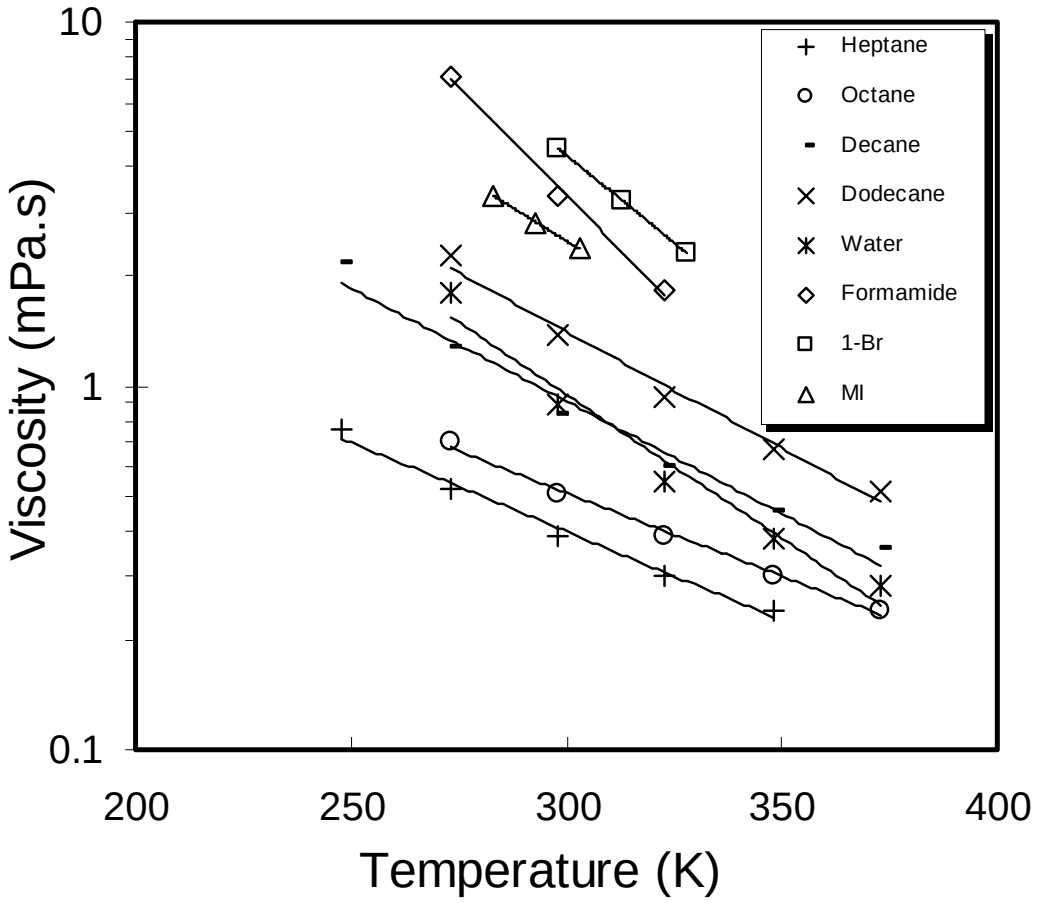

Figure 5.1 Viscosity of wicking liquids at different temperatures.

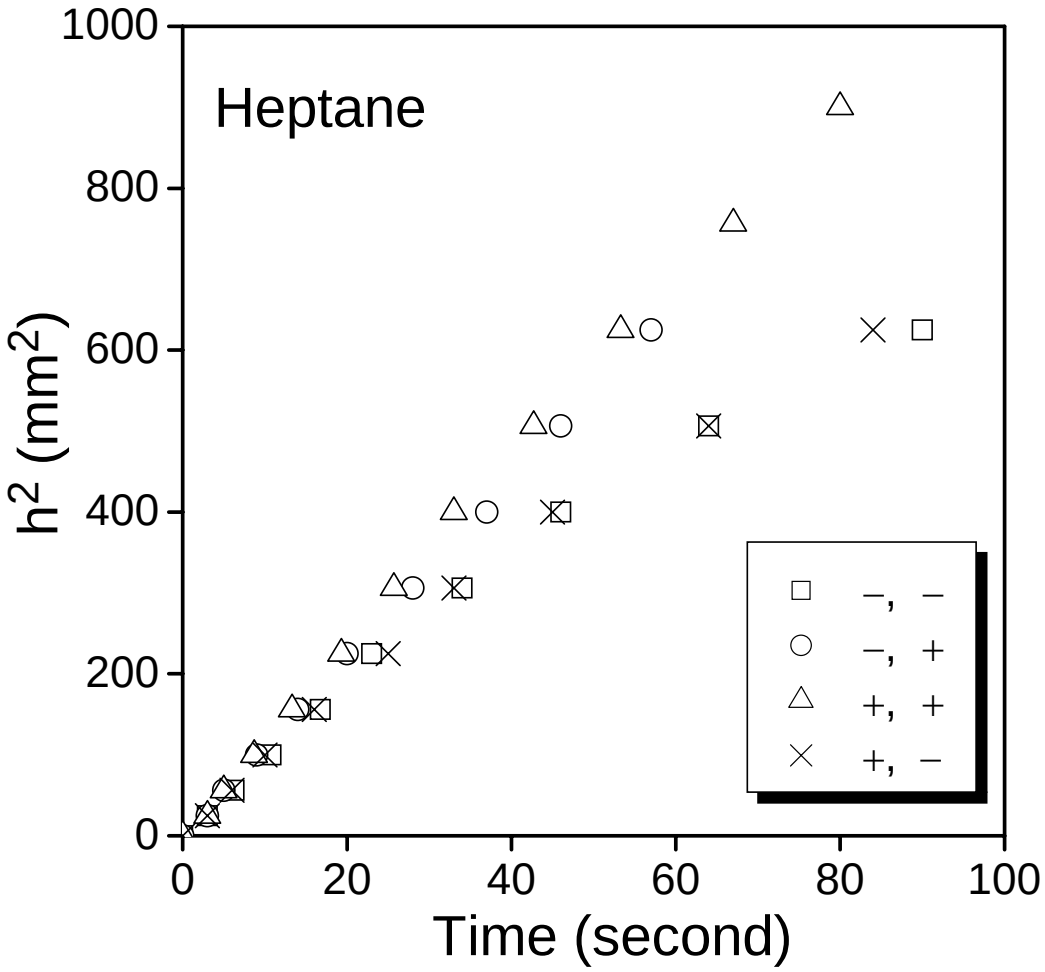

Figure 5.2a The relationship of h^2 vs time for talc sample Luz E obtained using the thin layer wicking technique with Heptane as the probe liquid. The legend shows the experiment conditions listed in Table 2.

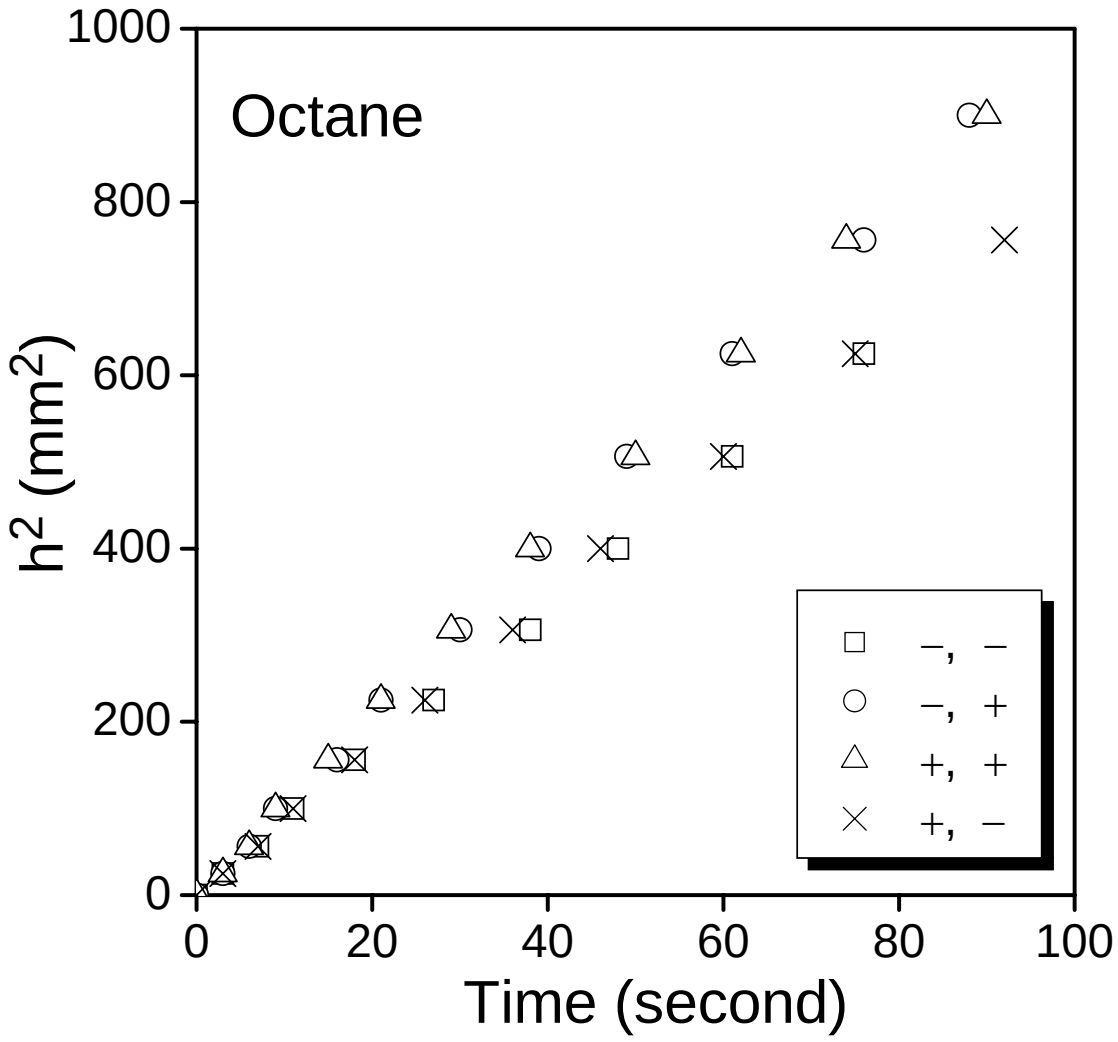

Figure 5.2b The relationship of h^2 vs time for talc sample Luz E obtained using the thin layer wicking technique with Octane as the probe liquid.

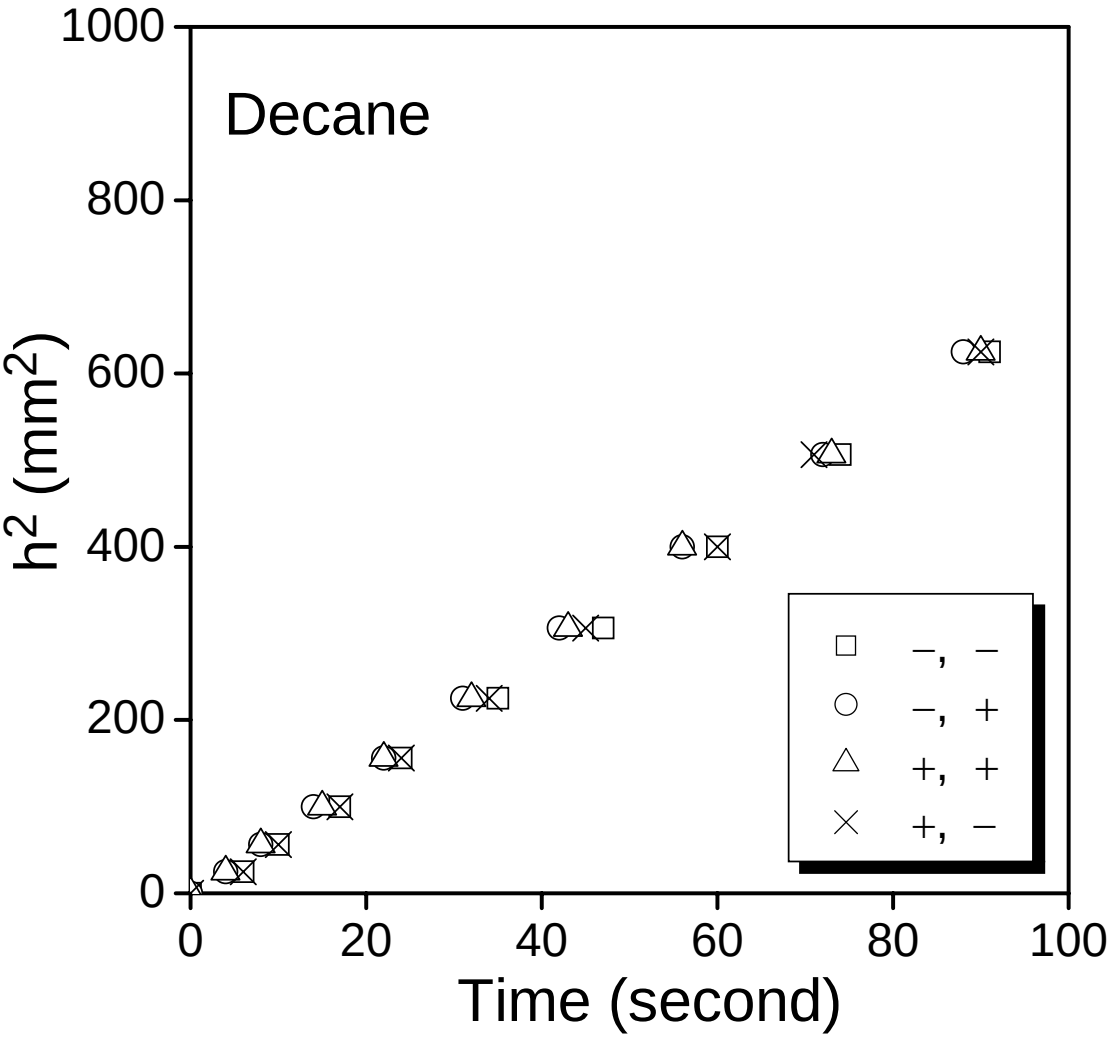

Figure 5.2c The relationship of h^2 vs time for talc sample Luz E obtained using the thin layer wicking technique with Decane as the probe liquid.

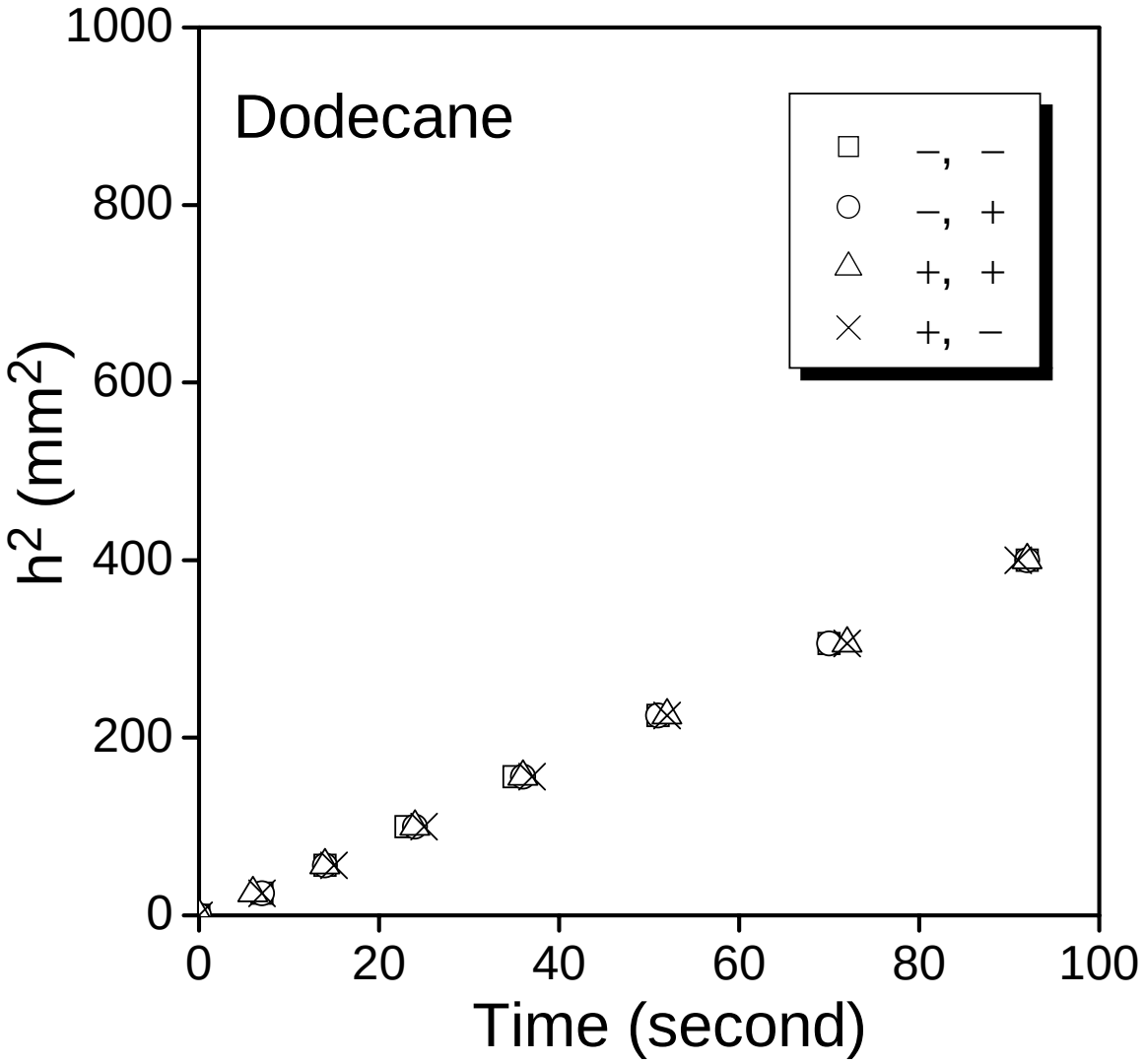

Figure 5.2d The relationship of h^2 vs time for talc sample Luz E obtained with the thin layer wicking technique using Dodecane as the wicking liquid.

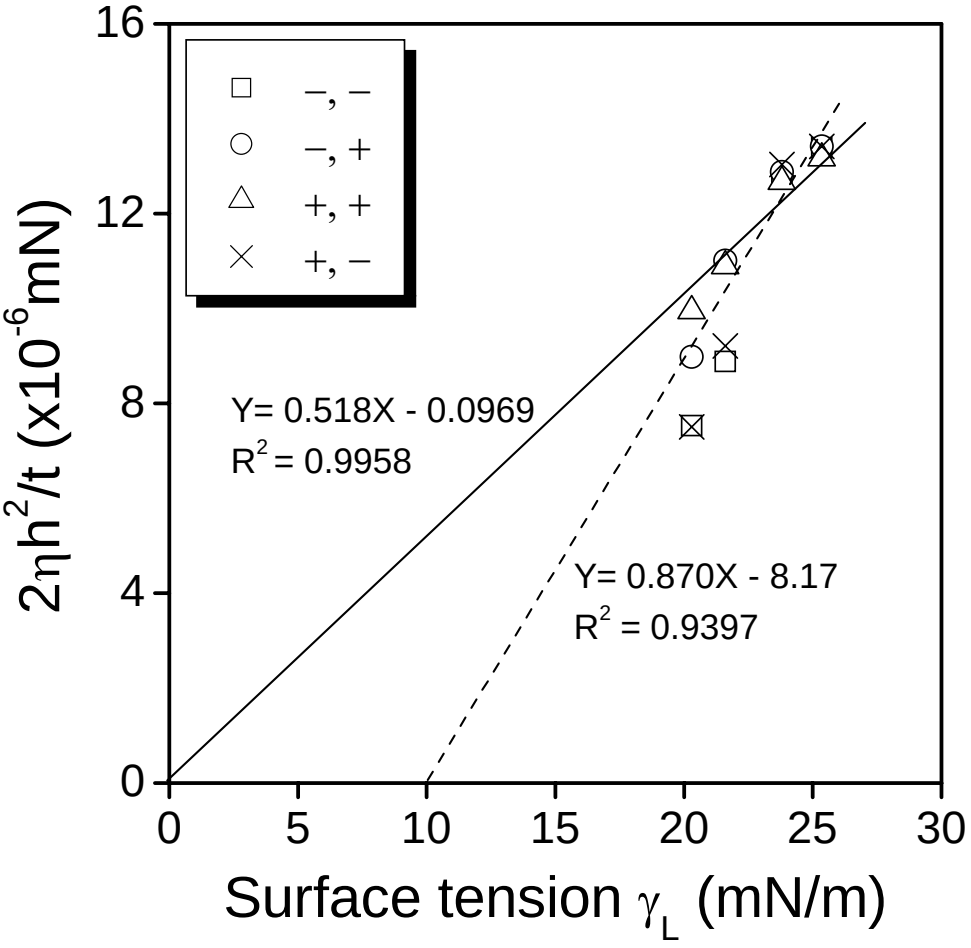

Figure 5.3 The relationship of $2\eta h^2/t$ vs surface tension γ_L for talc sample Luz E using low surface tension liquids as the wetting liquids in the thin layer wicking technique.

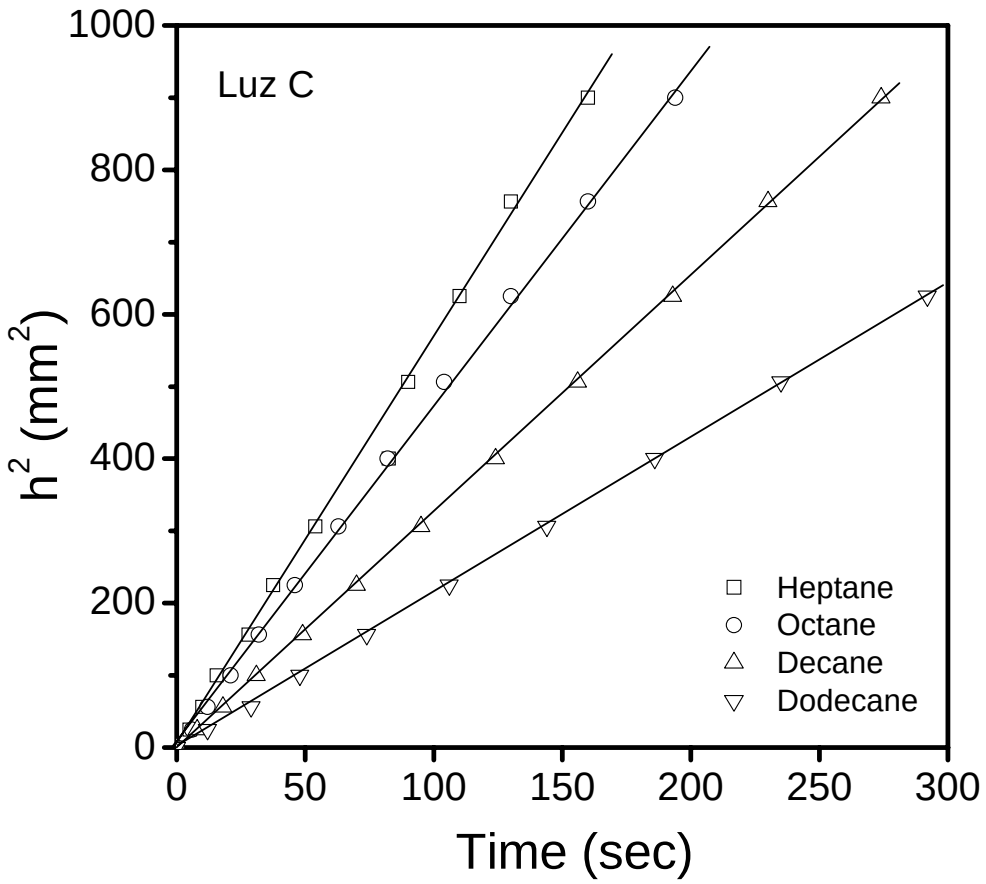

Figure 5.4a The relationship of h^2 vs time for talc sample Luz C obtained with the thin layer wicking technique using nonpolar alkanes as the wicking liquids.

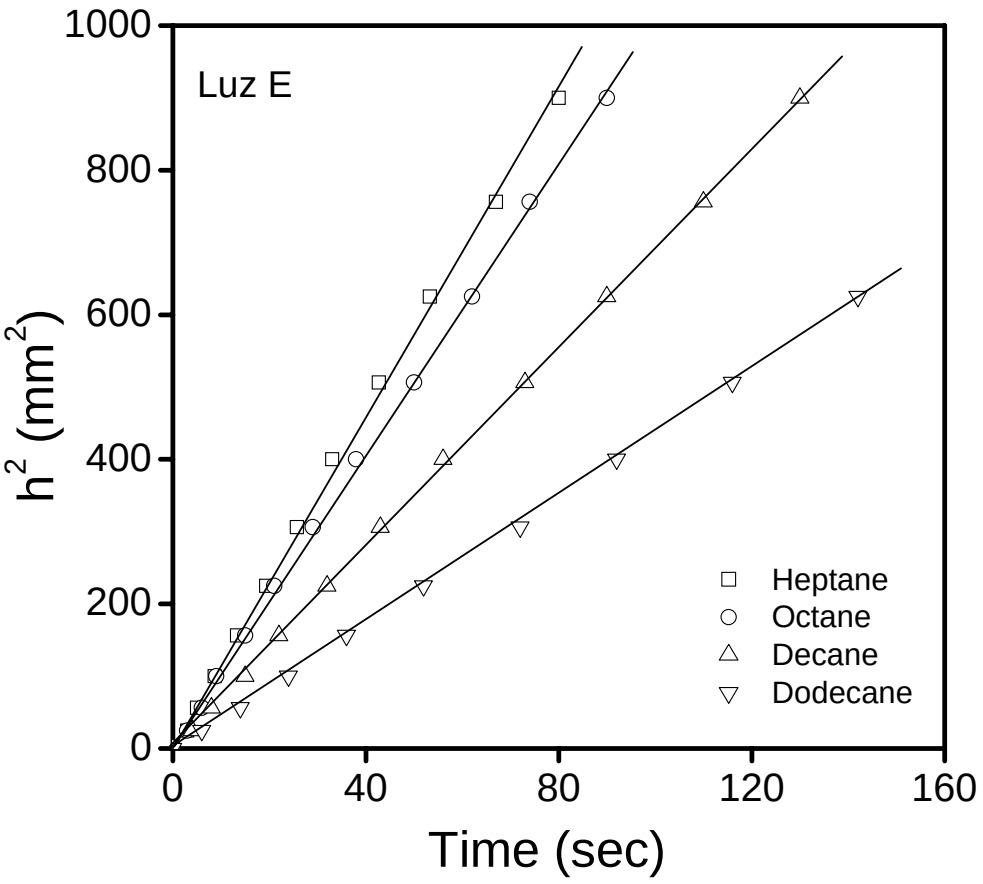

Figure 5.4b The relationship of h^2 vs time for talc sample Luz E obtained with the thin layer wicking technique using nonpolar alkanes as the wicking liquids.

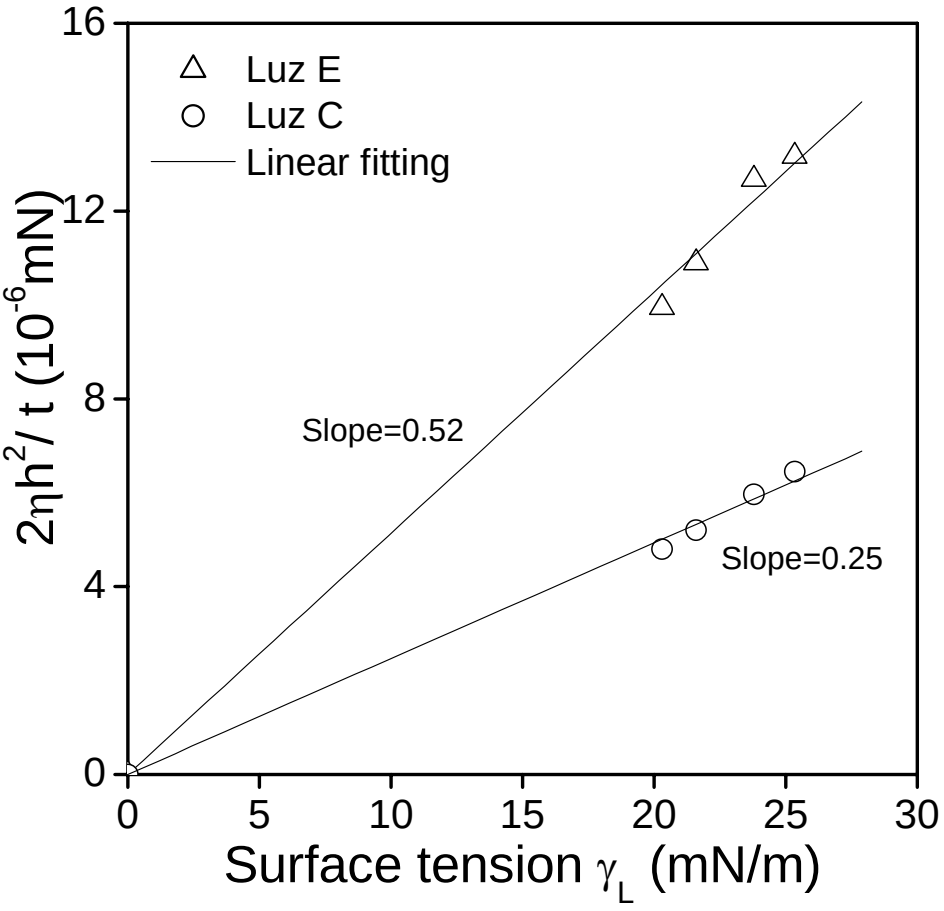

Figure 5.5 $2\eta h^2/t$ vs surface tension γ_L of Luz C and Luz E in thin layer wicking using wetting liquids. Linear fitting results, such as fitting line and equation, are also shown in the figure. The slope given in the fitting equation equals the R_{eff}, in the unit of μm, in thin layer wicking experiments.

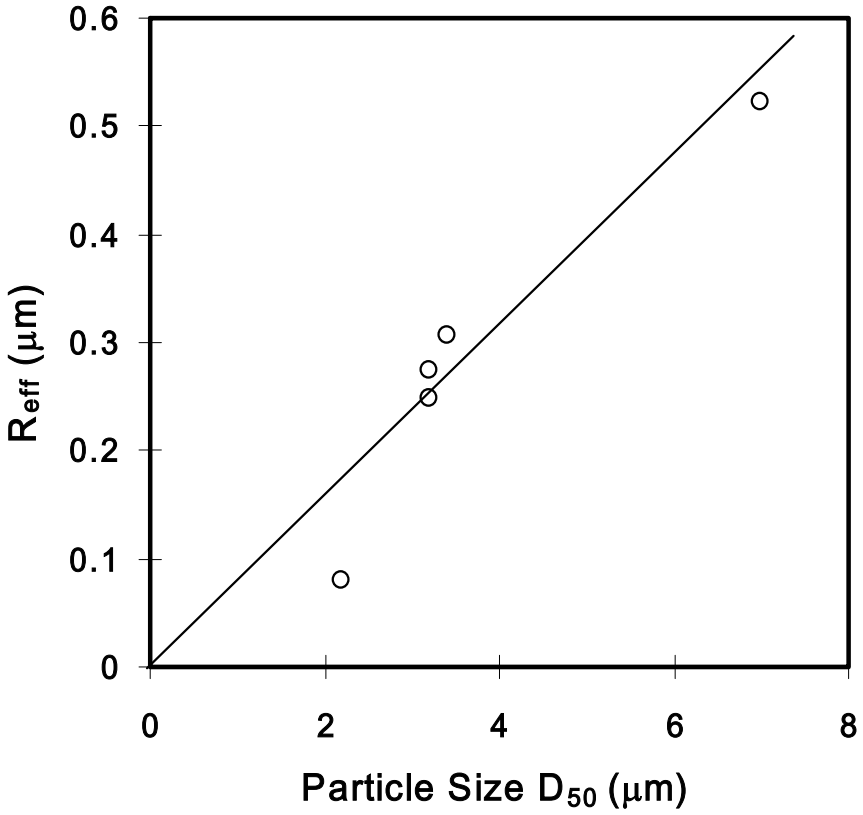

Figure 5.6 R_{eff} vs. Particle size D_{50} of different talc powder samples from Luz A to Luz E using thin-layer wicking technique.

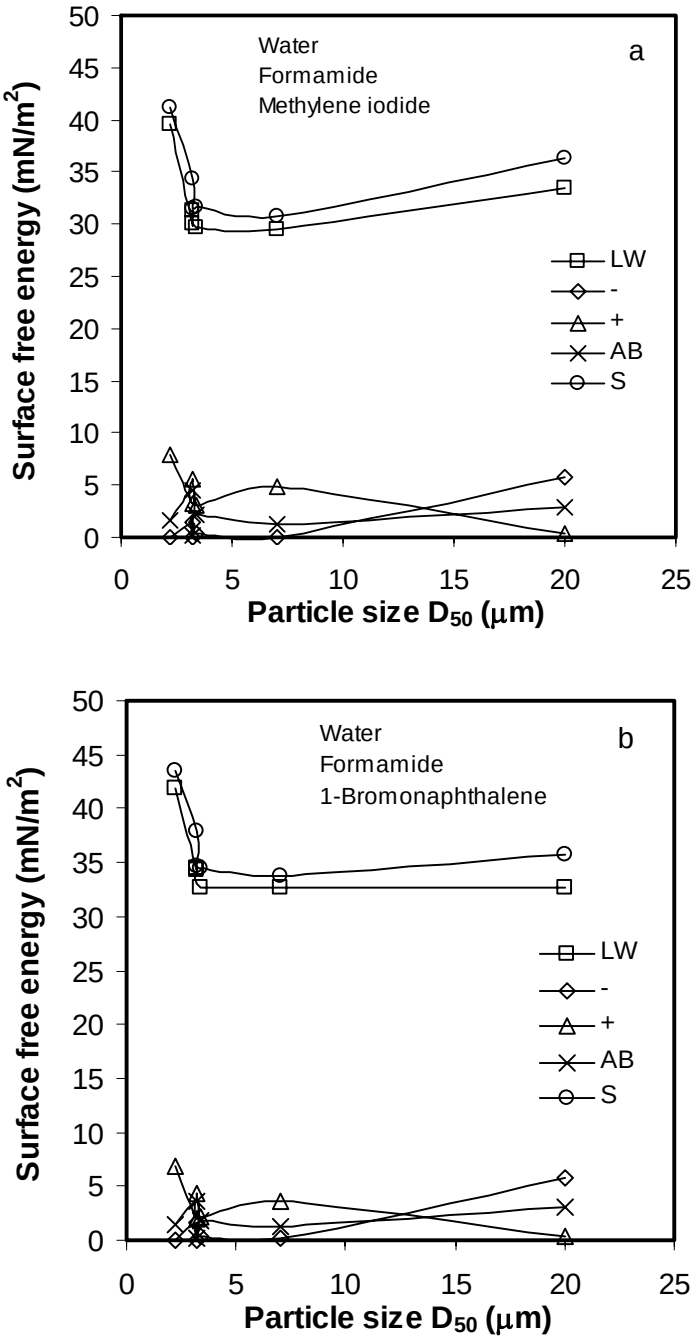

Figure 5.7 The relationship between average particle size D_{50} and surface free energy components of talc samples. In the legend, LW represents London-van der Waals apolar component of solid surface free energy; - represents the basic component; + represents the acid component; AB represents the polar component and S represents the total solid surface free energy. (a) surface free energy parameters of talc samples are calculated using water, formamide and methylene iodide as wicking liquids; (b) surface free energy parameters of talc samples are calculated using water, formamide and 1-bromonnaphthalene as wicking liquids.

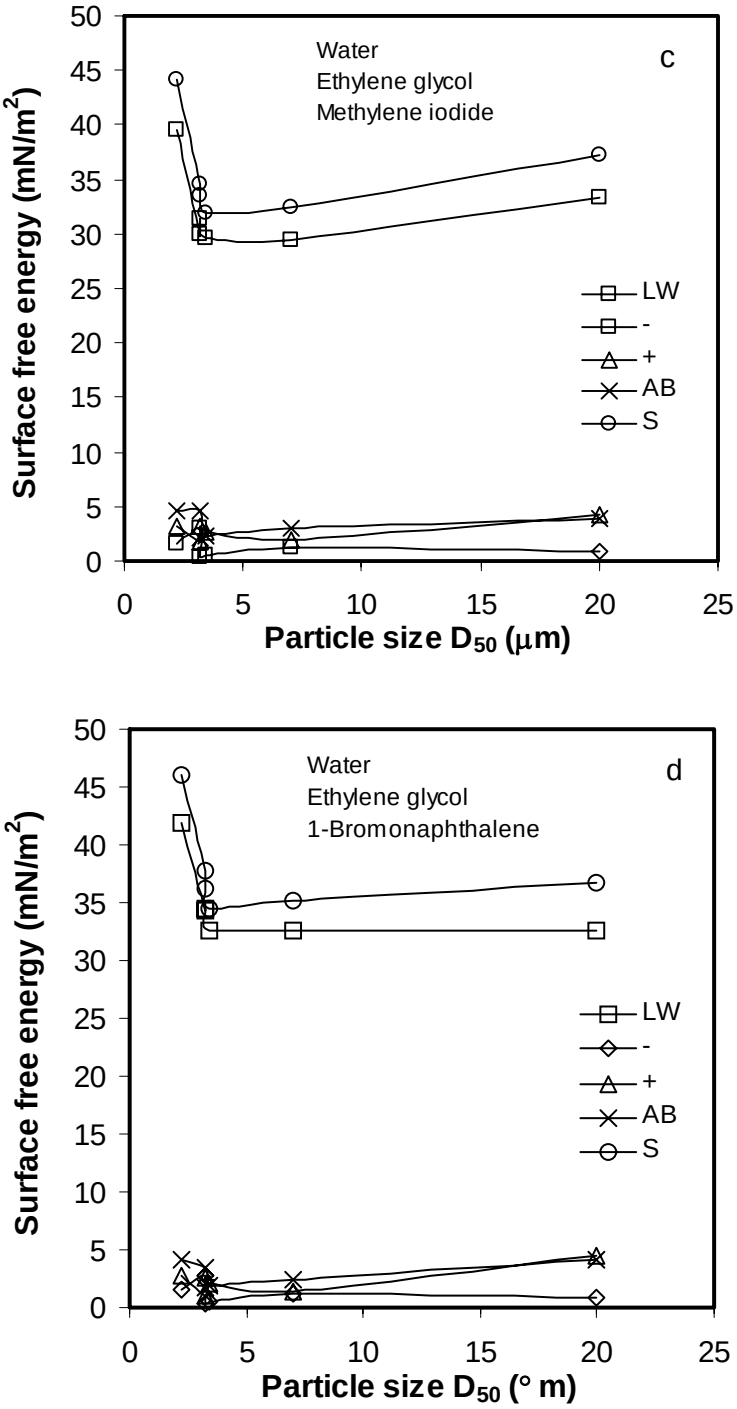

Figure 5.7 The relationship between average particle size D_{50} and surface free energy components of Luzenac talc samples. (c) Surface free energy parameters of talc samples are calculated using water, ethylene glycol and methylene iodide as wicking liquids; (d) Surface free energy parameters of talc samples are calculated using water, ethylene glycol and 1-bromonnaphthalene as wicking liquids.

Chapter 6

Effects of Chemicals on the Surface Free Energies of Talc Powders

ABSTRACT

In present work, thin layer wicking technique was used to determine the contact angles (θ) of several wicking liquids on powdered talc samples. The obtained contact angle values were used to calculate the surface free energy components of talc using the acid/base interaction theory developed by van Oss-Chaudhury-Good (OCG). The obtained surface free energy data of talc powders, in quantity, describe the surface properties, e.g. hydrophobicity, of talc. The thin layer wicking results of talc coated with CMC (carboxymethyl cellulose sodium salt) shows that the wetting reagents make talc surface hydrophilic by increasing solid surface free energy, especially the γ^{-lw} and γ^{-}. Also, increasing CMC reagent level from 0.4wt% to 1wt% doesn't change the solid surface free energy further. Adsorption of higher molecular weight CMC, FinnFix30, results in a higher γ_s^{-}. However the increase of γ_s^{-} and surface hydrophilicity are limited. Addition of EO/PO only weakly increases the zeta potential of talc sample; however, it increases γ^{-} and γ^{AB} greatly. Therefore, talc sample was made hydrophilic when being coated with dispersion reagents. Addition of SOPA alone has little effect on γ^{-} and γ^{AB}; while it changes the zeta potential of talc powder greatly. The reagent is designed to change surface charge rather than surface free energy. This information obtained in present investigation will be helpful for the application of these chemicals as a depressant/wetting reagent on talc in flotation and paper industry.

6.1 Introduction

Talc ($Mg_3Si_4O_{10}(OH)_2$) (1) is a natural mineral of which the elementary sheet is composed of a layer of magnesium-oxygen/hydroxyl octahedral sandwiched between two tetrahedral silica layers (2, 3). Its main surface, the face surface, of an elementary sheet shows a high hydrophobicity with no hydroxyl groups or active ions; whereas the edge surface shows some hydrophilicity because of the existence of pH dependent SiOH and MgOH sites (4, 5). Generally the elementary sheets stakes on one another and the lamellarity results in a larger than 1 face-to-edge surface area ratio (6), which makes talc a natural hydrophobic and floatable mineral. The hydrophobicity of talc has been studied by Fowkes and Harkins (7) by directly measuring contacts angle on a polished talc surface. Later on, wicking technique has been applied to measure the contact angle on talc powders (8). The reported water contact angle on talc surface is larger than 80° and this confirm talc's high natural hydrophobicity.

Talc is used for various applications, including paper coatings, pitch control, ceramics manufacture, and as filler in the plastics, polymer, paint and cosmetics industries. Particles of talc have the shape of platelets due to the layer structure of the mineral. In many of the industrial applications, this dual surface property of the mineral plays an important role. In the paper industry, for the pitch and sticky control applications, the hydrophilic property of the edges allows the particles to be dispersed in aqueous media, while the hydrophobic property of the basal surfaces attract the sticky hydrophobic substances present in wood pulp.

For filler applications, proper control of the adhesion between talc filler and the matrix is essential in controlling the property of the composite material. The strength of adhesion depends on the surface properties of the filler and of the matrix. In general, strong filler-matrix interactions result in improved processability, impact strength, and surface quality, while interactions that are too weak lead to decreased strength and increased deformability of the composite. The role of acid-base interactions is crucially important in the use of minerals as filler.

The properties of face and edge surfaces of talc also determined its application in other industry practice. Generally the wettability of talc surface can be modified by coating with polysaccharide reagents, such as dextrin, guar and carboxymethyl cellulose (9-14). Sodium carboxymethyl cellulose (CMC), which is the sodium salt of carboxymethyl ether of cellulose, is commonly used to change the wettability of talc surface. In flotation practice, CMC has been long used as talc depressant (13, 14). In paper industry, CMC is widely used as wetting reagent to increase talc stability in slurry. Despite of the well known depressing/wetting function of CMC on talc surface, its impact on solid surface properties has not been quantified yet. Due to the shortage in the knowledge of surface properties (e.g. surface free energy) change after CMC adsorption, the application of CMC in industry practice is hindered.

Solid surface properties, such as wettability and flotability etc., are generally evaluated by solid surface free energy, which is calculated through contact angles of liquids on solid surface. However, the studied talc sample in industry practice is generally in powder form, for which the direct contact angle measurement is not possible. The capillary rising technique (15, 16) has to been evoked to indirectly obtain the contact angle on powders using the Washburn equation. Further Subrahmanyam *et al*. (17) used this technique to get the different liquids contact angles on quartz particles which were

hydrophobized by adsorption of surfactant. Because the conventional powder column wicking method is not suitable for clay particles, which will further settle at the wicking beginning (8). Furthermore, the wetting front line is not sharp and clear, which increases the experiment error. In 1992, van Oss *et al*. (8) proposed a both simple and reliable capillary rising technique, which is called the thin-layer wicking technique, as an alternative for the column wicking when dealing with clay powders. From then on, many practices (18-24) have been carried out to study the surface properties of powdered materials using this technique. Chibowski (19-21) described this technique in both detailed theory and experiment practice based on the thermodynamics analysis of the wicking process. It is interesting to mention that, during these works, some authors focused in the effect of reagent coating on solid surface free energy. For example, Wu et *al*. (23) studied the effect of plurivalent counterions adsorption on flocculation of particle suspension by measuring the change of solid surface free energy. Li *et al*. (24) studied the surface thermodynamic properties of talc treated with octadecylamine. Chen and Zhu (25) studied the effect impact of lipopolysaccharide coating on clay particles wettability.

In this communication, the thin-layer wicking technique is applied to determine the surface free energy of talc powders before and after reagent coating. Thus the effect of chemicals coating on talc surface properties is evaluated and qualified based on the measured solid surface free energy values.

6.1.1 Acid/Base theory

Surface free energy is a fundamental parameter to quantify the wetting and adhesion phenomena which have been widely studied due to their importance in many industry applications. For example, a low solid surface free energy value suggests a poor wetting of water on this solid and a strong adhesion between the solid particles in aqueous solution. For non-polar materials, the surface free energies values can be directly measured or simply calculated from the van der Waals force interaction. However, how to quantify the surface free energies of polar materials is still under hot debate. The Surface-Tension-Component theory or the Acid/Base Theory developed by van Oss *et al*. (26-30) is by far the mostly used and applicable theory for the characterization of surface free energies of materials in both fundamental research and industry practice, even though some problems still have to be addressed. The theory can be briefly described as follows.

Fowkes (31-32) first proposed that the surface free energy of a material *i* can be subdivided into separate components:

$$\gamma_i = \sum_j \gamma_i^j \qquad [1]$$

where j refers to types of surface free energy component, e.g., dispersion, H-bonding, and metallic interactions. Later, Van Oss *et al*. (28-30) considered the surface tension as a sum of apolar Lifshitz-van der Waals, γ^{LW}, and polar acid/base interactions, γ^{AB}. Therefore, Eq. [1] can be expressed as:

$$\gamma_i = \gamma_i^{LW} + \gamma_i^{AB} \qquad [2]$$

in which γ_i^{LW} and γ_i^{AB} refer to the non-polar and polar (acid-base) surface free energy components, respectively. The former can be represented by the Lifshitz-van der Waals (or LW) interactions that include the dispersion (London), induction (Debye) and orientation (Keesom) components. The latter represents interactions between Lewis acids (electron acceptor) and bases (electron donor) on the surface.

van Oss *et al.* used the geometric mean combining rule to define γ_i^{AB} as follows:

$$\gamma_i^{AB} \equiv 2\sqrt{\gamma_i^+ \gamma_i^-} \qquad [3]$$

where γ_i^+ is the acidic component of the surface tension and γ_i^- is the basic component. Therefore, Eq. [2] can be transformed into

$$\gamma_i = \gamma_i^{LW} + 2\sqrt{\gamma_i^+ \gamma_i^-} \qquad [4]$$

It can be readily shown also that the free energy change (ΔG) associated with the adhesion of a liquid on a solid in the air is given by:

$$\Delta G = -2\left(\sqrt{\gamma_S^{LW}\gamma_L^{LW}} + \sqrt{\gamma_S^+\gamma_L^-} + \sqrt{\gamma_S^-\gamma_L^+}\right) \qquad [5]$$

where γ^{LW} is the Lifshitz-van der Waals component of the surface energy, γ^+ the acidic component, and γ^- is the basic component of the interacting solid (subscript S) and liquid (subscript L) surfaces.

Combining Eq. [5] with the well known Dupre equation:

$$\Delta G_{SL} = \gamma_{SL} - \gamma_S - \gamma_L \qquad [6]$$

one obtains:

$$\gamma_{SL} = \gamma_S + \gamma_L - 2\left(\sqrt{\gamma_S^{LW}\gamma_L^{LW}} + \sqrt{\gamma_S^+\gamma_L^-} + \sqrt{\gamma_S^-\gamma_L^+}\right) \qquad [7]$$

Combining Eq. [7] with the Young's equation,

$$\gamma_L \cos\theta = \gamma_S - \gamma_{SL} \qquad [8]$$

where θ is contact angle, one obtains the van Oss-Chaudhury-Good (OCG) equation:

$$(1+\cos\theta)\gamma_L = 2\left(\sqrt{\gamma_S^{LW}\gamma_L^{LW}} + \sqrt{\gamma_S^+\gamma_L^-} + \sqrt{\gamma_S^-\gamma_L^+}\right) \qquad [9]$$

which can be used to characterize a solid surface in terms of its surface free energy components, i.e., γ_S^{LW}, γ_S^+, and γ_S^-. In order to determine these values, it is therefore necessary to determine contact angles of three different liquids of known properties (i.e. γ_L^+, γ_L^-, γ_L^{LW}) on the surface of the solid of interest. One can then set up three equations

with three unknowns, which can be solved simultaneously to obtain the values of γ_S^{LW}, γ_S^+, and γ_S^-.

6.1.2 Thin layer wicking

In practice, however, it is impossible to directly measure the contact angle of liquid on powdered solids, especially for clay particles. Thin layer wicking technique is a convenient way to measure contact angles of liquids on powdered materials by determining the capillary rise rate of the wicking liquids in packed beds of those particulate materials. The wicking process follows the Washburn's equation (33):

$$\frac{2\eta h^2}{t} = R_{eff} * \gamma_L * \cos\theta \qquad [10]$$

in which η is the viscosity of the liquid, h is the height to which wicking liquid has risen at time t, R_{eff} is the effective interstitial pore radius of packed powder bed, γ_L is the surface tension of wicking liquid and θ is the contact angle.

The parameter R_{eff} of Eq. [10] is generally determined by wicking with low-energy spreading alkanes, for which the contact angle θ is assumed to be zero. Thus, Eq. [10] is reduced into the following equation:

$$\frac{2\eta h^2}{t} = R_{eff} * \gamma_L \qquad [11]$$

After wicking with several low energy alkanes, one can draw a plot of $2\eta h^2/t$ vs. γ_L. The slope of the straight fitting line passing through origin gives the effective interstitial pore radius R_{eff}.

The contact angle of high energy liquid, such as water, on powder surface can be obtained by wicking with the liquid on thin powder layer. Using the R_{eff} value obtained from wicking result with low energy alkanes, one can get the water contact angle by solving Eq. [10], in which contact angle is the only unknown parameter.

6.1.3 Surface free energy characterization of basal/edge surfaces

In order to determine the surface free energy components at the basal and edge surfaces of talc, surface free energy characterization studies must be conducted at two different sizes (D_1 and D_2) (6). The solid surface free energy (γ_s) and its components (i.e., γ_s^{LW}, γ_s^+, and γ_s^-) of each sample are obtained using the above described thin layer wicking technique. From the known f_e and f_b values obtained from flow microcalorimetry, one can then set up the following equation (6):

$$\gamma_s^{D_1} = f_b^{D_1}\gamma_s^b + f_e^{D_1}\gamma_s^e \qquad [12]$$

in which γ_s^b is γ_s at the basal surface and γ_s^e is γ_s at the edge surface. Eq. [12] suggests that the value of γ_s is a composite of γ_s^b and γ_s^e in proportion to f_b^{D1} and f_e^{D1}. Similarly, one can set up the following equation at size D_2:

$$\gamma_s^{D_2} = f_b^{D_2}\gamma_s^b + f_e^{D_2}\gamma_s^e \quad [13]$$

An explicit assumption in writing Eqs. [12] and [13] is that γ_s^b and γ_s^e are intensive properties of talc and do not change with particle size, which is a reasonable assumption. By solving Eqs. [12] and [13] simultaneously, one can determine the values of γ_s^b and γ_s^e. Likewise, one can set up simultaneous equations for γ_s^{LW}, γ_s^{AB}, γ_s^+, and γ_s^-, and obtain the respective values at the basal and edge surfaces of talc. After wicking with several low energy alkanes, one can draw the plot of $2\eta h^2/t$ vs. γ_L. The slope of the straight fitting line passing through origin gives the effective interstitial pore radius R_{eff}.

The contact angle of high energy liquid, such as water, on powder surface can be obtained by wicking with the liquid on thin powder layer. Using the R_{eff} value obtained from wicking result with low energy alkanes, one can get the water contact angle by solving Eq. [10], in which contact angle is the only unknown parameter. Using the measured contact angle of three different liquids of known properties (i.e. γ_L^+, γ_L^-, γ_L^{LW}) one can obtain the values of γ_S^{LW}, γ_S^+, and γ_S^- by solving three sets of Eq. [9] simultaneously. Thus the surface free energy values of solid powders are known.

It is worthwhile to mention that the contact angle obtained using thin layer wicking technique is the advancing contact angle rather than the equilibrium contact angle or Young's contact angle (8, 34, 35). Taking the advancing contact angle for granted the equilibrium contact angle generally results in lower solid surface free energy values, because the former is generally larger than the later. However, due to the fact that the capillary rising technique is the only available way to measure contact angles on solid powders, it is still useful to get solid surface free energy information before and after CMC addition using this technique.

6.2 Experimental

Materials

Nanopure water was obtained by Nanopure III (Barnstead, IA) water system. The conductivity of the water was 18.2 MΩ/cm at 23°C and the surface tension was 72.5mN/m at 22°C. Pre-cleaned glass microslides (75x25 mm, Corning, NY) were used without further cleaning.

Wicking liquids used in the present work, Alkanes, such as Heptane, Octane, Decane and Dodecane (Aldrich Chemical Company) were HPLC grade (>99.5% purity). The surface tension and viscosity data of these wicking liquids are listed as Table 6.1. HPLC-grade acetone and butanol were purchased from Fluka and both had purities greater than 99.5%.

Powdered talc samples of different particle sizes, labeled Luz A to Luz F, were kindly provided by Luzenac America (Englewood, CO.). They are readily used without further treatment. The mean particle size (D_{50}) was determined by Luzenac America using a Sedigraph and by sieve analysis at Virginia Tech laboratories. The effective pore sizes of the thin powder layer obtained using the thin layer wicking technique are listed in Table 6.2.

FinnFix5 and FinnFix30 (CMC, Carboxy Methyl Cellulose sodium salt) and PE23EX CMC (Carboxy Methyl Cellulose sodium salt) were also obtained from Luzenac

America. The abbreviation FF indicates their belonging to the Finnfix reagent series. The numbers indicate the relative viscosity of the reagents. FinnFix30 has a large viscosity and molecular weight than FinnFix5.

Thin layer wicking

10 g Talc powders were added into 190 ml water to make a 5% (wt.) solution and the suspension was stirred for 2 hours. Then 3.5 ml talc suspension was withdrawn with a pipette and evenly sprayed onto a glass microscope slide, which was kept strictly horizontal. The slide with talc suspension on it was dried in ambient situation overnight and further dried in oven at 110ºC for at least 2 hours to remove residual pore water; then it was cooled down in a vacuum desiccator and ready for wicking experiments. In practice, a uniform thin layer of talc powder was found firmly adhere to the glass slide and the front line of wicking liquid on the slide is both sharp and clear. All these merits ensure the wicking results show a quite good repeatability.

When the coating effect of FinnFix5 and FinnFix30 (CMC) was studied, a specific amount of reagent (0.4%, 0.7% and 1% in weight ratio to solid) was added into talc suspension and mixed for 2 hours using a magnetic stirrer.

It was proposed that, before the wicking experiments were carried out, the powder-coated slides should be kept in a sealed vessel filled with wicking liquid for 2 hours. This procedure makes the solid surface equilibrated with liquid vapor and a duplex film formed on the surface, which is proposed to ensure the complete spreading precondition applies (19, 21). In previous chapter, the results have shown that for high energy liquids pre-equilibration with liquid vapor has little effect on the wicking speed. The wicking experiments were performed by immersing the powder-coated glass slides vertically in the wicking liquid, which is filled at the bottom of a sealed vessel (8), and the time for the wicking liquid to travel through every 2.5mm height is recorded. Because the glass slides were vertically placed in present work, a 5cm wicking distance was set as the final wicking point in order to minimize the effect of gravity force. For each wicking liquid, the tests were repeated at least three times and the values listed here were the arithmetic average over three sets of experiment data. The value of R_{eff} in the Eq. [11] was determined using liquids of low surface free energy (heptane, octane, decane and dodecane), which completely spread over the solid surface (i.e., $\theta=0$). Experiment results show that the $2\eta l^2/t$ vs. γ_L yielded a straight line passing through the origin. This finding confirms that the Washburn equation, Eq. [11] is applicable under the wicking conditions in present work. Furthermore, the liquids contact angles on CMC coated thin powder layer were calculated using Eq. [10] with the obtained R_{eff}.

6.3 Results and Discussion

Luzenac America is producing and developing various surface-modified talc products. Various reagents, which include polymers, surfactants, polyelectrolytes, electrolytes, hydrolizable cations, and silanes, are used to modify the surface properties and, thereby, enhance the performance of talc for different applications. In principle, all of the modifications should result in changes in surface free energies.

It was, therefore, proposed to carry out free energy characterization for some of modified talc products from Luzenac America. It would be of interest to study the effect

of a surface modifying reagent on the changes in the surface free energies of the basal and edge surfaces of a talc sample. The results would be useful to determine if the reagent adsorbs preferentially on the basal or edge surfaces. Such information will be useful for further improving the performance of existing products and developing entirely new product lines.

In the present work, the effects of several different wetting and dispersion agents have been studied. The reagents include some chemicals as follow: Finnfix 5 (carboxy methyl cellulose, sodium salt; low molecular weight); Finnfix 30 (carboxy methyl cellulose, sodium salt; high molecular weight); PE23EX (carboxy methyl cellulose, sodium salt and poly anionic cellulose); Dowfax WP-310 (ethylene oxide/propylene oxide co-polymer), and K-Flow D (sodium polyacrylate); cationic and anionic surfactants. The chemical structures of these regents are shown as Figure 6.1 to Figure 6.3.

In this task, talc samples Heliocote-pt (d_{50}= 3.2 μm) and Mistrofil-pt (d_{50}=7.0 μm) were treated with the reagents listed above and characterized. Both talc samples are from a Canadian deposit (macrocrystalline talc) and ground to different particle sizes at Luzenac America plants. The thin-layer wicking technique was used to determine the contact angles, while surface free energy components at the basal and edge surfaces of talc were obtained using the methodology described in Chapter 5. The basal/edge aspect ratios of talc powders were determined using the techniques also discussed in Chapter 5.

6.3.1 Effects of CMC addition

6.3.1.1 Effects of CMC addition on contact angles of talc powders.

The contact angles of high energy wicking liquids on talc powders, Heliocote-pt and Mistrofil-pt, before and after being treated with CMC, i.e. FinnFix5, FinnFix30 and PE23EX, at different reagent level are listed in Table 6.3 and plotted as Figure 6.4, Figure 6.5 and Figure 6.6. Results show that contact angles of Methylene iodide and 1-Bromonaphthalene on talc samples decrease after addition of CMC at different reagent levels. For example, as shown in Figure 6.4, after addition of FinnFix5 the contact angle of 1-Bromonaphthalene on Heliocote-pt decreases from 41 to 18.4~25.2 degree; that on Mistrofil-pt decreases from 44.1 to 25.5~28.9 degree. The same trend was found both for Heliocote-pt and Mistrofil-pt samples when FinnFix30 is added. Figure 6.5 shows that after addition of FinnFix30, the contact angle of 1-Bromonaphthalene on Heliocote-pt decreases from 41.0 to 16.6~21.4 degree and that on Mistrofil-pt decreases from 44.1 to 28.6~31.8 degree.

When apolar liquids Methylene iodide and 1-Bromonaphthalene are used in wicking experiments, Eq. [9] can be simplified as the following:

$$(1+\cos\theta)\gamma_L = 2\sqrt{\gamma_S^{LW}\gamma_L^{LW}} \qquad [9a]$$

Because the polar components γ_l^+ and γ_l^- of these liquids equal zero, $\sqrt{\gamma_S^+\gamma_L^-}+\sqrt{\gamma_S^-\gamma_L^+}$ in the right side of the OCG equation equals zero. Thus the interactions between the liquid and solid are through apolar/apolar, or Lifshitz-van der Waals (LW) interactions and the contact angle is only determined by γ_s^{LW}. The decreasing of contact

angle suggests an increase of the apolar component of solid surface free energy γ_s^{LW} after CMC addition. In later section, we will describe the surface free energy change due to CMC addition in detail.

It is also shown in Table 6.3 and Figure 6.4-6.6 that the contact angles of formamide on talc powders increase with CMC addition both in the case of Heliocote-pt and Mistrofil-pt. For example, as shown in Figure 6.4, the contact angle on Heliocote-pt increase from 44.4 to 58.5~61.1 degree and that on Mistrofil-pt increases from 48.2 to 54.5~62.1 degree when talc samples were coated with FinnFix5. When FinnFix30 is added, the contact angle on Heliocote-pt increases from 44.4 to 62.8~69.6 degree and that on Mistrofil-pt increases from 48.2 to 64.9~73.9 degree. After the addition of PE23EX, the contact angles of wicking liquids on talc surface change in a similar trend as obtained with FinnFix5 and FinnFix30, with only some difference in magnitude.

A high contact angle is due to a weak attraction between the solid and the liquid. Therefore the increase of formamide contact angle on talc samples suggests that the solid/liquid attraction becomes weaker. Formamide is known as a polar liquid and its polarity comes mainly from its basic component of surface free energy. As shown in Table 6.1, the basic component γ_s^- of formamide is 39.6mJ/m^2 and the value is much larger than its acid component γ_s^+, which is only 2.28mJ/m^2 in value. It is known from the decrease of contact angle of Methylene iodide and 1-Bromonaphthalene that CMC addition increases γ_s^{LW} and this will decreases contact angle. So the increase of formamide contact angle must come from the decrease of the polar interaction between solid and formamide. In addition, its magnitude should overcome the increased non-polar interaction due to the increased γ_s^{LW}.

It was also shown in Table 6.3, Fig. 6.4 and Fig. 6.5 that the water contact angles on talc samples decrease after the addition of CMC. For example, as shown in Figure 6.4, when FinnFix5 is added, the water contact angle on Heliocote-pt decreases from 87.1 to 78.0~78.4 degree and that on Mistrofil-pt decrease from 87.6 to 74.8~75.7 degree. The same conclusion is drawn for both talc powder samples when FinnFix30 is added. As shown in Figure 6.5, the water contact angle on Heliocote-pt decreases from 87.1 to 76.7~78.2 degree and that on Mistrofil-pt decreases from 87.6 to 69.9~76.6 degree. It is well known that the lower the contact angle is, the less hydrophobic the surface is. So the wicking results clearly shown that addition of CMC can decreases the water contact angle on talc powders and make the talc surface become hydrophilic. This is definitely the purpose of wetting reagent in paper making or depressant in flotation.

It is worth while to mention that before CMC addition, the measured contact angles on talc samples respectively are: θ_{water}=87.1~87.6°, $\theta_{Metgylene\ iodide}$=55.5~58.3° and $\theta_{1\text{-}Bromonaphthalene}$=41~44.1°. These values are comparable to those from Ref. (36).

6.3.1.2 Effect of CMC addition on solid surface free energy of talc powders

Combining three sets of Eq. [9], one can calculate the surface free energy components of Heliocote-pt and Mistrofil-pt samples before and after CMC addition. The values were listed in Table 6.4. Further, these values were plotted as Figure 6.7 and 6.8. Fig. 6.7a) shows the effect of FinnFix5 coating on the solid surface tension of Heliocote-pt. It is clearly seen that after CMC addition, γ_s^{LW} increases from 34.2 to 40.3~42.2 mJ/m^2, γ_s^- increases from 0 to 7.9~9.2 mJ/m^2, γ_s^+ decreases from 4.3 to 0 ~0.1 mJ/m^2, γ_s^{AB} increases from 0.4 to 0.6~1.9 mJ/m^2 and total solid surface free energy γ_s increases from 34.6 to

40.8~42.7 mJ/m^2. Increasing the reagent level does not change the surface free energy components further. Fig. 7b) shows the effect of FinnFix5 coating on the solid surface tension of Mistrofil-pt. A same trend of solid surface free energy change as the one obtained with Heliocote-pt was found also applicable for Mistrofil-pt. γ_s^{LW} increases from 32.8 to 39.0~40.2 mJ/m^2, γ_s^- increases from 0.1 to 8.6~12.1 mJ/m^2, γ_s^+ decreases from 3.7 to 0.1 mJ/m^2, γ_s^{AB} increases from 1.1 to 1.6~2.2 mJ/m^2 and total solid surface free energy γ_s increases from 33.9 to 41.3~41.8 mJ/m^2. The change of surface free energy is not sensitive to reagent level any more.

Fig. 6.8a) shows the effect of FinnFix30 coating on the solid surface tension of Heliocote-pt. γ_s^{LW} increases from 34.2 to 41.4~42.6 mJ/m^2, γ_s^- increases from 0 to 11.7~14.6 mJ/m^2, γ_s^+ decreases from 4.3 to 0.3 ~1.2 mJ/m^2, γ_s^{AB} increases from 0.4 to 3.9~8.3 mJ/m^2 and total solid surface free energy γ_s increases from 34.6 to 46.3~50.3 mJ/m^2. The effects of FinnFix30 coating on the solid surface tension of Mistrofil-pt are shown in Fig. 8b). γ_s^{LW} increases from 32.8 to 38.0~39.1 mJ/m^2, γ_s^- increases from 0.1 to 20.1~23.4 mJ/m^2, γ_s^+ decreases from 3.7 to 0.6~1.7 mJ/m^2, γ_s^{AB} increases from 1.1 to 7.1~12.5 mJ/m^2 and total solid surface free energy γ_s increases from 33.9 to 46.3~50.5 mJ/m^2. Similar as the one obtained with FinnFix5, the reagent level does not have an impact on the solid surface free energy.

From the above descriptions, the effect of CMC addition on solid surface free energy can be summarized as the followings: γ_s^{LW} increases to 39~42 mJ/m^2; γ_s^- increases to 7.9~23.4 mJ/m^2; γ_s^+ decreases to nearly 0mJ/m^2; γ_s^{AB} increases only by a little for FinnFix 5; however as much as 10mJ/m^2 for FinnFix 30; γ_s increases by 10~20mJ/m^2, which is mainly due to the increase of γ_s^{LW} and γ_s^-.

Till now, there is no consensus on the adsorption mechanism of CMC at talc/water interface yet. It was proposed that the interaction between CMC and talc surface may comes from one or a combination of electrostatic interaction, chemical, hydrogen and hydrophobic bonding (11-14,37,38). However, which interaction is the dominant driving force for CMC adsorption is still under debate. The obtained information of surface free energy change after CMC addition brings out useful information of CMC adsorption at talc surface.

The increase of γ_s^{LW} attributes to the fact that polymer generally has a higher apolar surface free energy component because of the rather long hydrocarbon segments. It is very likely that the hydrocarbon backbone lays flat on talc face and fully covers the solid surface, because 40mJ/m^2, the obtained γ_s^{LW} value, is a typical value for polysaccharide (30). Increase of γ_s^- suggests that the hydrophilic hydroxyl and carboxyl groups of CMC polymer protrudes away from talc surface and make a hydrophilic layer with higher γ_s^- on the solid surface. It is interesting to note that by comparing the effects of FinnFix5 and FinnFix30 on γ_s^-, one can see that FinnFix30 coating results in a higher γ_s^-. This may be due to the fact that FinnFix30 has a higher molecular weight, which results in a higher adsorption density, more hydrophilic hydroxyl and carboxyl groups protruding away from talc surface; thus a higher γ_s^-. However, the difference of γ_s^- is only about 10mJ/m^2 and the wettibilities, i.e. water contact angle, are nearly the same. This finding corresponds to the work by Shortridge *et al*. (13) that CMC molecular weight has no decisive effect on the depression of the talc. It also suggests that CMC adsorption on talc

powders can only increases the surface hydrophilicity to a limited extent, which results in a relatively weak depressing ability of CMC on talc in flotation (13).

The decrease of γ_s^+, which is a characteristic parameter of the edge surface of talc, suggests that some CMC polymers also adsorb onto the edge surface of talc powder through the acid/base interaction between hydroxyl and carboxyl groups and acidic sites, therefore a decrease in γ_s^+.

6.3.2 Effect of EO/PO and SOPA Addition

6.3.2.1 Effect of EO/PO and SOPA addition on surface free energies of talc powders

The surface free energies of talc powders before and after the coating of EO/PO and SOPA were shown as Fig. 6.10 and Fig. 6.11, which suggested that the addition of these chemicals had a pronounced effect on the solid surface free energies.

Figure 6.10 a) shows the effects of EO/PO and SOPA addition on the surface free energies of Heliocote-pt talc powders using MI, water and Formamide combinination. γ^{LW} does not change much after the coating of EO/PO or co-adsorption of EO/PO and SOPA. It only fluctuates from 28 to 34 mJ/m^2. γ^- increases greatly with the addition of chemicals. The magnitude can be as high as 10 mJ/m^2. γ^+, on the other hand, decreases with the addition of chemicals by the magnitude of about 5 mJ/m^2. The value of γ^{AB} increases by 7~8 mJ/m^2 and this increases is mainly due to the increase of γ^-. In all, the total surface free energy of talc sample, γ, increases after being treated with varying amounts of EO/PO and SOPA, indicating that chemicals increased the hydrophillicity of the solid. It is also interesting to note that adding SOPA alone has little effect on γ^- and γ^{AB}. That is, addition of SOPA alone will not change the polar components of the surface free energy of talc sample.

Figure 6.10 b) shows the effects of EO/PO and SOPA addition on the surface free energies of Heliocote-pt sample using 1-Br, water and Formamide as high energy wicking liquids. The figure also showed that with the addition of chemicals, γ^+ decreases a little; however, γ^- increases greatly and this makes the polar surface free energy component, γ^{AB}, increase by 7~8 mJ/m^2. In all, the total surface free energy, γ, increases after being treated with varying amounts of EO/PO and SOPA. It was also shown that addition of SOPA alone has no effect on γ^- and γ^{AB}.

Figure 6.11 a) and Figure 6.11 b) show the effects of EO/PO and SOPA addition on the surface free energies of Mistrofile-pt talc sample. The change of surface free energy components due to chemicals adsorption follows the same trend as obtained with Heliocote-pt sample. The talc sample becomes hydrophilic after the addition of dispersion reagent.

6.3.2.2 Effect of EO/PO and SOPA addition on zeta-potentials of talc powders

Figure 6.12 a) and Figure 6.12 b) show the changes in zeta-potential respectively for Heliocote-pt and Mistrfil-pt talc samples after the addition of EO/PO and SOPA. Both the figures show that talc samples are generally negatively charged in neutral pH range with a p.z.c. as low as approximately pH3. Addition of EO/PO alone increases the zeta potential of talc sample a little. On the other hand, addition of both EO/PO and SOPA greatly increases the negative potential of talc sample. Comparing the results obtained

with zeta potential to those attained with surface free energies, one can tell that the acid/base interaction is different from the positive/negative electrostatic interaction. Addition of EO/PO increases γ^- greatly; while has minor effect on the zeta-potential. Addition of SOPA alone has no effect on γ^-; while it increases the negative zeta-potential greatly. The difference between acid/base interaction and electrostatic force has been discussed by van Oss *et al*. before (22, 23, 30). The use of K-Flow D alone causes relatively little changes in the surface free energies of talc. The reagent is designed to change surface charge rather than surface free energy

6.3.2.3 Adsorption of EO/PO copolymer on the basal/edge surfaces of talc sample

From the obtained surface free energy data of talc sample after the addition of EO/PO chemicals, using the technique described in previous section, one can calculate the change of surface energies and infer the adsorption of chemicals on the basal/edge surfaces.

The calculated results of surface free energies on base/edge surfaces were listed as Table 6.5. It is shown in the table that γ^- on the basal surface increases to as large as 14.49 mJ/m^2, which is much larger than that on bare talc samples. (see Table 5.6) By comparison, one can also see that γ^+ on edge surface decreases a little. As discussed in Chapter 5, the fact that negative surface free energies values were seen in Case 1 may origin from the similarity in surface properties between the two talc samples and the experimental errors associated with contact angle measurements. For example, as shown by Case 2, when the surface base/edge ratio changes a little, the negative disappeared. However, the trend that the chemicals adsorption results in γ^- increasing on basal surface and γ^+ decreasing on edge surface does not change at all. Furthermore, as shown in Case 3, by changing the surface free energies of measured talc sample a little, one can also get positive results, with the same trend of surface free energies change on both base and edge surfaces.

The increase of γ^- on the basal surface and decrease of γ_S^+ on the edge surface suggests that the polymer adsorbs on the edge surface with the EO group in contact with the surface, and the PO group pointing toward the solution. On the contrary, the polymer adsorbs on the basal surface with the PO group in contact with the surface, and the EO group pointing toward the solution. The adsorption behavior is schematically described by Figure 6.13.

6.4 Conclusions

In present work, thin layer wicking technique was used to determine the contact angles (θ) of wicking liquids on powdered talc samples. The obtained contact angle values were used to calculate the surface free energy components of talc using the acid/base interaction theory developed by van Oss-Chaudhury-Good. Thus the effects of CMC addition on talc wettability is evaluated according to change of the solid surface free energy.

It is concluded that under present experiment condition, the penetration of liquids in powder layer follows the Washburn's equation and the effective interstitial pore radius R_{eff}, which is obtained by wicking with low-energy alkenes, is linear proportional to powder size, D_{50}. The measured high water contact angle on talc surface confirms the

natural hydrophobicity of talc powders. The wicking results of thin layer of talc coated with CMC shows that the wetting reagents make talc surface hydrophilic by increasing solid surface free energy, especially the γ^{-lw} and γ^{-}. Increasing CMC reagent level from 0.4wt% to 1wt% doesn't change the solid surface free energy further. Despite of a higher γ_s^{-} when FinnFix30, a higher molecular weight CMC, is added, the increase of γ_s^{-} and surface hydrophilicity are limited. The results in present work quantify the effect of CMC addition on talc's wettability and the information will make help in the application of CMC as depressant/wetting reagent on talc in flotation and paper industry.

Addition of EO/PO only weakly increases the zeta potential of talc sample; however, it increases γ^{-} and γ^{AB} greatly. Therefore, talc sample was made hydrophilic when being coated with dispersion reagents. Addition of SOPA alone has little effect on γ^{-} and γ^{AB}; while it changes the zeta potential of talc powder greatly. The reagent is designed to change surface charge rather than surface free energy.

6.5 References

1. E. Z. Orowan, Phys. 1933, 82, 235.
2. B. W. Evans, S. Guggenheim, Rev. Min. 1988, 19, 225
3. A.U. Gehring, Clay Minerals, 1988. 33. 661-664
4. P. Jenkins, J. Ralston, Colloids and Surfaces A, 1998, 139, 27–40
5. L. J. Michot, F. Villiéras, M. Franqois, J. Yvon, R. Le Dred, and J. M. Cases Langmuir 1994,10, 3765-3773
6. I. Yildirim, Ph.D. Thesis, Virginia Tech, April 2001
7. F. M. Fowkes, William D. Harkins, J. Am. Chem. Soc., 1940, 62(12), 3377-3386
8. J. C. Van Oss, R. F. Giese, Z. Li, K. Murphy, J. Norris, M. K. Chaudhury, and R. J . Good, J. Adhesion Sci. Technol, 1992 Vol. 5, No. 4, 413-428,
9. S. Subramanian, J. S. Laskowski, Langmuir, 1993, 9(5), 1330-1333
10. R. K. Rath, S, Subramanian, J. S Laskowski, Langmuir 1997, 13(23), 6260-6266
11. C. W. Hoogendam, A. de Keizer, M. A. Cohen Stuart, and B. H. Bijsterbosch, Langmuir 1998, 14, 3825-3839
12. Q. Liu, Y. Zhang, J. S. Laskowski, Int. J. Miner. Process. 2000, 60, 229–245
13. P.G. Shortridge, P.J. Harris a, D.J. Bradshaw a, L.K. Koopal, Int. J. Miner. Process. 2000, 59, 215–224
14. G. E. Morris, Daniel Fornasiero, John Ralston, Int. J. Miner. Process. 2002, 67, 211–227
15. R. E. Ayala, E. Z. Casassa and G. D. Parfitt, Powder Technology, 1987, Vol. 51, 1, 3-14.
16. C. A. Prestidge, G. Tsatouhas, International Journal of Pharmaceutics, 2000,Vol. 198, 2, 201-212
17. T. V. Subrahmanyam, M. B. M. Monte, A. Middea, E. Valdiviezo and F. F. Lins, Minerals Engineering, 1999, Vol. 12, 11, 1347-1357
18. C. J. van Oss, W. Wu and R. F. Giese, Jr. Particulate Science and Technology, 1993, 11, 193-198
19. E. Chibowski, L. Holysz, Langmuir, 1992, 8(2), 710-716
20. L. Holysz, E. Chibowski, Langmuir, 1992, 8(2), 717-721
21. E. Chibowski, F. Gonzalez-Caballero, Langmuir, 1993, 9(1), 330-340

22. W. Wu, R. F. Giese, Jr. and C. J. van Oss, Colloids and Surfaces A, 1994, Vol. 89, 23, 241-252
23. W. Wu, R. F. Giese, Jr. and C. J. Van Oss, Powder Technology, 1996,Vol. 89, 2, 129-132
24. Z. Li, R. F. Giese, C. J. van Oss, Langmuir, 1994, 10(1), 330-333
25. G. Chen and H. Zhu, Colloids and Surfaces B, 2004, Vol. 35, 2, 143-147
26. C. J. Van Oss, R. J. Good, and M. K. Chaudhury, J. of Colloid and Interface Science, 1986, 111, 378
27. C. J. van Oss, M. K, Chaudhury, and R. J. Good, Adv. in Colloid Interface Sci., 1987, 28, 35
28. C. J. Van Oss, R. J. Good, and M. K. Chaudhury, Langmui, 1988, 4, 884
29. C. J.Van Oss, M. K. haudhury, and R. J. Good, J. of Colloid and Interface Science, 1988, 128, 313,
30. C. J.Van Oss, "Interfacial forces in aqueous media", Marcel Dekker, 1994
31. F. M. Fowkes, J. Phys. Chem., 1962, 66, 382
32. F. M. Fowkes, J. Phys. Chem., 1963, 67, 2538-2541
33. E.W. Washburn, Physical Review, 1921, 1, 273
34. P. M. Costanzo, W. Wu, R. F. Giese, C. J. van Oss, Langmuir, 1995, 11(5), 1827
35. E. Chibowski and Rafae Perea-Carpio, Adv. in Colloid and Interface Science, 2002, Vol. 98, 2, 245-264
36. F. E. Bartell, H. H. Zuidema, J. Am. Chem. Soc., 1936, 58(8), 1449-1454
37. E. Steenberg, 1982, PhD thesis, University of Potchefsroom, South Africa
38. J.Wang, P. Somasundaran, J. Colloid and Interface Science, 2005. 291, 1, 75-83.

Table 6.1 Surface tension (mJ/m) and viscosities (mPa • s) values of wicking liquids (@ 20ºC)

Liquid	γ_l^{LW} (mJ/m)	γ_l^+ (mJ/m)	γ_l^- (mJ/m)	η(mPa • s)
Heptane	20.3	0	0	0.409
Octane	21.6	0	0	0.542
Decane	23.8	0	0	0.907
Dodecane	25.35	0	0	1.493
1-Bromonaphthalene	44.4	0	0	4.89
Methylene iodide	50.8	0	0	2.82
Water	21.8	25.5	25.5	1.08
Formamide	39.0	2.28	39.6	4.03

Table 6.2. Effective pore size, R_{eff} of Luzenac talc obtained with the thin layer wicking technique using low surface free energy liquids.

Talc Sample	Particle Size D_{50} (μm)	Effective Pore Size R_{eff} (μm)
Luz A	2.2	0.08
Luz B	3.2	0.27
Luz C	3.2	0.25
Luz D	3.4	0.31
Luz E	7	0.52
Luz F	20	1.30

Table 6.3 Contact angle values of talc samples after being treated with CMC.

Reagent Level (%)		Contact angle θ (degree)							
		Heliocote-pt				Mistrofil-pt			
		water	For	MI	1-Br	water	For	MI	1-Br
FinnFix 5	0	87.1	44.4	55.5	41.0	87.6	48.2	58.3	44.1
	0.4	78.0	58.5	35.9	18.4	74.8	54.5	42.4	28.9
	0.7	78.0	61.1	42.5	19.4	74.9	60.3	43.2	25.5
	1	78.4	60.3	44.8	25.2	75.7	62.1	37.7	28.1
FinnFix 30	0	87.1	44.4	55.5	41.0	87.6	48.2	58.3	44.1
	0.4	76.7	62.8	53.1	17.4	69.9	64.9	35.5	28.6
	0.7	77.0	67.4	50.8	16.6	73.6	72.6	44.1	31.8
	1	78.2	69.6	46.6	21.4	76.6	73.9	43.0	31.4
PE23EX	0	87.08	44.38	55.47	41.01	87.6	48.2	58.3	44.1
	0.4	73.51	75.31	52.40	41.45	68.28	57.43	47.35	30.31
	0.7	75.65	75.67	50.34	42.66	69.01	62.22	45.09	32.11
	1	74.98	75.00	48.15	39.75	68.50	61.52	43.74	29.91

Table 6.4 Surface free energies of talc powders after being treated with CMC.

Reagent level (%)		Surface free energy (mJ/m^2)									
		Heliocote-pt					Mistrofil-pt				
		γ_s^{LW}	γ_s^-	γ_s^+	γ_s^{AB}	γ_s	γ_s^{LW}	γ_s^-	γ_s^+	γ_s^{AB}	γ_s
FinnFix5	0	34.2	0.0	4.3	0.4	34.6	32.8	0.1	3.7	1.1	33.9
	0.4	42.2	7.9	0.0	0.6	42.7	39.0	8.6	0.1	2.2	41.3
	0.7	41.9	9.2	0.1	1.9	43.8	40.2	12.0	0.1	1.6	41.8
	1	40.3	8.4	0.0	0.6	40.8	39.3	12.1	0.1	2.0	41.4
FinnFix30	0	34.2	0.0	4.3	0.4	34.6	32.8	0.1	3.7	1.1	33.9
	0.4	42.4	11.7	0.3	3.9	46.3	39.1	21.8	0.6	7.1	46.3
	0.7	42.6	14.5	1.0	7.7	50.3	38.0	23.4	1.7	12.5	50.5
	1	41.4	14.6	1.2	8.3	49.7	38.1	20.1	1.7	11.8	50.0
PE23EX	0	34.2	0.0	4.3	0.4	34.6	32.8	0.1	3.7	1.1	33.9
	0.4	34.0	26.0	1.5	12.5	46.5	38.5	17.8	0.0	0.7	39.3
	0.7	33.4	22.9	1.3	10.9	44.3	37.9	20.6	0.2	4.0	41.9
	1	34.7	23.4	1.5	11.7	46.4	38.7	20.8	0.2	4.2	42.9

Table 6.5 Effect of EO/PO addition on Surface free energy and its components at the base/edge surfaces of powdered talc samples obtained with the thin layer wicking technique.

	Mistrofil-pt (1% EO/PO)	Heliocote-pt (1% EO/PO)	1		2		3	
			Base surface	Edge surface	Base surface	Edge surface	Base surface	Edge surface
γ_s^{LW}	32.09	31.03	29.42	36.44	30.51	34.02	-	-
γ_s^-	7.64	10.34	14.49	-3.55	11.69	2.68	13.16	0.89
γ_s^+	3.35	1.44	-1.49	11.24	0.48	6.85	0.19	8.50
γ_s^{AB}	10.11	7.71	4.02	20.04	6.50	14.51	-	-
γ_s	42.20	38.74	33.44	56.48	37.01	48.53	-	-

* In case 1, f_b^1=0.62 for Mistrofil-pt sample and f_b^2=0.77 for Heliocote-pt sample have been used to calculate the surface free energies on base/edge surfaces. In case 2, f_b^1=0.55 for Mistrofil-pt sample and f_b^2=0.85 for Heliocote-pt sample were used. In case 3, f_b^1=0.62 for Mistrofil-pt sample and f_b^2=0.77 for Heliocote-pt sample have been applied; while the value of γ_s^- for Mistrofil-pt is purposely changed from 7.64 to 8.5mJ/m^2 and the γ_s^+ value for Heliocote-pt is purposely changed from 1.44 to 2.1 mJ/m^2 only to show the effects of experiment variance on the final calculation results.

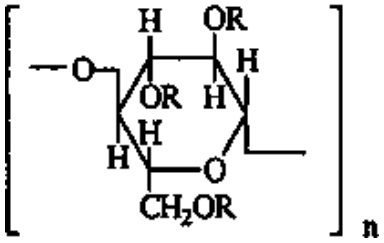

$[C_6H_7O_2 (OH)_x (OCH_2COONa)_y]_n$
where n is the degree of polymerization
x = 1.50 to 2.80
y = 0.20 to 1.50
x + y = 3.0

Figure 6.1 Chemical structure of carboxy methyl cellulose, sodium salt (i.e., Finnfix 5 and Finnfix 30).

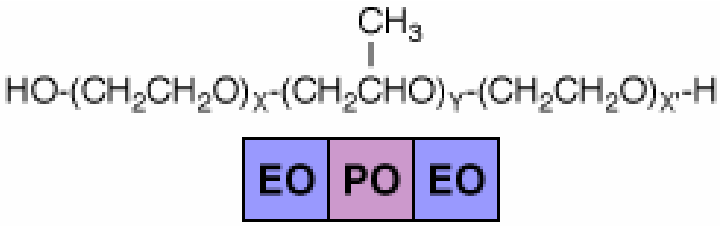

Figure 6.2 Chemical structure of ethylene oxide (EO) / propylene oxide (PO) block co-polymer (Dowfax WP-310).

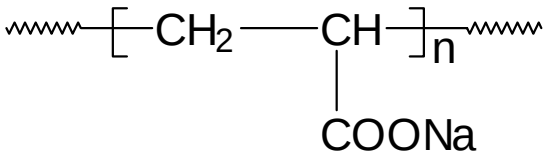

Figure 6.3 Chemical structure of sodium poly acrylate (K-Flow D)

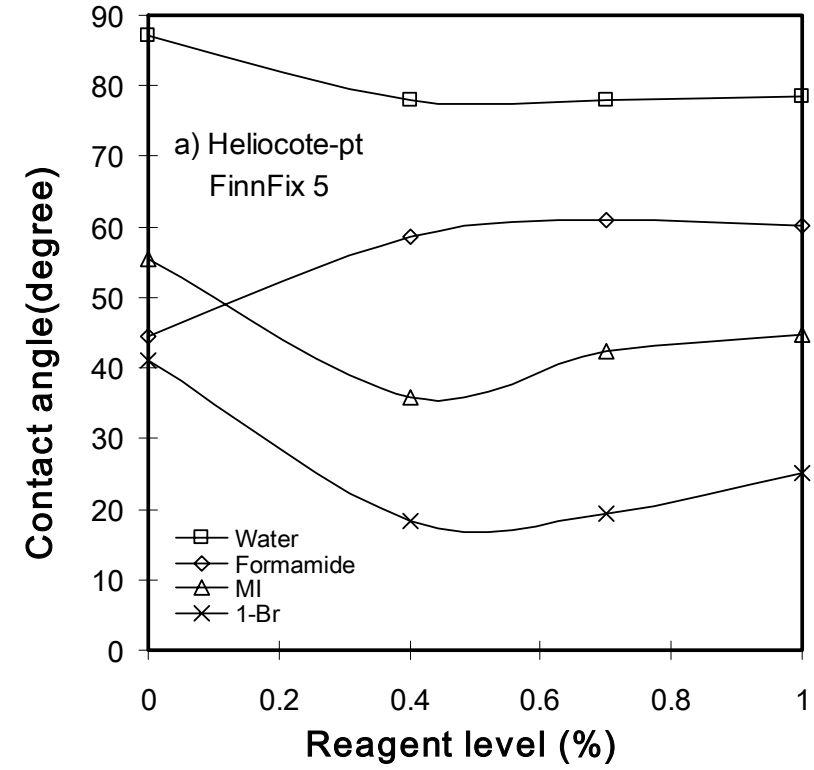

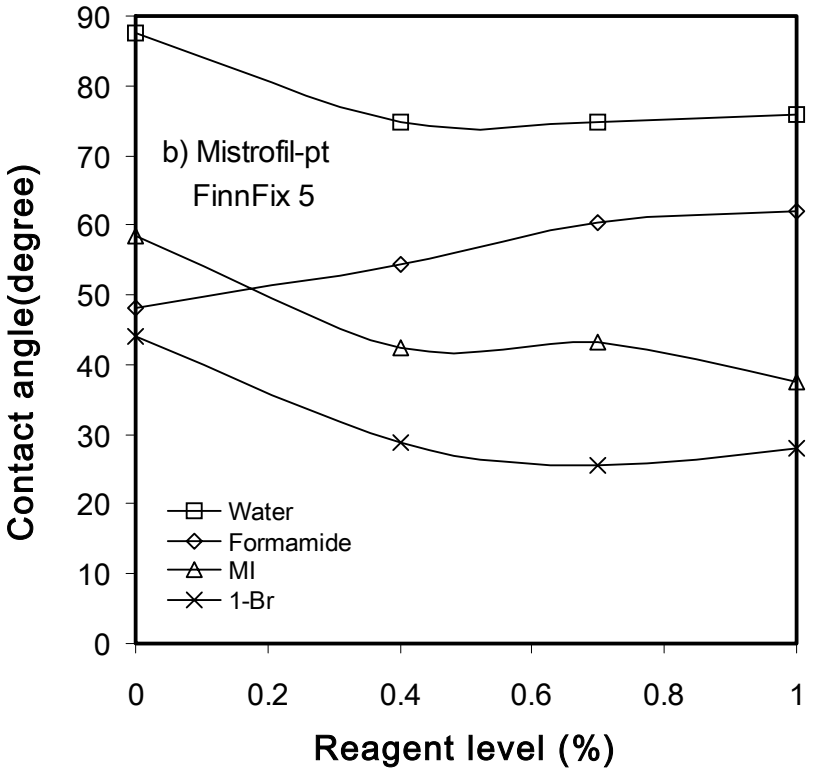

Figure 6.4 Effects of FinnFix5 addition on contact angles on talc powders.

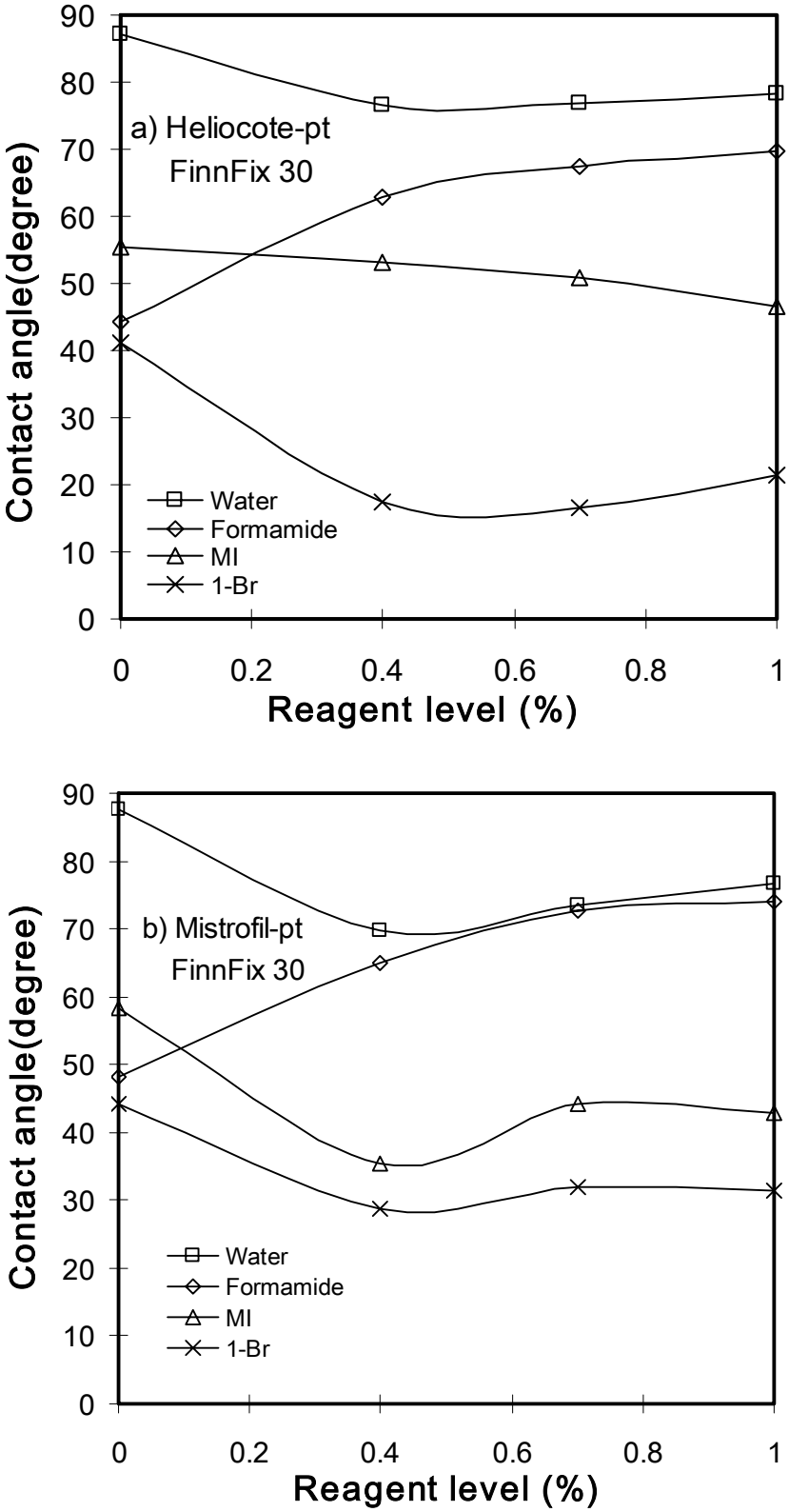

Figure 6.5 Effects of FinnFix30 addition on contact angles on talc powders.

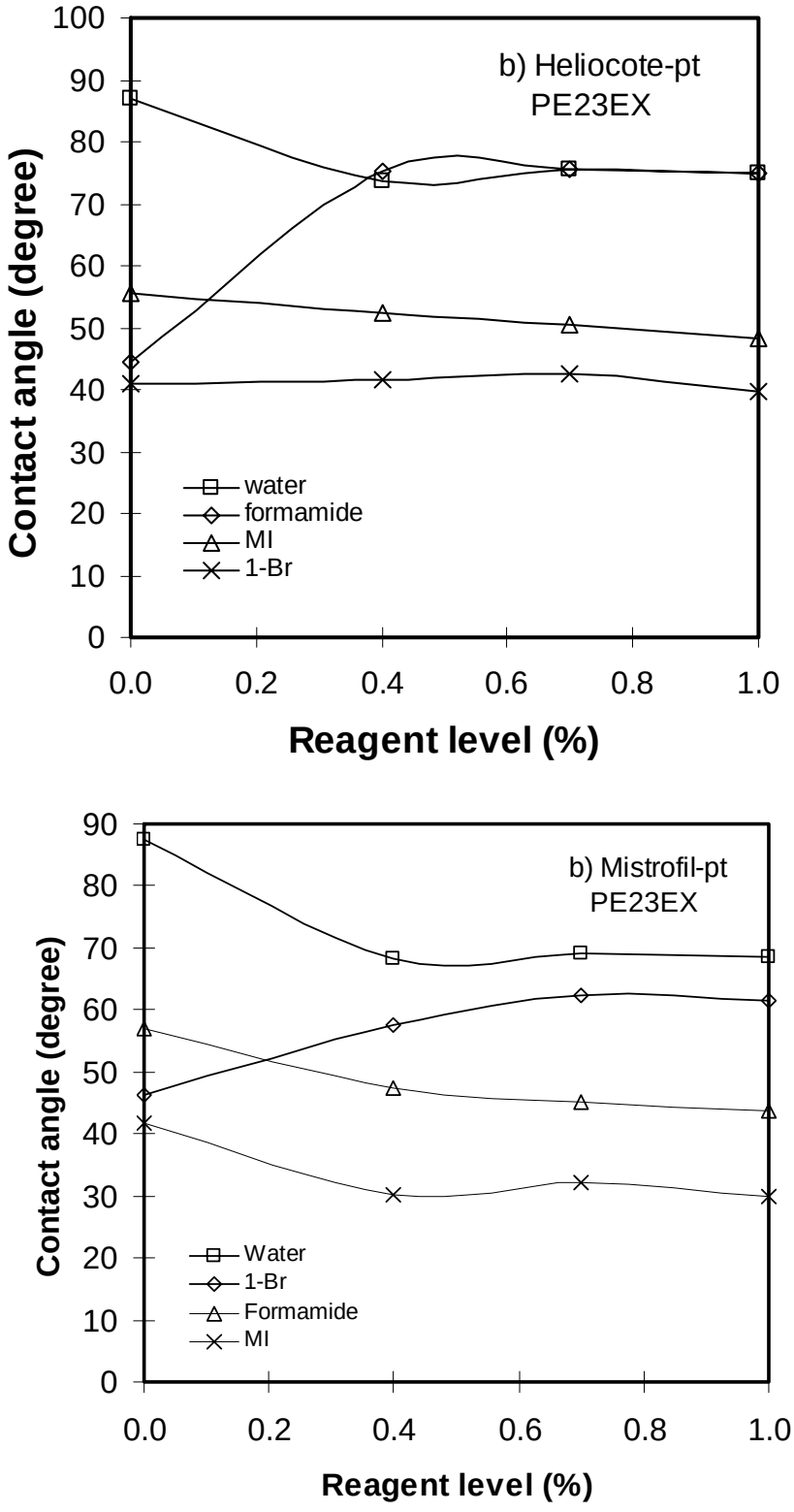

Figure 6.6 Effects of PE23EX addition on contact angles on talc powders.

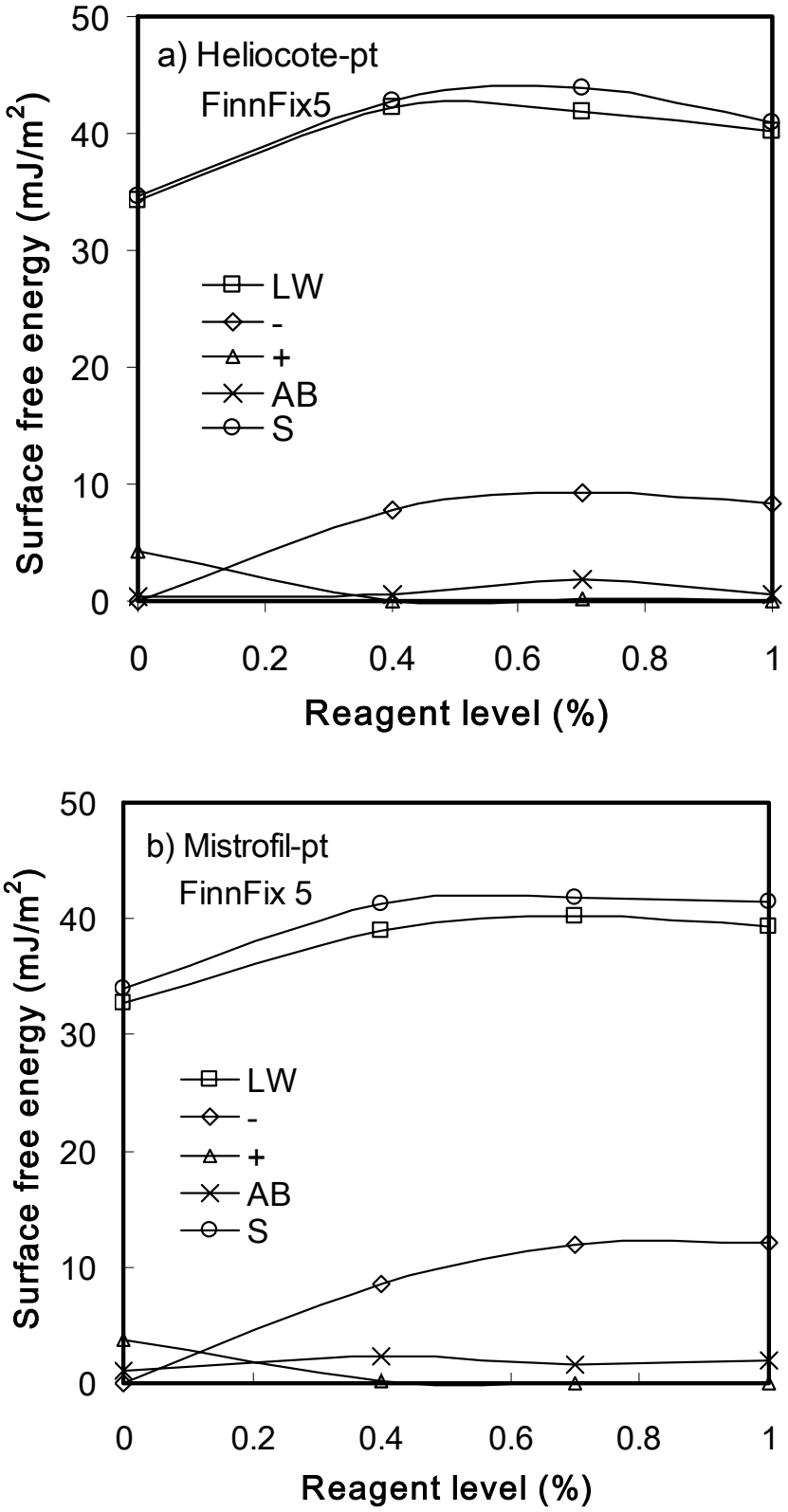

Figure 6.7 Effects of FinnFix5 addition on surface free energy on talc powders.

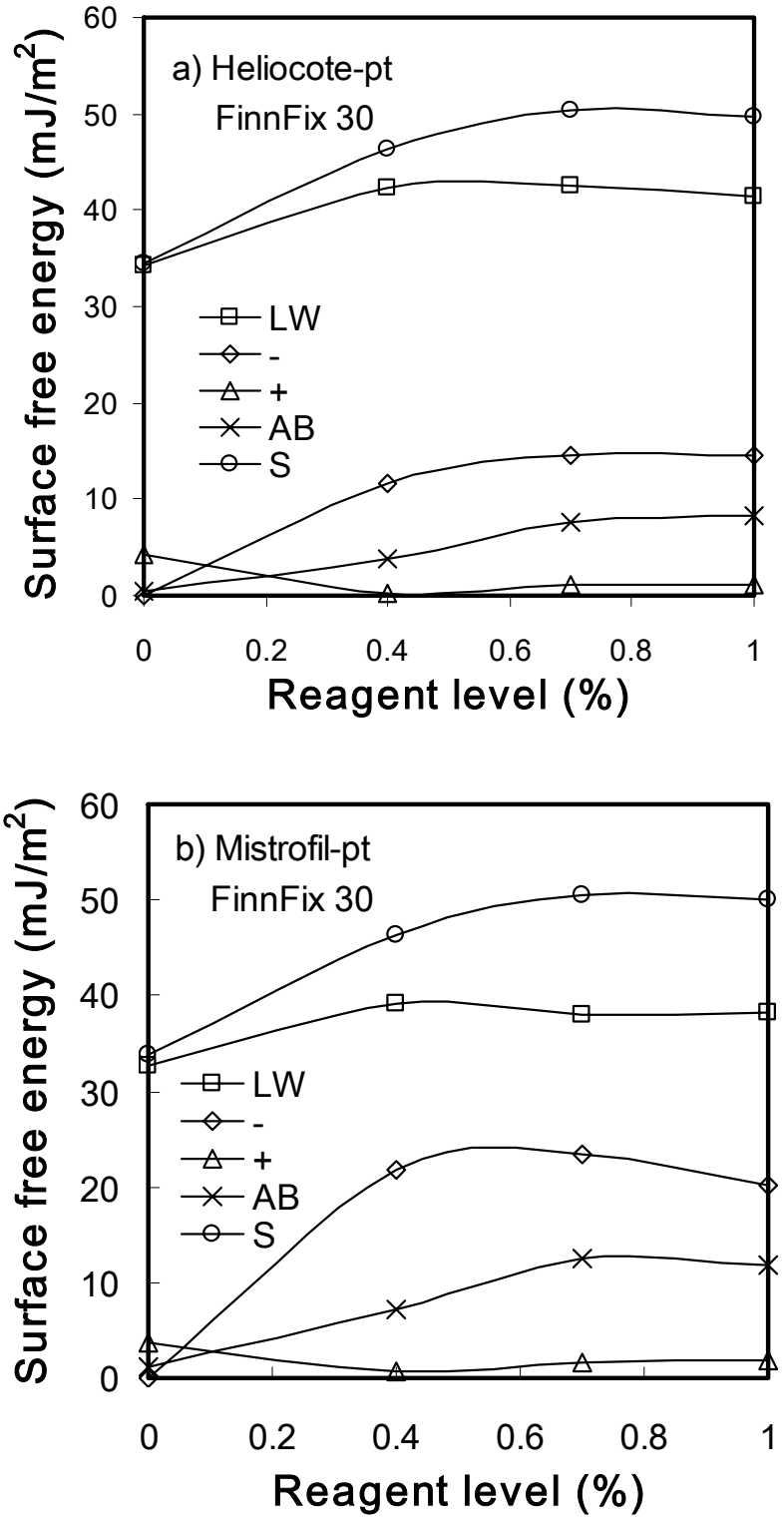

Figure 6.8 Effects of FinnFix30 addition on surface free energy on talc powders.

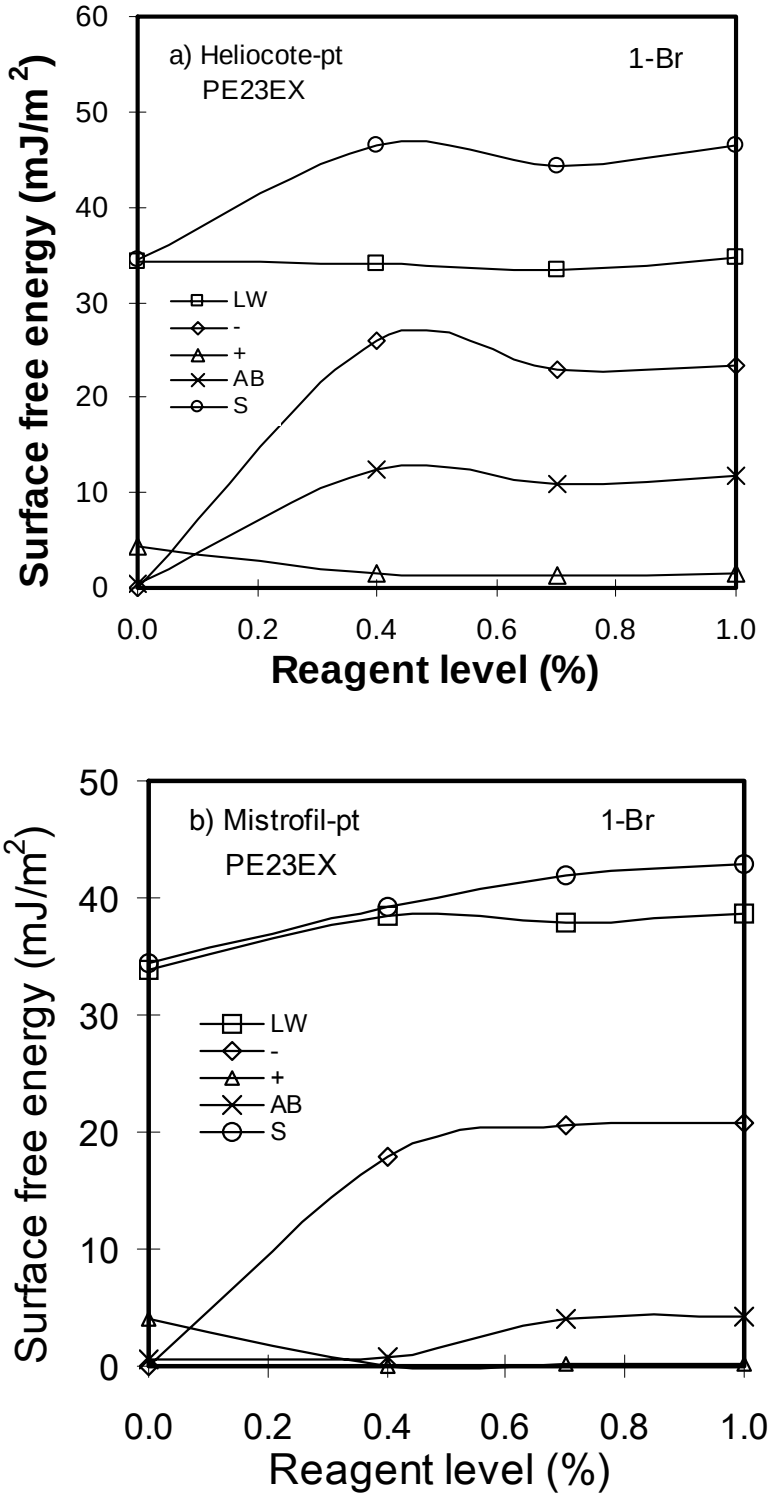

Figure 6.9 Effects of PE23EX addition on surface free energy on talc powders.

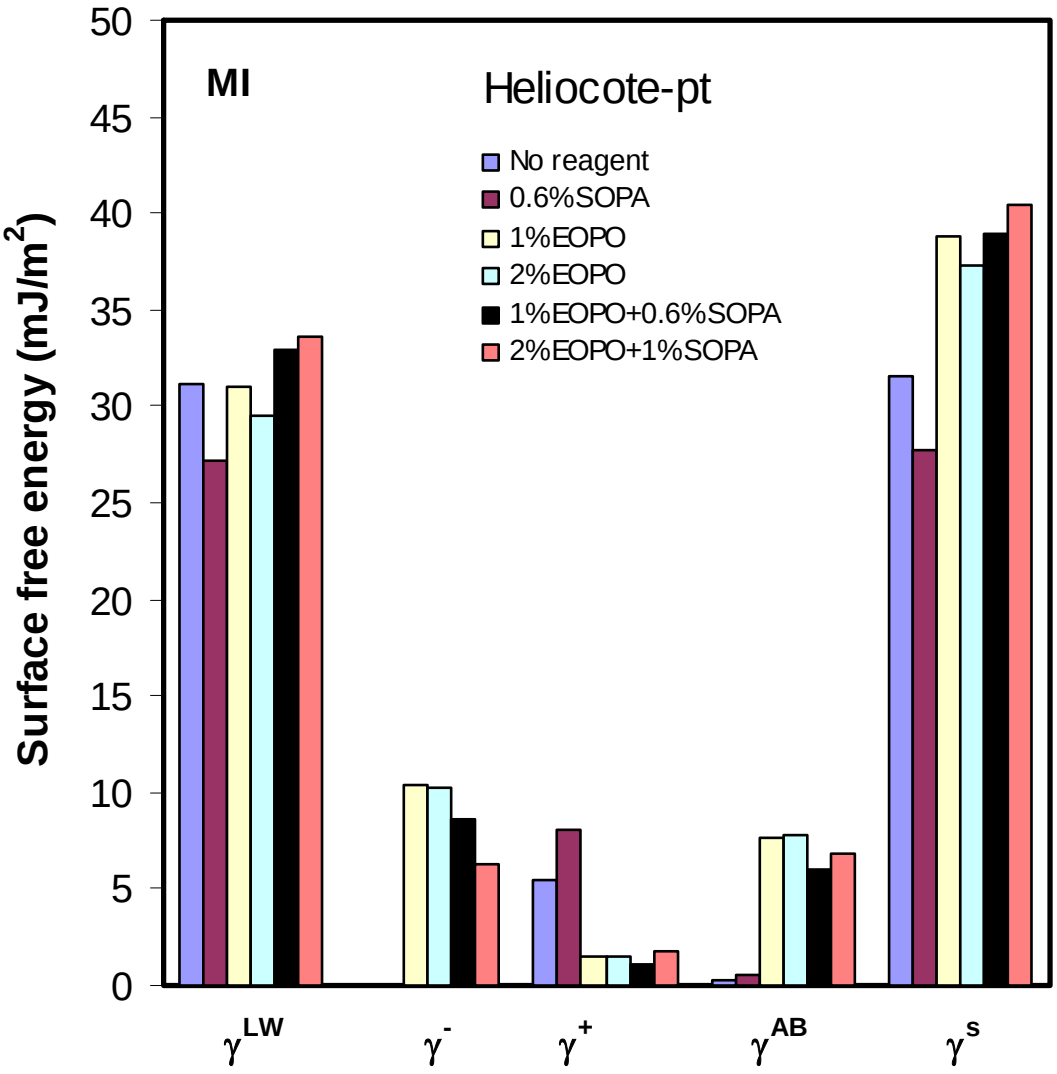

Figure 6.10 a) Effects of EO/POand SOPA addition on the surface free energies of talc powders using MI, water and Formamide combinination.

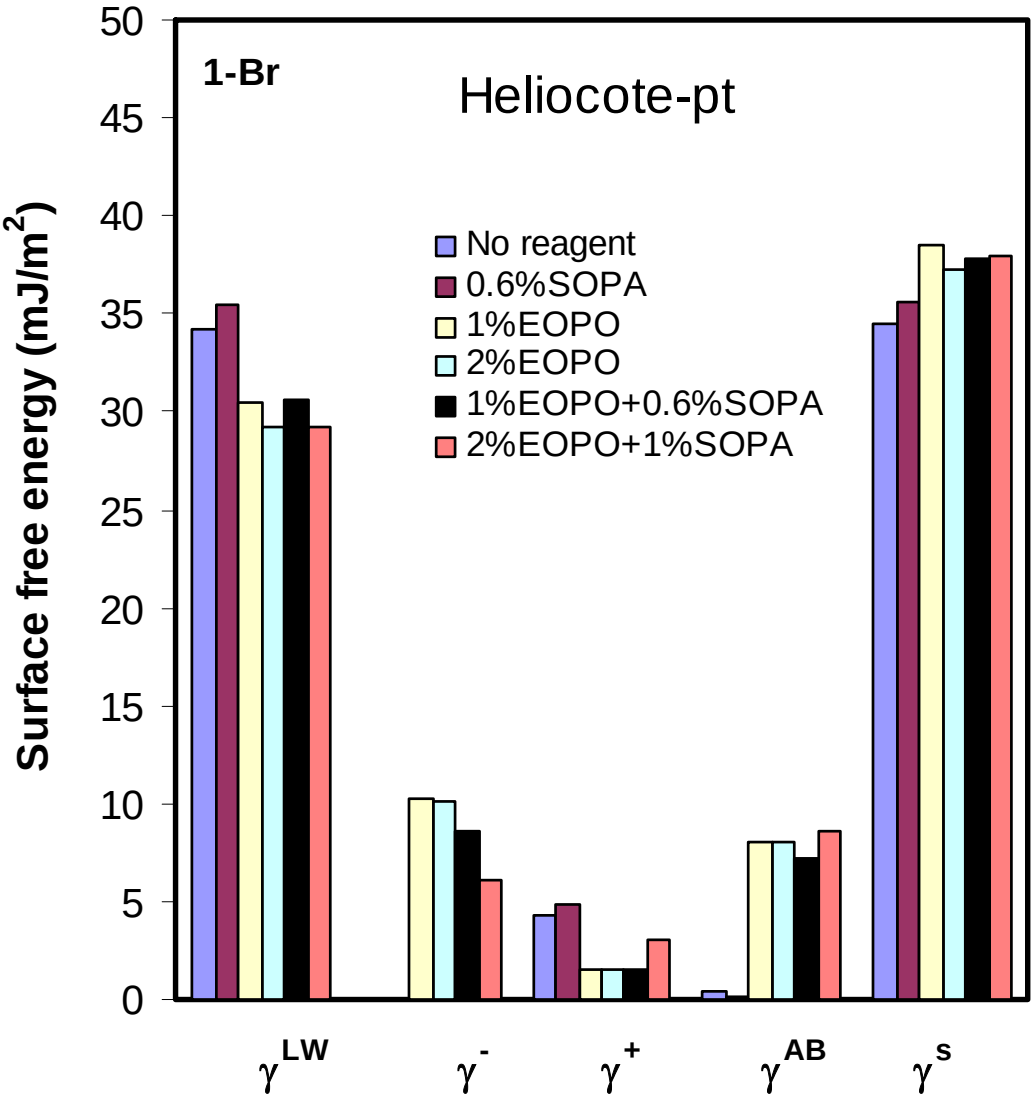

Figure 6.10 b) Effects of EO/POand SOPA addition on the surface free energies of Heliocote-pt talc powders using 1-Br, water and Formamide combinination.

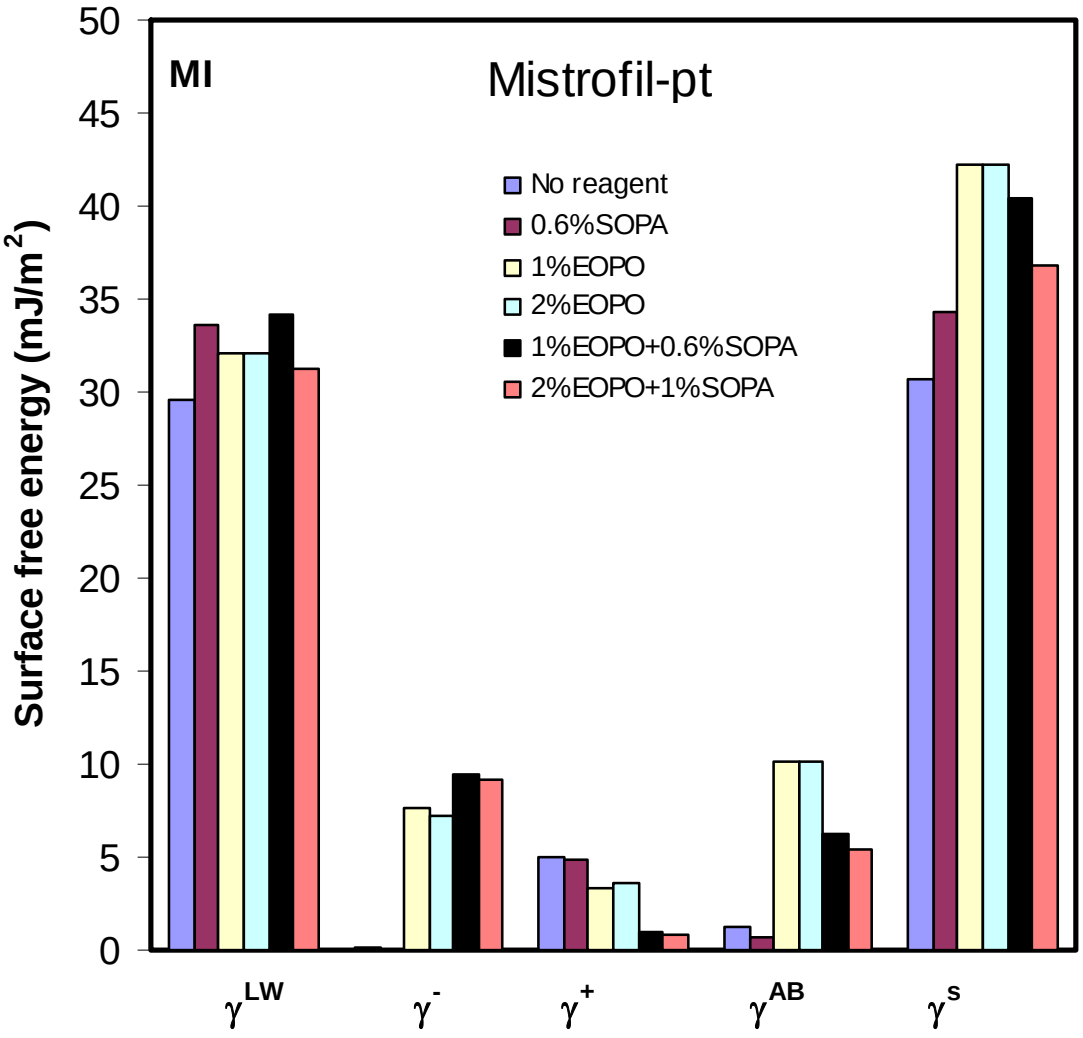

Figure 6.11 a) Effects of EO/POand SOPA addition on the surface free energies of Mistrofil-pt talc powders using MI, water and Formamide combinination.

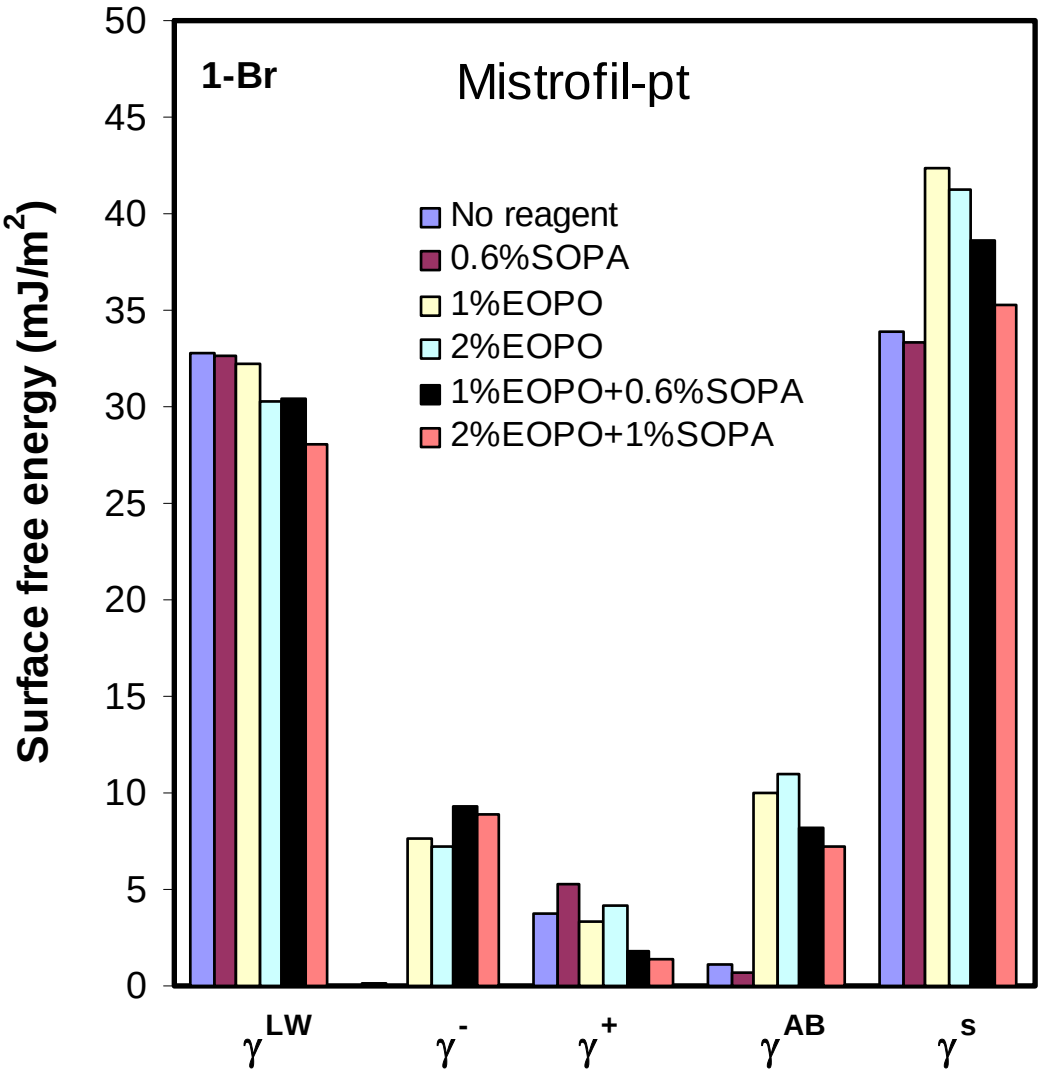

Figure 6.11 b) Effects of EO/POand SOPA addition on the surface free energies of Mistrofil-pt talc powders using 1-Br, water and Formamide combinination.

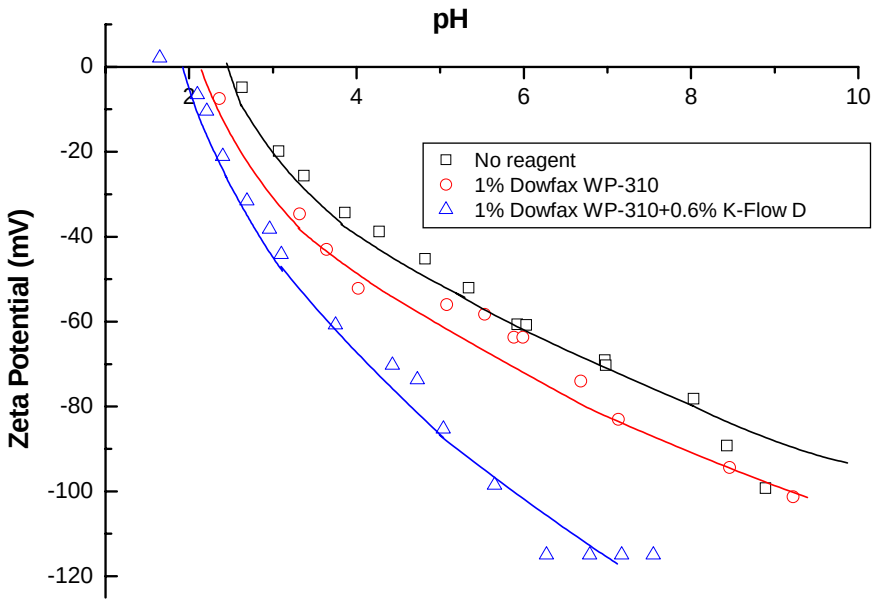

Figure 6.12 a) Effect of EO/PO and SOPA addition on zeta potential of Mistrofil-pt talc sample.

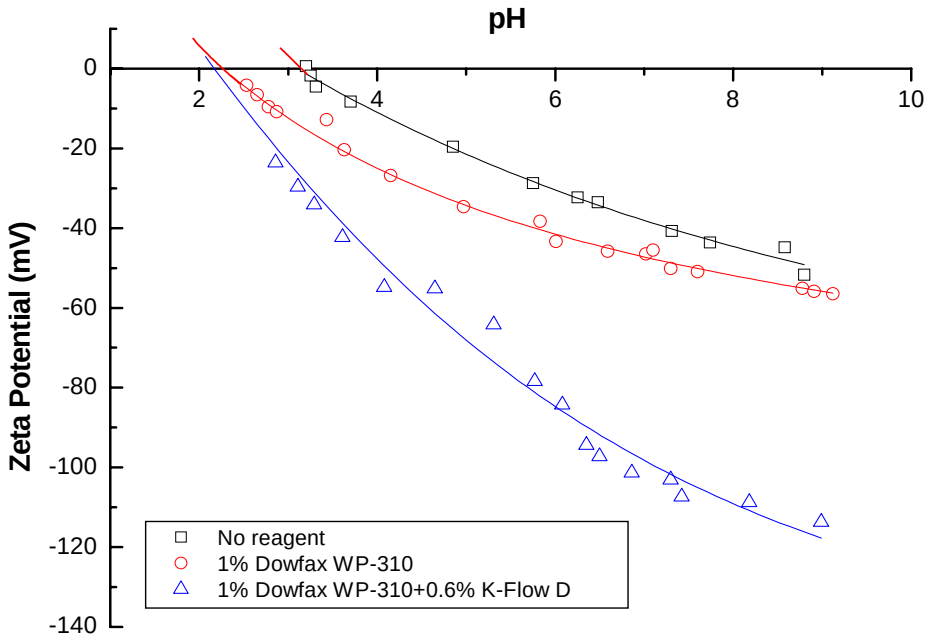

Figure 6.12 b) Effect of EO/PO and SOPA addition on zeta potential of Heliocote-pt talc sample.

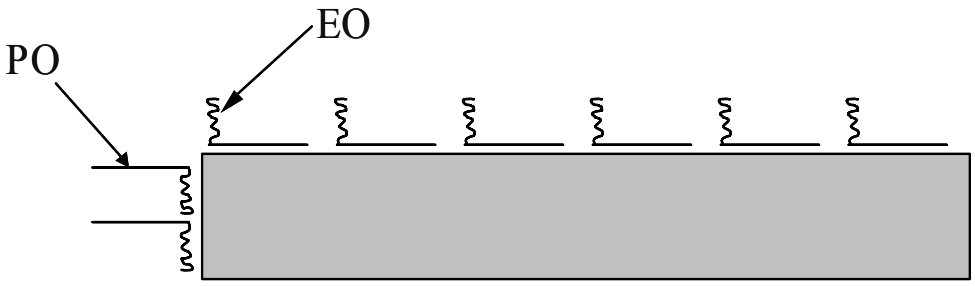

Figure 6.13 The adsorption mechanism of Dowfax-310 (EO/PO co-polymer) on the basal and edge surfaces of a talc lamella

CHAPTER 7

Surface Force and Surface Free Energy

Abstract

The silica/water interfacial surface free energy γ_{sl} was calculated from the detachment forces measured between silica surfaces in C_nTACl solutions using an AFM. In addition, the value of γ_{sl} was also calculated from the surface free energy parameters of C_nTACl coated silica particles, which were obtained from the thin layer wicking technique. Despite of a little difference between the absolute γ_{sl} values attained through two different techniques, the trends that interfacial surface free energy, γ_{sl}, increases with surface hydrophobicity (water contact angle) are of the same. It was also found that the surface free energy components γ_s^{lw} and γ_s^+ of silica decreases with surface hydrophobicity increasing. The fact that the change in Gibbs free energy, ΔG_{131} and ΔG_{132} both become more negative when contact angle increases suggests that the process of coagulation or floatation of silica particles in the aqueous solution becomes much easier to occur with surface hydrophobicity increasing.

7.1 Introduction

In minerals engineering, hydrophobicity of minerals surface usually play a decisive role. For example, coagulation and flotation can only be possible when the target mineral surface is made hydrophobic. Yoon et al. has schematically shown that hydrophobic force increases with solid surface hydrophobicity. Furthermore, surface hydrophobicity is believed to affect the flotation kinetics, as predicted in a flotation model. The most widely used measure of hydrophobicity is the water contact angle, which is a thermodynamic property and can be used to determine whether coalescence, adhesion or wetting process can occur. As shown in Chapter 5, contact angle has been used to calculate the surface free energy parameters on the talc powder samples. The information then can be used to calculate the interfacial surface tension, γ_{sl}, between the mineral and aqueous solution using the surface tension components theory.

It has been discussed in Chapter 3 that, in another way, the interfacial free energy can be calculated from the detachment force, which is related to the work of adhesion, between two solid surfaces in aqueous media. According to the DMT and JKR models, a high interfacial free energy results in a high detachment force.

In present work, it is interesting to compare the values of interfacial free energy obtained separately from the two methods and study the relationship between surface force, interfacial free energy and surface hydrophobicity. Further, the change in Gibbs free energy, ΔG_{131} and ΔG_{132} related to the coagulation and flotation process can be calculated from the interfacial free energy results.

7.1.1 Interfacial free energy (γ_{12}) vs. detachment force

The adhesion force between a sphere and a plate can be obtained starting from the Derjagurin approximation. The DMT (Derjaguin-Muller-Toporov) relation applies for the rigid materials (1),

$$F_{adhesion} / R \cong 4\pi\gamma_{12} \qquad [1]$$

where γ_{12} is the interfacial surface free energy and the adhesive contact is assumed ideal. For glass sphere and plate immersed in C_nTACl surfactant solution, the γ_{12} can be expressed as γ_{sl}, in which, *s* stands for solid and *l* stands for aqueous solution.

For elastic materials, the surface deformations are no longer negligible and the JKR (Johnson, Kendal, Roberts) theory applies instead (2),

$$F_{adhesion} / R \cong 3\pi\gamma_{12} \qquad [2]$$

Generally speaking, real materials are in a state between rigid an elastic. Thus the DMT theory gives an up limit; whereas the JKR theory gives a low limit for the adhesion force.

In AFM force measurement, as discussed in Chapter 3, the adhesion force can be calculated from the detachment force curve using the same treatment as applied to the approach force curves. Thus the interfacial surface free energy γ_{12} is obtained by solving the Eq. [1] or Eq. [2]. Both the equations show that the adhesion force increases with interfacial surface free energy γ_{12}.

7.1.2 Interfacial free energy (γ_{12}) calculated from the Acid/Base theory

As described in Chapter 5, solid surface free energy can be described by the surface tension components theory or the Acid/Base theory developed by van Oss *et al*. (3-7). The theory is briefly described as follows.

Fowkes (8, 9) firstly proposed that the surface free energy of a material *i* can be subdivided into separate components:

$$\gamma_i = \sum_j \gamma_i^j \qquad [3]$$

in which j represents types of surface free energy component, e.g., dispersion, H-bonding, and metallic interactions. Van Oss *et al*. (3-7) considered the surface tension as a sum of apolar Lifshitz-van der Waals, γ^{LW}, and polar acid/base interactions, γ^{AB}. Thus,

$$\gamma_i = \gamma_i^{LW} + \gamma_i^{AB} \qquad [4]$$

where γ_i^{LW} and γ_i^{AB} are respectively the non-polar and polar (acid-base) surface free energy components. The former can be represented by the Lifshitz-van der Waals (or LW) interaction that includes the dispersion (London), induction (Debye) and orientation (Keesom) components. The latter represents interactions between Lewis acids (electron acceptor) and bases (electron donor) on the surface.

van Oss *et al*. used the geometric mean combining rule to define γ_i^{AB} as follows:

$$\gamma_i^{AB} \equiv 2\sqrt{\gamma_i^+ \gamma_i^-} \qquad [5]$$

where γ_i^+ is the acidic component of the surface tension and γ_i^- is the basic component. Therefore, Eq. [4] can be expressed as

$$\gamma_i = \gamma_i^{LW} + 2\sqrt{\gamma_i^+ \gamma_i^-} \qquad [6]$$

It is therefore readily drawn that the change in surface free energy (ΔG_{SL}) associated with the adhesion of a liquid drop on a solid plate in the air can be given by:

$$\Delta G_{SL} = -2\left(\sqrt{\gamma_S^{LW}\gamma_L^{LW}} + \sqrt{\gamma_S^+\gamma_L^-} + \sqrt{\gamma_S^-\gamma_L^+}\right) \qquad [7]$$

in which γ^{LW} is the Lifshitz-van der Waals component of the surface free energy; γ^+ and γ^- are respectively the acidic and basic components of the materials. S represents solid, while L represents liquid. Combining Eq. [7] with the Dupre equation:

$$\Delta G_{SL} = \gamma_{SL} - \gamma_S - \gamma_L \qquad [8]$$

one obtains:

$$\gamma_{SL} = \gamma_S + \gamma_L - 2\left(\sqrt{\gamma_S^{LW}\gamma_L^{LW}} + \sqrt{\gamma_S^+\gamma_L^-} + \sqrt{\gamma_S^-\gamma_L^+}\right) \quad [9]$$

Combining Eq. [9] with Young's equation,

$$\gamma_L \cos\theta = \gamma_S - \gamma_{SL} \quad [10]$$

in which, θ is the contact angle, one gets the van Oss-Chaudhury-Good (OCG) equation:

$$(1 + \cos\theta)\gamma_L = 2\left(\sqrt{\gamma_S^{LW}\gamma_L^{LW}} + \sqrt{\gamma_S^+\gamma_L^-} + \sqrt{\gamma_S^-\gamma_L^+}\right) \quad [11]$$

which is used to characterize a solid surface in terms of its surface free energy components, i.e., γ_S^{LW}, γ_S^+, and γ_S^-. To determine these values, it is necessary to determine contact angles of three different liquids of known properties (*i.e.* γ_L^+, γ_L^-, γ_L^{LW}) on the surface of the solid of interest. One can then set up three equations with three unknowns, which can be solved simultaneously to obtain the values of γ_S^{LW}, γ_S^+, and γ_S^-.

7.1.3 Thin layer wicking

In practice, however, it is not practical to directly measure the contact angle of liquid on powdered solids, especially for clay particles. Thin layer wicking technique is a convenient way to measure contact angles of liquids on powdered materials (10-14) by determining the capillary rise rate of the wicking liquids in packed beds of those particulate materials. The wicking process follows the Washburn's equation (15):

$$\frac{2\eta h^2}{t} = R_{eff} * \gamma_L * \cos\theta \quad [12]$$

where η is the viscosity of the liquid, h is the height to which wicking liquid has risen at time t, R_{eff} is the effective interstitial pore radius of packed powder bed, γ_L is the surface tension of wicking liquid and θ is the contact angle.

The parameter R_{eff} of Eq. [12] is generally determined by wicking with low-energy spreading alkanes, for which the contact angle θ is assumed to be zero. Thus, Eq. [12] is reduced into the following equation:

$$\frac{2\eta h^2}{t} = R_{eff} * \gamma_L \quad [13]$$

After wicking with several low energy alkanes, one can draw a plot of $2\eta h^2/t$ vs. γ_L. The slope of the straight fitting line passing through origin gives the effective interstitial pore radius R_{eff}.

The contact angle of high energy liquid, such as water, on powder surface can be obtained by wicking with the liquid on thin powder layer. Using the R_{eff} value obtained from wicking result with low energy alkanes, one can get the water contact angle by solving Eq. [12], in which contact angle is the only unknown parameter.

The obtained contact angle for each liquid is then imputed into Eq. [11]. Three equations with three unknowns are set up and solved simultaneously to obtain the values of γ_S^{LW}, γ_S^+, and γ_S^-. Imputing the known water and solid surface free energy components into Eq. [9], one then obtain the solid/water interfacial surface free energy, γ_{12}. What is more, one can get the change in Gibbs free energy for the processes, as shown in Figure 1, of a) coagulation process: a solid particle 1 adheres to a solid particle in liquid media 2,

$$\Delta G_{131} = -2\gamma_{12} \qquad [14]$$

and b) flotation process: a solid particle 1 adhere to a air bubble 3 in liquid media 2,

$$\Delta G_{132} = \gamma_{12} - \gamma_{13} - \gamma_{23} \qquad [15]$$

It is clearly seen that ΔG_{131} is related to the coagulation process of solid particles in suspension while ΔG_{132} represents the floatability of particles in a flotation tank.

7.2 Experimental

Materials

Nanopure water was obtained by using the Nanopure III (Barnstead, IA) water system. The conductivity of the water was 18.2 MΩ/cm at 25°C and the surface tension was 72.5 mN/m at 22°C. Liquid reagents, such as chloroform (99.9%, Burdick & Jackson), H_2SO_4 (98%, VMR International) and H_2O_2 (30%, VMR International) were used as received without further purification. The surfactants used in the present work included dodecyltrimetyl-ammonium chloride (C_{12}TACl), tetradecyltrimetylammonium chloride (C_{14}TACl), hexadecyltrimetylammonium chloride (C_{16}TACl) and octadecyltrimetylammonium chloride (C_{18}TACl) all from TCI and of greater than 97% purity. They were used without further purification. Solutions of a low concentration were prepared in containers with a volume of at least 100 mL to prevent significant depletion of surfactant *via* adsorption onto the glass walls.

Quartz plates (Hereaus Amersil Inc.) and silicon wafers (100 oriented, Polished Wafer, Sumco, Ore-gon) were boiled in a H_2SO_4/H_2O_2 solution (7: 3 by volume) at 110 ℃ for 60 minutes. The plates were rinsed thoroughly with a large amount of Nanopure water, equilibrated with the water in a sealed vial for at least 20 minutes, removed and dried by blowing pure nitrogen gas over the surface, and then used for experiments.

Pre-cleaned glass microslides (75x25 mm, Corning, NY) were used without further cleaning. Wicking liquids used in the present work, Alkanes, such as Decane and Dodecane (Aldrich Chemical Company) were HPLC grade (>99.5% purity).

Surface Force Measurements

Surface forces were measured using a Digital Instrument Nanoscope IIIa AFM (Digital Instruments, CA) at room temperature (22±1℃) using the colloidal probe technique (16,17). The separation distance (*H*) between the probe (glass sphere) and the substrate (silica plate) was measured by monitoring the deflection of the cantilever on which the probe was attached. Silicon-nitride NP-20 cantilevers were obtained from Veeco, CA.

Triangular cantilevers with spring constant of 0.58 N/m were used. The spring constants were determined using the resonant frequency technique (18). Errors associated with this technique were within ±7%. The glass spheres (12-20μm in diameter) were obtained from Polysciences Inc., Warrington, PA. They were soaked in chloroform for 30 minutes and UV-irradiated for 30 minutes to remove possible organic contaminants. In each experiment, a glass sphere was glued onto a cantilever with EPON 1004 resin (Shell Chemical Co.). Measured forces (F) were normalized by dividing with the radii (R) of the spheres. Combined errors between the measurements of the spring constants and the sphere diameters were within ±12% in force/diameter (F/R) calculations.

For a given surfactant, surface forces were measured at different concentrations. For a given set of measurements, the surfactant solutions were injected into an AFM liquid cell starting from the lowest concentration and continuing to the highest. At each concentration, the glass sphere and silica plate were equilibrated for 1 hour before starting the measurements.

Contact Angle Measurements

A silica plate was immersed in a surfactant solution for a desired period of time. The contact angles were measured by means of a contact angle goniometer using the captive bubble technique, in which silica plates were kept in solution while air bubbles were brought to contact. A total of five contact angles were measured at a given experimental condition and averaged.

Thin Layer Wicking Experiment

10 g glass spheres (<2 μm) were added into 190 ml C_nTACl (n=12,14,16,18) surfactant solutions at the concentration of respective p.c.n., which is obtained from the force measurement in Chapter 3, to make a 5% (wt.) solution. The suspension was stirred for 2 hours and then 5 ml silica/surfactant suspension was withdrawn with a pipette and evenly sprayed onto a glass microscope slide, which was kept strictly horizontal. The slide with the solution of hydrophobized glass on it was dried in ambient situation overnight and further dried in oven at 110ºC for at least 2 hours to remove residual pore water; then the slide was cooled down in a vacuum desiccator and ready for wicking experiments. In practice, a uniform thin layer of talc powder was found firmly adhere to the glass slide and the front line of wicking liquid on the slide is both sharp and clear.

The wicking experiments were performed by immersing the powder-coated glass slides vertically in the wicking liquid, which is filled at the bottom of a sealed vessel (19), and the time for the wicking liquid to travel through every 2.5mm height is recorded. Because the glass slides were vertically placed in present work, a 5cm wicking distance was set as the final wicking point in order to minimize the effect of gravity force. For each wicking liquid, the tests were repeated at least three times and the values listed here were the arithmetic average over three sets of experiment data. The value of R_{eff} in the Equation [13] was determined using liquids of low surface free energy (Decane and Dodecane), which completely spread over the solid surface (i.e., θ=0). Experiment results show that the $2\eta l^2/t$ vs. γ_L yielded a straight line passing through the origin. This finding confirms that the Washburn equation, Eq. [12] is applicable under the wicking conditions

in present work. Furthermore, the liquids contact angles on C_nTACl coated thin glass powder layer were calculated using Eq. [12] with the obtained R_{eff}

7.3 Results and Discussion

7.3.1 Detachment force vs. Interfacial surface free energy (γ_{sl})

Figure 7.2 shows the detachment force measured between glass sphere and silica plate in C_nTACl solutions at the concentration of respective p.c.n. using an AFM. When the surfactant changes from $C_{12}TACl$ to $C_{18}TACl$, the detachment force correspondingly increases from 13 to 60 mN/m. The variance associated with the detachment force measurement is about $\pm$ 5 mN/m; therefore, the results clearly show that the adhesion force obtained in long chain surfactant solution is much higher than that for a short chain surfactant. As shown by Eq. [1] and [2], the adhesion force is directly related to the solid/liquid interfacial free energy. It suggests that interfacial free energy between silica/$C_{18}TACl$ solutions should be larger than that at silica/$C_{12}TACl$ solutions interface. The interfacial surface free energy, γ_{sl} is calculated using Eq. [2], i.e., the JKR model and the results are listed in Table 7.1. As expected, the interfacial energy increases from 1.38 mJ/m^2 to 2.44 mJ/m^2 when surfactant changes from $C_{12}TACl$ to $C_{14}TACl$ because of the stronger adhesion force measured in the later case. The γ_{sl} value further increases to 5.2 mJ/m^2 for the case of $C_{16}TACl$ and amounts to as high as 6.37 mJ/m^2 at the silica/$C_{18}TACl$ solutions interface.

It is known that the interfacial surface free energy γ_{sl}, is directly related to the solid surface hydrophobicity. The results of contact angle measurement show that the water contact angle increases from 47 to 62 degrees when the surfactant changes from $C_{12}TACl$ to $C_{18}TACl$. This finding corresponds to the trend of interfacial energy increasing with surfactant chain length. It is therefore concluded that for long chain surfactant a more hydrophobic surfactant layer is formed at solid/water interface at the p.c.n.. This in turn introduces an increase of interfacial surface free energy γ_{sl} and thus the adhesion force between glass sphere and silica plate in aqueous solution. Figure 7.3 shows that the adhesion force (detachment force) increases with contact angle increasing. When the contact angle increases from 47 degree to 64 degree, correspondingly, the detachment (pull-off) force increases from 13 to 60 mN/m. The figure also shows that the decay length of the strongest long rang attraction in respective C_nTACl solutions at the p.c.n also increases with contact angle. For example, the decay length, D increases from 3 to 32 nm accordingly when the contact angle increases from 47 degree to 64 degree. The results indicate that both the approach and the detachment force increase with surface hydrophobicity! It may be stated in another expression that it is easy for the hydrophobic solid particles to aggregate while difficult to disperse in aqueous media.

7.3.2 Thin layer wicking of glass sphere

Figure 7.4 shows the thin layer wicking results of glass particles coated with $C_{14}TACl$ surfactant. The slope of the straight line of $2\eta h^2/t$ *vs*. surface tension γ_L gives the effective pore radius, R^*, which is included in Eq. [12] and [13]. However, one can see from the figure that the $2\eta h^2/t$ value for Formamide is above the straight line obtained with the low surface tension wicking liquids, decane and dodecane, of which the wicking contact angle is assumed to be zero. It suggests that for formamide the value of cosθ in Eq. [12] should

be larger than 1! Therefore, the contact angle of formamide can not be available when calculated using Eq. [12] Further more, the surface free energy components of the glass spheres accordingly can't be calculated using the OCG equation due to the lack of contact angle data in Eq. [11].

The reason can be explained by the facts that the wicking liquid, formamide is a strong basic liquid with a γ^- value as high as 39.6 mJ/m^2. From Eq. [7], one can see that the solid with a high acidic surface free energy component γ^+ will result in a more negative surface free energy change for the process of adhesion. At this situation, contact angle is no longer a good criterion for the solid hydrophilicity because the contact angle is already zero. It is therefore not applicable to first get contact angle and calculate the surface energy components using the contact angle values using Eq. [11]. However, we manage to find one way to overcome the difficulty. Without obtaining the contact angle value in Eq. [12], we directly impute the cosθ attained from Eq. [12] into Eq. [11] and setup three equations for three wicking liquids. Thus the solid surface free energies are still can be calculated. The calculation results are also shown in Table 7.1.

7.3.3 Solid surface free energies

The solid surface free energy components of glass spheres are listed in Table 7.1 and some free energy parameters are also shown in Figure 7.5. The glass sphere without reagent coating shows such a high acid surface free energy component γ^+ as 41.5 mJ/m^2. It confirms the previous assumption and explains why the glass surface is so hydrophilic. As mention by van Oss (7), one surface free energy component, either γ^+ *or* γ^-, is higher than 28.5 mJ/m^2, the surface is hydrophilic. Also, the fact that the acid component is very high correlates to that the P.Z.C for silica is at about pH 2-3.

It is clearly shown in Figure 7.5 that when contact angle (surface hydrophobicity) increases, the solid surface free energy γ^+ decreases. For example, the value decreases from 41.5 mJ/m^2 to only 27 mJ/m^2 when silica sphere is hydrophobized by C_{12}TACl with a result contact angle as 43 degree. When C_{14}TACl is applied, the contact angle increases to 47.5 degree and the γ^+ further decreases to 24 mJ/m^2. When silica powder is coated with C_{16}TACl, the contact angle is 59 degree and γ^+ is as low as 19 mJ/m^2. Finally, addition of C_{18}TACl increase the contact angle to 65 degree and γ^+ is further lowed to12.7 mJ/m^2. γ^-, however, does not change much after the adsorption of C_nTACl surfactants. Therefore, the addition of surfactant increases silica surface hydrophobicity mainly by decreasing surface free energy.

7.3.4 γ_{sl} calculated from the thin-layer wicking technique

The solid/water interfacial surface free energy γ_{sl}, is thus calculated using the surface free energies data of glass spheres obtained in the previous section. The results show that from C_{12}TACl to C_{18}TACl, γ_{sl} increases with surface hydrophobicity increasing. For example, γ_{sl} is -5 mJ/m^2 in the case of no surfactant being added. The negative sign suggests that the uncoated silica surface is very hydrophilic and the silica surface attracts the water molecules stronger than by water molecule themselves. That is the reason why silica particle disperse very well in water and form stable suspension. The value increases to as high as 11.16 mJ/m^2 when the silica surface is coated with C_{18}TACl surfactant and the contact angle is 65.74 degree.

In addition, the interfacial free energy calculated using Eq. [2] from the detachment force obtained from the AFM force measurement is also plotted in Figure 7.5 for comparison. It seems that there is a little difference between the absolute γ_{sl} values attained using two different techniques. For example, the value of γ_{sl} , at contact angle 62 degree, is 6.37 mJ/m^2 from the detachment force measurement; while the value is 11.16 mJ/m^2 with a 65.74 degree contact angle from the thin layer wicking technique. The difference may be due to surface roughness and the experiment errors associated with the two different techniques. However, the results both show a same finding. That is, the interfacial surface free energy, γ_{sl}, increases with surface hydrophobicity (water contact angle).

7.3.5 The change in Gibbs free energy (ΔG)

From the attained interfacial surface free energy, one can calculate the Gibbs free energy change for the process of coagulation (ΔG_{131}) and flotation(ΔG_{132}) using Eq. [14] and [15]. The calculated values are listed in Table 7.1 and plotted as Figure 7.6. For the bare hydrophilic silica, ΔG_{131} is 10 mJ/m^2 and it suggests that it is not favorable in thermodynamics for two hydrophilic silica particles adhere to each other. Instead they disperse well in water. ΔG_{132} is only -1.5 mJ/m^2 and the very close to 0 value means that the attachment of a bubble to a hydrophilic silica sphere is not quite an automatic thermochemical process.

When the silica surface is hydrophobized by surfactant adsorption, the solid/water interfacial tension increases. The hydrophobization also introduces more negative change in Gibbs free energy. For example, when coated with C_{12}TACl, the ΔG_{131} is -3.22 mJ/m^2 and ΔG_{132} is -22.9 mJ/m^2. The negative values suggest that when being hydrophobized, solid particles are no longer stable or dispersed in water. It becomes more and more possible for the coagulation and flotation process to automatically occur. When the solid surface becomes even hydrophobic, the ΔG_{131} value further decreases to -8.27 mJ/m^2 and ΔG_{132} decreased to -23.6 mJ/m^2. The ΔG_{131} value further decreases to -12.9 mJ/m^2 and ΔG_{132} decreased to -35.5 mJ/m^2 with contact angle increasing further. Finally, when C_{18}TACl is used, contact angle increase to about 65 degree. Correspondingly, the ΔG_{131} value further decreases to -22.3 mJ/m^2 and ΔG_{132} decreased to -42.95 mJ/m^2. The glass spheres become more and more unstable in aqueous solutions.

7.4 Conclusions

The detachment forces between glass/silica surfaces in C_nTACl solutions, obtained from AFM surface force measurement, are used to calculate the silica/water interfacial surface free energy γ_{sl} using the JKR model. The values are compared to those obtained from thin layer wicking technique, through which the surface free energy components of silica particles are attained. The results shows that the detachment force and interfacial surface free energy, γ_{sl} increases with surface hydrophobicity (water contact angle). The surface free energy components γ^{lw} and γ^{+} of silica decreases with surface hydrophobicity increasing. The fact that the changes in Gibbs free energy, ΔG_{131} and ΔG_{132}, both become more negative when contact angle increases suggests that the instability and the floatability of silica particles in the pulp solution increase with surface hydrophobicity.

7.5 References

(1) B. V. Derjaguin, V. M. Muller and Yu. P. Toporov, J. Colloid Interface Sci., 1975, 53, 2, 314-326.
(2) K.L. Johnson, K. Kendall, A.D. Roberts, Proc. R. Soc. London, A324, 1971, 301.
(3) C. J. Van Oss, R. J. Good, and M. K. Chaudhury, Colloid and Interface Science, 1986, 111, 378.
(4) C. J. van Oss, M. K, Chaudhury, and R. J. Good, Adv. in Colloid Interface Sci., 1987, 28, 35.
(5) C. J. Van Oss, R. J. Good, and M. K. Chaudhury, Langmuir, 1988, 4, 884
(6) C. J. Van Oss, M. K. haudhury, and R. J. Good, Colloid and Interface Science, 1988, 128, 313.
(7) C. J.Van Oss, "Interfacial forces in aqueous media", Marcel Dekker, 1994.
(8) F. M. Fowkes, J. Phys. Chem., 1962, 66, 382.
(9) F. M. Fowkes, J. Phys. Chem., 1963, 67, 2538-2541.
(10) I. Yildirim, Ph.D. Thesis, Virginia Tech, April 2001.
(11) E. Lobato, Master Thesis, Virginia Tech, November 2004.
(12) E. Chibowski, L. Holysz, Langmuir, 1992, 8(2), 710-716.
(13) L. Holysz, E. Chibowski, Langmuir, 1992, 8(2), 717-721.
(14) E. Chibowski, F. Gonzalez-Caballero, Langmuir, 1993, 9(1), 330-340.
(15) E.W. Washburn, Physical Review, 1921, 1, 273.
(16) W. A. Ducker; T. J. Senden; R. M. Pashley, Nature 1991, 353, 239-241.
(17) W. A. Ducker; T. J. Senden; R. M. Pashley, Langmuir 1992, 8, 1831-1836.
(18) J. P. Cleveland; S. Manne, D. Bocek, P. K. Hansma, Rev. Sci. Instrum. 1993, 64, 403-406.
(19) E. Lobato, J. Zhang, I. Yildirim, R.-H. Yoon and J. Yordan, "Characterization of Surface Free Energies of Talc Powders using Thin-Layer Wicking Technique", SME Annual Meeting, March, 2006.
(20) I. Yildirim, J. Zhang, and R-H Yoon, "Effect of Surface Treatment on the Acid-base Properties of Fillers and Pigments", SME Annual Meeting, 2003.

Table 7.1 Water contact angle, surface free energy components and solid/liquid interfacial energy of glass particles obtained using the thin layer wicking technique, also with the solid/liquid interfacial energy of silica substrates obtained from AFM surface force measurement.

Method		Water	C_{12}TACl	C_{14}TACl	C_{16}TACl	C_{18}TACl
Thin layer wicking	Contact angle (º)	11.65	43.00	47.49	59.16	65.74
	γ_s^{LW}	48.02	40.10	41.04	32.95	30.18
	γ_s^-	2.01	1.20	1.57	1.54	2.33
	γ_s^+	41.5	27.00	24.04	18.96	12.69
	γ_s^{AB}	18.28	11.38	12.29	10.82	10.89
	γ_s	66.3	51.48	53.33	43.76	41.07
	γ_{12}	-5	1.61	4.13	6.44	11.16
	ΔG_{131}	10	-3.22	-8.27	-12.9	-22.3
	ΔG_{132}	-1.5	-22.9	-23.6	-35.5	-42.9
AFM force measurement	γ_{12}	-	1.38	2.44	5.20	6.37
	Contact angle (º)	0	47	51	58	62

* Surface free energy components and solid/liquid interfacial energy are in the unit of mJ/m^2.

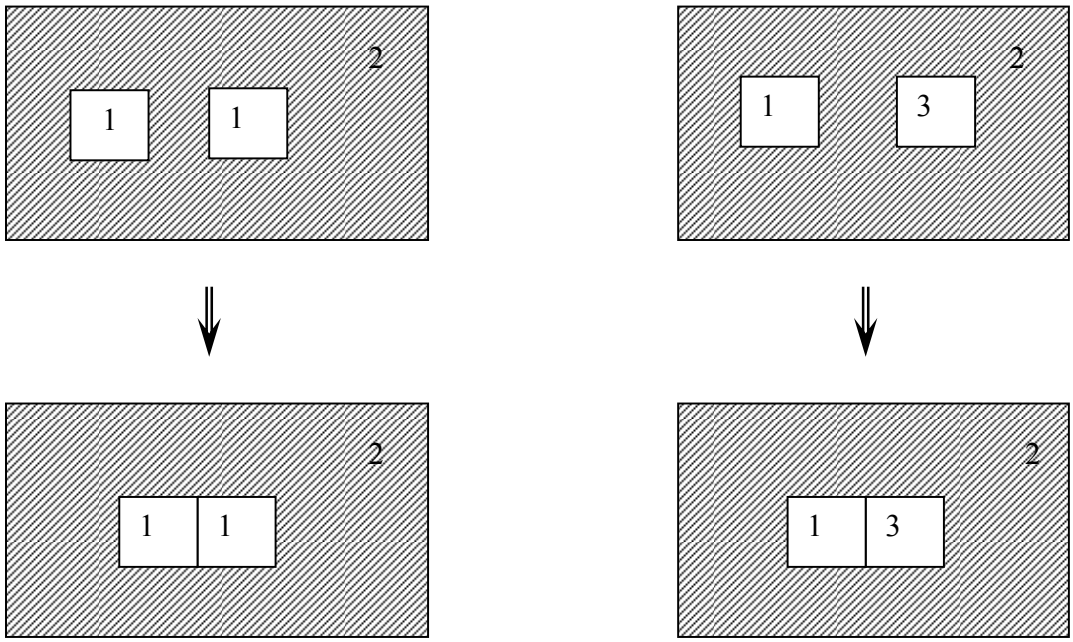

a) $\Delta G_{131} = -2\gamma_{12}$ b) $\Delta G_{132} = \gamma_{13} - \gamma_{12} - \gamma_{23}$

Figure 7.1. The changes in Gibbs free energy for the processes of a) coagulation process: a solid particle 1 adheres to another solid particle in liquid media 2; b) flotation process: a solid particle 1 adheres to an air bubble 3 in liquid media 2.

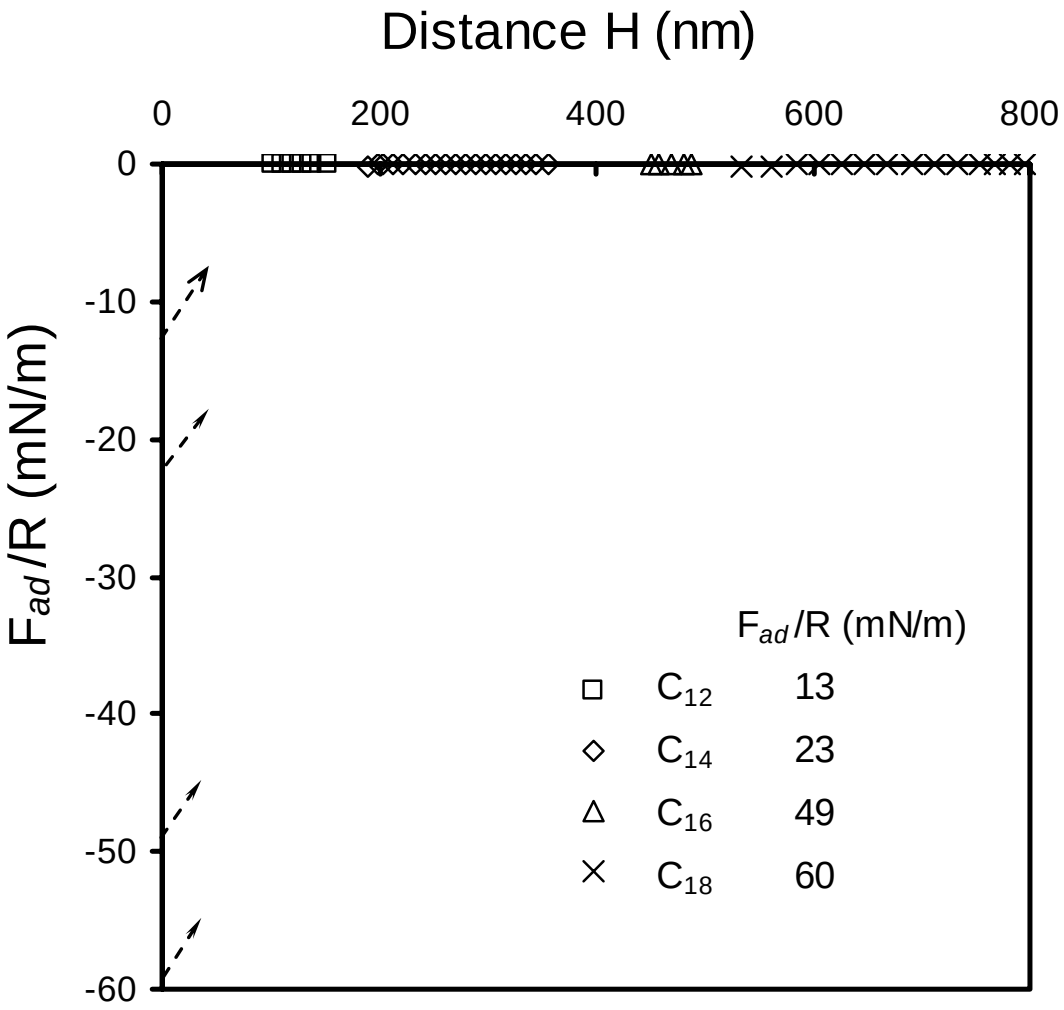

Figure 7.2 Detachment force between glass/silica surfaces submerged in C_nTACl solutions at the concentration of respective p.c.n. The forces are normalized by the radius of glass sphere, R.

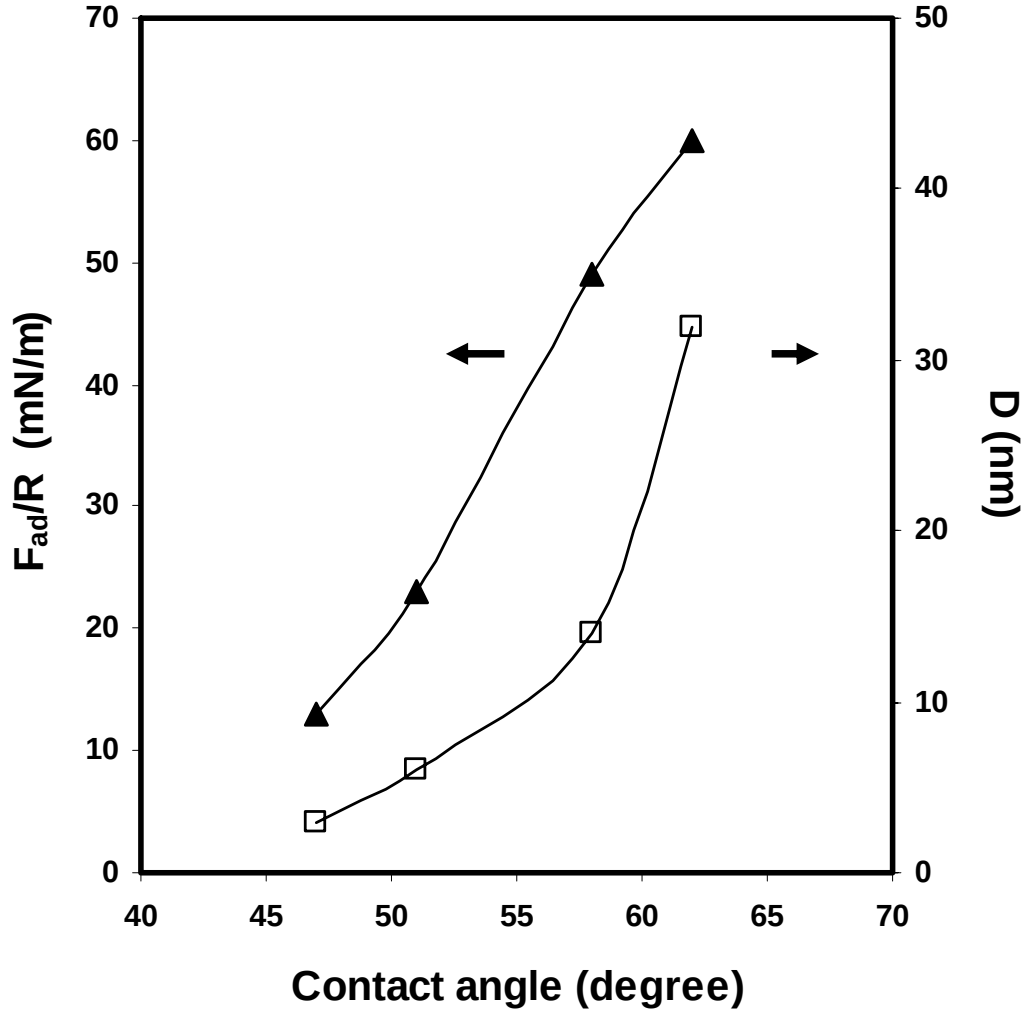

Figure 7.3 Relationship between the detachment force, the Decay length of the strongest long range attraction between silica/glass surfaces submerged in C_nTACl solutions and the surface hydrophobicity at the concentration of respective p.c.n.

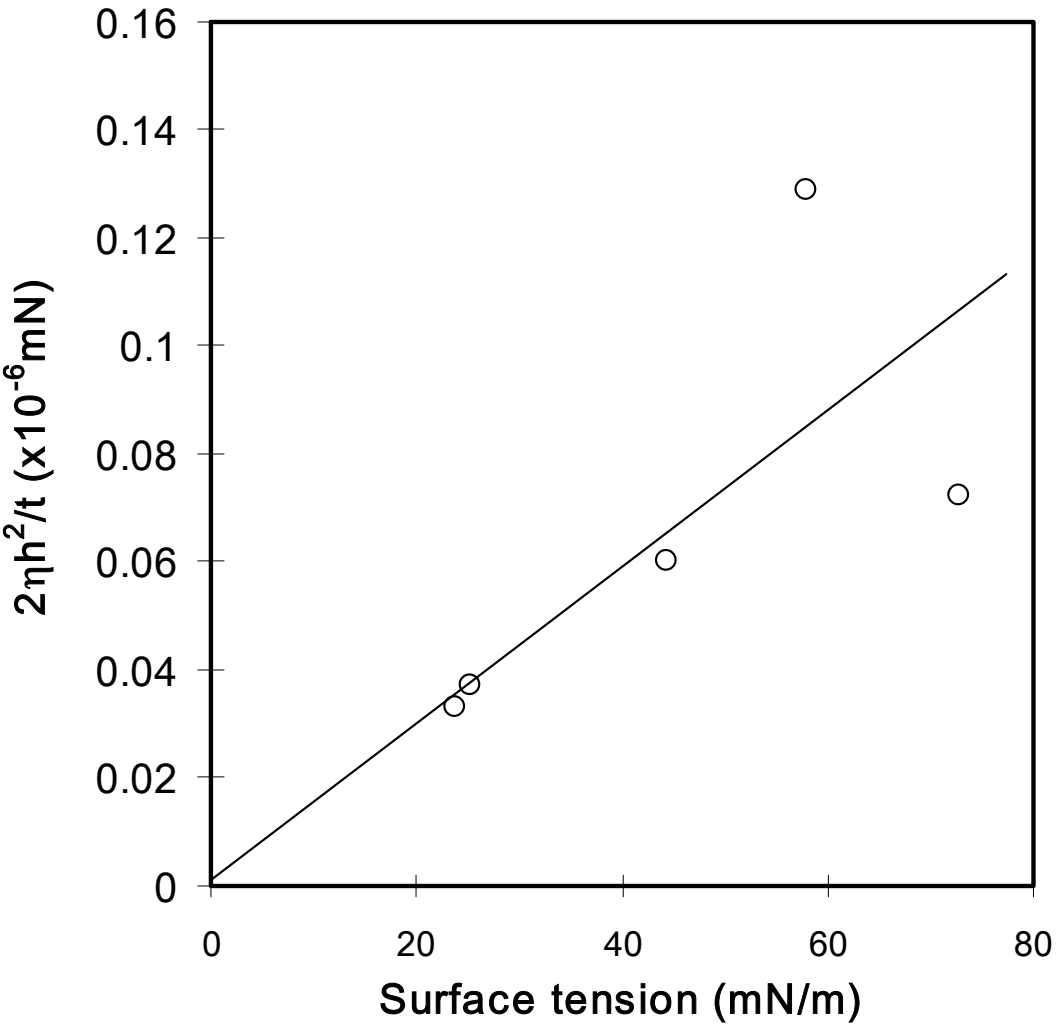

Figure 7.4. $2\eta h^2/t$ *vs*. surface tension γ_L of silica powders coated with C_{14}TACl surfactant using the thin layer wicking technique.

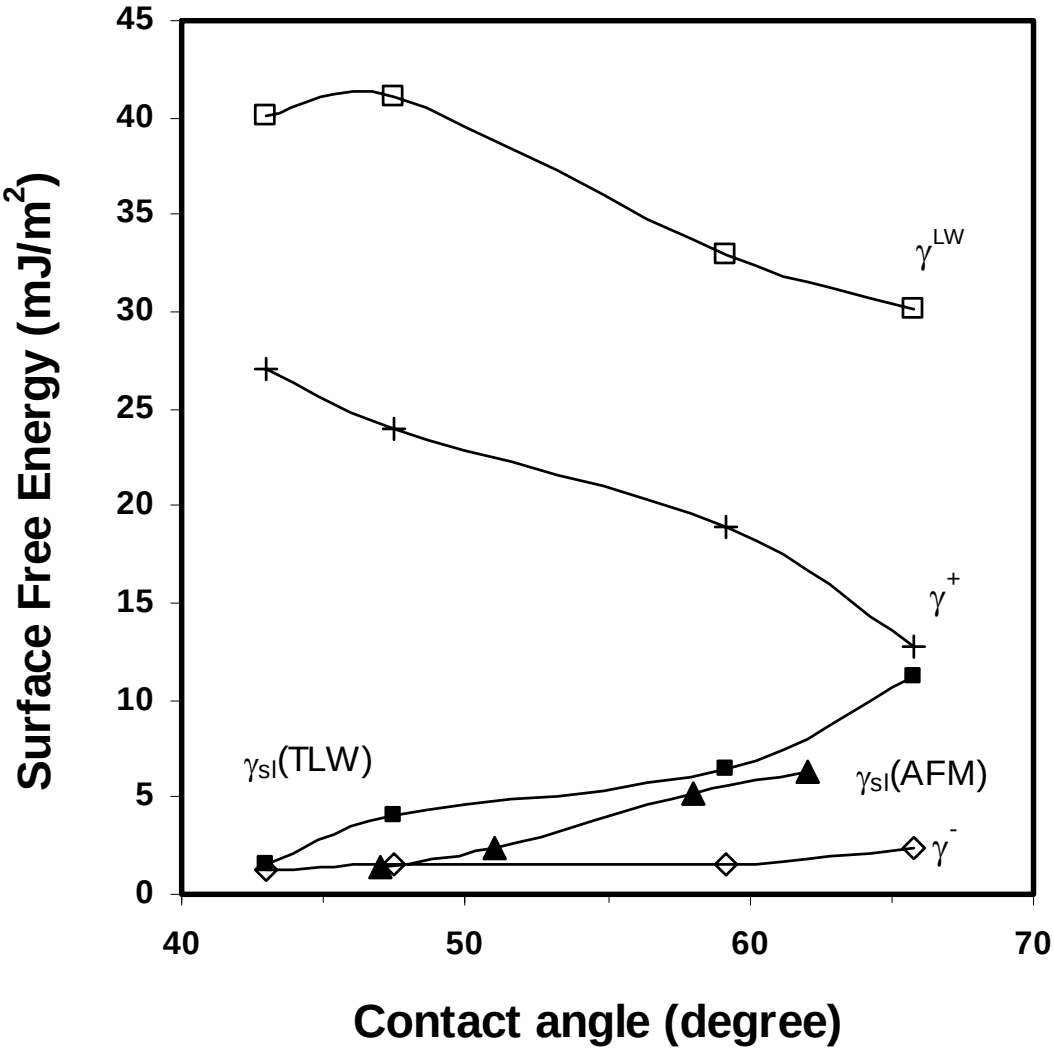

Figure 7.5 The relationship between solid surface free energy and the solid hydrophobicity (water contact angle). It also shows the relationship between the solid/liquid interfacial surface free energy, obtained from both the AFM force measurement and the thin layer wicking technique, and the solid hydrophobicity (water contact angle).

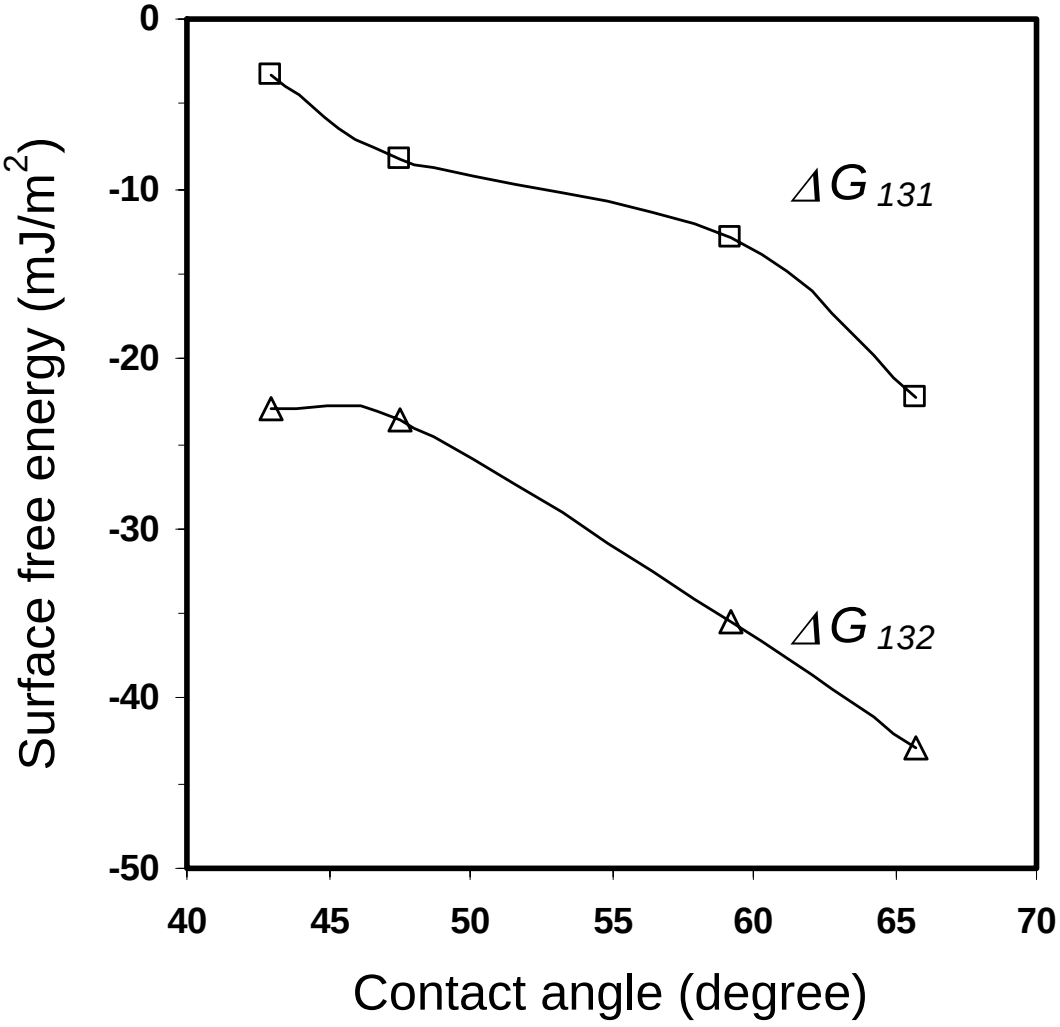

Figure 7.6 Relationship between the contact angle and stability and flotability of solid particles in water. ΔG_{131} is the change of surface free energy for the attachment of two talc powders in water. ΔG_{132} is the change of surface free energy for the attachment of a talc powder and an air bubble in water. 1 represents solid, i.e. silica ; 2 represents air phase and 3 represents liquid, i.e. water.

CHAPTER 8

Future work

Based on the results obtained in the present work, the future work may be recommended to be carried out listed as follows:

1. In present work, a study of salt effect has been carried out in the in-situ adsorption surfactant/adsorbate system. The hydrophobic force at the p.c.n. was found to decreases with salt addition. However, the adsorption of surfactant at the solid/liquid interface may be disturbed by the addition of salt due to the uncertainty of exact p.c.n. associated with experiment difficulties. Therefore, a robust hydrophobic surface, such as silica surface coated by OTS with chemically adsorption, is recommended for the study of salt effect on hydrophobic force. The results will help verify the origin of the long range hydrophobic force.

2. Surface force measurements are suggested to be carried out at different temperatures between chemically hydrophobized solid surfaces, which are rather robust and will remain nearly the same as temperature changes. Considering the water structure origin of the hydrophobic force, the change in media temperature will introduce changes in water structure; therefore the change in hydrophobic force. The obtained force results will make better understanding of the origin of hydrophobic force in a thermodynamics consideration.

VITA

Jinhong Zhang was born in August, 1973 in Lianyungang, Jiangsu, China. He received B.S. in Minerals processing in China University of Mining and Technology, Xuzhou, China in July, 1995. He graduated with a master degree in Minerals processing in China University of Mining and Technology (Division of Graduates), Beijing, China in July, 1998. He enrolled in the Mining and Minerals Engineering Department of Virginia Polytechnic Institute and State University in August, 2001 to pursue his Ph.D. He has been a research assistant in Virginia Tech since then.